A Characterisation and Radiation Resistance Study of a Mixed-Modifier Borosilicate Glass for HLW Vitrification.

Jonathan Mark Roderick
B.Sc. (Hons.)

A thesis submitted to the University of Warwick in partial fulfilment of the requirement for the degree of Doctor of Philosophy

Department of Physics

February 2001

This thesis is dedicated to Melly.

THE UNIVERSITY OF WARWICK

LIBRARY DECLARATION

Candidate's name: JONATHAN RODRICK

Date of birth: 27-04-1977 ID Number: 9765274

I agree that this thesis shall be made available by the University Library in accordance with the regulations governing University of Warwick theses.

I agree that the summary of this thesis may be submitted for publication.

I agree that the thesis may be photocopied (single copies for study purposes only) (YES) / NO
(please delete as appropriate)

Theses with no restriction on photocopying will also be made available to the British Library for microfilming. The British Library may supply copies to individuals or libraries, subject to a statement from them that the copy is supplied for non-publishing purposes. All copies supplied by the British Library will carry the following statement: "Attention is drawn to the fact that the copyright of this thesis rests with its author. This copy of the thesis has been supplied on condition that anyone who consults it is understood to recognise that its copyright rests with its author and that no quotation from the thesis and no information derived from it may be published without the author's written consent."

Author's Signature: JM Rodrick Date: 27-02-01

USER'S DECLARATION

1. I undertake not to quote or make use of any information from this thesis without making acknowledgement to the author.

2. I further undertake to allow no-one else to use this thesis while it is in my care.

DATE	SIGNATURE	ADDRESS

Contents

List of Figures

List of Tables

Abbreviations

BO	Bridging Oxygen
DTA	Differential Thermal Analysis
ESR	Electron Spin Resonance
EXAFS	Extended X-ray Absorption Fine-Structure
HLW	High Level Waste
LBS	Lanthanum-sodium-lithium borosilicate
MA	Mixed alkali
MAS	Magic Angle Spinning
MQMAS	Multiple Quantum Magic Angle Spinning
NBO	Non-Bridging Oxygen
NBS	Sodium-lithium borosilicate
NMR	Nuclear Magnetic Resonance
TEM	Transmission Electron Microscopy
XRD	X-ray Diffraction

Acknowledgements

I would like to thank the Department of Physics for providing the facilities that have made this work possible. In addition, I'd like to thank everyone who has helped me to complete this thesis in one way or another over the last three years.

I'd like to thank Dr. Diane Holland for her wit, guidance and unstinting enthusiasm for glass science. I owe much to the efforts of Keith Briggs, Dave Hammond, Dan Lee, Andy Sheffield and Geoff Diamond for their invaluable technical expertise. Special thanks are due to Dr. Andrew Howes, for incalculable assistance with NMR spectrometry, and Dr. Nobby Clarke and Bob Green, for their time and co-operation at the Birmingham University Radial Ridge Cyclotron facility. I would also like to thank BNFL, and Mr. Charlie Scales in particular, for providing financial assistance and direction for the work.

I am very grateful to the other members of the Glass-Ceramics and Crystallography groups, particularly Dr. Ian Gee, Dr. Glyn Jones, Tom Lyford, Dr. Andy Wootton and Dr. Steve Ison, with whom I have spent much of my time, both professionally and socially. I also owe an incredible amount to my very good friends in Earlsdon, who all deserve some kind of medal for putting up with me over the last few months. Thanks must also go to Mr. Reamonn Lydon and the Fiat for getting me around this year.

Finally I would like to thank my family for supporting me throughout the three long years it has taken for my research to come to fruition.

Declaration

The work for this thesis was carried out in the Department of Physics at the University of Warwick, and the ESR and the Radial Ridge Cyclotron facilities were made available at Birmingham University. The work was completed during the period from October 1997 to September 2000 and, except where specifically acknowledged in the text, is the result of my own independent research and has not been previously submitted at the University of Warwick, or any other institution, in respect of a higher degree. Parts of this thesis have been published or submitted for publication with the following references:

1. *Characterisation and radiation resistance of a mixed-alkali borosilicate glass for high-level waste vitrification*, **J M Roderick**, D Holland & C R Scales, Proc. 3rd Int. Conf. on Borate Glasses, Crystals and Melts, Phys. Chem. Glasses, **41** (6) (2000) p.392-395

2. *Characterisation and radiation resistance of a mixed-alkali borosilicate glass for high-level waste vitrification*, **J M Roderick**, D Holland & C R Scales, *Scientific Basis for Nuclear Waste Management* **23** (2000), Eds. R W Smith & D W Shoesmith.

3. *Density-structure relations in mixed-alkali borosilicate glasses by ^{29}Si and ^{11}B MAS-NMR*, **J M Roderick**, D Holland, A P Howes & C R Scales, Proc. 8th Int. Conf. On Non-Crystalline Materials, J. Non-Cryst. Solids, in press.

The abstracts to each of these publications can be found in appendix A. It is anticipated that further parts of this thesis will be submitted for publication in due course.

26 February 2001
Date

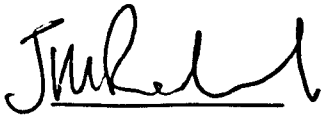
J M Roderick

Abstract

The short-range structural order, in glasses from the technologically important Na_2O-Li_2O-B_2O_3-SiO_2 system, is investigated using NMR and thermophysical techniques. The change in the populations of tetrahedrally coordinated borate units and various trigonal borate units is deduced from ^{11}B NMR and compared with the most widely accepted, NMR based, structural model of Dell, Bray and Xiao[1]. Differences from the model are discussed and substantiated with results obtained from ^{29}Si NMR. Structure sensitive properties such as density, glass transition temperature and thermal expansion coefficient are reported across a wide range of modifier concentrations. This information is then related to and compared with the structural arrangements obtained from NMR studies of less complex systems. An empirical density model[2,3] designed for the single-modifier borosilicate systems has been used to gain information regarding the structural arrangements in the current system.

Investigation of specific, carefully controlled, compositional changes to the current HLW vitrification glass, MW, has been carried out. The effect of B_2O_3 concentration on the chemical durability of glasses from this system has been studied using dynamic leach tests. In addition, the role of La_2O_3, a waste simulant, has been investigated using similar analytical methods, and suggestions as to its primary function in the glass have been discussed.

Finally, a preliminary study of the interaction of several compositions, related to MW, with high-energy α-particles and UV-radiation, has been pursued. The presence of radiation induced structural and physical changes has been probed using ESR and γ-ray spectroscopy, enabling suggestions for the types of defects produced and nuclear reactions taking place to be made.

[1] W. J. Dell, P. J. Bray & S. Z. Xiao, J. Non-Cryst. Solids **58** (1983) p.1
[2] D. Feil and S. Feller, J. Non-Cryst. Solids **119** (1990) p.103
[3] K. Budhwani & S. Feller, Phys. Chem. Glasses **36** (4) (1995) p.183

Chapter 1- Introduction

1.1 Overview

The theory and practice of High-Level Waste (HLW) storage has as yet failed to determine a definitive method of safe, reliable, durable isolation of wastes generated by the nuclear power and weapons industries. Containment systems currently utilised around the world include a variety of glasses and glass-ceramics, cements and synthetic minerals. A key requirement is the development of predictive models, based on sound experimental data of the effects of radiation and physical degradation, that will allow the long-term assessment of the suitability of the chosen isolating matrix.

Borosilicate glass is the current system favoured by waste disposal facilities in the United States, France and Great Britain and much work has been carried out on formulations based around the generic borosilicate system. Its desirable combination of chemical and thermal stability, ease of processing and ability to accommodate large variations in waste composition make it a suitable candidate medium for the final long-term storage of HLW. However, the relative complexity of the borosilicate system requires fuller investigation, of its chemical and physical properties, than those of less complex glass-forming systems.

1.2 Aim of the Work

The objectives of the following work have been two-fold. Firstly, effort has been directed towards investigating the effect, on chemical and radiological behaviour, of variations to the base borosilicate composition currently used to store HLW by British Nuclear Fuels Ltd. Experimental simulation of the interactions that may take place between the storage medium and radioactive elements present in the waste, alongside dynamic chemical durability tests, have been used to carry out this evaluation.

Secondly, a more fundamental study of the chosen mixed-alkali borosilicate glass system has been attempted. This has involved the preparation and analysis, using numerous chemical and structural techniques, of a range of compositions covering the low to medium alkali content of the glass-forming region. No

published work currently exists specifically covering the mixed-alkali borosilicate glass system and it is hoped that an improvement in the state of knowledge will aid the refinement and subsequent selection of a final storage solution.

1.3 Thesis Structure

This thesis consists of 8 chapters of which this is a brief introduction to chapters 2-8, as outlined below.

Chapter 2 begins with a review of the theory of glass structure and an introduction to the mixed-alkali borosilicate system in particular. There then follows an examination of the structural and physical property modelling that has been carried out on less complex borate, silicate and borosilicate systems. This information is essential in understanding the subsequent approach taken towards analysis of the experimental data presented here.

Chapter 3 presents an introduction to the theory and practice of HLW disposal, concentrating on a description of the processes and conditions that determine the choice of storage material to be used. Consideration of the radiochemistry and composition of a typical commercial waste stream is used to describe the radiochemical effects that must be anticipated when choosing a suitable storage medium.

Chapter 4 is used to outline the theory and practice behind the experimental techniques used in this work.

Chapter 5 presents the first results chapter, concentrating on structural and physical characterisation of the borosilicate glass using NMR and DTA techniques. Measurement of the density variation is also used alongside NMR data to identify structural changes that occur upon variation of the base composition, whilst high-temperature leach tests are used to investigate the chemical stability of the glass compositions studied. The same analytical techniques are also used to study the influence of a simulated waste component, La_2O_3, added to the base composition.

Chapter 6 concentrates on the results of radiation exposure tests on the samples analysed in Chapter 5. The results of efforts to monitor the effect of high-energy α-particle bombardment, via ESR and γ-ray spectroscopy, are explained, ranging from determination of the number of structural defects produced, to interpreting their nature and longevity.

Chapter 7 reports the results of detailed physical and structural analysis of samples taken across a large composition range. The findings are put in context with simpler systems with the results of attempts to model properties such as glass transition temperature, T_g, density and boron and silicon coordination. The results of investigation of the mixed-alkali effect, via ionic-conductivity measurements, are also presented.

Chapter 8 discusses overall conclusions from the experimental results and suggests possibilities for future work.

Note: References are presented at the end of each chapter.

Chapter 2 – Glass structural theories and properties

2.1 Introduction

2.1.1 Glass Definition and properties

The material known as glass is so abundant in our world that its presence often goes unnoticed, yet, it is a fascinating and diverse substance that mankind has been producing, by increasingly sophisticated means, for thousands of years. To begin with, it is well known that most technical glasses contain silica, but we know that silica is not an essential ingredient. Glasses are traditionally produced from a hot melt, but other means of processing such as vapour deposition and sol-gel processing of solutions do not require melting. The vast majority of glasses are inorganic but it is also possible to produce glasses from organic materials such as glycerol. Obviously, it is not possible to define a glass simply from its chemical nature. In fact, no definition of a glass has been assembled that is suitably specific and yet covers the wide range of properties that glasses possess. In truth, it is not possible to completely describe the macroscopic structure of glasses because we do not yet know the complex microscopic structure that glasses possess.

At the same time, glasses *can* be characterised by well-defined properties which, though common to them, are different from those of liquids and crystalline solids. X-ray and neutron diffraction studies have shown that glasses do not possess any long-range periodic order of their constituent atoms [1]. Their similarity to liquids can be illustrated by comparison of the radial distribution functions as shown in Fig. 2.01 Furthermore, the relationship between crystal, liquid and glass can be explained by means of a volume-temperature diagram as shown in Fig. 2.02.

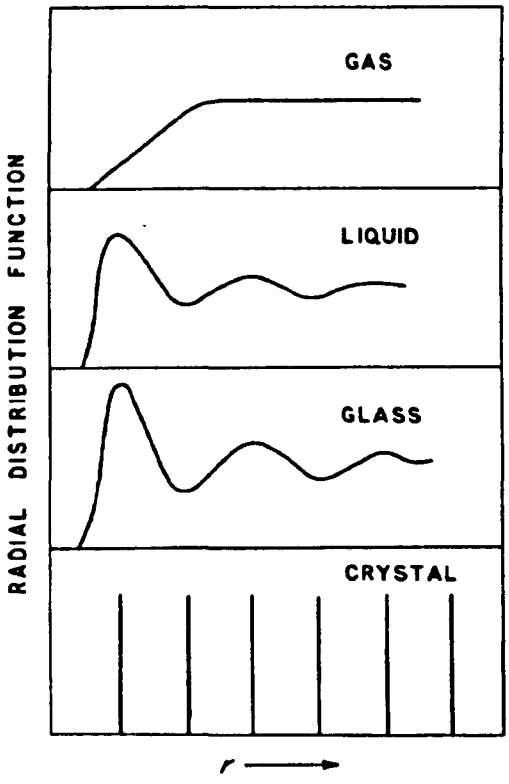

Fig. 2.01 Comparison of the radial distribution function of a glass with that of a gas, liquid and crystal [1].

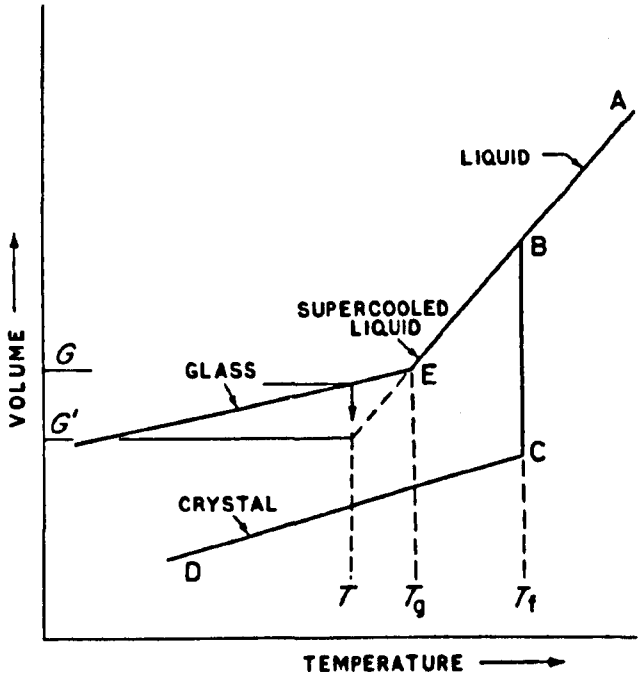

Fig. 2.02 The method of transition from a liquid to a glass [1].

If the liquid is cooled sufficiently slowly from point A, the volume will decrease along AB until point B, where, especially if nuclei are present, crystallisation will take place and the volume of the material will decrease rapidly along BC. The crystal will then continue to contract and cool along CD. However, if the liquid is cooled sufficiently quickly to avoid extensive crystallisation, the volume will continue to decrease along BE. At a certain temperature, the graph undergoes a significant gradient change and the material then continues to contract along EF, almost parallel to CD. The point at which the gradient change occurs is known as the glass transition temperature, T_g, though it is more accurate to describe it as a region since the gradient change is not abrupt. Only below this temperature may the material truly be called a glass. A glass can thus be defined as 'an amorphous solid completely lacking in long range, periodic atomic structure and exhibiting a region of glass transition behaviour'.

2.1.2 Glass forming oxides

Silica (SiO_2) is a common but not essential component of most man-made glasses. Extensive studies have shown that most oxides with a high degree of covalency will form glasses either by themselves or when combined with other oxides. Those oxides are termed 'network formers' and examples include SiO_2, B_2O_3, GeO_2 and P_2O_5. Oxides containing cations that have a more ionic bond with oxygen behave in a manner that is intermediate between those oxides that always form glasses and those that never do. These oxides are known as 'intermediates' and include oxides such as Bi_2O_3, Al_2O_3, Ga_2O_3 and MoO_3. Finally, cations that form highly ionic bonds with oxygen never act as network formers or intermediates and serve only to modify the network structure created by the network forming oxides. These are termed 'modifiers' and include Na_2O, Li_2O and CaO.

2.1.3 Structural theories of glass formation

As already explained, in principle, many liquids, if cooled rapidly enough through the transition region, can be made to form a glass. The fact that different systems require different cooling rates in order to form glasses has led to different atomistic theories correlating the nature of the chemical bond and shape of the structural units involved with the ease of glass formation. As with the definition of a

glass, no one has yet developed a unified theory that is capable of explaining the wide range of phenomena observed in the formation and properties of glasses.

Several structural theories have been proposed since the physical and chemical characterisation of glasses began with Goldschmidt in 1926. He correlated the relative sizes of the oxygen and A atoms with the ability of the A_2O_3 system to form a glass. Based on the observation that glasses formed most easily when the cation-oxygen radius ratio was between 0.2 and 0.4, he suggested that the tetrahedral packing produced by this radius ratio was a requirement of easy glass formation. It has since been shown that cations with a coordination number of 6 can be present in significant quantities in a glass, whilst BeO, with a radius ratio of 0.221, does not form a glass [1].

Later, the seminal work of Zachariasen in 1932 extended the ideas of Goldschmidt and attempted to explain why certain coordination numbers might favour glass formation over others. He observed that those silicate compositions that readily formed glasses possessed network, instead of close-packed, structures. The difference between the structure of a hypothetical crystalline compound A_2O_3, (a), and the Zachariasen model for the glassy form of the same compound, (b), is shown in Fig. 2.03.

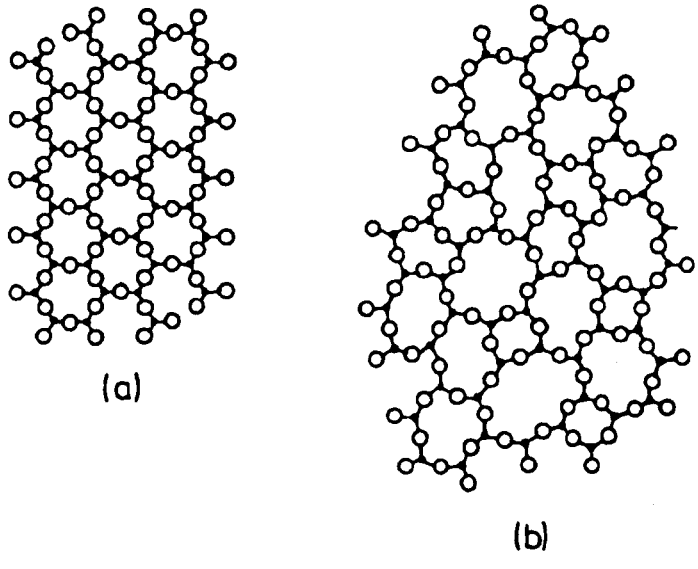

Fig. 2.03 Schematic two-dimensional representation highlighting the structural differences between (a) a crystalline compound and (b) a glassy form of the same compound [1].

Zachariasen assumed that the oxygen polyhedra found in oxide crystals (trigonal, tetrahedral and octahedral) would also be present in glasses, but without the well-defined, periodic orientation found to exist in crystals. It was found that non-periodicity could be introduced into the network structure by variation of the bond angles (for two-dimensions) or bond angles and 'dihedral' angles (the relative angle of twist between neighbouring units for three-dimensions). In this way, it is possible to construct a *continuous random network* (CRN), containing the same structural units as the crystalline material, but with a random orientation preventing the introduction of significant medium- or long-range order.

From this, Zachariasen proposed a set of rules to be satisfied if an oxide is to be glass forming

1) no oxygen must be linked to more than two atoms of A.
2) the number of oxygen atoms surrounding A must be small (typically 3 or 4).
3) the oxygen polyhedra share only corners, not edges or faces.

A fourth rule was added to ensure the three-dimensional nature of the network

4) at least three corners in each oxygen polyhedron must be shared.

Again it should be noted that, although Zachariasen's ideas have generally been accepted, there are notable exceptions where the coordination number of oxygen may not equal two [2]; also, whereas the coordination numbers of silicon, phosphorus and boron in glass are 4, 4, and 3 or 4, respectively, the coordination number of tellurium in $PbO\text{-}TeO_2$ glasses is 6; and finally, Hagg [3] has pointed out that the presence of certain atomic structures negates the requirement that the network is three-dimensional.

Futher structural theories have been put forward by Smekal [4], who suggested the need for partly ionic-partly covalent bonding as a requirement for glass formation, and Sun [5] attempted to use the interatomic bond strength of an oxide to predict its glass-forming ability. Some modifications to these structural theories have been made by other workers but none of the suggested hypotheses are really capable of explaining the driving force and mechanism behind glass-formation.

2.1.4 Phase Separation in glasses

This phenomenon, occurring in many glass-forming systems, is one of great importance in the science of HLW isolation. The thermodynamic basis for phase separation is not of great relevance to this research and so is not discussed here. In essence, phase separation in a glass takes place when it is energetically favourable for the melt to separate into two viscous liquids, or phases. If a glass melt is cooled rapidly below its transition temperature and the viscosity of the phases is sufficiently high, we will be left with a solid that contains droplets of one liquid in a matrix of the other, depending on the relative concentrations of each phase. In the solid state, metastable immiscibility can occur giving two types of separation, termed either *nucleation and growth* or *spinodal* immiscibility. The resulting glass is now phase separated as a result of stable *liquid-liquid* immiscibility. The sodium borosilicate glass system, in particular, exhibits a region of spinodal phase separation at low alkali contents. This effect is used as a method of producing non-crystalline silica by the selective acid leaching of the phase separated sodium-borate phase in the sodium borosilicate system. The extent of phase separation in the modifier borosilicate system can possess such fine scale morphology that it is undetectable by the eye. However, it is this separation that can contribute to the degradation of the chemical resistance of glasses used to store radioactive waste. The composition of the final wasteform glass is therefore carefully chosen to prevent the possibility of any phase separation occurring, whilst maintaining suitable processing parameters and chemical and physical properties.

2.1.5 Multicomponent glass structural theories

It may seem a little strange to talk of the 'structure of glasses' when they are defined, primarily, as lacking a long-range, periodic structure. Fortunately, it is possible to reproduce glasses of given properties from the same nominal composition, which leads to the belief that, even though glass behaviour is determined by non-periodicity, structure still exists at a small enough level that can control properties. Whilst the models of Goldschmidt and Zachariasen attempted to elucidate the qualifying properties required for glass formation in simple oxides, rarely are modern technological glasses found to contain fewer than four components, making it even more difficult to assign specific structural arrangements

to a specific glass property. Most structural models used today only address the formation of a network and do not attempt to study the issues of bond length or bond angle rotation and distribution inherent to the random network model. In fact, the lack of a unified glass structure model is not helped by the manner in which many models seek only to support a trend observed in a property of a particular glass system, at the same time ignoring substantial amounts of data that conflict with the proposed model.

2.2 Structural studies of important glass systems

2.2.1 Single and mixed-alkali borate glasses

Vitreous boric oxide, B_2O_3, is the simplest borate glass and has been studied in detail by X-ray diffraction and nuclear magnetic resonance (NMR) techniques for over forty years. Boron can be trigonally- or tetrahedrally-coordinated in crystalline compounds, to three or four bonding oxygens respectively, giving $[BO_3]$ or $[BO_4]$ polyhedra.

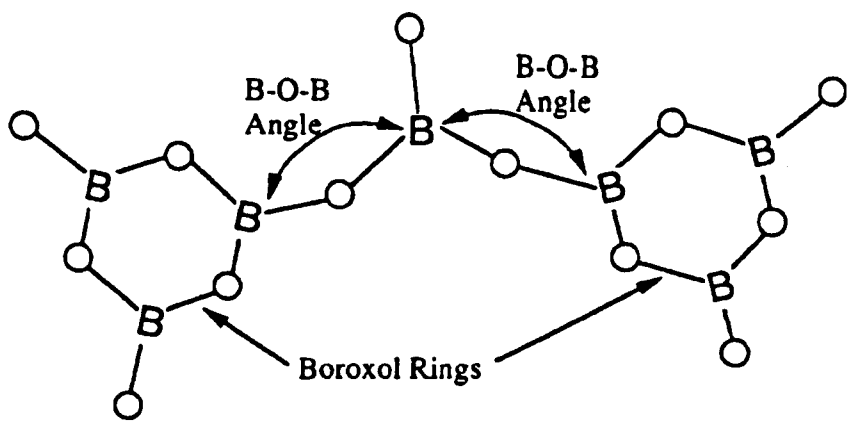

Fig. 2.04 The boroxol ring structure, B_3O_3, present in vitreous boric oxide and alkali borate glasses. [8]

Extensive studies of boric oxide [6,7] by Raman spectroscopy have indicated that, at an intermediate level, structural units known as boroxol rings are predominant. The boroxol group is a six-membered planar ring, as illustrated in Fig. 2.04.

The vast majority of boron atoms in vitreous boric oxide are three-coordinated to oxygen. A three-dimensional structure is obtained from these planar

structural units by folding or 'crumpling' of the network. However, the bonds between the structural units (Van der Waals in this case) are weak, making the structure easily disrupted and thus explaining the very low glass transition temperature of boric oxide, 260°C, compared to vitreous silica, 1100°C.

There is currently much discussion in the literature of the extent to which the structure of vitreous B_2O_3 is based around these boroxol rings. Support exists both for the boroxol ring model, where the fraction, f, of boron atoms in boroxol groups is ~0.8 [9], and the [BO_3] triangle model with f<0.1 [10]. Several workers have obtained well-resolved NMR spectra indicating two distinct sites, assignable to boron within boroxol rings and boron outside rings [11,12].

2.2.1.1 Nuclear Magnetic Resonance (NMR) studies

Despite the fact that borate glasses are of less technological importance than silicate glasses, much effort has been directed toward establishing a clearer understanding of the structural behaviour of the system. Even prior to the advent of more powerful analytical techniques, ^{11}B wideline NMR has been a particularly useful structural probe, with which Bray and co-workers [13-15] gained detailed insights into the structure of borate glasses. An understanding of the structure of these relatively simple glasses is essential for any meaningful examination of the more complex alkali borosilicate systems to be made. Whilst debate continues today on the extent to which glassy B_2O_3 is based on the six-membered boroxol ring [16], vast numbers of studies have focused on the effect of inclusion of alkali species in the borate network [1,13,14,17-19].

There are five borate units hypothesized to exist at various alkali borate compositions and these will be designated as follows: -

f_1 – a trigonal boron unit with all bridging oxygens
f_2 – a tetrahedral boron unit with all BOs and one alkali ion associated with it
f_3 – a trigonal boron unit with one NBO and one alkali ion associated with it
f_4 – a trigonal boron unit with two NBOs and two alkali ions associated with it
f_5 – a trigonal boron unit with three NBOs and three alkali ions associated with it

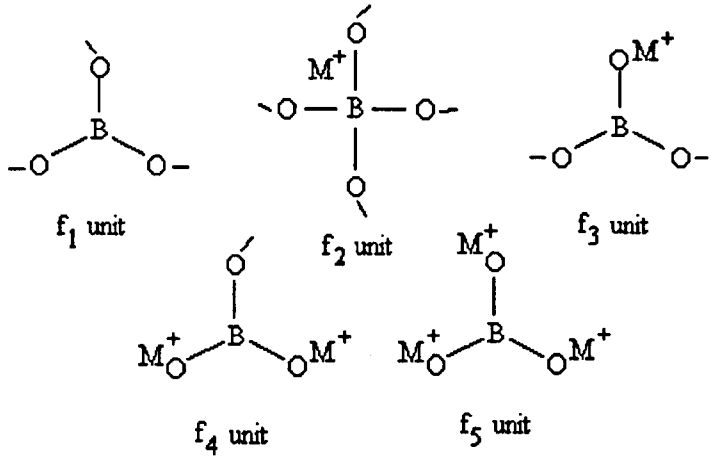

Figure 2.05 The five borate structural units deduced from NMR spectroscopy.

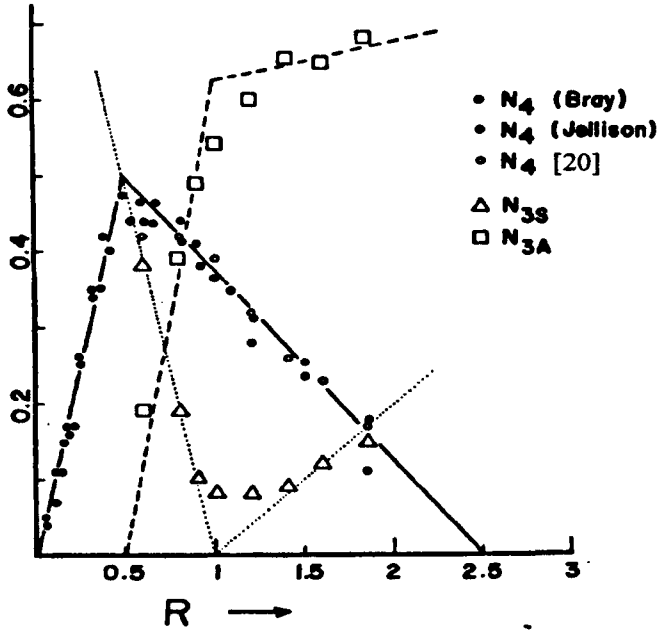

Fig. 2.06 The quantitative variation in N_4 with alkali content in the sodium borate system [20].

At low alkali concentrations each alkali unit, M_2O, is used to convert two f_1 boron units from three- to four-coordination, f_2. Hence, the fraction of tetrahedral boron units, $N_4 = f_2/\Sigma f$, increases with R = [mol% M_2O]/[mol% B_2O_3]. Fig. 2.06 illustrates how N_4 varies upon addition of alkali to a Li_2O-B_2O_3 glass as deduced from NMR spectroscopy [20]. It can be seen that a maximum is reached at R=0.5, whereafter N_4 decreases, eventually to zero, at a higher value of R. With the subsequent destruction of f_2 units, asymmetric f_3 and f_4 units with non-bridging oxygens are formed. Further studies have reported the influence of different cations and found that for a given value of R, N_4 decreases in the order Li->Na->K->Rb->Cs [21].

2.2.1.2 Glass transition temperature (T_g)

The technological significance of the glass transition temperature has led to attempts to integrate nuclear magnetic resonance measurements and T_g data into a model capable of describing the variation in T_g by the change in structural configuration as the composition of the glass changes. Qualitative connections have been made by Shelby [23] and Button [24] between the variation in T_g and concentration of tetrahedral borons at low *R* values. This is illustrated for the lithium borate system in Fig. 2.07.

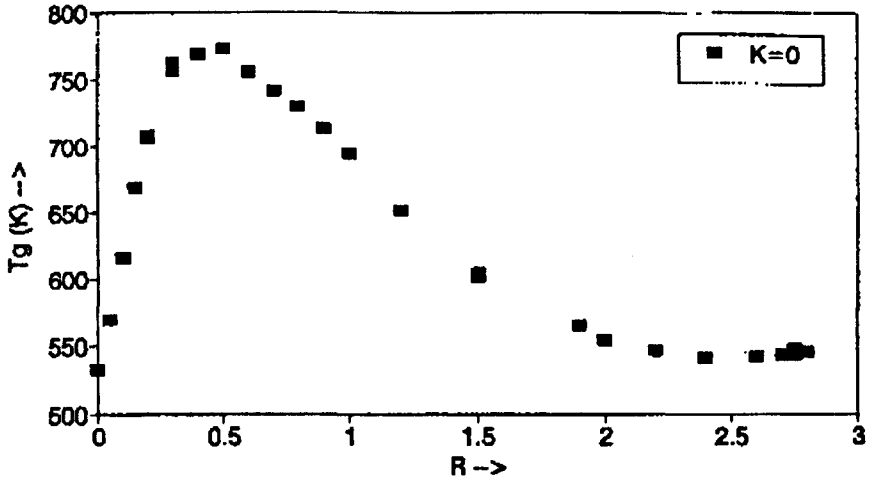

Fig. 2.07 The variation in glass transition temperature with alkali content in the lithium borate system [25].

As the trigonal f_1, f_3, f_4 and f_5 boron units are essentially planar, the growth of tetrahedral f_2 units increases the dimensionality of the network, leading to an increase in T_g. The subsequent destruction of f_2 units, and replacement by f_3 and f_4 units reduces the cross-linking of the network, leading to a decrease in T_g.

2.2.2 Single and mixed-alkali silicate glasses

The structure of vitreous silica, the simplest silicate glass, adheres rigidly to the rules of glass formation identified by Zachariasen. The basic building block is the silicon-oxygen tetrahedron with a coordination number of 4. Fig 2.08 shows a two-dimensional representation of the structure of vitreous silica, where the missing fourth oxygen would sit directly above each silicon atom.

The three dimensionality of the network is produced by linking of these tetrahedra at their corners. The existence of long-range order is prevented by

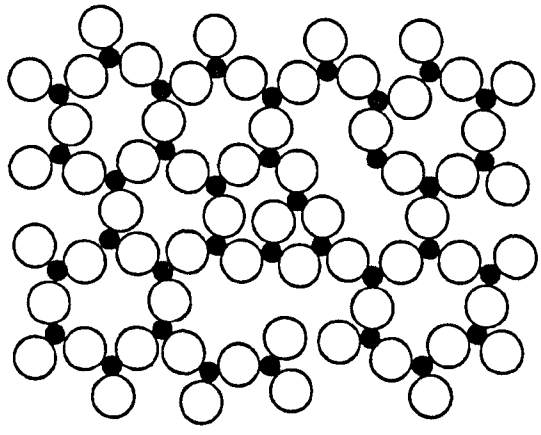

Fig. 2.08 A two-dimensional representation of the structure of vitreous silica, SiO_2, where • - silicon, o – oxygen [26].

variations in the Si-O-Si angle connecting adjacent tetrahedra and also by rotation around the oxygen atom linking adjacent tetrahedra. Though any long-range order in the network is destroyed by variation of the dihedral angles, evidence for the high degree of short-range order represented by the basic tetrahedral unit is given by the very small variations in the Si-O and O-O distances, ≈0.162nm and ≈0.265nm, respectively [26]. At the intermediate structural level, the distance between silicon atoms in the centres of linked tetrahedra, there is a wide distribution of values centred around ≈0.312nm as a result of the distribution in Si-O-Si dihedral bond angles. The exact distribution of Si-O-Si angles, clustered around ≈144°, but ranging from 120° to 180°, is subject to disagreement in the literature but this empirical description serves as the basis for a rudimentary understanding of vitreous silica structural details.

2.2.2.1 Nuclear Magnetic Resonance (NMR) studies

Alkali silicate systems were investigated initially in 1974 using wideline NMR [27], and subsequent studies have provided answers to questions surrounding 1) the Si-O-Si bond angle distribution, 2) the distribution of NBOs introduced by network modifiers, 3) the spatial distribution of alkali/alkaline earth metal cations and 4) the role and distribution of intermediate oxides. As a result, it is well understood that incorporation of alkali oxides into glassy silica leads to depolymerisation of the network, where one molecular unit of oxide leads to the breakage of one Si-O-Si bridge, resulting in two non-bridging oxygens. It is thought that this network disruption could lead to the formation of the five silicon

environments, Q^n units, observed in the crystalline silicates, where n represents the number of bridging oxygens attached to the silica tetrahedron, illustrated in Fig. 2.09(a). The number of NBOs per [SiO_4] unit depends on the amount of alkali oxide present, however, some controversy has arisen over the exact nature of the distribution, split between a binary distribution theory where the structure consists of a maximum of two Q^n species [28,29], and a more statistical distribution [30]. In the binary distribution, in the region $0 < R_2O < 33.3$mol%, Q^4 units convert to Q^3 units whilst in the region $33.3 < R_2O \leq 50$mol%, Q^3 units convert to Q^2 units. Upon further addition of alkali, $50 < R_2O \leq 60$mol%, Q^2 units convert to Q^1 units and between $60 < R_2O \leq 66.7$mol% Q^1 units convert to Q^0. For $R_2O \geq 66.7$mol%, all the silicate units are hypothesised to have all non-bridging oxygens.

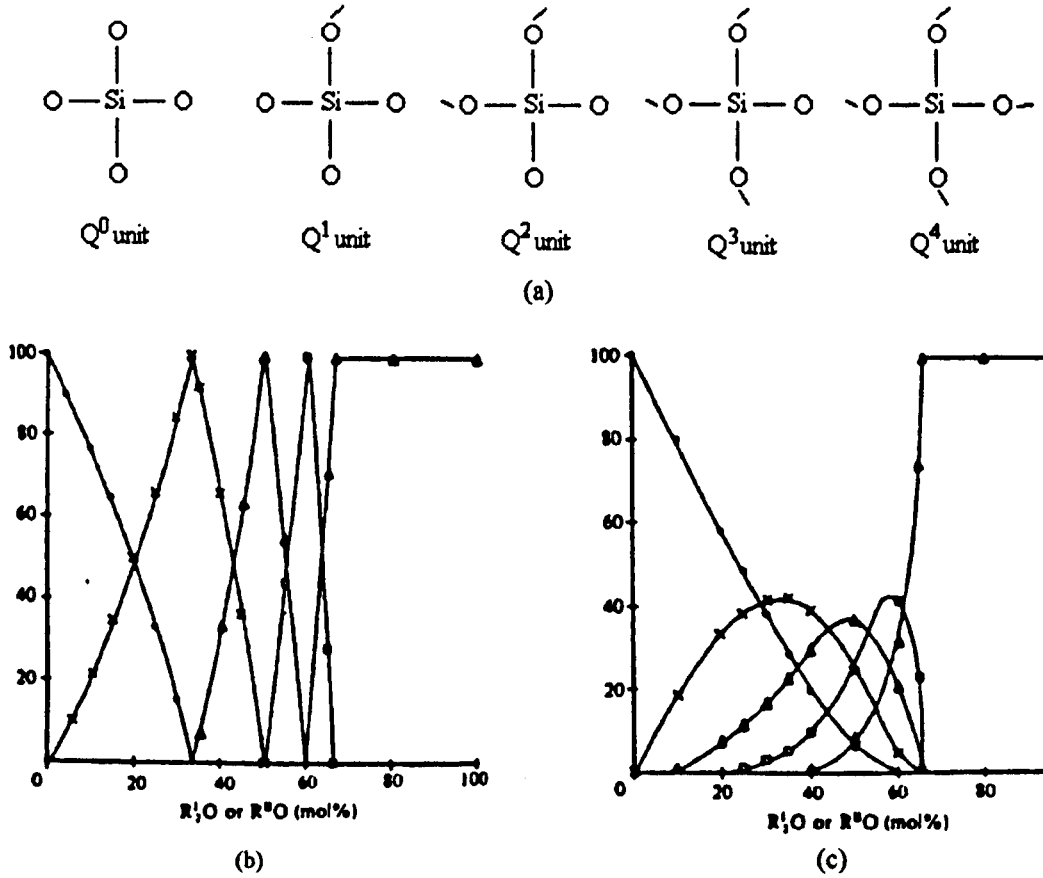

Fig. 2.09 (a) The five structural units hypothesized to exist in silicate glasses, deduced from NMR spectroscopy, alongside comparison of the two models of silicate unit distribution hypothesised to exist in alkali silicate glasses (b) constrained (binary), (c) unconstrained (statistical) (taken from [31]).

The statistical distribution is similar to that in the alkali borate system, where there is destruction and creation of progressive Q^n units as the modifier content is increased. Both ideas are illustrated in Fig. 2.09(b) and (c).

2.2.2.2 Glass transition temperature (T_g)

The addition of alkali oxide to silica leads to a large decrease in the melting and transition temperatures of the glass, a phenomenon that has the advantage of easier glass processing but the disadvantage of a final wasteform that is less resistant to large increases in ambient temperature. Fig. 2.10 shows the glass transition temperatures of samples from the lithium silicate system, investigated by Boekenhauer *et al.* [25], where J corresponds to the molar ratio of Li_2O to SiO_2 present in the glass.

As explained in the previous section, this decrease in T_g is brought about by the generation of non-bridging oxygens on the silica tetrahedra. The overall trend of decreasing T_g can be seen as J increases, until a constant value, within experimental errors, is reached at $J > 1.3$. Boekenhauer deduced from this that no change in T_g is brought about as the third of four non-bridging oxygens is added to the silica unit.

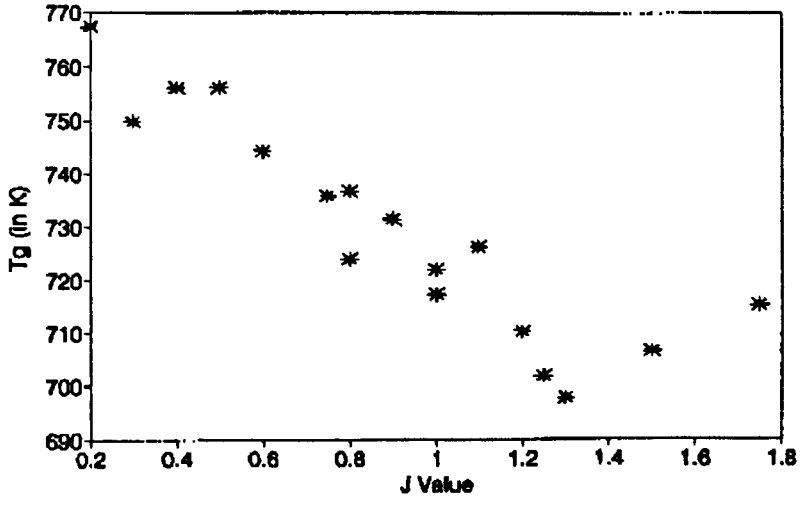

Fig. 2.10 The variation in glass transition temperature in the lithium silicate system (taken from [25]).

2.2.3 Single-alkali borosilicate glasses

The more complex alkali borosilicate glasses have been the subject of extensive studies due to their wide technological importance, not only in the field of HLW isolation. Though, as explained previously, the loaded wasteform may consist of >30 components, an understanding of the structural and physical properties of the base composition is necessary to facilitate the selection of an optimum storage matrix.

There are three main physical and structural properties that have been studied in considerable depth in the single-alkali borosilicate system: spectroscopic information obtained by NMR methods, density variations and also changes in T_g with composition. In the field of HLW isolation, the change in glass transition temperature with composition is a major factor that must be controlled to ensure the viability of the final wasteform. At the same time, much of the information linking structural arrangements to the changes in glass transition and density can only be determined by NMR methods, so all three properties have an important role to play in structure-property determination in glasses.

2.2.3.1 ^{11}B and ^{29}Si NMR models

^{11}B MAS NMR has been used extensively, as in the less complex alkali borate systems, to investigate the structural arrangements adopted by the 3- and 4-coordinated boron units as alkali is introduced into the system. The currently accepted structural model, based on the sodium-borosilicate system, was developed by Dell, Bray and Xiao [32] from earlier work by Yun and Bray [20,33]. They have postulated that the single alkali borosilicate system can be subdivided into regions delineated by certain alkali oxide/boron oxide ratios, *R*. These regions are explained in detail below:

Region 1: $R < 0.5$

Here, the ternary system behaves similarly to the binary borate system, where any added alkali is associated with the borate network only, with extra oxygens converting trigonal boron units to tetrahedral boron units. Within this region no interaction between the borate and silicate networks is expected to occur; a possible explanation as to why glasses in this composition region have a tendency to phase separate.

Region 2: $0.5 \leq R \leq R_{max}$

In this region, added alkali combines with the $[BO_3]$ and $[BO_4]$ units, in the form of diborate units, to form the reedmergnerite unit, a boron tetrahedron bonded to four silica tetrahedra. If we assume *m* moles of Na_2O are added to the $R=0.5$ composition, based on one mole of B_2O_3, the conversion process can be written as:

$$\tfrac{1}{2}(Na_2O{\cdot}2B_2O_3) + K(SiO_2) + m(Na_2O)$$

$$\longrightarrow$$

$$(\tfrac{1}{2}-m)(Na_2O{\cdot}2B_2O_3) + 2m(Na_2O{\cdot}B_2O_3{\cdot}8SiO_2) + (K-16m)SiO_2 \qquad (2.01)$$

where $R=m+0.5$ and the formulae represent the structural units present. It can be seen that the process will end when $K=16m$ or $R_{max}=\tfrac{1}{2}+K/16$.

Region 3: $R_{max} \leq R \leq R_{d1}$

According to the Dell model, additional alkali added to the glass is used to form non-bridging oxygens (NBOs) on the silica tetrahedra in the reedmergnerite units. This implies no change in the abundance of tetrahedral boron units, resulting in the same unit fractions over the whole region.

It is reported that the best fit of the experimental data occurs when each pair of reedmergnerite groups has absorbed 1.5 additional molecules of Na_2O. Hence, the end point of the process can be deduced from

$$R_{D1}(Na_2O){\cdot}B_2O_3{\cdot}K(SiO_2) = (\tfrac{1}{2}-K/16)(Na_2O{\cdot}2B_2O_3) + K/8(2.5Na_2O{\cdot}B_2O_3{\cdot}8SiO_2) \qquad (2.02)$$

Region 4: $R_{d1} \leq R \leq R_{d3}$

In this region it is assumed that the alkali oxide combines with the remaining diborate groups and reedmergnerite groups, dividing itself proportionately according to the numbers of B and Si atoms in each unit. If m_1 moles of Na_2O go to the diborate groups and m_2 moles of Na_2O go to the reedmergnerite groups, we can write

$$(\tfrac{1}{2}-K/16)(Na_2O{\cdot}2B_2O_3) + m_1(Na_2O)$$

$$\longrightarrow$$

$$(\tfrac{1}{2}-K/16-\tfrac{1}{3}m_1)(Na_2O{\cdot}2B_2O_3) + \tfrac{2}{3}m_1(2Na_2O{\cdot}B_2O_3) \qquad (2.03)$$

and

$$(K/8)^*(2.5Na_2O{\cdot}B_2O_3{\cdot}8SiO_2) + m_2(Na_2O)$$

$$\longrightarrow$$

$$(K/8-2m_2/15)(2.5Na_2O{\cdot}B_2O_3{\cdot}8SiO_2) + 2m_2/15[(2Na_2O{\cdot}B_2O_3) + 8(SiO_2 + Na_2O)] \qquad (2.04)$$

where $(m_1+m_2) = R-R_{D1}$ and $m_1/m_2 = (2-K/4)/(K+K/4)$

These processes end when the diborate units are fully converted, i.e. $(1/2 - K/16 - m_1/3) = 0$, and the reedmergnerite units are fully converted, when $(K/8 - 2m_2/15) = 0$. This occurs at $R_{D3} = (m_1+m_2) + R_{D1} = 2+K$, at which point $N_4 = 0$ and $N_3 = 1$. Within each of these regions, the fractions of the individual borate units can be found using the equations given in Table 2.01

Borate unit	Fraction of unit present at this composition
$0.5<R<R_{max}$	
f_1	R
f_2	$1-R$
f_3	0
f_4	0
$R_{max}<R<R_{d1}$	
f_1	R_{max}
f_2	$1-R_{max}$
f_3	0
f_4	0
$R_{d1}<R<R_{d2}$	
f_1	$(1 - K/8)\cdot(3/4 - R/(2 + K))$
f_2	$(8+K)\cdot((1/12) - R/(24 + 12K))$
f_3	$(1/3)\cdot(R - R_{D1})\cdot(2 - K/4)/(2 + K)$
f_4	$\frac{1}{2}(R - R_{D1})\cdot(2 - K/4)/(2 + K) + 2/3(KR/(8 + 4K) - K/16)$
$R_{d2}<R<R_{d3}$	
f_1	0
f_2	$(8+K)\cdot((1/12) - R/(24 + 12K))$
f_3	$(4/3 - K/6)\cdot(1 - R/(2 + K))$
f_4	$\frac{1}{2}(1 - K/8) + (R - R_{D2})\cdot(2 - K/4)/(2 + K) + 2/15(5KR/(8 + 4K) - 5K/16)$

Table 2.01 Equations used to calculate the fractions of each borate unit present at different compositions from the model of Dell et al.[32].

Combining the fractions of each unit over the whole composition range leads to the trends illustrated in Fig. 2.11, illustrating that at low modifier content, $[BO_3]$ units are steadily converted to $[BO_4]^-$ units. At R_{D1}, trigonal borate units with one and two NBOs, respectively, begin to form at the expense of both the f_1 and f_2 units still remaining. The f_4 unit is expected to become dominant at the further expense of

the f_3 units at very high modifier contents, until the network is sufficiently disrupted that glass formation becomes impossible.

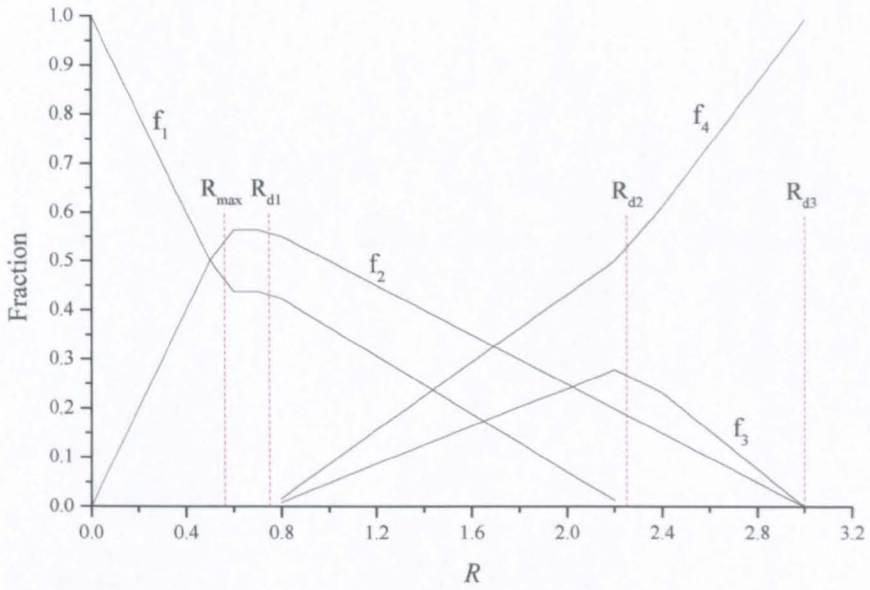

Fig. 2.11 The change in concentration of borosilicate units with alkali content from the model [32] for K=1.

Information regarding the arrangements of silicon atoms in the borosilicate system has been obtained by the use of ^{29}Si MAS NMR. As with the borate and silicate systems, the chemical environment around the silicon atom changes as the alkali oxide concentration increases. Fig. 2.12 illustrates how the chemical shift, an identifier of the structural arrangements present, becomes more positive as *R*, the ratio of alkali oxide to boron oxide, increases. This indicates that depolymerisation of the network is taking place via the creation of non-bridging oxygens on the silica tetrahedra. It can be noted from the figure that the rate at which the depolymerisation occurs is related to *K*, the ratio of silica to boron oxide. This can be explained by the fact that the higher silica concentration in the glass requires more alkali to be added for the modifications to be observed [34]. This also leads to the idea that some kind of sharing of the alkali between the borate and silicate networks occurs. One of the most debated points relates to the nature of this sharing and whether the alkali is preferentially associated with one network over the other.

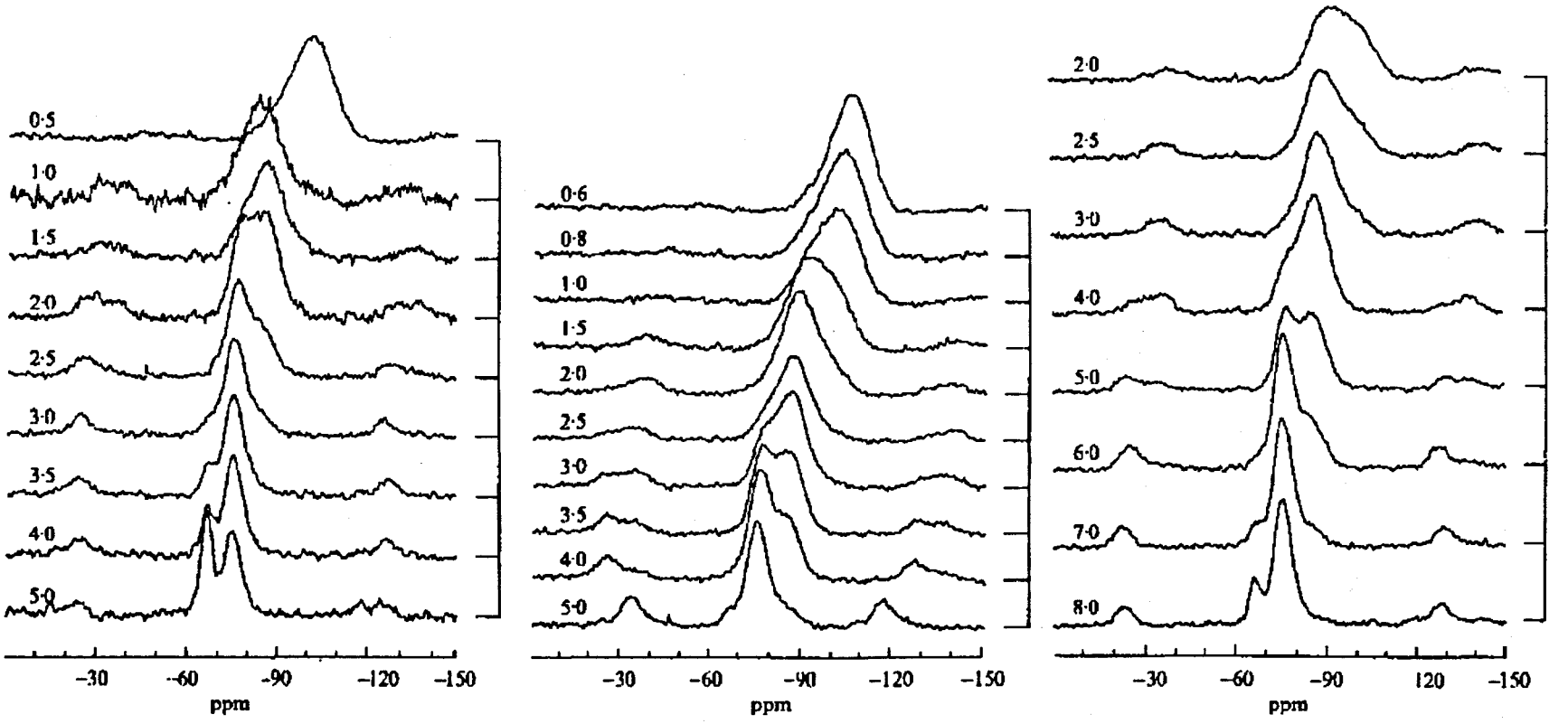

Fig. 2.12 The change in chemical shift of the silicate species in a sodium borosilicate glass with alkali content, R, and different values of K ($[SiO_2]/[B_2O_3]$) = (a) 2, (b) 4 and (c) 6 (taken from [34]).

Many workers have used the method of expressing the number of Q^n units in terms of the added oxygen to silicon ratio, O_A/Si, which allows comparison of the different structural models and also of results obtained for the alkali silicate systems. Three such models will be described; one based on the ^{29}Si NMR studies of Mackenzie [34] *et al.*, and two based on the ^{11}B NMR data of Wu *et al.* [35], Zhong *et al.* [36] and Dell [32].

In the Mackenzie model, proportional sharing of the alkali begins at R_C, below which the alkali oxide is thought to be completely associated with the borate network and the speciation of silicate units is expressed in terms of the added oxygen (associated with silicon) to silicon ratio, O_A/Si. Therefore, the amount of alkali associated with the silicate network, R_{Si}, can be written as

$$R_{Si} = O_A/Si = 0 \text{ for } 0 < R < R_C \tag{2.05}$$

$$R_{Si} = O_A/Si = (R-R_C)/(K+1) \text{ for } R_C < R < R_C+2(1+K) \tag{2.06}$$

The models of Wu and Zhong allow for other values of R_C at which sharing begins, although equations 2.05 and 2.06 above still apply. The values for R_C found by Zhong and Mackenzie are reported as

K	R_C	R_C	R_C
	Wu	Zhong *et al.*	Mackenzie *et al.*
2	0.4	0.312	0.184
4	0.4	0.408	0.227
6	0.4	0.426	0.361

Table 2.02 Comparison of the points at which proportional sharing of the alkali between the silicate and borate networks is hypothesised to begin.

From the model of Dell described earlier, the expressions for R_{Si} and O_A/Si are found to be

$$R_{Si} = O_A/Si = 0 \text{ for } 0 < R < R_{max} \tag{2.07}$$

$$R_{Si} = (R-R_O) \text{ for } R_C < R < R_{D1}$$

$$\therefore O_A/Si = (R-R_C)/K \text{ for } R_C < R < R_{D1} \tag{2.08}$$

$$R_{Si} = K[3/16 + (65/16)(R-R_{D1})/(8+4K)] \text{ for } R_{D1} < R < R_{D3}$$

$$\therefore O_A/Si = 3/16 + (65/16)(R-R_{D1})/(8+4K) \text{ for } R_{D1} < R < R_{D3} \quad (2.09)$$

Comparisons of the Q^n species present with the O_A/Si ratio for each model are shown below in Figs. 2.13(a-d) and analysis of the data has found that the best agreement between model and experiment is obtained for a simple proportional sharing of alkali between the networks at R_O=0. With reference to the model of Dell, it can be seen that this result disagrees with the results based on ^{11}B NMR, which assumes that sharing begins at much higher values of *R* which are also dependent on *K*. Part of the scope of the current work has been to investigate the details of the boron and silicon speciation in the mixed-alkali borosilicate system through the combined results of ^{11}B and ^{29}Si MAS NMR.

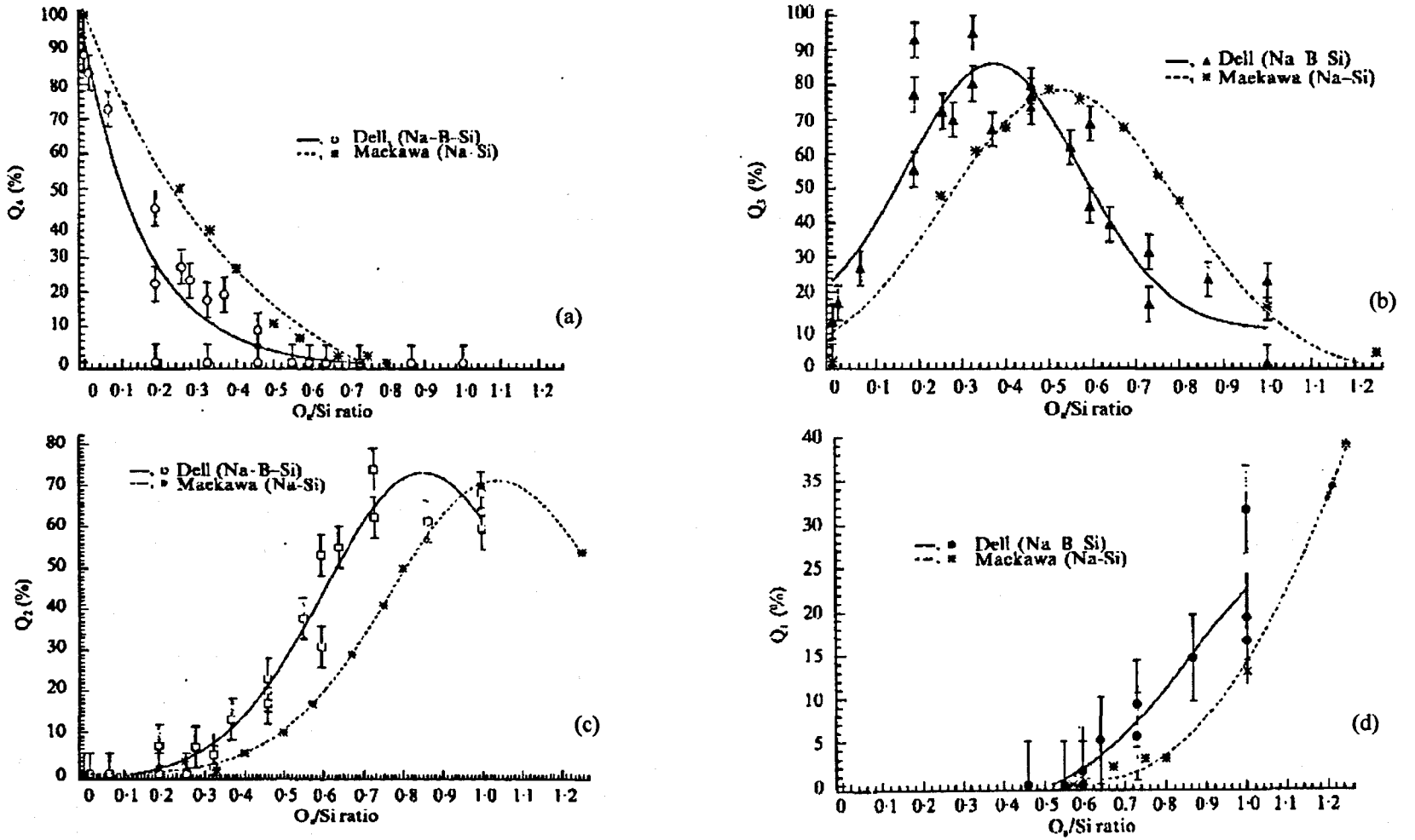

Fig. 2.13 The variation in the concentration of (a) Q^4 species, (b) Q^3 species, (c) Q^2 species and (d) Q^1 species with the added oxygen (associated with silicon) to silicon ratio for the data from Bhasin et al. [37] and the models of Dell [32] and Maekawa [38].

2.2.3.2 Glass transition temperature

It has been mentioned previously that the addition of alkali oxide to silica leads to a decrease in the T_g of alkali silicate glasses, whilst the opposite effect is seen in alkali borate glasses. Though an exact explanation of this phenomenon has not yet been developed, the consequences for the use of an alkali borosilicate glass waste disposal matrix are clear. Fig. 2.14 illustrates how the glass transition temperatures of a sodium borate, lithium borate and their corresponding borosilicate glasses vary with composition. Fig. 2.15 shows the change in T_g in the sodium borosilicate system as *K* increases, i.e. more silica is added.

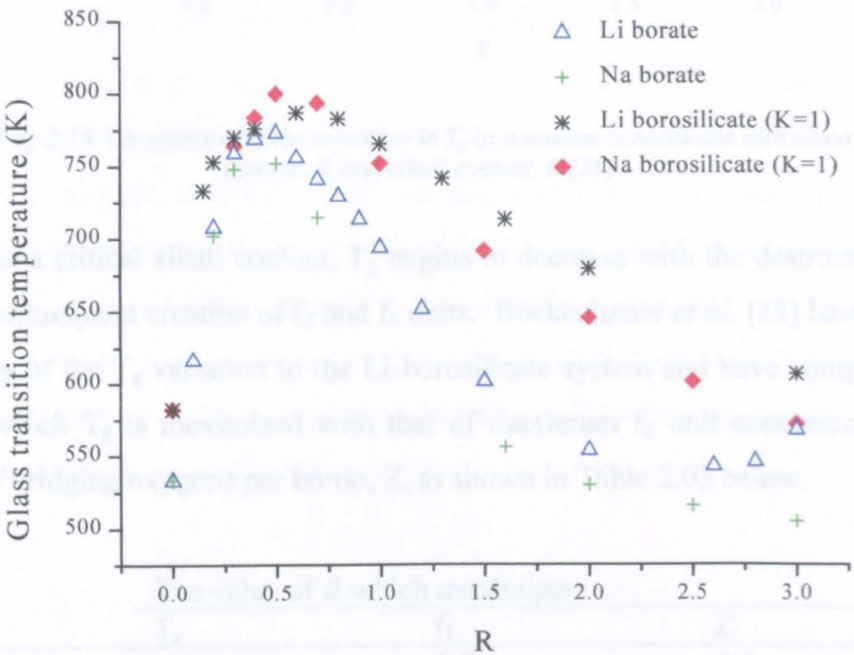

Fig. 2.14 Comparison of the variation in T_g of several alkali borate and borosilicate glasses with alkali content, R [39].

It can be seen that the initial addition of any type of alkali leads to a rapid increase in T_g, up to a certain value of *R*, at which point it begins to decrease to below the *K=0* value at very high *R*. This results from the conversion of trigonal f_1 units to tetrahedral f_2 units, increasing the connectivity of the network and consequently T_g, the temperature at which structural rearrangements may begin to take place. The maximum in T_g, however, does not correspond exactly to the maximum in f_2 [25], and, in addition, the maximum value of f_2 increases with *K* [39] whereas the maximum in T_g is the same for all K.

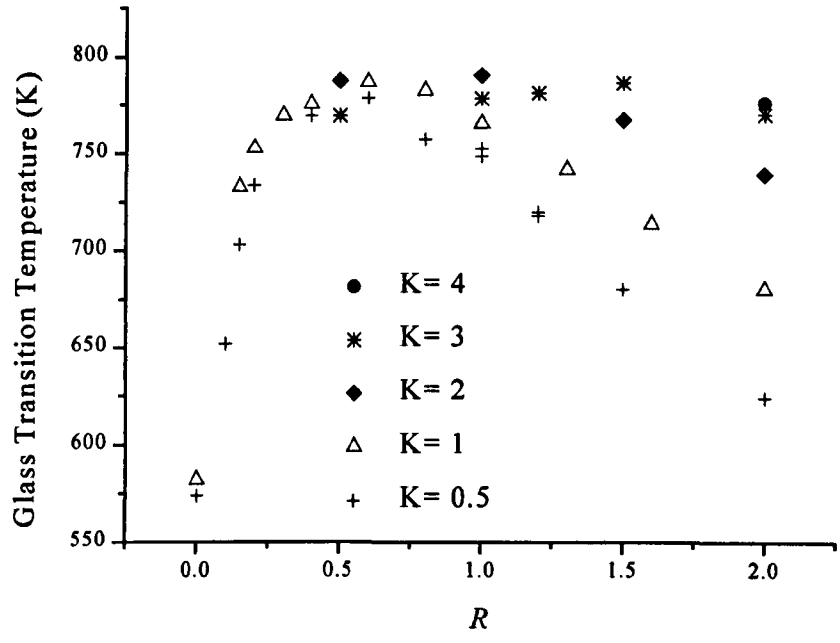

Fig. 2.15 Comparison of the variation in T_g in a sodium borosilicate with silica content, K and alkali content, R [39].

Past a critical alkali content, T_g begins to decrease with the destruction of f_2 units and subsequent creation of f_3 and f_4 units. Boekenhauer *et al.* [25] have carried out a study of the T_g variation in the Li-borosilicate system and have compared the value at which T_g is maximized with that of maximum f_2 unit concentration and number of bridging oxygens per boron, *Z*, as shown in Table 2.03 below.

K	The value of *R* which maximises:		
	T_g	f_2	Z
0.0	0.5	0.8	0.4
0.5	0.6	1.0	0.5
1.0	0.6	1.1	0.6
2.0	1.0	1.5	0.8
3.0	1.5	1.8	0.9

Table 2.03 Comparison of data for varying K indicating the values of R which maximise structural and physical properties.

This indicates that there is better agreement, at lower K values, between the values of *R* which maximise T_g and the number of bridging oxygens per boron, than the values of *R* which maximise T_g and the concentration of f_2 units. Hence, the idea that the f_2 unit plays a dominant role in determining some of the physical properties of the glass may not be applicable across all compositions. It can also be seen from the figures that the T_gs of the borates and borosilicates are approximately equal at

low alkali contents, indicating that the silicate network plays no part in the interactions occurring in the glass within this region, thereby supporting the theory of Dell outlined earlier [32]. The presence of the silicate network does, however, have an effect on the value of R that maximises T_g and also on the rate at which T_g decreases with R. The addition of alkali will eventually lead to the creation of NBOs on the silicate units which will tend to decrease the T_g of the glass.

2.3 Structural & physical property modelling

2.3.1 Glass transition temperature in modifier borates

The relationship between the fraction of f_2 boron units and the glass transition temperature has been included in a semi-empirical model developed by Affatigato *et al.* [40], making use of the structural unit information obtained by NMR studies to investigate the variation of T_g in lithium and lithium-sodium borates. In this model, it is hypothesized that the five structural units, described previously, that exist in alkali borate glasses are associated with their own 'characteristic' transition temperature. Hence, a general formula can be written to describe the sum of each characteristic transition temperature as

$$T_g = f_1 T_{g1} + f_2 T_{g2} + f_3 T_{g3} + f_4 T_{g4} + f_5 T_{g5} \qquad (2.10)$$

where f is the fraction of each of the five known borate units determined from NMR studies. A least squares analysis of equation 2.10 using the known NMR fractions and experimental data leads to values for each characteristic T_g as shown in Table 2.04.

Structural unit	Lithium borate (K)	Sodium-lithium borate (K)
f_1	570	567
f_2	1104	1002
f_3	417	348
f_4	460	429
f_5	582	483

Table 2.04 Characteristic transition temperatures of the five borate units determined from NMR models (taken from [40]).

Inferences regarding the role of the lithium and sodium ions in borates can also be made from this result. Firstly, the f_1, f_3, f_4 and f_5 units in the lithium borate system have similar characteristic T_gs, indicating that lithium does not have a significant effect on the structure of these trigonal units. Secondly, the addition of sodium ions lowers the characteristic transition temperature of the f_3, f_4 and f_5 units, demonstrating that the structural arrangements of the planar trigonal units are disturbed by the presence of the larger sodium ion. Affatigato has also commented on the presence of a mixed-alkali effect in the lithium-sodium borate system, where a series of Li-Na borate glasses possess lower T_gs than the corresponding single-modifier glasses.

Chryssikos [41] has incorporated the idea that network connectivity is a dominant feature in the variation of physical properties by considering the relationship between the number of bridging oxygens associated with a boron unit, Z, and T_g. Fig. 2.16 shows how the glass transition temperatures of a series of Li- and Na-borate glasses vary alongside Z, where Z has been determined from the Li-borate and Na-borate NMR fractions reported by Chong *et al.* [42].

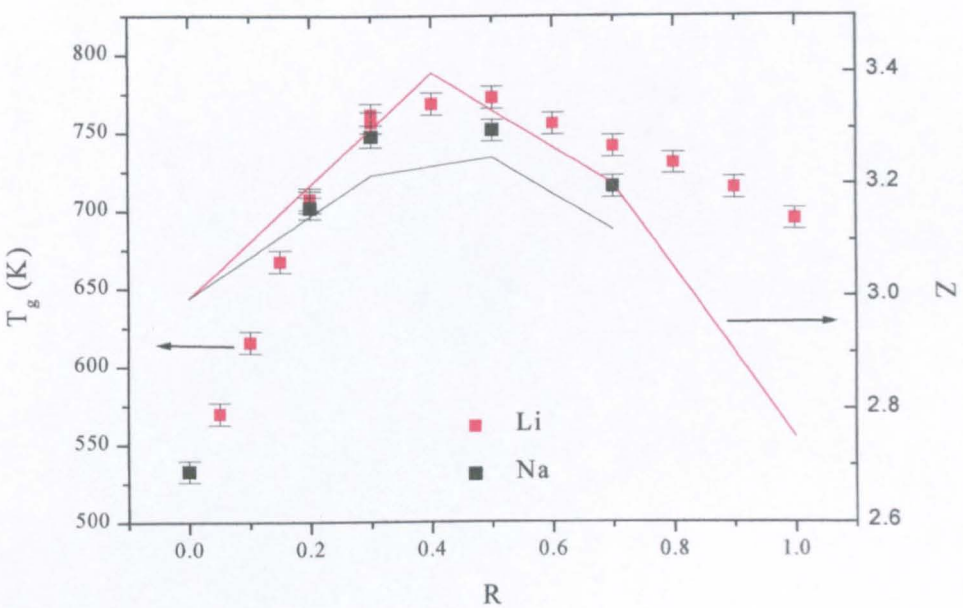

Fig. 2.16 Comparison between the variation of T_g and Z in single-modifier borate glasses (data taken from [39]).

2.3.2 Density modelling

2.3.2.1 Modifier borate glasses

Density modelling presents a suitable test of the reliability of NMR deduced structural theories and has been used extensively to elucidate some structural ideas that are occasionally insensitive to NMR techniques. Most recent studies have focused on relating the change in density as a function of R, the molar ratio of alkali oxide to boric oxide, to the arrangement of the five borate structural units mentioned earlier. Density variations in lithium- and sodium-borate glasses were measured by **Shibata** *et al.* [43] and Karki *et al.* [44] fifteen years ago, representing the initial **stages** of the use of then recently discovered NMR information to obtain physical property information. Figure 2.17 shows the density variation of a lithium-borate glass [43] as a function of R. As mentioned previously, it can be seen that the plot of density versus R has a similar shape to that of N_4 versus R, reiterating the idea that the presence of tetrahedral f_2 units strongly influences the physical properties of the glass.

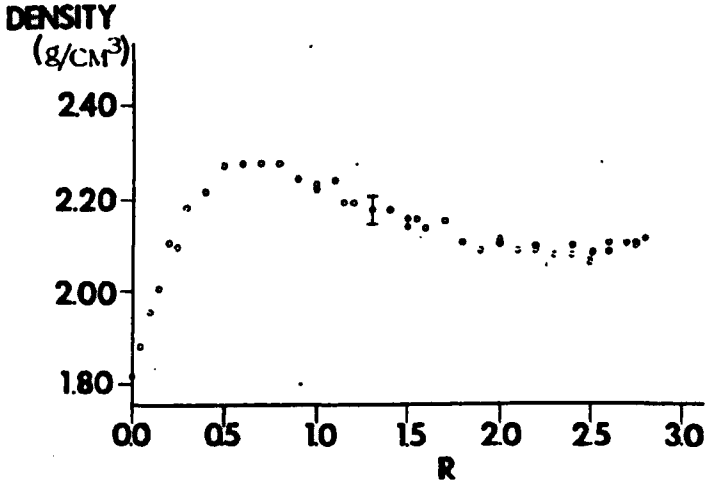

Fig. 2.17 Density variation with R in the Li-borate system (taken from [43]).

In studies of single- and mixed-alkali borates, the following semi-empirical equation has been used to express the change in density of the glass with composition

$$\rho = \rho_0 \frac{\sum f_i M_i}{\sum f_i V_i} \qquad (2.11)$$

where f_i, M_i and V_i correspond to the fractions, masses and associated volumes of the borate structural units and ρ_0 is the density of pure B_2O_3. In all calculations involving density, the mass and volume of each unit are relative to that of the trigonal $[BO_3]$ unit, i.e. the mass of the $[BO_4]^-M^+$ unit is given by [B+2O+M]/[B+1.5O]. Chong *et al.* [42] have reported results from Bray that the structural arrangement of the borate units is affected by the presence of more than one alkali, as illustrated in Table 2.05.

Li-Na borate system

	$0.0 \leq R \leq 0.28$	$0.28 \leq R \leq 0.61$	$0.61 \leq R \leq 1.0$
f_1	$1-R$	$1-R$	$1-R$
f_2	$0.853\,R$	$0.342\,R+0.197$	$-0.439\,R+0.5625$
f_3	$0.147\,R$	$0.658\,R-0.197$	$1.439\,R-0.625$
f_4	0	0	0
f_5	0	0	0

Li borate system

	$0.0 \leq R \leq 0.4$	$0.4 \leq R \leq 0.7$	$0.7 \leq R \leq 1.0$
f_1	$1-R$	$1-R$	$1-R$
f_2	R	$0.167\,R+0.333$	$-0.25\,R+0.5625$
f_3	0	$0.833\,R-0.333$	$1.25\,R-0.625$
f_4	0	0	0
f_5	0	0	0

Na borate system

	$0.0 \leq R \leq 0.335$	$0.25 \leq R \leq 0.75$	$0.75 \leq R \leq 1.0$
f_1	$1-R$	$1-R$	$1-R$
f_2	$0.862\,R$	$0.173\,R+0.288$	$-0.362\,R+0.664$
f_3	$0.138\,R$	$0.827\,R-0.288$	$1.362\,R-0.664$
f_4	0	0	0
f_5	0	0	0

Table 2.05 Illustration of the modifier dependence on the NMR fractions in single- and mixed-modifier borate glasses (taken from [42]).

The results of a least-squares analysis of equation 2.11 performed by Chong [42], using the structural unit information provided in Table 2.05, generate best fit values for each V_i, highlighting the differences in borate unit volume upon the inclusion of more than one alkali species, as shown in Table 2.06. This information is of importance to the current work as we have investigated the structure and properties of a multi-alkali species borosilicate glass.

Unit	Relative volume of unit compared with trigonal boron unit with 3 bridging oxygens (at R = 0)				
	Li-Rb	Li-Na	Rb	Na	Li
(a) using fractions independent of alkali type					
f_1	0.98	0.98	0.99	0.96	0.98
f_2	1.42	1.03	1.89	1.19	0.91
f_3	1.86	1.49	2.30	1.65	1.32
f_4	2.53	1.87	a)	2.15	1.69
f_5	3,28	2.35	a)	2.80	1.95
(b) using fractions dependent on alkali type					
f_1	0.98	0.97	0.98	0.95	0.98
f_2	1.24	1.02	1.76	1.17	0.91
f_3	1.81	1.38	2.29	1.62	1.32
f_4	a)	a)	a)	a)	a)
f_5	a)	a)	a)	a)	a)

Table 2.06 Volumes of the five borate units deduced from least squares analysis of the corresponding alkali borate system density data. a) no data available

2.3.2.2 Single-modifier borosilicate glasses

The model used by Karki *et al.* [44] and Chong *et al.* [42] to determine the density trend in the sodium borate system was expanded by Feil and Feller [45], and later by Budwhani and Feller [46], in an attempt to model the sodium, lithium and potassium borosilicate systems. Instead of considering only the total mass and volume of the borate units in the glass, they also incorporated several terms to account for the extra mass and volume introduced by the presence of the silicate units. The extra terms include the change in mass and volume of the tetrahedral unit as non-bridging oxygens are introduced by the addition of Na_2O molecules. The modified equations used to model the density are shown below

$$\rho = \frac{\sum f_1 M_1 + (K/2)^* M_{Si}}{\sum f_1 V_1 + (K/2)^* (V_6 + (N(K,R)^* dV_{6a}))} \qquad N(K,R) \le 1 \qquad (2.12)$$

$$\rho = \frac{\sum f_1 M_1 + (K/2)^* M_{Si}}{\sum f_1 V_1 + (K/2)^* (V_6 + dV_{6a} + (N(K,R)-1)^* dV_{6b})} \qquad 1 \le N(K,R) \le 2 \qquad (2.13)$$

where V_6 is the associated volume of an $[SiO_4]$ tetrahedron, dV_{6a} is the differential volume represented by the addition of a single alkali ion resulting in the

conversion of a bridging oxygen to a non-bridging oxygen, such as $Q^4 \rightarrow Q^3$, and dV_{6b} represents the differential change in volume of a silica unit as a second alkali ion is added and a Q^3 unit is converted to a Q^2 unit. The term N(K,R) represents the number of (M^{+1} + ½O^{-1}) added to the silica system per silica unit, and is defined within the regions outlined earlier in the Dell NMR model as follows

$$N(K,R) = 0 \qquad R < R_{max} \tag{2.14}$$

$$N(K,R) = 2\frac{(R - R_{max})}{K} \qquad R_{max} < R < R_{D1} \tag{2.15}$$

$$N(K,R) = \frac{9 + 52S}{24} \qquad R_{D1} < R < R_{D3} \tag{2.16}$$

The masses of the five borate units, M_i, remain unchanged from the simple borate system and the best fit volumes of the borate units, V_i, were found by a least squares analysis of Eq. 2.11 (borates only) using the experimental alkali borate density data. The value of the volume of each unit for each alkali is shown in Table 2.07 below.

Alkali	*Borates*			*Silicates*			
	V_1	V_2	V_3	V_4	V_6	dV_{6a}	dV_{6b}
Li	0.98	0.93	1.27	1.61	1.43	0.24	0.35
Na	0.95	1.25	1.62	2.12	1.43	0.47	0.59
K	0.95	1.67	2.07	2.94	1.43	0.82	1.01

Table 2.07 Variation in the volume of several borate units and the [SiO_4] tetrahedron in borate and silicate glasses with different modifier species.

The mass of the silicate part of the glass will change as alkali is added to the system, hence, we can represent this variation using the following terms

$$M_{Si} = \left[\frac{SiO_2}{BO_{1.5}}\right] \qquad R < R_{max} \tag{2.17}$$

$$M_{Si} = \frac{[SiO_2] + \frac{(R - R_{max})([M_2O])}{K}}{[BO_{1.5}]} \qquad R_{max} < R < R_{dl} \tag{2.18}$$

$$M_{Si} = \frac{[Si] + \left(\frac{13}{12}S + \frac{35}{16}\right)([O]) + \left(\frac{26}{12}S + \frac{3}{8}\right)([M])}{[BO_{1.5}]} \qquad R < R_{d3} \qquad (2.19)$$

where $S = (R\text{-}R_{d1})/(2+K)$, [X] is the atomic or molecular mass of X and the addition of alkali is assumed to cause simple lever rule changes to the nature of the silicate unit ($Q^4 \rightarrow Q^3 \rightarrow Q^2$). The corresponding volume of the silicate unit is defined over all regions of interest as shown in Eqs. 2.17-2.19. Throughout all sections of the model, the masses and volumes of the structural units have been referenced to those of the $BO_{1.5}$ unit, thus the factor (K/2) has been introduced into Eqs. 2.12 and 2.13 to account for the fact that K is referenced to the B_2O_3 unit. The model has been designed to end when $R = 2+K$ or $N(K,R) = 2$, depending on whichever comes first. The results of the model in the three alkali systems are shown in the Figs. 2.19(a)-(c).

It can be seen that the accuracy with which the model is capable of predicting the change in density with composition decreases as K increases. Since the volumes of the borate units used in the model were derived from the borate system density data, Feil and Feller [45] explain that the fit of the model improves as the glass composition moves towards the binary system. The model does, however, provide a very good empirical correlation between the structural units, their arrangements in the glass, and observed experimental density changes. They suggest that the consistent underestimation is the result of some kind of 'compaction' of the structural units, most notably f_2, the tetrahedral borate unit.

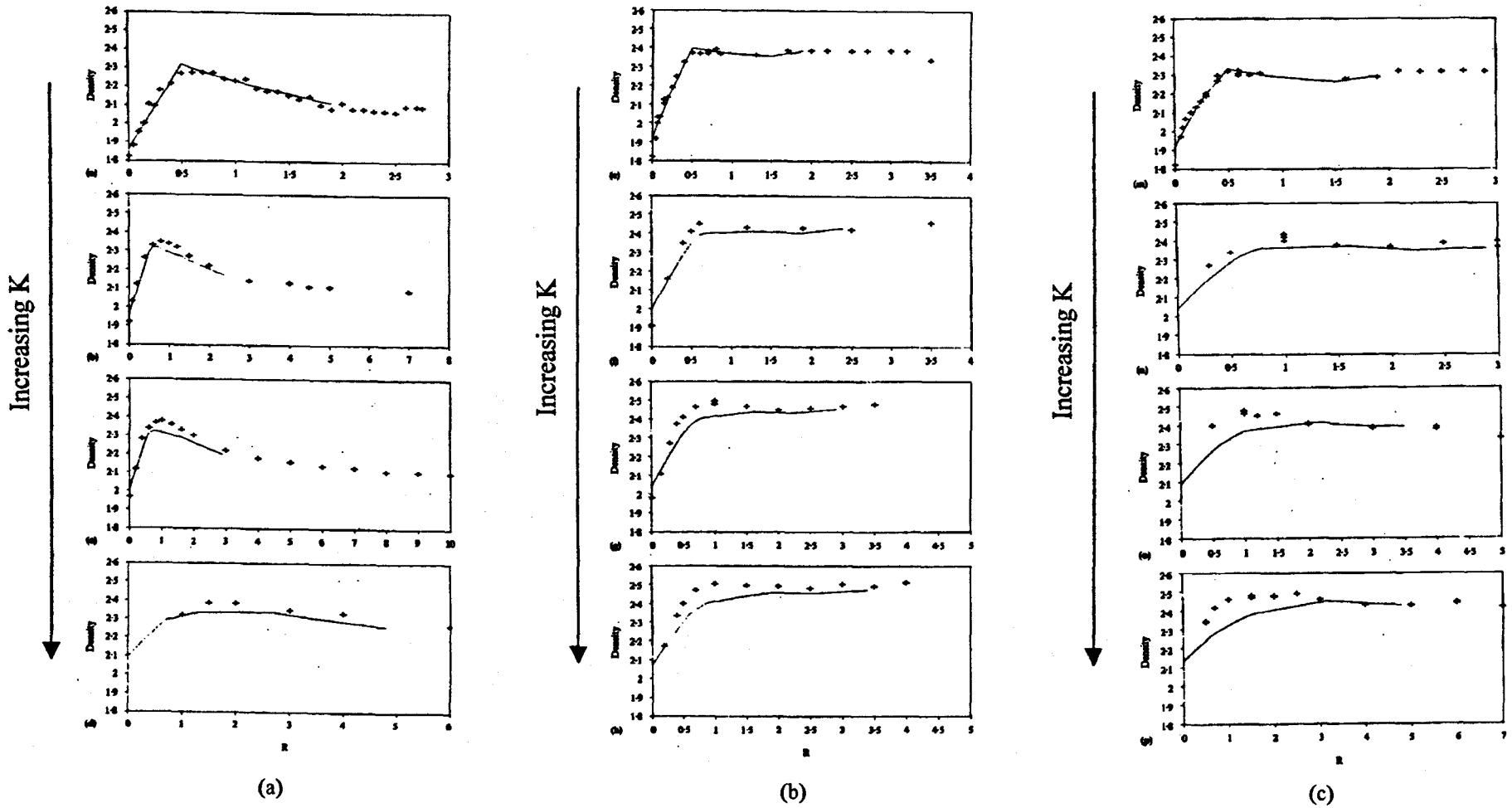

Fig. 2.18 Comparison of the density data for the lithium (a), sodium (b) and potassium (c) borosilicate systems, overlaid with the results of the model proposed by Budwhani and Feller [46].

2.4 References

[1] A. Paul, Chemistry of Glasses, Chapman & Hall, London (1990) p.1
[2] J. F. Baugher & P. J. Bray, Phys. Chem. Glasses **10** (1969) p.77
[3] G. Hagg, J. Chem. Phys. **3** (1935) p.42
[4] A. Smekal, J. Soc. Glass Technol. **35** (1951) p.411
[5] K. H. Sun, J. Am. Ceram. Soc. **30** (1947), p.277
[6] J. Goubeau & J. Krogh-Moe, K. Norke Vidensk. Selsk. Forh **27** (1954), p.18
[7] J. Krogh-Moe, Acta Chem. Scand. **7** (1958) p.611
[8] J. E. Shelby, Introduction to Glass Science and Technology, Royal Society of Chemistry Paperbacks, (1997) p.91
[9] A. C. Hannon, D. I. Grimley, R. A. Hulme, A. C. Wright & R. N. Sinclair, J. Non-Cryst. Solids **177** (1994) p.299
[10] J. Swenson & L. Börjesson, *Proc. Second Int. Conf. On Borates, Glasses, Crystals and Melts*, Society of Glass Technology (1997) p.425
[11] S. Gravina & P. J. Bray, J. Magn. Reson. **89** (1990) p.515
[12] R. E. Youngman & J. W. Zwanziger, J. Non-Cryst. Solids **168** (1994) p.293
[13] P. J. Bray & A. H. Silver, Modern Aspects of the Vitreous State, edited by J. D. MacKenzie, Butterworth, London (1960) p.92
[14] W. Müller-Warmuth, Glastech. Ber. **38** (1965) p.121
[15] G. E. Jellison & P. J. Bray, Borate Glasses, Structure, Properties, Applications, edited by D. L. Pye, V. D. Frechette & N. J. Kreidl (1978) p.353
[16] C. G. Joo, U. Werner-Zwanziger & J. W. Zwanziger, Phys. Chem. Glasses **41** (5) (2000) p.317
[17] P. J. Bray & G. O'Keefe, Phys. Chem. Glasses **4** (1963) p.37
[18] H. M. Kriz, M. J. Park & P. J. Bray, Phys. Chem. Glasses **12** (1971) p.45
[19] C. Rhee & P. J. Bray, Phys. Chem. Glasses **12** (1971) p.65
[20] Y. H. Yun & P. J. Bray, J. Non-Cryst. Solids **44** (1981) p.227
[21] J. Zhong & P. J. Bray, J. Non-Cryst. Solids **111** (1989) p.67
[22] H. Eckert, Progress in NMR Spectroscopy **24** (1992) p.219
[23] J. E. Shelby, J. Am. Ceram. Soc. **66** (1982) p.225
[24] J. Button, J. Non-Cryst. Solids **49** (1982) p.129
[25] R. Boekenhauer, H. Zhang, S. Feller, D. Bain, S. Kambeyanda, K. Budhwani, P. Pandikuthira, F. Alamgir, A. Michael Peters, S. Messer and Kong L. Loh, J. Non-Cryst. Solids **175** (1994) p.141
[26] J. E. Shelby, Introduction to Glass Science and Technology, Royal Society of Chemistry Paperbacks, (1997) p.79
[27] B. D. Mosel, W. Müller-Warmuth and H. Dutz, Phys. Chem. Glasses **15** (1974) p.154
[28] R. Dupree, D. Holland and D. S. Williams, J. Non-Cryst. Solids **68** (1984) p.399
[29] A. R. Grimmer, M. Mägi, M. Hähnert, H. Stade, A. Samoson, W. Wieker and E. Lippmaa, Phys. Chem. Glasses **25** (1984) p.105
[30] C. M. Schramm, B. H. W. S. de Jong and V. E. Parziale, J. Am. Ceram. Soc **106** (1984) p.4396
[31] R. Dupree, N. Ford & D. Holland, Phys. Chem. Glasses **28** (1987) p.78
[32] W. J. Dell, P. J. Bray & S. Z. Xiao, J. Non-Cryst. Solids **58** (1983) p.1
[33] Y. H. Yun and P. J. Bray, J. Non-Cryst. Solids **27** (1978) p.363

[34] J. W. MacKenzie, A. Bhatnagar, D. Bain, S. Bhowmik, C. Parameswar, K Budhwani, S. A. Feller, M. L. Royle & S. W. Martin, J. Non-Cryst. Solids **177** (1994) p.269

[35] X. W. Wu, F. Tian, X. Q. Zhang, L. Z. Pan & S. L. Wu, Collected Papers XIV Intl. Congress on Glass **1** (1986) p.32

[36] J. Zhong, X. Wu, M. L. Liu and P. J. Bray, J. Non-Cryst. Solids **107** (1988) p.81

[37] G. Bhasin, A. Bhatnagar, S. Bhowmik, C. Stehle, M. Affatigato, S. Feller, J. Mackenzie & S W Martin, Phys. Chem. Glasses **39** (5) (1998) p.269

[38] H. Maekawa, T. Maekawa, K. Kawamura & T. Yokohawa, J. Non-Cryst. Solids **127** (1991) p.53

[39] S. A. Feller, J. Kottke, J. Welter, S. Nijhawan, R. Boekenhauer, H. Zhang, D. Feil, C. Parameswar, K. Budhwani, M. Affatigato, A. Bhatnagar, G. Bhasin, S. Bhowmik, J. Mackenzie, M. Royle, S. Kambeyanda, P. Pandikuthira and M. Sharma, *Proc. 2nd Int. Conf. On Borate Glasses, Crystals and Melts*, (1997) p.249

[40] M. A. Affatigato, S. Feller, E. J. Khaw, D. Feil, B. Teoh and O. Mathews, Phys. Chem. Glasses **31** (1) (1990) p.19

[41] E. I. Kamitsos, G. D. Chryssikos, A. M. Karakassides, Phys. Chem. Glasses **29** (3) (1988) p.121

[42] B. C. L. Chong, S. H. Choo, S. Feller, B. Teoh, O. Mathews, E .J. Khaw, D. Feil, K. H. Chong, M. Affatigato, D. Bain, K. Hazen and K. Farooqui, J. Non-Cryst. Solids **109** (1989) p.105

[43] M. Shibata, C. Sanchez, H. Patel, S. Feller, J. Stark, G. Sumcad and J. Kasper, J. Non-Cryst. Solids **85** (1986) p.29

[44] A. Karki, S. Feller, H. P. Lim, J. Stark, C. Sanchez and M. Shibata, J. Non-Cryst. Solids **92** (1987) p.11

[45] D. Feil and S. Feller, J. Non-Cryst. Solids **119** (1990) pp.103-11

[46] K. Budhwani & S. Feller, Phys. Chem. Glasses **36** (4) (1995) p.183

Chapter 3 – Waste Disposal Science and Procedure

3.1 Introduction to High-Level Waste (HLW) management

3.1.1 Introduction

The disposal of high-level radioactive waste (HLW) from nuclear weapons production, naval propulsion programs and the reprocessing of commercial spent fuels in technologically advanced countries is a growing global issue. Both in Europe and, in particular, the United States, the legacy of 50 years of research, power generation and weapons testing is a vast quantity of liquid and solid HLW stored in underground tanks at several government sites, awaiting a more permanent storage solution. The complex nature of the waste composition, as illustrated in the table below, must be accommodated in the development of a storage material that is capable of withstanding the physical and radiological changes that are expected to occur over the lifetime of the wasteform.

Component	Wt% in glass	Component	Wt% in glass
SiO_2	46.1	SrO	0.3
TiO_2	0.01	NiO	0.37
Al_2O_3	6.58	B_2O_3	15.9
Fe_2O_3	3.0	Li_2O	4.07
CaO	0.01	RuO_2	0.7
MgO	5.74	MoO_3	1.62
K_2O	0.01	Cs_2O	1.11
Na_2O	8.29	Nd_2O_3	1.44
P_2O_5	0.26	Sm_2O_3	0.22
Cr_2O_3	0.58	CeO_2	0.84
ZrO_2	1.45	La_2O_3	0.48
HfO_2	0.02	Pr_6O_{11}	0.44
BaO	0.5	Y_2O_3	0.1

Table 3.01 A typical fully loaded high-level waste glass composition.

The wasteform structural changes produced by the extremely high levels of radioactivity, generated by the actinide elements and fission products in the waste, have led to much research taking place into simulation of the expected low-dose, long-term damage mechanisms with high-dose, short-term analogues [1-4]. The extent to which these effects can be simulated with accuracy has been questioned but

no alternative method of assessing the performance of the storage material is available at present [5].

3.1.2 HLW storage matrices

A range of candidate storage materials have been investigated over the last 30 years, including glasses, glass ceramics, ceramics and cements, each possessing individual properties that may be tailored by precise composition control. Table 3.02 gives details of the compositions of some of the materials that have been considered as potential HLW storage solutions, along with information on more important physical and chemical properties.

	SG7 (a)	SON68 (a)	RUS4 (a)	UK209 (a)	Titanate (b)	Synroc-D (b)
Li_2O		2.4		5.4		
Na_2O	7.4	11.9	44.0	11.2		
K_2O						
MgO	1.0					
CaO	2.7	4.9	5.0		11.7	10.3
Fe_2O_3			5.0			
TiO_2					59.1	31.8
ZrO_2					27.3	8.5
ZnO		3.0				
B_2O_3	8.3	16.9	14.8	14.8		
Al_2O_3	8.6	5.9	10.0		1.9	33.6
SiO_2	72.0	54.9		68.6		15.8
P_2O_5			29.0			
Others			$7.0SO_3$			
Waste Loading (wt%)	15				≤ 12	69
T_g (K)			702			
Young's Modulus (Gpa)	73	84		90		158
Thermal Expansion (MK^{-1})	6.8	8.3	18.0	8.4	8.8	10.5
Thermal Conductivity ($W\,m^{-1}\,K^{-1}$)	1.30	1.09		1.29	5.8	2.6

Table 3.02 A selection of HLW storage solutions based on glass, ceramic, glass-ceramic and synthetic matrices [6], (a) – vitreous, (b)- crystalline.

There are several key requirements that a storage matrix must fulfil in order for it to be considered as a permanent vitrification solution [5]. Firstly, the material must be capable of retaining its physical and chemical durability over extremely long times, of the order of 10^6-10^7 years. Secondly, the material must be thermally stable

above and beyond the considerable ambient temperatures (~500°C) that may be generated by the decay of certain waste components. Thirdly, the processing of the material must be physically and economically viable, i.e. too high a processing temperature may result in unstable components being volatilised before they are isolated within the material. Finally, anticipated changes in nuclear power generation technology may generate wastes with different elemental compositions and much higher concentrations of radioactive isotopes, requiring the storage material to accommodate the physical effects of higher doses of radioactivity and unexpected waste compositions. With these criteria in mind, it is possible to identify suitable candidates for the final vitrification solution.

Although silica forms the basis of most commercially produced glasses and has properties that are well characterised and understood, it requires too high a processing temperature (~1500°C) for it to be considered as a candidate for use in HLW vitrification. In practice, boric oxide (B_2O_3) can be added to silica to significantly reduce the temperature required for glass formation. Borosilicate glass systems have become the popular choice as final storage solutions because they fulfil the requirements outlined above. Their amorphous structure and strong interatomic bonding allow a wide range of waste compositions to be accommodated in the glass matrix; they have been shown to be more chemically durable than other systems and can be processed relatively easily and at temperatures significantly lower than, for instance, silicate glasses.

Interest has also been shown in alternative, non-silicate based glass systems. For example, phosphate glasses have been identified as candidates because of their lower processing temperatures and high sulphate and metal oxide solubilities, whereas the chemical durability of silicates, in particular, is compromised by the presence of sulphate-containing wastes due to phase separation [6]. However, subsequent poor chemical durability and the high corrosiveness of the melt has resulted in the abandonment of most phosphates as a serious storage solution in all but a few laboratories in Europe and the USSR. More recent work has centred on the addition of Fe_2O_3, Al_2O_3 and ZnO to the phosphate composition, resulting in improved thermal stability and chemical durability. Favourable comparisons have been made with borosilicates with regard to actinide oxide storage potential but further work is required before definitive conclusions can be drawn.

The superior physical properties of silica have also been combined with Al_2O_3 to produce aluminosilicate glasses exhibiting improved durabilities with regard to borosilicates. Studies by Vance [7] have reported that substantial amounts of UO_2 could be retained by the glass upon carefully controlled cooling of the melt.

The process of sintering materials which would otherwise present persistent melt processing temperature problems is a possible alternative to vitrification and was first investigated by Ross in 1975 [8]. Subsequent studies have shown that the resultant wasteforms exhibit good chemical durability and mechanical strength [9]. Interestingly, SEM investigations have found that whilst the vitrification process dissolves the waste in the glass matrix, sintering encapsulates the waste in the framework of the crystalline phases present in the sintered glass. Sintering of an aluminosilicate glass to form a glass-ceramic has been investigated in depth by Luk and co-workers [10], with specific attention being paid to the effect on physical and chemical properties of encapsulating a simulated waste compositions consisting of Fe_2O_3, NiO, Cr_2O_3 and ZrO_2. Audero and co-workers [11] have also studied the effect of devitrification on the leaching behaviour of a sintered aluminoborosilicate glass, reporting that no significant change was observed between the as-sintered and devitrified samples.

3.2 Radiation Effects in High-Level Waste (HLW) Glasses

3.2.1 Radiation Sources

Radiation effects in HLW matrices are generated by two main processes; β-decay of the fission products (primarily Cs and Sr) and α-decay of the actinide elements (U, Np, Pu, Am and Cm). Spontaneous fission of some of the actinide isotopes and (α,n) reactions are sources of fission fragments and neutrons, but due to their low production rates these processes can usually be ignored. In general, β-decay of the fission products predominates during the first 500 years of storage with high radioactivities and heat generation. Alpha decay dominates over longer timescales with a much lower heat generation rate, as indicated in Fig. 3.01.

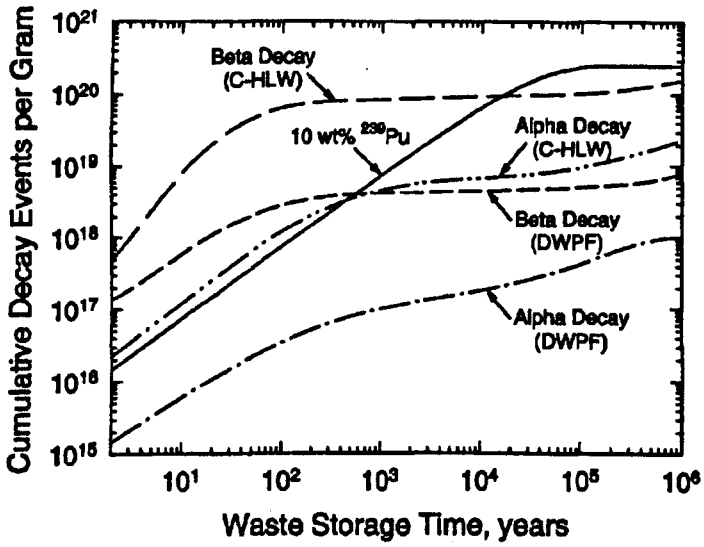

Fig. 3.01 The cumulative dose expected from different sources of α- and β-radiation during the lifetime of the storage matrix. Data is presented for DWPF (Defence waste processing facility, Savannah River) glass, C-HLW (a commerical nuclear waste glass) and a glass containing 10 wt.% plutonium (taken from [5]).

3.2.2 Interaction of radiation with glass and glass ceramics

Interaction of β- and α-decay radiation with the wasteform arises from the presence of β-particles, α-particles, recoil nuclei and γ-rays. Two broad categories can be defined containing these interactions: the transfer of energy to electrons (ionisation and electronic excitation) and the transfer of energy to atomic nuclei, primarily by ballistic processes involving elastic collisions. The processes controlling the effects of the radiation are governed by the partitioning of the available energy into electronic excitations and elastic nuclear collisions.

Both categories will be explained in more detail, but essentially, the energy transfer from β-particles and γ-radiation is dominated by ionisation processes. For the case of recoil nuclei and α-particles, the energy transfer partitioning depends on the relative velocity of the ions and that of the orbital electrons of the constituent ions of the glass. Ionisation processes will be the dominant method of energy transfer if the energy of the bombarding particle, in keV, is greater than its atomic weight but elastic collisions will dominate if the energy of the ion falls below this limit. In addition to the transfer of energy, the particles emitted through radioactive decay can themselves, in some cases, have a significant effect on the wasteform as a result of their deposition and accommodation in the glass structure.

3.2.2.1 Ionisation and electronic excitation

The effect of β- and α-radiation on a material as they pass through it is chiefly by interaction with the electrons of the constituent atoms. Processes of this kind may lead to the excitation or ionisation of the atoms and molecules, which in turn could result in covalent and ionic bond rupture, enhanced diffusion and localised electronic excitations. Radiolysis (the conversion of a localised electronic excitation into atomic motion) can be a very efficient displacement process, producing significantly more atomic displacements than ballistic collisions.

As the α-particle passes through the material, it will strip-off outer electrons from the atoms it interacts with, providing, of course, that the velocities of ion and electron meet the requirements stipulated in section 3.2.2. The ability of the α-particle to attract electrons will diminish with decreasing charge and energy, and as a result, at the end of its path, elastic collisions will start to occur between the α-particle and constituent atoms.

The interaction of β-particles with the material is in many ways similar to that of α-particles. The average energy loss per ion-pair formed is the same for β- and α-particles and primary ionisation by both particles only accounts for about 20-30% of the total ionisation. However, β-particles have, for a given energy, a higher velocity and therefore the specific ionisation is less for β-particles. Whereas an α-particle may travel several tens of μm before dissipating its energy, a β-particle may lose a large fraction of its energy in one collision. It is possible for an α-particle to produce several hundred well-separated atomic displacements, but a β-particle is incapable of doing the same.

3.2.2.2 Ballistic processes

Alongside the structural disruption produced by electronic excitation and ionisation, elastic collisions can cause direct atomic displacements and produce atomic-scale structural rearrangements. Since β-particles from the decay of fission products are not energetic enough to transfer sufficient energy to the atom, they account for only ~0.1 displacements per decay event. The primary source of atomic displacements by ballistic interactions is the α-particle and, more importantly, the α-recoil nucleus produced in an α-decay event.

Typical energies of these two particles range from 4.5-5.8MeV and 70-100keV, respectively. As stated previously, the α-particle will dissipate most of its energy via ionisation processes but is still capable of producing several atomic displacements through elastic collisions. The larger but less energetic α-recoil is responsible for the majority of displacements produced by ballistic processes in HLW glasses. The α-recoil loses nearly all of its energy in elastic collisions over a very short range (30-40nm), producing highly localised damage (displacement cascade or thermal spike).

In an α-decay event, the α-particle and α-recoil are released in opposite directions and produce distinct damage separated by several microns. The average number of displacements generated per α-decay event by decay of the actinides in HLW glasses is expected to be similar and is ~2300 per decay event.

3.2.2.3 Transmutation and Gas production

Along with the energy transferred to the glass, β- and α-decay also lead to transmutation of the radioactive parent nuclei. The two main sources of transmutations are the intermediate-lived fission products, ^{137}Cs ($\tau_{1/2}$ 30.2 years) and ^{90}Sr ($\tau_{1/2}$ 28.1 years), which undergo the following decay schemes shown below.

$$Cs^{137} \rightarrow Ba^{137m} + \beta^- \rightarrow Ba^{137} \tag{3.01}$$

$$Sr^{90} \rightarrow Y^{90} + \beta^- \rightarrow Zr^{90} + \beta^- \tag{3.02}$$

Transmutations can involve valence changes and major changes in atomic radii. The transmutation of ^{137}Cs leads to an ionic radius decrease of 20%, while for ^{90}Sr the decrease is 29%. Glass wasteforms are more likely to tolerate these changes as ceramic wasteforms have ordered structures that are likely to be less accommodating.

Another feature of α-decay that must be considered is the production of He atoms, which result from the capture of two electrons by an α-particle. These atoms must be accommodated in the glass interstitially, be trapped at internal defects, aggregate to form bubbles or be released at the glass surface [12,13].

3.3 Irradiation Techniques

3.3.1 Actinide-Doping

The α-decay of actinides present in high-level wasteforms consists of two separate, simultaneous processes; 1) An α-particle (E~5MeV) with a range of 10,000-20,000nm, dissipates most of its energy by ionisation. However, at low velocities near the end of its track, it displaces 100-200 atoms creating Frenkel defect pairs. (2) The α-recoil atom (E~0.1MeV) with a range of 10nm produces ~2000 atomic displacements creating 'tracks' of disordered material. The two areas of damage are separate and distinct and will have different effects on the atomic structure of the solid, particularly for crystalline materials [14].

The long-term effects of these α-decay events have been simulated in several waste glass compositions [4,12,15-18] by incorporating short-lived actinides such as ^{238}Pu ($\tau_{1/2}$ 87.7 years) or ^{244}Cm ($\tau_{1/2}$ 18.1 years) [19] in sufficient concentrations to achieve 10^{18}-10^{19} α-decay events per gram over several years. This technique effectively simulates the α-recoil and α-particle effects, albeit at accelerated dose-rates, that are expected over 10^3-10^6 years for HLW glasses. Phase separation and partial devitrification can result in the non-homogeneous distribution of actinides in actual waste glasses. This can be readily simulated using actinide incorporation techniques and appropriate processing to produce similar phase separation or crystallinity.

3.3.2 Neutron Irradiation

Neutron irradiation is one method that has been used in the past to simulate and study radiation damage in HLW and by their very nature, neutrons are excellent for use in irradiation studies. Being without charge, they will dissipate their energy by ballistic processes, producing significant numbers of atomic displacements. There is one slight drawback, however, in that they only moderately simulate the effects of the ballistic interactions of α-particles and recoils [12]. In addition, there is no analogue of the build-up of He also found due to α-decay [20].

Another approach that has been used with, in particular, borosilicate glasses is irradiation in a thermal neutron flux to generate a 1.78MeV α-particle as a result of the very high $^{10}B(n,\alpha)^7Li$ cross-section. With this technique, high rates of He

production are possible but again there is a drawback in that the process does not simulate the dense collision cascade produced by the α-recoil.

Similar to charged-particle irradiation, fast and/or thermal neutron irradiation produces nearly homogeneous damage that cannot simulate the heterogeneous distribution of actinides or fission products that would be contained within the crystalline areas of the wasteform.

3.3.3 Charged particle irradiation

The usefulness of charged particle irradiations that have been employed to simulate radiation effects in glass lies in their ability to achieve high doses in very short timescales (minutes). Conversely, the damage layer produced by α-irradiation is thin (the penetration depth of a 5.5MeV α-particle is ~ 0.005mm), making subsequent analysis difficult. However, it is possible, alongside the complementary technique of heavy-ion implantation, to effectively simulate the effects of α-particle and α-recoil damage. Both of these methods have been used to study α-decay damage effects in nuclear waste glasses and ceramics.

3.3.4 Natural Analogues

It is common in nature for natural glasses to contain ^{238}U, ^{235}U and ^{232}Th together with their daughter products. Unfortunately, these glasses are of limited use due to the low doses of radiation generated by the low quantities of actinides present. However, despite low uranium concentrations, ranging from 0.1 μmole/g to a few μmole/g, fission tracks have occurred in sufficient abundance to allow over 400 successful age determinations on volcanic glasses. Fission tracks represent an extreme in radiation damage caused by massive particles (fission fragments) of high energy (hundreds of MeV), with the tracks being up to several nm in length. The fission fragment yield in nuclear waste glasses is very much lower than that of α-decay events, and so is not considered a major damage mechanism. It has been suggested, however, that fission tracks provide an opportunity for the study of track annealing in an aperiodic solid, and such results may be relevant to the evaluation of the persistence of damage tracks in nuclear waste glasses.

3.4 Radiation Effects in HLW Glasses

3.4.1 Introduction

Effects of radiation in nuclear glasses are complex and even fundamental understanding of the damage processes taking place is limited. The high-radiation environment provided by α- and β-decay can effect the release of radionuclides to the biosphere through physical and chemical changes produced by the radiation at both the atomic and macroscopic level. At present, the only data available on simulated waste glasses are of measured macroscopic data, though glasses for HLW immobilisation are expected to exhibit radiation-induced defect centres similar to those found in simple glasses.

There are several measurable macroscopic properties of the glass that can be used to characterise the extent of the damage to the structure and integrity of the simulated waste form.

3.4.2 Volume Changes

The majority of all data on radiation induced volume changes has been generated in actinide-doping studies of alpha-decay damage. The volume of HLW glasses can decrease (compaction), increase (expansion), or remain unaltered as a result of radiation damage [12]. Volume changes can introduce internal stresses which could lead to microcracking and fracture of the glass.

The macroscopic volume changes, are usually determined by density measurements and generally follow an exponential dependence on dose, D [17];

$$\Delta V / V_O = A^*[1 - e^{(-BD)}] \qquad (3.03)$$

where A is the volume change at saturation and B is the amount of glass damaged per unit dose. Volume changes normally saturate within the range ±1.2% at a dose equivalent to ~$1x10^{18}$ α-decays g^{-1} ($1x10^{11}$ R) as illustrated in Fig. 3.02 for several HLW glasses [12,21] from work in the United States and Europe.

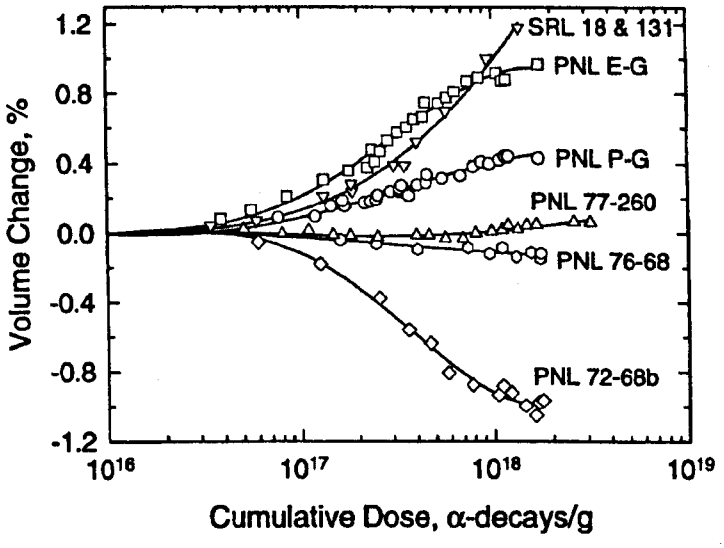

Fig. 3.02 The impact of large doses of α-radiation on the volume of several defence-waste glass storage matrices. [12,21]

Recent studies of actinide-dopes glasses in Japan [22,23] show expansions of similar magnitude for similar doses. In one study, the expansion determined by density measurements ranged from 0.4%-0.6% and is in excellent agreement with the volume change (0.51%) determined from the measured size and concentration of irradiation induced He or O_2 bubbles. Data obtained for other irradiation techniques, including fast neutron irradiation, are also within the bounds observed for actinide-doped glasses.

Very little data has been obtained regarding the effect of irradiation temperature on volume changes, notably that for a simulated waste glass doped with ^{238}Pu [24], where the rate of expansion was seen to be greater at low temperatures than at higher temperatures.

By considering the limited data available it is difficult to determine whether the volume changes induced by α-decay are due to ballistic or ionisation processes. Studies by Arnold [25,26] have strongly indicated that ionisation processes are the dominant damage mechanisms in borosilicate HLW glasses.

3.4.3 Stored Energy

Studies of actinide-doped waste glasses at the Pacific Northwest Laboratory [12,27], AERE-Harwell [28] and under a collaborative European Communities program [29], have shown that α-decay can lead to a rapid increase in stored energy

that saturates at values generally less than 150J/g (~0.03 ev/atom) as shown in Figure 3.03.

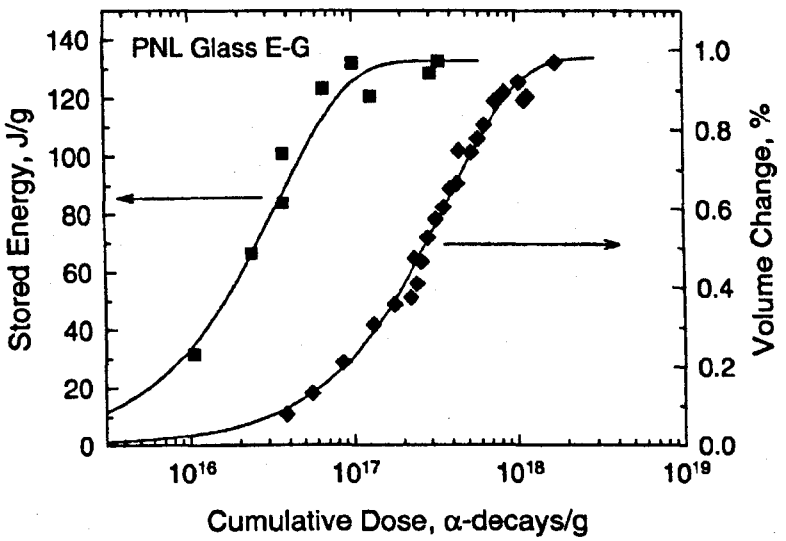

Figure 3.03 Variation in stored energy with radiation dose for several waste glasses.

The changes in bonding and structure that occur with radiation damage processes can result in the storage of latent energy, which is released as heat at elevated temperatures. This release of energy is of importance because of the risk of catastrophic failure of the wasteform should a very large amount of energy be released. It can be seen that saturation occurs at a much lower dose than for the volume changes. This indicates that the defects giving rise to the stored energy precede the structural rearrangements that manifest as volume changes.

In one glass doped with ^{244}Cm, it was found that the stored energy decreased linearly with irradiation temperature and was completely absent at 350°C [27]. The stored energy in actinide-doped simulated waste glasses is released over a broad range of temperatures from 100°C to 600°C [14,27], leading to a maximum temperature rise, arising from the rapid release of the stored energy, of only 50-125°C [17]. Temperature increases of this magnitude should present no serious problem so long as they are not superimposed on an existing high ambient temperature.

3.4.4 Helium Accumulation

The α-particle released during α-decay can capture two electrons to form He, which must then be accommodated interstitially, diffuse to internal defects or be released at the glass surface. Any build-up of He can lead to embrittlement or swelling, seriously weakening the ability of the wasteform to be an effective barrier to radionuclide release. The diffusivities of He in simulated waste glasses are one to two orders of magnitude lower than those in silica or alkali silicate and have been reported to decrease by several orders of magnitude with increasing radiation dose. This suggests that the He becomes trapped at radiation induced defects [20,30].

Low-level He concentrations (<100 atomic parts per million) introduced by (n,α) reactions under neutron irradiation have resulted in bubble formation after post-irradiation annealing at 600°C [31]. Higher He concentrations (up to 10^4 appm) have produced bubble formation at ambient temperatures (<100°C) [31]. Actinide-doped wasteforms containing ^{244}Cm have also shown bubble formation after $8x10^{18}$ α-decays g^{-1} at ambient temperature [22] and the integrated volume of bubbles correlated with the measured volume change. Though the exact nature of the bubbles was not established in any of these studies, they are assumed to be He or He/O_2.

3.4.5 Mechanical Properties

In a recent study of a simulated nuclear waste glass doped with ^{238}Pu and ^{244}Cm [32], the hardness and Young's modulus decreased exponentially with dose while the fracture toughness increased exponentially with dose. The maximum values for the relative changes were -25%, -30%, and +45%, respectively. The changes in fracture toughness are strongly correlated with the presence of bubbles that were observed in the glasses [22]. These changes in hardness and Young's modulus were recovered during annealing above 673K but complete recovery of the fracture toughness was never observed. The bubbles, which can impede crack propagation, anneal with kinetics similar to the recovery of the fracture toughness. In the study of an α-irradiated HLW glass [33], the hardness decreased by 15% and the fracture toughness increased by 80% with dose, as shown in Fig. 3.04. A similar decrease in hardness (24%) was observed in an actinide-doped glass [34]. These

large increases in fracture toughness may also be associated with bubble formation but lack of complete analysis means this has not been confirmed.

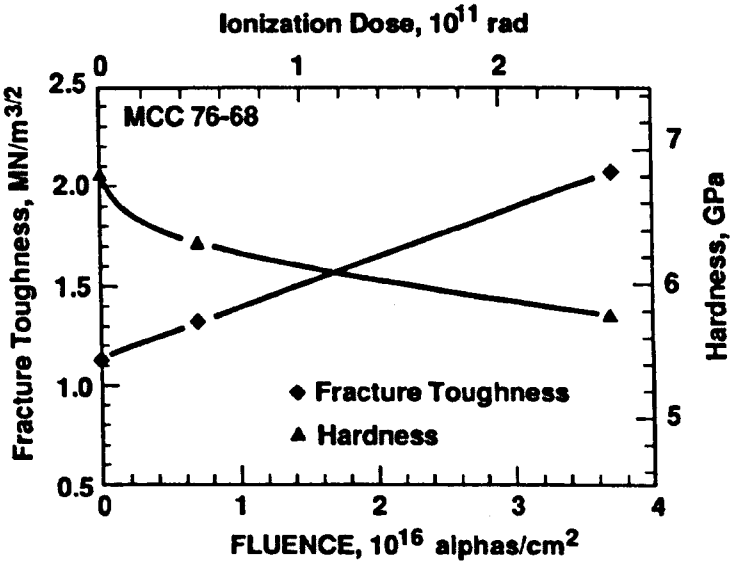

Fig. 3.04 The variation in fracture toughness and hardness, with radiation dose, of a high-level waste storage matrix (taken from [33]).

3.4.6 Radionuclide Release

The release rate of radionuclides to the biosphere will be determined by the release rate from the HLW glass, the solubilities of the radionuclides in the ground water and transport characteristics of the repository geology. One of the reasons that the aluminosilicate glass system has been selected for study is because it offers superior durability for the encapsulation of waste compared with other waste glasses. Since nearly all rock formations are rich in Al and Si components, a percolating ground water would be already saturated or near-saturated, prior to contact with the wasteform.

One way in which radiation can affect the rate of release of radionuclides is through microfracturing of the glass, effectively increasing the surface area available for radionuclide release. Changes in differential volume, microstructure and mechanical properties will all affect the extent of microfracturing but lack of information available at present makes it difficult to predict the extent of the damage produced; suffice to say that it is expected to occur.

The dissolution rate of the glass may be affected by changes in chemistry, microstructure and network bonding, but there is some uncertainty over the

reliability of the data concerning the effects of α-decay on the leach rates of HLW glasses. Short-term tests prior to 1982 were based solely on weight loss and the results from these predict no more than a factor of three increase in the short-term dissolution rate. However, it has since been established that short-term tests based solely on weight loss can underestimate the change in dissolution rate by a factor of three to four [21,35,36]. Consequently, based on the limited database of results available, a conservative estimate might be that radiation effects are not expected to increase the dissolution rates by more than a factor of 10. This assessment has been supported by the study [37] of a 17-year-old borosilicate glass containing 4 wt% ThO_2, where the Th daughter product release rate was increased 15 to 45% due to dissolution along the recoil tracks produced by the α-recoil nucleus. Therefore, the radiation enhanced radionuclide release rates can be expected to increase in proportion to the increase in surface area, times a factor of approximately 10 for enhanced dissolution. Any temperature dependence of the radiation effects could affect the level of enhancement expected.

3.5 Analysis of radiation induced defects

3.5.1 Electron Spin Resonance (ESR) - introduction

Electron spin resonance (ESR) spectroscopy, also known as electron paramagnetic resonance (EPR), was first discovered in 1944 by Zavoyskiy and has since become a particularly powerful method for the identification and characterisation of radiation-induced defects in vitreous materials. As will be explained in more detail in Chapter 4, ESR spectroscopy involves the monitoring of the behaviour of unpaired electrons with a magnetic field. The sister technique to ESR, nuclear magnetic resonance (NMR), adopts an analogous operational methodology and has since become the more widely used of the two, despite having been discovered 4 years later and also being ~2000 times less sensitive due to the relative magnetic moments of the electron and proton.

Whereas most as-quenched insulating glasses contain insufficient numbers of unpaired electrons for meaningful ESR analysis, the effect of irradiation by x-rays, γ-rays and α-particles is to produce significant concentrations of vacancies and

interstitials in the otherwise perfect random network. Subsequent trapping of radiation-generated electrons or holes by these species leads to the creation of paramagnetic defect centres that may be studied using ESR techniques.

3.5.2 Defect structure-glass structure relations

The nature of the defects introduced into the glass network as a result of irradiation has been found to alter depending on the constituents of the glass [38]. The figure below is a schematic representation of the structure of a glass and the radiation-induced defects that are hypothesised to occur.

Although not shown explicitly, the network formers R, R_A and R_B are tetrahedrally coordinated with the network forming species at the centre. Fig. 3.05(a) shows that silicon is always tetrahedrally coordinated unless an oxygen vacancy is present. This vacancy can act as an electron trap, termed an E' centre [39], and is denoted by (4) in the figure.

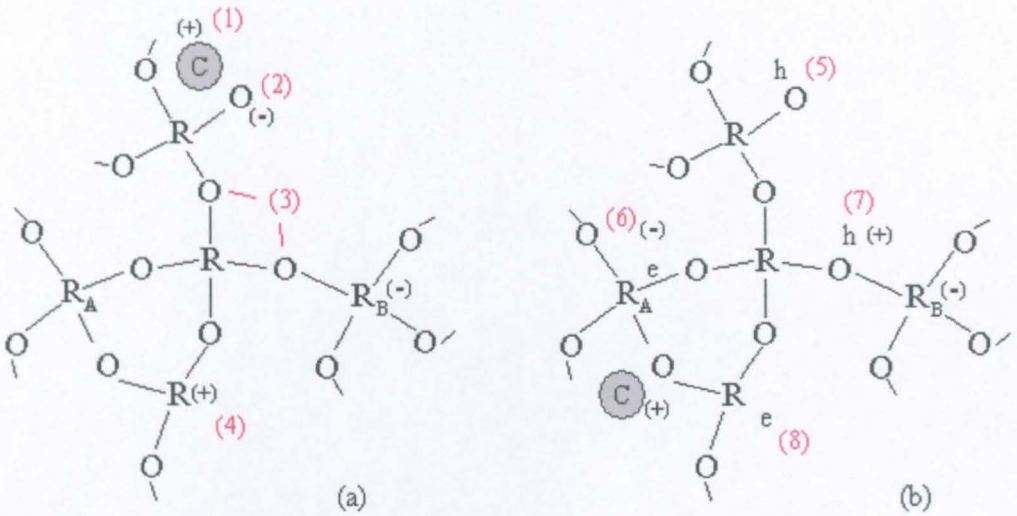

Fig. 3.05 Schematic representation of an oxide glass showing several types of radiation induced paramagnetic defect centres and pre-existing defects: (1) Interstitial cation, (2) Non-bridging oxygen, (3) bridging oxygens, (4) oxygen vacancy, (5) hole trapped on non-bridging oxygen, (6) electron trapped on R_A-O bond, (7) hole trapped on bridging oxygen near R_B, (8) electron trapped at oxygen vacancy (taken from [40].

When silica is not the main network forming oxide, i.e. in borates, germanates or phosphates, other defect centres can arise. In the case of boron and aluminium, the addition of alkali oxide results in a change of coordination, from 3 to 4 (boron) or 4 to 6 (aluminium), as they accept an extra electron from the modifying cation. The resulting $(R_B)O_4$ may be considered as a negative point defect or hole

trap and is denoted by (7) in the figure. The addition of alkali oxide to silica, however, results not in a change of coordination but a change in the number of bonding oxygens per silica atom, i.e. non-bridging oxygens (NBOs) are introduced onto the silica unit. Without the charge compensation of a nearby cation, the non-bridging oxygen can be thought of as another type of hole-trap. Finally, electron traps can also arise when the network former R_A possesses the same valency as R but a greater electron affinity, i.e. when R_A=Ge and R=Si. In low temperature irradiations, upon warming, these somewhat unstable centres are often stabilised by the diffusion of cations into positions nearby.

3.5.3 ESR studies of borate & silicate glasses

ESR studies of radiation-induced damage centres in glasses containing boron have been reported as early as 1953, less than ten years after the inception of the technique. In 1963, Lee and Bray [41] performed a thorough study of the nature of the ESR spectra observed in a selection of alkali borate glasses, irradiated by γ-ray and thermal neutrons. Fig. 3.06 shows the ESR spectra of a γ-ray irradiated $15Na_2O.85B_2O_3$ glass before and after thermal annealing at 250°C for 10 minutes.

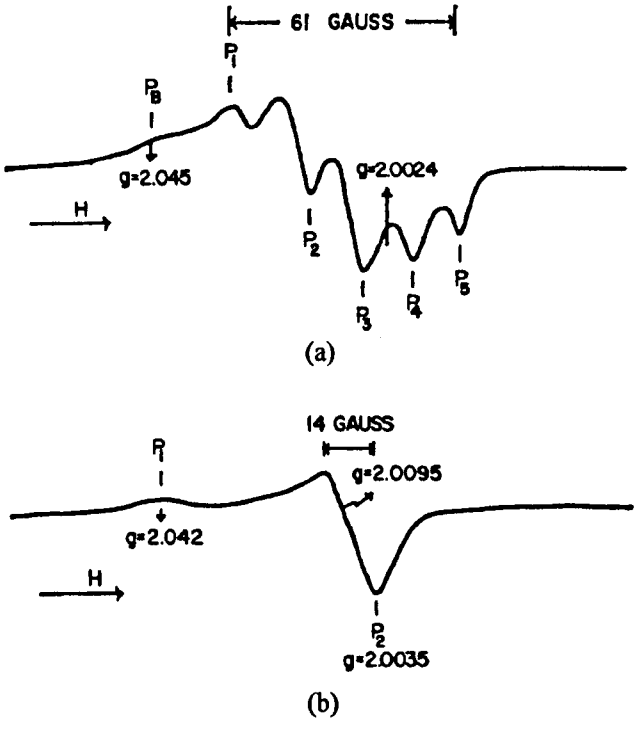

Fig. 3.06 The X-band ESR spectra of a γ-ray irradiated ($1x10^8$ R) $15Na_2O.85B_2O_3$ glass (a) before and (b) after thermal annealing at 250°C (taken from [41]).

It can be seen that the first spectrum is partially resolved into five major absorption lines. Subsequent substitution of the sodium by alternative alkali species makes no difference to the appearance of the five line structure, though the composition $5Na_2O.95B_2O_3$ displays a spectrum that consists of both the five-line and structureless resonance seen after thermal treatment, as shown in Fig. 3.07.

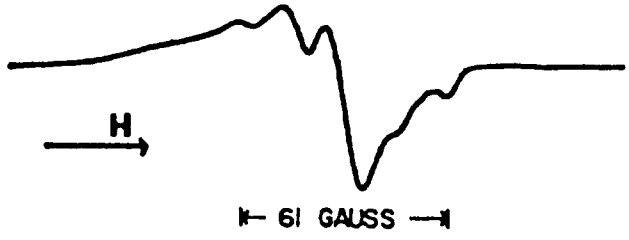

Fig. 3.07 ESR spectrum of a γ-ray irradiated ($1x10^8$ R) $5Na_2O.95B_2O_3$ glass (taken from [41]).

Comparison of these results with that from an irradiated "pure" B_2O_3 glass shows that the intensity of the five-line spectrum in the pure B_2O_3 glass is roughly 20 times less than that of the $15Na_2O.85B_2O_3$. One theory that has been proposed from these results is that the alkali ions or impurities present in the glass are not responsible for the five-line structure. Also, with the exclusion of hydrogen as a possible cause [41], the nucleus responsible for the structure must be either ^{11}B, ^{10}B or ^{17}O. Since a completely different spectrum, Fig. 3.08, is observed when the alkali borate glass is enriched with the ^{10}B isotope, ^{17}O can be ruled out as the cause of the observed structure.

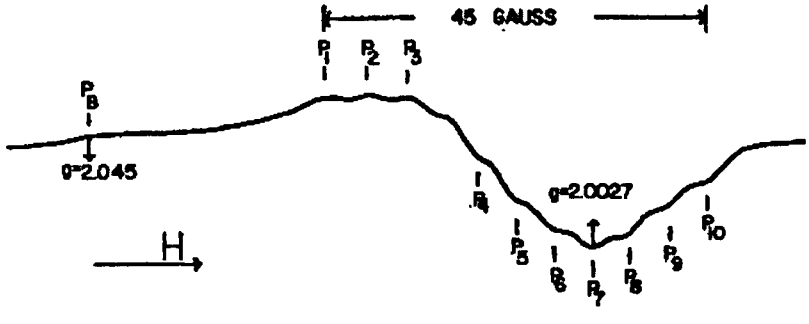

Fig. 3.08 An example of the characteristic lineshape observed from ESR studies of borate glasses due to a hyperfine interaction with the ^{10}B nucleus. (taken from [41]).

From this, is has been concluded that the five-line resonance arises from a hyperfine interaction with the ^{11}B nuclei, whilst the ten-line resonance is the result of a hyperfine interaction with the ^{10}B nuclei [41]. Lee and Bray are also able to hypothesise, from the intensity of the ESR spectra and knowledge of ^{11}B NMR data that the ^{11}B nuclei responsible for the five-line resonance lie at the centre of BO_4 tetrahedral units.

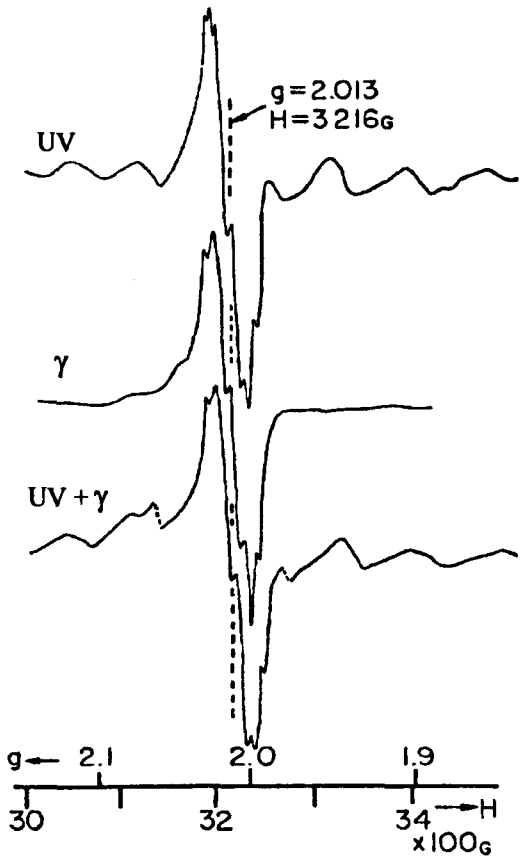

Fig. 3.09 ESR spectra obtained from a lithium borate glass irradiated by (a) UV-radiation, (b) γ-radiation, (c) UV- + γ-radiation (taken from [42]).

A number of workers have investigated the influence of high-energy ultra violet (UV) radiation on borate, silicate and aluminosilicate glasses [42,43]. Their results indicate a difference in the ESR signals obtained for each system and Fig. 3.09 illustrates the spectral differences between the UV-, γ- and UV+γ-irradiated samples.

The UV- + γ-irradiated sample ESR spectrum differs from both the samples irradiated by only one type of radiation. In explanation, similarly to Lee and Bray [41] and Beekenkamp [44], the multiple lines are attributed to a hole trapped on a

bridging oxygen between a $[BO_3]$ and $[BO_4]$ group, interacting weakly with the B^{11} nucleus on the $[BO_4]$ group.

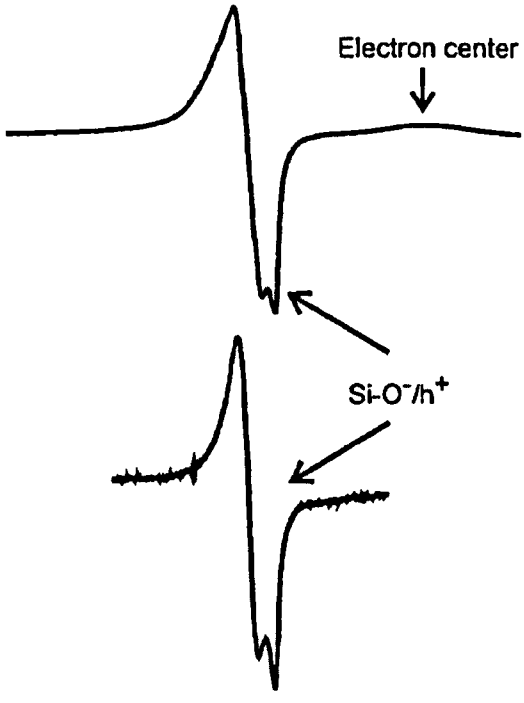

Fig. 3.10 ESR spectra of (a) a barium silicate glass and (b) a calcium-aluminosilicate glass, irradiated with γ-rays at room temperature. Certain traps attributable to holes and electrons are indicated. [43]

Fig. 3.10 shows the ESR spectra obtained from a $30BaO{\cdot}70SiO_2$ and a $33CaO{\cdot}5Al_2O_3{\cdot}62SiO_2$ glass irradiated by γ-rays at room temperature. The hole and electron traps described earlier in Fig. 3.05 can be elucidated from these spectra, i.e. the addition of alumina to a silicate glass leads to an increase in the concentration of Si-O-Al linkages on the SiO_4 units, which, in competition with NBOs, can then act as sites for the $Si\text{-}O^-/\ h^+$ trap, as indicated.

3.5.4 UV-spectroscopic studies of oxide glasses

UV/Visible spectrophotometry is a valuable analytical technique in the study of the modifying effects of cations such as Na^+, Li^+ and La^{3+}, and of defects, or *colour centres*, produced by exposure to energetic ions or electromagnetic radiation. It is often used in conjunction with ESR spectroscopy to provide a detailed picture of the types of species responsible for the physicochemical changes that the glass undergoes as a result of radiation exposure. Although not discussed further here, it is

worth mentioning that the presence of colour centres results in changes to the glass melting characteristics, due to changes in the radiative characteristics of the glass, which themselves are dependent on the glass near infra-red transmission [45].

A typical UV-transmission curve always exhibits a sharp drop to zero at a particular wavelength, called the ultra-violet absorption edge. Studies [46,47] have shown that the precise wavelength of this *cut-off* is dependent on glass composition, as shown in Fig. 3.11. Observations made by Scholze [46], namely that the transmission of glasses in the UV is dependent on the number of nonbridging oxygens present, have been shown to be in agreement with that predicted by the network theory of glasses.

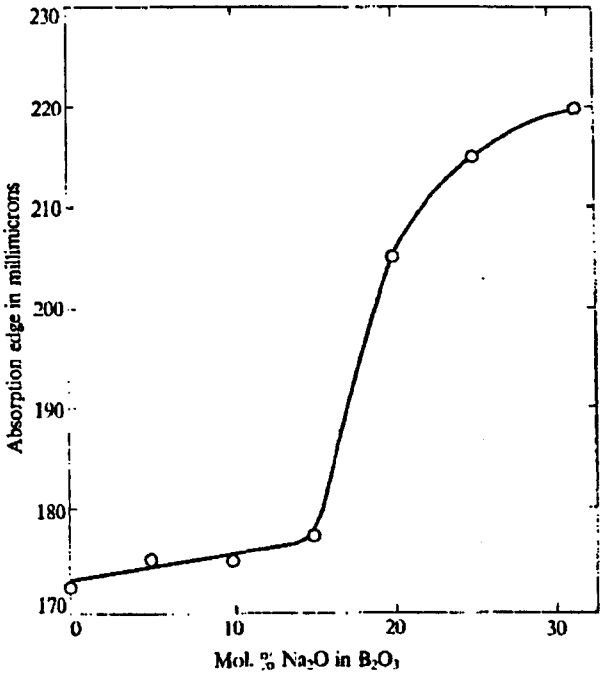

Fig. 3.11 Evidence for the influence of glass composition on the UV- transmission characteristics of a sodium borate glass [46]

3.6 References

[1] Hj. Matzke, Nucl. Instrum. Methods in Phys. Rev. B **32** (1988) p.453

[2] W. J. Weber, L. K. Mansur, F. W. Clinard Jr & D. M. Parkin, J. Nucl. Mater. **184** (1991) p.1

[3] D. J. Wronkiewicz, Effects of Radionuclide Decay on Waste Glass Behaviour – A Critical Review, ANL-93/45 (Argonne National Laboratory, Argonne, IL 1993)

[4] W. G. Burns & A. E. Hughes, *Scientific Basis For Nuclear Waste Management V*, p.339, edited W. Lutze (Mater. Res. Soc. Symp. Proc. **11** Pittsburgh, PA, 1982)

[5] W. J. Weber, R. C. Ewing, C. A. Angell, G. W. Arnold, A. N. Cormack, J. M. Delaye, D. L. Griscom, L. W. Hobbs, A. Navrotsky, D. L. Price, A. M. Stoneham & M. C. Weinberg, J Mater. Res. **12** (8) (1997) p.1950

[6] I. W. Donald, B. L. Metcalfe & B. N. J. Taylor, J. Mater. Sci., **32** (1997) p. 5851

[7] E. R. Vance, S. Urquhart, D. Anderson & I. M. George in "Advances in Ceramics", Vol. 20, "Nuclear Waste Management II", edited by D. E. Clark, W B White & A T Machiels (Am. Ceram. Soc., Westerville, OH, 1986) p.249

[8] W. A. Ross, Report No. BNWL-SA-5362 (Pacific Northwest Laboratory, Battelle, 1975)

[9] S. Gahlert & G. Ondracek in "Radioactive Wasteforms for the Future", edited W. Lutze & R. C.Ewing (North Holland, Amsterdam, 1988) p.161

[10] K. L. Luk, PhD Thesis, University of Warwick, 2000.

[11] M. A. Audero, A. M. Bevilacqua, N. B. M. de Bernasconi, D. O. Russo & M. E. Sterba, J. Nucl. Mater. **223** (1995) p.151

[12] W. J. Weber & F. P. Roberts, Nuclear Technology **60** (1983) p.178

[13] W. J.Weber, Journal of Minerals, Metals and Materials Society **43** No.7 (1991) p.35

[14] W. J. Weber, J. W. Wald & W. J. Gray, *Scientific Basis For Nuclear Waste Management* **3**, p.441, edited by J. G. Moore, Plenum Press, New York.

[15] W. G. Burns, A. E. Hughes, J. A. C. Marples, R. S. Nelson & A. M. Stoneham, J Nucl. Mater. **107** (1982a) p.245

[16] D. H. Day, A. E. Hughes, J. W. Leake, J. A. C. Marples, G. P. Marsh, J. Rae & B. O. Wade, Rep. Prog. Phys. **48** (1985) p.101

[17] R. C. Ewing, W. J. Weber, F. W. Clinard Jr, Prog. In Nucl. Energy **29** (2) (1995) p.63

[18] R. C. Ewing, W. J. Weber & W. Lutze, *Scientific Basis For Nuclear Waste Management* **19**, p.25, edited by W. M. Murphy & D. A. Knecht (Mater. Res. Soc. Symp. Proc. **412**, Pittsburgh, PA, 1996)

[19] E. Browne, J. M. Daikiri *et al.*, Table of Isotopes, Ed. by C. M. Lederer & V. S. Shirley, 7th edition (J Wiley & Sons, New York, 1978)

[20] G. Malow & H. Andresen, *Scientific Basis For Nuclear Waste Management* **1**, p.109, edited by G. J. McCarthy, Plenum Press, New York, 1979.

[21] W. J. Weber, Nucl. Instr. Methods in Phys. Res. B **32** (1988) p.471

[22] Y. Inagaki, H. Furuya & K. Idemitsu, T. Banba, S. Matsumoto & S. Muraoka, *Scientific Basis For Nuclear Waste Management* **15**, p.199, edited by C. G. Sombret (Mater. Res. Soc. Symp. Proc., **257**, Pittsburgh, PA, 1992)

[23] T. Banba, S. Matsumoto & S. Muraoka, K. Yamada, M. Saito, H. Ishikawa & N. Sasaki, *Scientific Basis For Nuclear Waste Management* **18**, p.1397, edited by T. Murakami & R. C. Ewing (Mater. Res. Soc. Symp. Proc., **353**, Pittsburgh, PA, 1995)
[24] J. A. C. Marples, Nucl. Instr. Methods in Phys. Res. B **32** (1988) p.480
[25] G. W. Arnold, *Scientific Basis for Nuclear Waste Management* **8** p.617 Ed. by C. M. Jantzen, J. A. Stone & R. C. Ewing (Mater. Res. Soc. Symp. Proc. **44** Pittsburgh, PA, 1985)
[26] G. W. Arnold, Nucl. Instrum. Methods in Phys. Res. B **1** (1984) p.516
[27] F. P. Roberts, G. H. Jenks & C. D. Bopp, Radiation Effects in Solidified High-Level Stored Wastes – Part 1, Stored Energy, Report No. BNWL-1944 (Pacific Northwest National Laboratory, Richland, WA, 1976)
[28] A. R. Hall, J. T. Dalton, B. Hudson & J. A. C. Marples, Management of Radioactive Wastes from the Nuclear Fuel Cycle **2** IAEA-SM-207 p.3 (IAEA, Vienna, 1976)
[29] G. Malow, J. A. C. Marples & C. G. Sombret, Radioactive Waste Management & Disposal, edited by R. Simon & S. Orlowski, p.341 (Harwood Academic Publishers, Chur, Switzerland, 1980)
[30] R. P. Turcotte, Radiation Effects in Solidified High-Level Stored Wastes – Part 2, Helium Behaviour, Report No. BNWL-2051 (Pacific Northwest National Laboratory, Richland, WA, 1976)
[31] A. K. Dé, B. Luckscheiter, W. Lutze, G. Malow & E. Schiewer, Am. Ceram. Soc. Bull. **55** (1976) p.500
[32] Y. Inagaki, K. Furuya, Y. Ono, K. Idemitsu, T. Banba, S. Matsumoto & S. Muraoka, *Scientific Basis For Nuclear Waste Management* **16**, p.191, edited by C. G. Interrante & R. T. Palaban (Mater. Res. Soc. Symp. Proc. **294** Pittsburgh, PA, 1993)
[33] W. J. Weber, Hj. Matzke, European Applied Research Reports **7** (1987) p.1221
[34] R. A. Bonniaud, N. R. Jacquet Francillon, R. L. Laude & C. G. Sombret, in *Ceramics in Nuclear Waste Management*, Ed. by T D Chikilla & J E Mendel, CONF-790420 (National Technical Information Service, Springfield, VA, 1979), p.57
[35] J. H. Westick & C. O. Harvey, High temperature leaching of a simulated high-level waste glass, PNL-3172, (Pacific Northwest National Laboratory, Richland, WA, 1981)
[36] W. J. Weber, J. W. Wald, *Scientific Basis for Nuclear Waste Management* **8**, p.679, edited by C. M. Jantzen, J. A. Stone & R. C. Ewing (Mater. Res. Soc. Symp. Proc. **44** Pittsburgh, PA, 1985)
[37] Y. Eyal & R. C. Ewing in *Proceedings of the International Conference on Nuclear Waste Management and Environmental Remediation* **1** edited by D. Alexandre, R. Baker, R. Kohout & J. Marek, p.191 (ASME Press, New York, 1993)
[38] S. A. Al'tshuler & B. M. Kozyrev, "Electron Paramagnetic Resonance", Academic Press, London (1964) p.vii
[39] R. A. Weeks, J. Appl. Phys. **27** (1956) p.1376
[40] D. L. Griscom, J. Non-Cryst. Solids **13** (1973/74) p.253
[41] S. K. Lee & P. J. Bray, J. Chem. Phys. **39** (11) (1963) p.2864
[42] T. Kishii & K. Ŏoka, J. Phys. Soc. Japan **23** (1967) p.659

[43] M. Nofz, C. Reich, R. Stösser, J. Bartoll & E. Janata, Glastech. Berichte **72** (1999) p.76
[44] P. Beekenkamp, Philips Research Report Supplement (4) (1966)
[45] C. R. Bamford, Colour Generation and control in glass, Glass Science and Technology, Vol.2, Elsevier Scientific Publishing Company, Amsterdam (1977) p.166
[46] H. Scholze, Glastech. Ber. **32** (1959) p.81
[47] B. D. McSwain, N. F. Borelli & Gouq-Jen Su, Phys. Chem. Glasses **4** (1) (1963), p.1

Chapter 4 – Experimental Theory & Practice

4.1 Glass Preparation

4.1.1 General Procedure

All samples were prepared by fusion of the required combinations of reagent-grade silica (SiO_2), boric acid (H_3BO_3), sodium carbonate (Na_2CO_3), anhydrous sodium tetraborate ($Na_2B_4O_7$) and lithium carbonate (Li_2CO_3). Details of the calculation of the batch composition required to produce a given glass composition are given in Appendix D. Batches were melted in 90%Pt-10%Rh crucibles at temperatures ranging from 1323 to 1923 K, depending on silica content. After a hold time of 18 minutes at the melt temperature, each sample was quenched in de-ionised water and dried, before being remelted for a further 10 minutes and cast into blocks or splat-quenched, depending on the rate of devitrification. The short melting times were employed to ensure minimisation of any volatilisation of boron from the melt. A small amount of glass was powdered and analysed using thermal methods, whereupon the remaining sample was annealed at 50K below the glass transition temperature, T_g. Rods of each sample were cast in moulds for thermal expansion measurement and were also annealed at 50K below T_g.

4.1.1 Glass compositions

Fig. 4.01 below is a ternary phase diagram indicating the compositions of the samples used in the current work. It is known that there exists an especially large region of metastable phase separation in the low-alkali composition range in the lithium- and also the sodium-borosilicate system. The chemical analysis of the glasses and their leachates, generated by the chemical durability tests, was determined by X-ray fluorescence (XRF) and Inductively Coupled Plasma (ICP) techniques at Ceram Research [1]. All samples were polished before the irradiation and conductivity experiments using 70μm fixed diamond paper, followed by 7μm and 6μm aqueous diamond suspension. Samples awaiting further physical and structural analysis were stored in a desiccator until required.

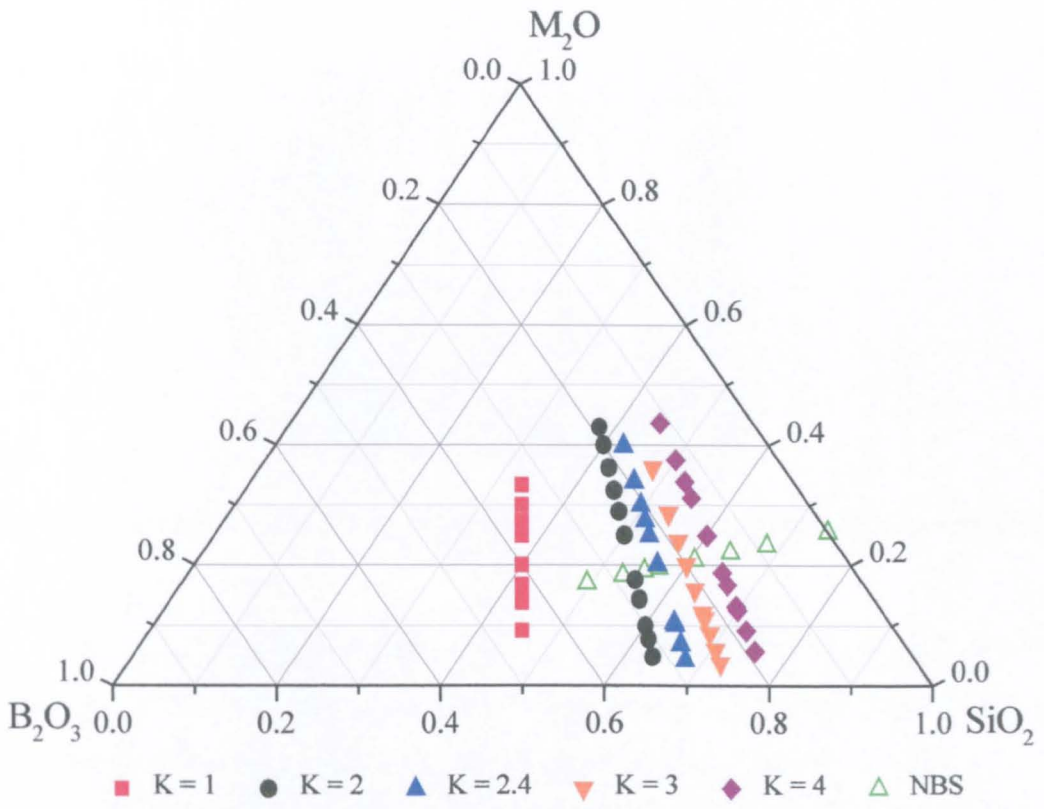

Fig. 4.01 Ternary phase diagram illustrating the mole fraction compositions of the glasses prepared and studied in the current work.

4.2 Characterisation techniques

4.2.1 Thermal techniques

4.2.1.1 Differential thermal analysis (DTA)

Differential Thermal Analysis is a simple but very useful technique for the characterisation of the thermal properties of a material. Essentially, the sample and a suitable reference material are heated simultaneously in a furnace whilst the temperature difference, ΔT, between them is monitored by a differential thermocouple. Any exothermic or endothermic processes that take place in the sample will show up as peaks or troughs in the DTA trace, depending on the orientation of the thermocouple. The resulting trace can be used to identify events such as melting, crystallisation and most usefully, in the case of this study, the glass transition temperature, T_g. A schematic representation of the experimental arrangement used is shown in Figure 4.02.

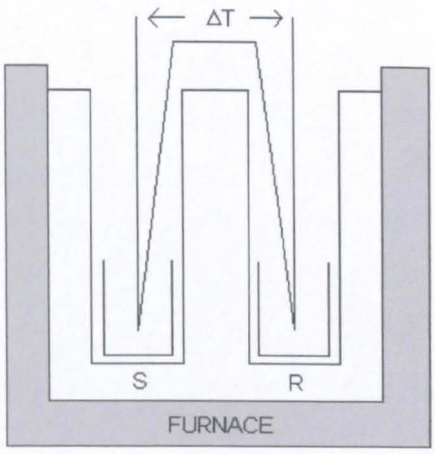

Fig. 4.02 Schematic diagram of DTA apparatus showing positions of sample (S), reference (R) and details of ΔT measurement.

Measurements were carried out on a Stanton-Redcroft 673-4 DTA and used mainly to identify the glass transition temperature, T_g, alongside the melting and crystallisation events taking place up to approximately 1500°C. Each run was carried out at a heating rate of 10°C min^{-1} under air at standard atmospheric pressure. The reference chosen was Al_2O_3, principally because of its lack of any exothermic or endothermic features, which may have interfered with the T_g signal. Fig. 4.03 shows a portion of a typical DTA trace obtained by the method described above, highlighting how a value for T_g is determined.

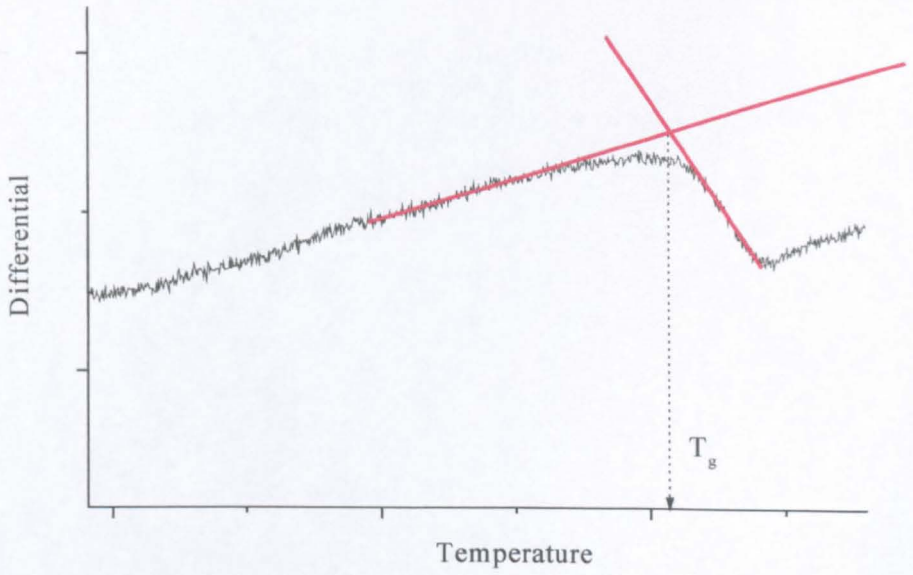

Fig. 4.03 An example of how the glass transition temperature, T_g, is determined from the DTA trace.

4.2.1.2 Dilatometry

Information on the influence of the glass components on the thermal expansion properties of the samples was acquired using a vertical quartz push-rod dilatometer, designed at the University of Warwick. The sample was placed between a movable quartz rod and a fixed base, with any movement of the rod being monitored by an LVDT and recorded on a computer. The temperature of the furnace surrounding the sample arrangement was increased at 2°C min^{-1} until approximately 20°C above the T_g determined by DTA. The linear coefficient of thermal expansion (CTE), α, was measured between 100°C and 300°C and was calculated according to equation 4.01,

$$\alpha_L = \frac{\Delta L}{L_O \Delta T} \tag{4.01}$$

where α_L is the linear coefficient of thermal expansion, ΔL is the change in sample length, L_O is the original sample length and ΔT the change in temperature.

In order to ensure reliability and reproducibility, a platinum rod was used to calibrate the equipment and obtain a value for the expansion of the quartz push-rod. This was found to be ~0.7 MK^{-1} over the temperature range of interest.

4.2.2 Structural Determination

4.2.2.1 NMR Spectroscopy

Since its discovery in 1945, NMR spectroscopy has been used to probe the structure of glasses using the interaction of nuclei possessing a non-zero magnetic moment with an external magnetic field. The role and behaviour of typical glass component nuclei such as ^{11}B and ^{29}Si within the network can be studied as a function of the composition. The technique is most commonly used in glass science to differentiate between the available coordination states of boron (3- and 4-coordinated), and the oxygen-silicon speciation, Q^n, where n corresponds to the number of bridging oxygens associated with the silica unit.

The phenomenon exploited by NMR spectroscopy is the energy difference in spin levels arising from the interaction between the nuclear magnetic moment and an externally applied magnetic field, B_o, in the z-direction. Excitation of the nuclear

magnetic moments with radio frequency (RF) energy, and detection of the subsequent spin system response can be achieved using continuous wave (CW) or pulsed spectroscopy. Both techniques possess their individual advantages, but pulsed NMR allows access to more detailed structural information as a result of improved spectrum resolution.

Used as an important analytical tool, the chemical shift is generated by the interaction of the nuclear spin angular momentum with surrounding electron clouds. The primary influence of the electron clouds is the magnetic shielding that arises when electronic orbitals are perturbed by the applied magnetic field [2]. This screening results in displacement of the Larmor precession frequency and is termed the chemical shift due to its dependence on the local chemical environment, enabling the determination of the structure of molecules from NMR spectra. Several factors can contribute to the size of the shift, including the co-ordination number of the atom; the type of neighbouring atom; bond angles and lengths; structural unit connectivity and next nearest-neighbour co-ordination sphere [3].

The Zeeman interaction is the interaction of spin angular momentum of a spin *I* with an externally applied magnetic field. The Zeeman Hamiltonian is given by:

$$H_Z = -\gamma_I \hbar \vec{I} \cdot \vec{B} \tag{4.02}$$

where γ_I is the gyromagnetic ratio of spin *I*. If the magnetic field is chosen to be in the z-direction and radial frequency units are used (i.e. dividing by *h*), the Hamiltonian becomes:

$$H_Z = \omega_o I_Z \tag{4.03}$$

where $\omega_o = -\gamma_I B_o$, the Larmor (precession) frequency in H_Z can, be used to calculate the energy of the transition between states. For the case of ^{11}B, with spin I = 3/2, the energy of the spin states can be found by obtaining the eigenvalues of the Zeeman Hamiltonian and are represented in Fig. 4.04.

The majority of nuclei routinely studied using NMR techniques, including ^{11}B, possess a spin-quantum number $I > ½$. Consequently, the electrical charge

distribution within the nucleus is non-spherically symmetric, giving rise to a nuclear electrical quadrupole moment (eQ).

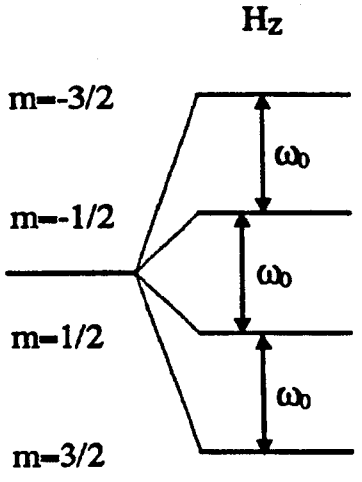

Fig. 4.04 Schematic representation of the available spin states and their energies resulting from the Zeeman interaction of an I = 3/2 nucleus.

For a quadrupolar nucleus in a magnetic field, two competing interactions exist: a) the magnetic field attempts to align the spins along the magnetic field and b) the quadrupole interaction attempts to orient the spins towards the most favourable orientation in the local electric field gradients. The interaction of the quadrupole moment with electric field gradients produces a shift in the position of the nuclear energy levels, as shown in Fig. 4.05.

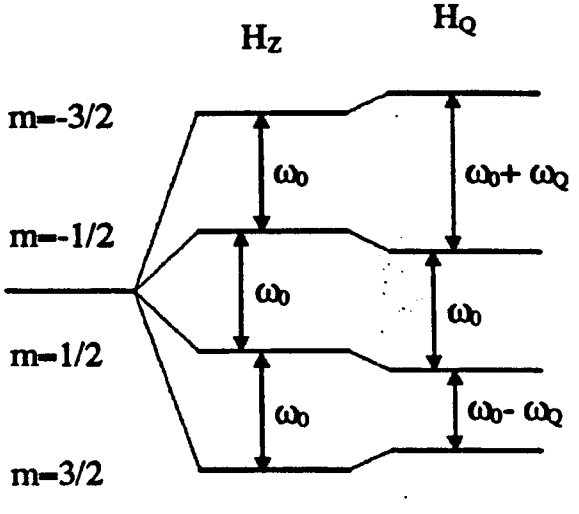

Fig. 4.05 The energy level diagram for a spin 3/2 nuclei in a magnetic field exhibiting Zeeman and quadrupolar interactions.

The macroscopic result of this is broadening of the central transition, causing overlap of the individual resonance contributions and smearing of the fine-detail of the NMR spectrum. An example of the characteristic quadrupolar lineshape for a spin 3/2 nucleus such as ^{11}B is shown in Fig. 4.06 (a), along with the lineshapes that can be observed with variation of the asymmetry and broadening parameters.

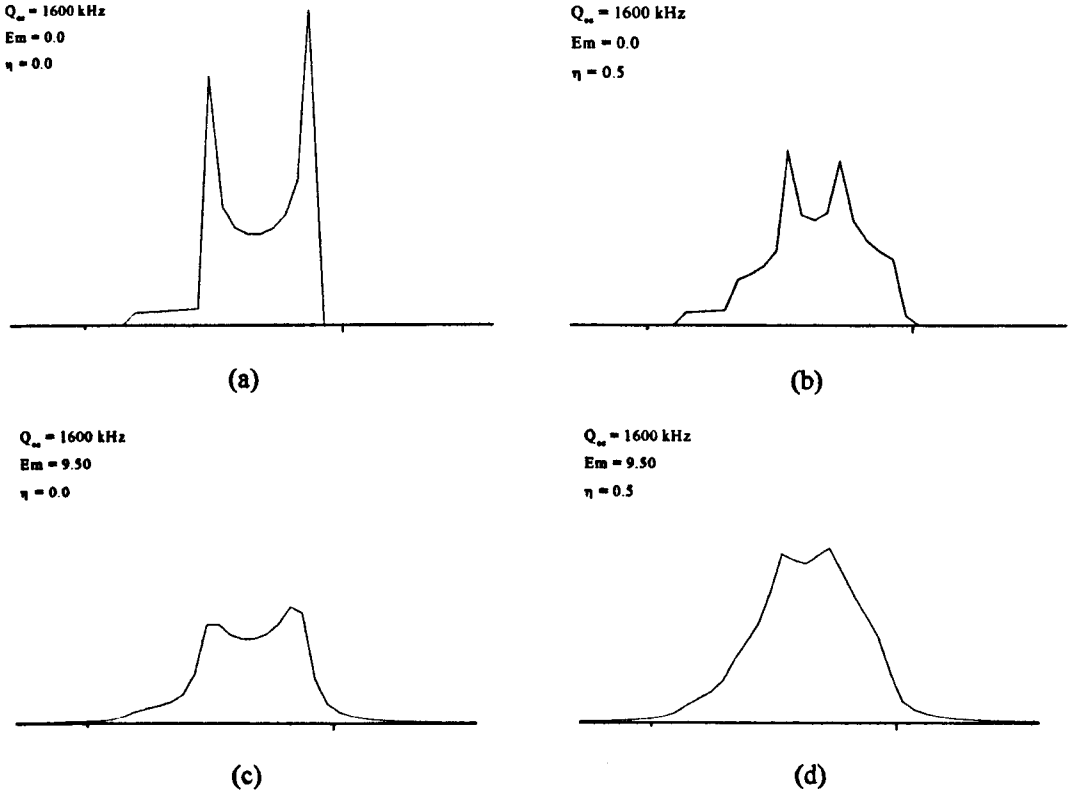

Fig. 4.06 Illustration of the nature of the second-order quadrupolar lineshape of a spin-3/2 nucleus, specifically ^{11}B, with variation of the quadrupolar coupling constant (Q_{cc}), asymmetry parameter (η) and line broadening (E_m). The isotropic chemical shift is at 0 ppm.

The MAS procedure that successfully averages dipolar and chemical shift effects in ^{29}Si (I = ½) does not eliminate second-order quadrupole effects, making the deconvolution of ^{11}B MAS NMR spectra inherently difficult. The characterisation of ^{29}Si spectra is more straightforward and can be achieved using combinations of Gaussian peaks.

In pulsed NMR, the whole frequency bandwidth of interest is irradiated simultaneously, producing a field B_1 in the x direction. When a pulse of length t_p, possessing angular frequency γB_1, is applied, the sum of the nuclear magnetic

moments will be rotated from their equilibrium position along the z-axis by the angle,

$$\theta_p = \gamma B_1 t_p \tag{4.04}$$

and will precess about the z-axis as shown in Fig. 4.07. Over time, spin-spin interactions and spin-lattice relaxation mechanisms return the magnetisation vector M to its equilibrium position. This decaying signal is termed the free induction decay (FID) and the fourier transform (FT) of this produces the NMR absorption spectrum. Improvements to this procedure have been made with the introduction of magic-angle spinning (MAS) NMR spectroscopy, where the sample is oriented at 54.74° to the magnetic field and spun very rapidly. The broadening mechanisms that reduce resolution are minimised at this precise angle and fine structural details once obscured become visible.

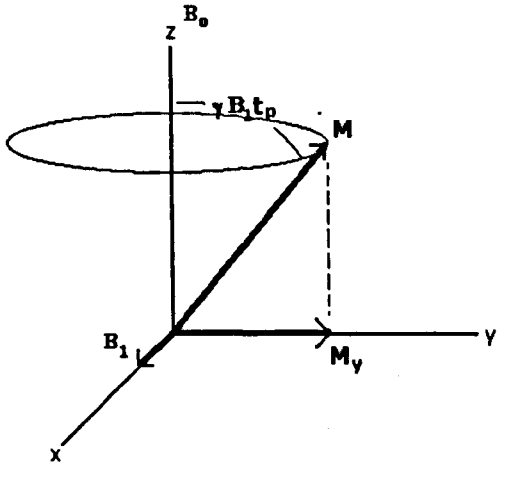

Fig. 4.07 Schematic representation showing the displacement and precession of the magnetic moment due the applied RF pulse.

A Varian/Chemagnetics Infinity 600 NMR spectrometer was used to acquire information regarding the type and abundance of borate structural units present in each sample. The ^{11}B magic-angle-spinning (MAS) NMR spectra were obtained from 1000 acquisitions at room temperature and a spinning speed of no less than 15kHz. A pulse length of 0.6μs and pulse delay of 1.5 seconds were used at a frequency of 192.504 MHz. The reference material used was Pyrex®, which allowed variations in the chemical shift of each sample to be measured and also allowed a

rough estimate of the boron content, prior to complete chemical analysis, to be made. Fig. 4.08 shows an example of the spectrum obtained from a mixed-modifier borosilicate glass and its possible deconvolution into the individual resonance contributions from different ^{11}B environments.

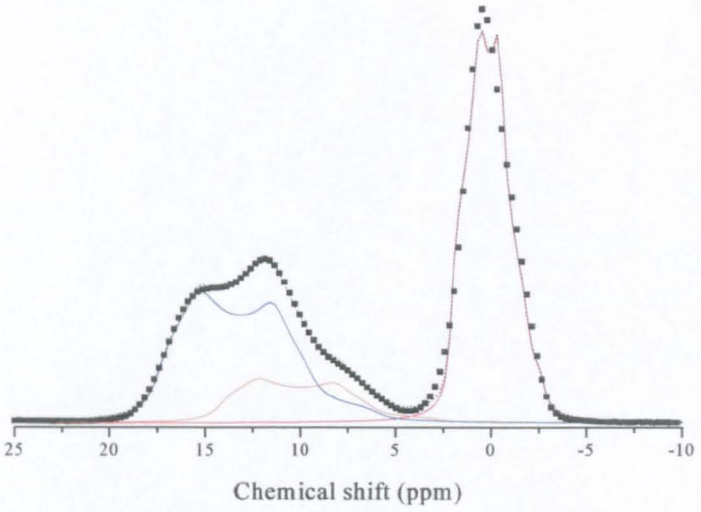

Fig. 4.08 Examples of the individual contributions used to fit the experimental ^{11}B MAS NMR spectra of the NBS and ABS glasses. ····· = data, – – – = overall fit, —— = tetrahedral [BO_4] units, —— = symmetric [BO_3] units, —— = asymmetric [BO_3] units

Experimental spectra were simulated using an NMR simulation program [4], using a minimum of three peaks exhibiting quadrupolar lineshapes. The isotropic chemical shift, δ_i, quadrupolar coupling constant, Q_{cc}, and asymmetry parameter, η, of each peak were recorded. The ^{29}Si MAS NMR spectra were obtained from 1000 acquisitions at room temperature on a Bruker MSL 360 spectrometer, at a spinning speed of 3kHz, pulse length of 2μs and pulse delay of 5 seconds at a frequency of 71.54 MHz. The pulse delay chosen was sufficiently long to avoid any magnetic moment saturation effects, spin relaxation having been enhanced by the inclusion of a small amount of Fe_2O_3 (0.1 mol%) in each sample. Experimental spectra were simulated by the minimum number of Gaussian lineshapes sufficient to generate a satisfactory fit to the data.

4.2.2.2 Density measurement

Variations in the density of glasses can be used to indicate changes in the type and abundance of structural units present. It is primarily used in this work to investigate the change in boron and silicon speciation with the amount of alkali

incorporated in the glass. Whilst measurement of the dimensions and mass can be used as a crude method of determining the density of a sample, a much more accurate technique is based on the mass-displacement theory of Archimedes. The density can be calculated from equation 4.05,

$$\rho = \frac{M_A \rho_W}{M_A - M_W} \tag{4.05}$$

where M_A is the mass of sample in air, M_w is the mass of sample in liquid, in this case distilled water, ρ_w is the density of water at the measurement temperature.

An average of four measurements were taken for each sample, leading to an estimated error of ± 0.01 gcm^{-3}. As far as possible, only samples that were free from bubbles and cracks were used in the measurement.

4.2.2.3 Ionic (DC) Conductivity

The kinetic behaviour of ions within a glass is of great importance in those fields where the glass is used as an electrical insulator, a fast-ion battery system or, in particular, where glasses are used to isolate HLW from its surroundings. The mobility of ions such as Na^+ and Li^+ affect the chemical durability of the wasteform and must be taken into consideration during the composition selection stage.

Though it has been known for over 100 years that ordinary glasses are conducting, the mechanism that describes this phenomenon has not been established absolutely. The simplest and most popular theory, based on the structure of alkali silicate glasses, involves the migration of the interstitial alkali ions present, as shown in Fig. 4.09(a). Cation mobility is dominant in many borate, phosphate and silicate glasses, though anionic motion has been observed and commented upon [5]. Mixed cation conduction has been studied extensively and is of particular interest to the Li_2O-Na_2O-B_2O_3-SiO_2 system. The most interesting feature of this is that the combination of different alkalis in the composition produces a distinct minimum in the conductivity at any given temperature. Figure 4.09(b) describes the variation in conductivity of a Li_2O-Na_2O-$2SiO_2$ glass alongside the change in molar volume.

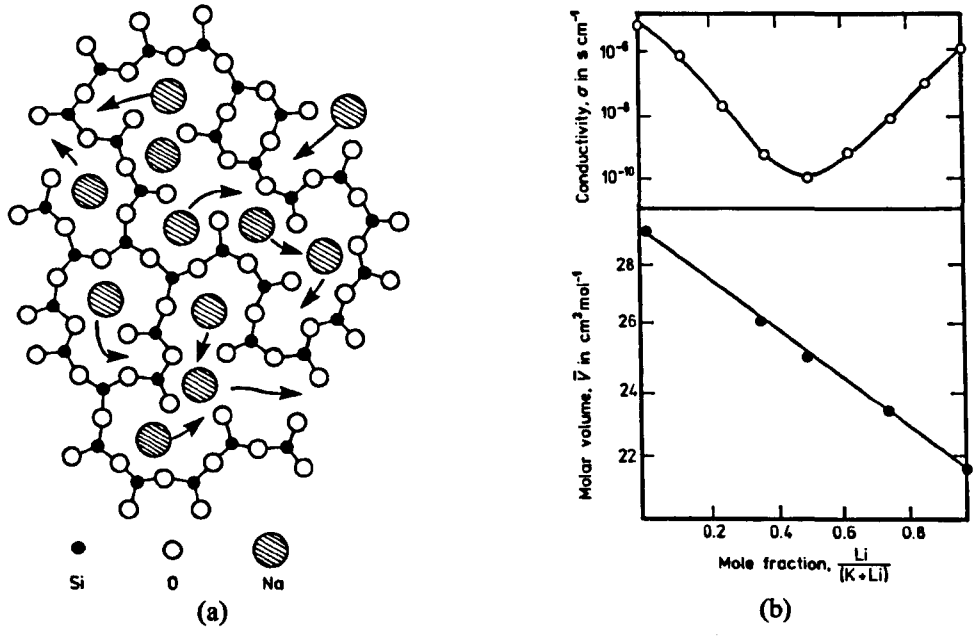

Fig.4.09 (a) A schematic representation of the mechanism by with ionic conduction is proposed to occur in alkali-silicate glasses [6] and (b) illustration of the mixed-alkali effect observed in a Li_2O-Na_2O-SiO_2 glass (after [7]).

Conventionally, the glass conductivity is measured by attaching electrodes to the surface and determining the complex impedance diagram over a 1-10^6 Hz range, using a frequency impedance analyser. This arrangement can be equated to a simple circuit including a parallel RC element, representing the glass, and a series capacitance, representing the electrode. A simulated impedance plot, alongside its equivalent circuit is shown in Fig 4.10.

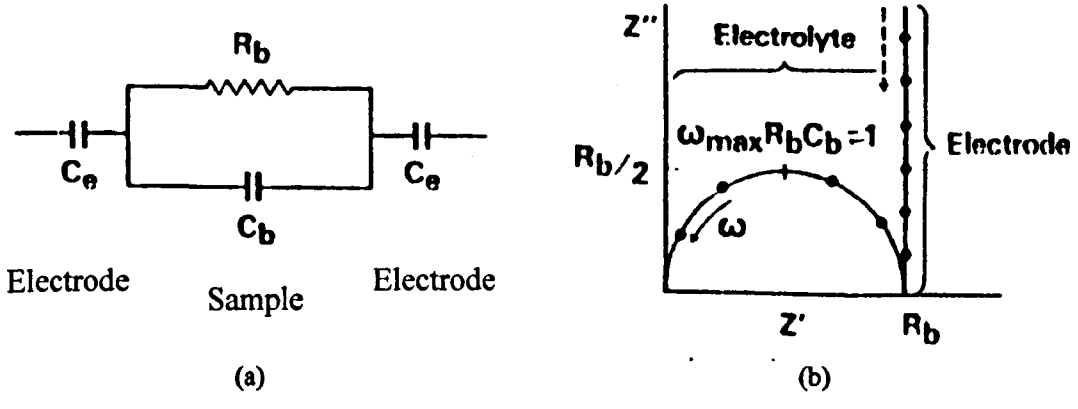

Fig. 4.10 (a) Schematic representation of the experimental arrangement for measurement of the dc conductivity of a glass. Typically $C_e = 10^{-6}$ Fcm^{-2}, $C_b = 10^{-12}$ Fcm^{-2}, $R_b = 10^2 - 10^8$ Ωcm. (b) Simulated complex impedance plot for the circuit in (a).

Appropriate manipulation of the acquired data can be used to determine information regarding the processes taking place within the sample. It is known that

conduction processes within the glass are thermally activated which can be described by Arrhenius behaviour below T_g, given by,

$$\sigma = \sigma_0 \exp\left(\frac{-E_A}{RT}\right) \tag{4.06}$$

where σ_0 is the conductivity at infinite temperature, E_A is the activation energy for conduction, R is the gas constant, and T is the temperature in Kelvin. A plot of log σ against 1/T has the gradient $(-E_A/RT)\log_{10} e$ and so the activation energy for conduction, i.e the energy required by the conducting ion to move through a potential barrier, can be determined.

A layer of platinum was deposited on both faces of the sample, providing a contact between the electrodes and the sample. It was decided to use platinum instead of the more usual gold coating due to prior evidence of gold diffusion into the sample at elevated temperatures. The sides of the samples were masked during electrode deposition to eliminate the possibility of short circuits. Fig. 4.11 shows the essential features of the conductivity jig design used to carry out the conductivity measurements. The equipment was originally designed and constructed at the Chemistry Department of Aberdeen University and a similar apparatus was built at the Physics Department of Warwick University.

The sample is pressed firmly between two ceramic discs, with a piece of gold foil inserted between the sample and each disc. Each gold electrode was attached to lengths of platinum wire connected to a Hewlett Packard 4192A Impedance Analyser, with a frequency range of 5Hz-13MHz, enabling a two-terminal impedance measurement to be made. The platinum wires were shielded by silica tubes to prevent stray capacitances and the whole arrangement fitted inside a large-bore pyrex tube, enabling the use of vacuum or other gas environments. A K-type thermocouple was positioned very close to the edge of the sample whilst an R-type thermocouple was used to monitor and control the temperature of the furnace. It was found that a typical sample did not begin to show signs of significant bulk conduction until the sample temperature was raised to approximately 185°C. Around ten measurements were made between 200°C and 400°C, for a frequency sweep of 5Hz-1MHz, with the results being interpreted using plots of modifier content against log σ, and Arrhenius (log σ v 1/T) plots.

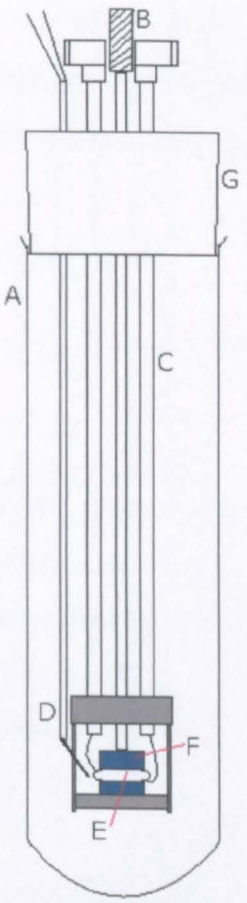

Fig. 4.11 Schematic of the ionic-conductivity jig design. A – pyrex glass tube, B – spring-loaded plunger, C – stainless steel tubes containing quartz glass tubes, D – sample thermocouple, E – sample, F – alumina spacers, G – rubber bung.

Fig. 4.12 shows an example of the variation in conductivity with frequency obtained from one of the mixed-modifier samples.

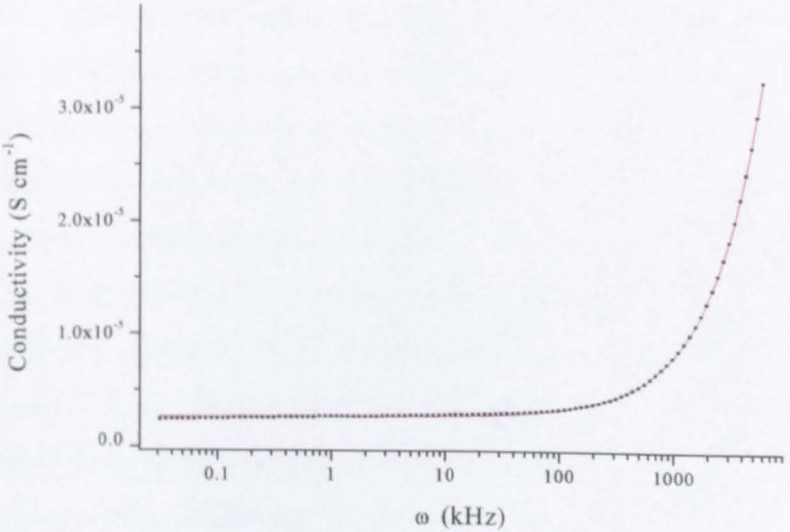

Fig. 4.12 An example of conductivity versus frequency used to determine the dc conductivity of the mixed-modifier glasses studied. The dc conductivity is found from fitting Eq. 4.07 (shown in red)

The data collected from each sample was fitted to Eq. 4.07, representing the ac (frequency dependent) conductivity of many materials (σ_{ac}) and enabling the dc (frequency independent) part of the conductivity (σ_{dc}) to be measured.

$$\sigma_{ac} = \sigma_{dc} + A\varpi^{S} \tag{4.07}$$

4.2.3 Chemical durability

4.2.3.1 Leach testing

The ability of the different glass compositions to withstand prolonged, moderate-temperature, dynamic water corrosion is naturally of concern as the final storage environment of the glass wasteform will present all three of these factors. This effect was simulated using a leach testing method [8] based on the International Standard Soxhlet Leach Test Procedure (ISO/TC85/SC5/WG5/N37). There were three main analytical stages involved:

1. Sample weight loss was monitored
2. Leachate pH was determined.
3. Elemental analysis of leachate was performed.

A schematic diagram of the soxhlet apparatus is shown in Fig. 4.13. The samples were first polished to the same standard as the ionic conductivity, viscometry and radiation exposure tests. They were then washed in acetone, dried in an oven and weighed. Sample dimensions were determined from an average of three measurements of sample thickness and diameter. An optical micrograph of each sample was taken prior to leaching to provide a comparison with the leached sample.

To begin the test, each round-bottomed flask was filled with 300ml of distilled water and a sample placed at the bottom of each soxhlet cup. The apparatus was connected as shown and the cooling water turned on. Isomantles were used to heat the water at a constant 100°C, which resulted in the sample experiencing a temperature of 75°C. A 'blank' was run alongside each set of samples to allow determination of the contribution to the leachate from the experimental apparatus itself. After two weeks, the isomantles were switched off and leachates allowed to cool, before pH measurements were made using standard pH 7 and pH 10 buffer

solutions, and a Hanna Instruments HI-931410 pH/mV meter. When all the leachates had been collected, they were acidified with 2.5M nitric acid to a final pH of approximately 2.7 and analysed using XRF for the presence of sodium and lithium [1].

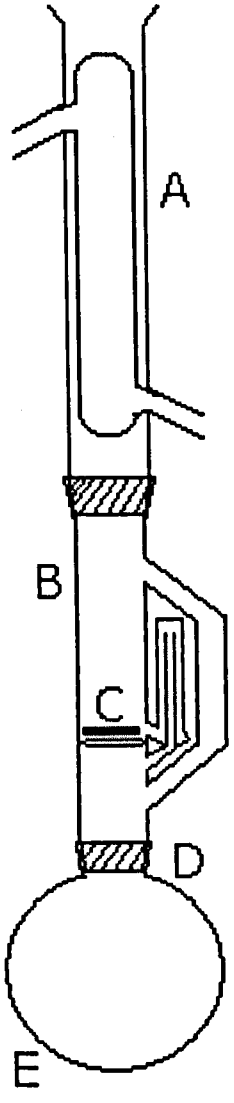

Fig. 4.13 Leach testing apparatus, detailing A – condenser, B – soxhlet, C – glass sample, D – flask, E – heat. Each sample was tested for 14 days at 75°C.

4.2.4 Radiation testing

4.2.4.1 Cyclotron irradiation

Widespread use of various kinds of radiation has been made in an attempt to simulate, over short timescales, those radiochemical processes and effects that are expected to occur over the lifetime of the wasteform. As highlighted in Chapter 3, the current typical wastestream contains elements that are considerable sources of

alpha and beta radiation and the effect of this radiation on the wasteform must be anticipated and countered. In particular, Cm^{242} produces 5.5MeV alpha particles via the alpha decay process shown in Eq. 4.08,

$$Cm_{96}^{242} \xrightarrow{\alpha\text{-}decay} \alpha_2^4 + Pu_{94}^{238} \qquad (4.08)$$

The subsequent interactions of the emitted alpha particles with components of the wasteform are of great importance. The future use of higher burn-up fuel presents further problems as the concentration of radiation sources in the wastestream is increased and any damage mechanisms or interactions occur at a faster rate.

All compositions in the NBS series and La-doped NBS series were irradiated with α-particles to simulate the effect of the decay processes of waste elements such as Cm^{242} and Am^{241}. The irradiations were carried out at Birmingham University on their Radial Ridge Cyclotron facility, which is capable of producing 25MeV α-particles. To simulate realistically the effects of the decay processes, the beam was reduced to 5.5MeV using aluminium or tantalum foils of the required mass-density (determined as shown in Appendix B), placed immediately in front of the sample. To prevent overheating and melting of the 1mm-thick sample, a water-cooled backing plate was incorporated into the design of the sample holder. Samples were irradiated at a range of beam currents depending on their thicknesses. Any charge incident on the sample was detected by a Brookhaven Model 1000c Integrator. This then allowed the total dose given to each sample to be calculated by the following equation:

$$\text{Total dose} = \text{No. of } \alpha\text{-particles incident on sample} = \frac{I*(2*10^{-8})}{C_\alpha} \qquad (4.09)$$

where I is the integrator reading at the end of the irradiation, $(2*10^{-8})$ is an instrument scaling factor and C_α is the charge on an α-particle. An estimate of the total dose can also be calculated from the knowledge of the applied beam current and irradiation time. The total dose was converted into the dose $gram^{-1}$ or dose cm^{-3}, depending on the analysis required.

Estimates of the activity of HLW waste over the period of its lifetime show that this cumulative dose corresponds to a period of storage from several tens to several hundreds of years, depending on the type of waste considered (see Chapter 3, section 3.2.1). Post-irradiation, the samples were allowed to 'cool' before either being monitored using a γ-ray Ge-scintillator or stored for electron spin resonance (ESR) analysis. Figures 4.14 and 4.15 show a photograph of the cyclotron beamline and a schematic representation of the target assembly.

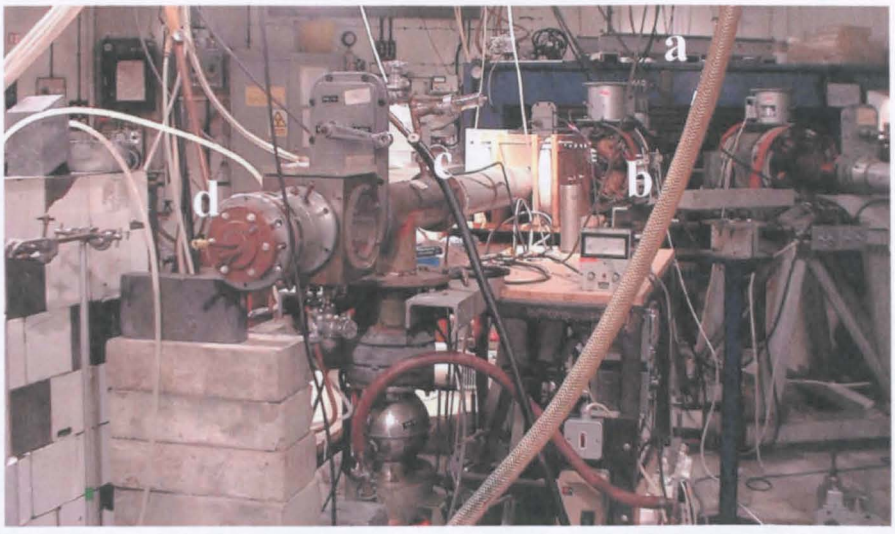

Fig. 4.14 Photograph of the beamline used in the irradiation studies, indicating a) main bending magnet, b) focussing quadrapole magnet, c) sweep coils and d) target

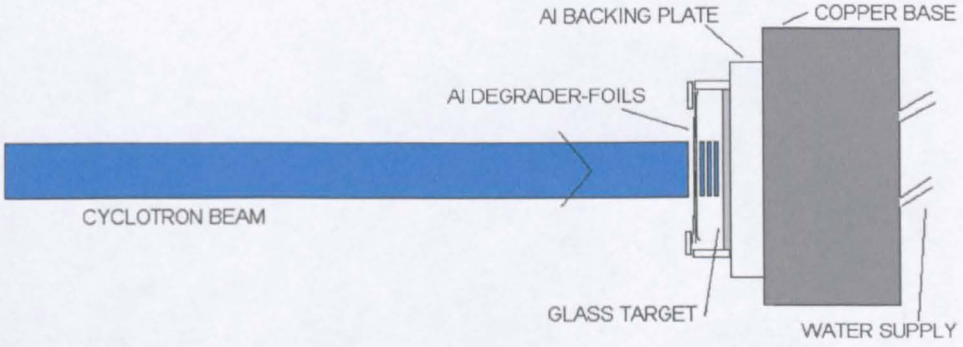

Fig. 4.15 Schematic representation of the sample irradiation target assembly, indicating the positions of sample, energy degrading foils and cooling system.

4.2.4.2 Electron Spin Resonance (ESR) spectroscopy

As discussed earlier in Chapter 3, exposure of a solid to high-energy radiation can lead to the formation of point defects within the glass network. It is true that many point defects are paramagnetic and so their nature and behaviour can be studied by means of their ESR spectra. Vacancies produced by ballistic

processes, impurities, interstitial atoms and trapped hole centres can all be used to probe the extent of irradiation damage in a solid.

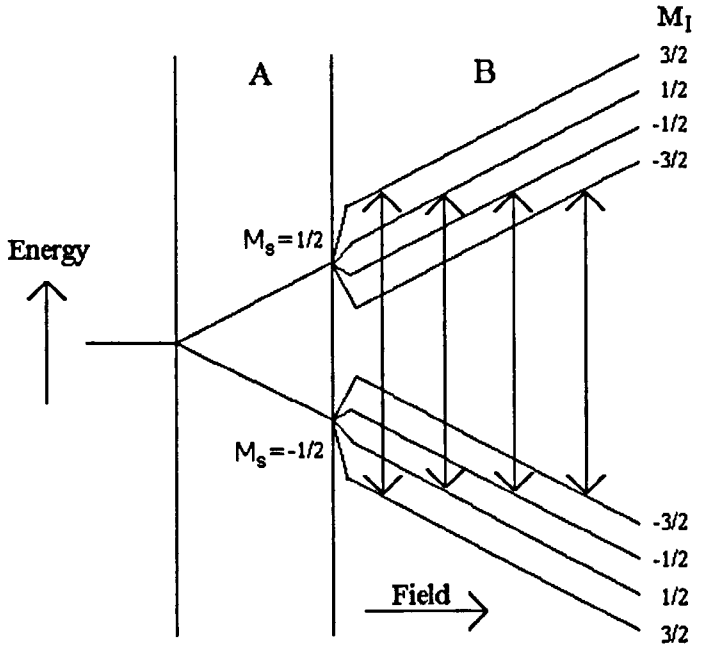

Fig. 4.16 Schematic representation of the available electron spin-states, $\Delta M_s = \pm 1$, and the subsequent Zeeman and hyperfine splitting used in ESR spectroscopy for a spin ½ nucleus.

Essentially, ESR spectroscopy utilises the fact that unpaired electrons in a material will interact with an applied field, producing a change in the energy state of the electrons. As with NMR theory, we can define the magnetic dipole moment, μ, of a species as:

$$W = -\mu.H \tag{4.10}$$

where **W** is the energy of the dipole and **H** is the magnitude of the magnetic field. From quantum theory, we know that an isolated electron with spin quantum number S=½ may align its spin parallel or anti-parallel to the applied magnetic field. We can consider the electron to possess only spin angular momentum and so Eq. 4.10 can be written as,

$$W = g\beta H M_S \tag{4.11}$$

where $\mathbf{M_s}$ is the quantised value of spin angular momentum in the direction of **H**, g is the electronic g-value and β is the Bohr magneton, $\beta = eh/4\pi m_e$. Application of an electromagnetic field of appropriate frequency, ν, can induce transitions between the two Zeeman levels if the photon energy, hν, matches ΔW, the energy level separation. Then,

$$\Delta W = h\nu = g\beta H_r \tag{4.12}$$

where H_r is the magnetic field at which the resonance condition is met.

ESR spectra were acquired at a centre field of 3.485kG and sweep width of 300G. Microwaves of X-Band frequency were used, at approximately 9.7GHz, with modulation amplitude of 10G and microwave power of 1mW. All samples were swept five times to produce the final spectrum. Fig. 4.17 gives a schematic description of the essential elements of the ESR spectrometer.

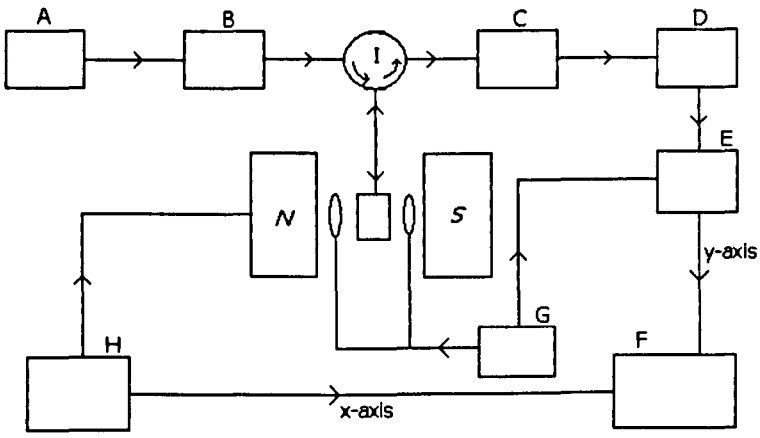

Fig. 4.17 Schematic representation of modern ESR spectrometer. A – microwave source, B – attenuator, C – microwave detector, D – amplifier, E – phase-sensitive detector, F – recorder, G – modulation power and reference, H – magnetic field power and sweep, I – circulator.

4.2.4.3 UV-Visible Spectroscopy

The UV-Visible spectra were obtained on a Varian DMS 90 UV/Visible spectrophotometer using a deuterium arc lamp (190-350nm) and tungsten halogen lamp (350-900nm). Some samples were measured after irradiation in a cyclotron with 5.5MeV α-particles, whilst other samples received a post-irradiation treatment with a ~100W UV lamp operating at 252nm. After various irradiations and thermal

treatments, the samples were analysed in the spectrophotometer and the transmittance recorded over the 190-900nm range.

4.3 References

[1] CERAM Research Ltd, Queens Road, Penkhull, Stoke-on-Trent, ST4 7lQ, England.

[2] P. T. Callaghan in Principles of Nuclear Magnetic Resonance Microscopy, Clarendon Press, Oxford (1991) p.49

[3] R. Dupree & D. Holland, Glasses and Glass-Ceramics, edited by M H Lewis, Chapman & Hall (1989) p.5

[4] D. Massiot, dmfit #20000916, http://crmht.cnrs.orleans.fr/Pole1/ThemeDM/structureDynamique.html

[5] C. M. Mari, Solid State Ion. **12** (1984) p.419

[6] M. D. Ingram, Materials Science and technology: A Comprehensive Treatment **9**, edited by J. Zarzycki, (1991) p.719

[7] D. E. Day, J Non-Cryst. Solids **21** (1976) p.343

[8] High Temperature Processes – Leach Tests, BNFL Research and Technology Operating Instruction HTP 07, Issue 2 (12/99)

Chapter 5 – Physical & Structural Characterisation

5.1 NBS series

5.1.1 Composition details

The base composition, MW, used as a starting point for the study is shown in Table 5.01, alongside the variations to this composition also used in the chemical durability and irradiation experiments.

			Mol% content							
NBS	K	R	SiO_2		B_2O_3		Na_2O		Li_2O	
			a	b	a	b	a	b	a	b
11	-	-	74.42	74.48	0.00	0.05	12.95	12.54	12.69	12.36
7	7.94	2.72	68.1	70.99	8.57	8.55	11.8	8.65	11.56	11.79
6	4.90	1.65	64.33	64.90	13.57	13.24	11.2	10.91	10.93	10.94
MW	3.26	1.12	60.61	60.61	18.57	18.57	10.55	10.55	10.3	10.3
8	2.51	0.82	56.88	57.91	23.57	23.07	9.9	9.51	9.67	9.49
14	1.51	0.53	55.39	49.65	25.57	32.84	9.64	8.81	9.41	8.68
9	1.4	0.48	53.16	49.88	28.57	33.88	9.25	8.11	9.03	8.13
10	1.23	0.53	49.44	44.5	33.57	36.3	8.6	12.1	8.4	7.0

Table 5.01 Mol% compositions of NBS series samples. Note: a – nominal composition, b – analysed composition (± 1% of value)

5.1.2 Structural characterisation

5.1.2.1 NMR spectroscopy

a) ^{11}B NMR – spectra

Fig. 5.01 shows the ^{11}B NMR spectra obtained from the NBS series glasses. The B_4 peak in each NBS glass exhibits a chemical shift ranging between 0.54 and –1.17 ppm, whilst there are two distinct features visible at approximately +12 and +15 ppm, respectively. Other studies have referenced their ^{11}B NMR data to $Et_2O:BF_3$ and assigned the contribution from the tetrahedral boron site in pyrex a chemical shift of +1.8 ppm. Hence, to compare the current work with any other, a factor of 1.8 ppm must be added to the observed chemical shifts. The variation in shift of the B_4 peak can be considered within the bounds of experimental error, though the gradual negative shift of the B_4 signal from 0.54 to –1.17 ppm could be explained by the observation of van Müllen and Müller-Warmuth [3] that the isotropic chemical

shift of the BO_4 unit becomes more negative if it is surrounded by other $[SiO_4]$ and $[BO_4]$ tetrahedra rather than by trigonal polyhedra. Since the fraction of trigonal boron atoms decreases and the silica content increases as we move from NBS 10 to NBS 11, increasing numbers of silica and boron tetrahedra will be available to produce these conditions, as reported in other studies [3]. Other workers [4] have attempted to fit the complex trigonal signal in several Na-borosilicate glasses using multiple peaks, corresponding to the symmetric and asymmetric BO_3 units described in Chapter 2. Computer simulations of these two sites were reported to give values of +17.2 and +12.9 ppm (referenced to $Et_2O:BF_3$) for the isotropic chemical shifts of the symmetric and asymmetric $[BO_3]$ units respectively.

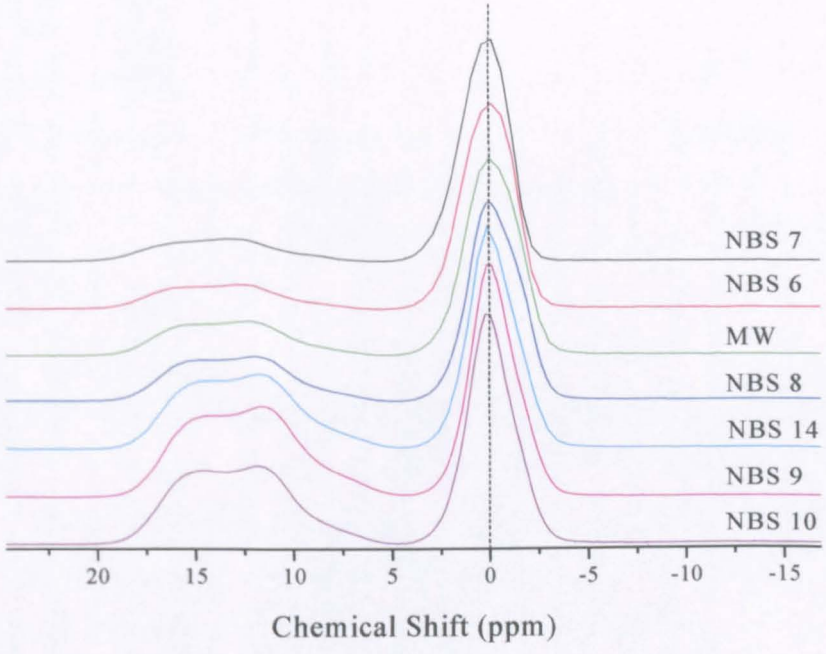

Fig. 5.01 ^{11}B MAS NMR spectra of NBS glasses (normalised and shift referenced to pyrex).

A deconvolution of the contributions to each NBS spectrum has been carried out, assuming the presence of one tetrahedral site and two trigonal sites, all exhibiting a quadrupolar interaction. The values of the isotropic chemical shift, δ_I, quadrupolar coupling constant, Q_{CC}, and asymmetry parameter, η, were recorded and are shown in Appendix C. The shift values reported by Bunker *et al.* lie close to the +18 ±1 and +15 ±1 ppm shift values observed in the NBS glasses, suggesting that these peaks also arise from symmetric and asymmetric $[BO_3]$ sites. Some modification of the local environment surrounding them could lead to the less positive chemical shifts of these peaks, such as the shielding effect of silicon in the

second coordination sphere. There is an inherent difficulty in resolving the B_3 signal into its individual contributions as there is a high degree of overlap between each peak. The lack of spectral features at low B_2O_3 concentrations makes it almost impossible to generate a unique fit to the data.

b) ^{11}B NMR – B_3/B_4 co-ordination

The fractions of tetrahedrally coordinated boron atoms, N_4, were calculated from the NMR spectra as described in Chapter 4, and are summarised in Fig. 5.02. To allow meaningful comparison of the results, N_4 has been plotted as a function of the ratio of silica to boron oxide, K, and modifier oxide to boron oxide, R, in addition to simple boron oxide content.

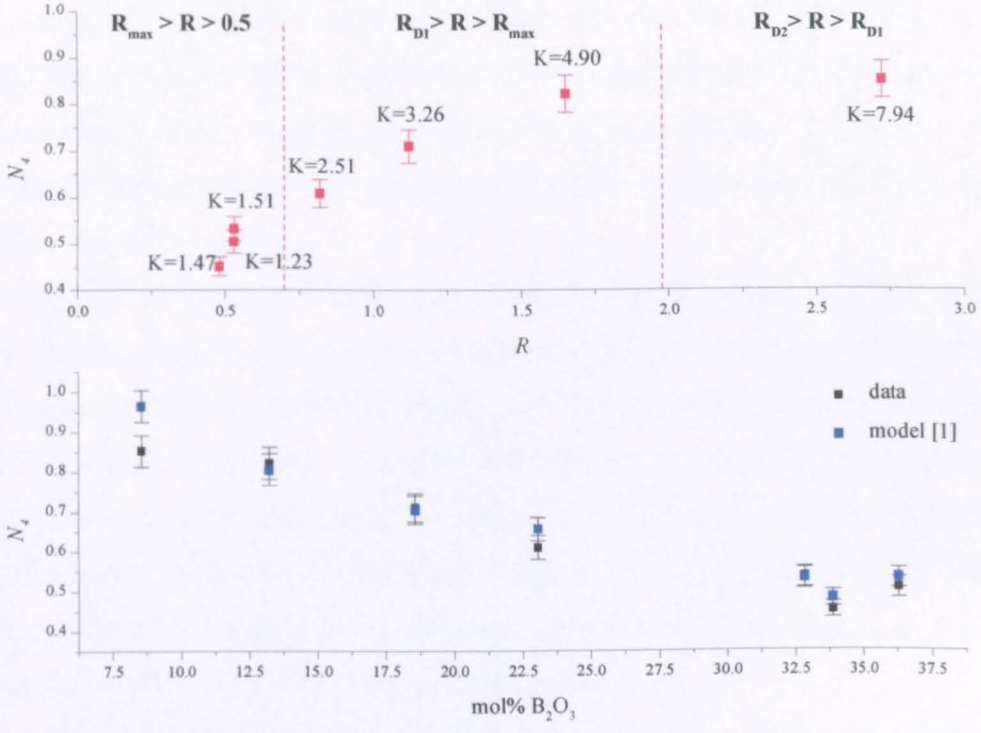

Fig. 5.02 Change in fraction of tetrahedral boron units with addition of B_2O_3 to the NBS glasses.

It can be seen from Table 5.01 and Fig. 5.02 that the introduction of increasing amounts of B_2O_3 into the mixed-modifier silicate composition, NBS 11, leads to a gradual decrease in the fraction of tetrahedrally coordinated boron atoms present in the glass. This can be explained by the fact that the continued replacement of silica and modifier atoms by boron will eventually lead to a 100% B_2O_3 glass,

already known to consist entirely of trigonal [BO_3] groups in the form of individual [BO_3] units and boroxol rings [2]. Since a decrease in the fraction of tetrahedral boron units leads to a decrease in the *connectivity* of the glass network, the physical and chemical durability of the glass should decrease accordingly. Other properties such as glass transition temperature should also be influenced by the structural reorganisations that take place as the composition of the glass changes.

Also shown in Fig. 5.02 are the N_4 fractions predicted by the model of Dell and Xiao [1], indicating that good agreement exists between the data obtained from the mixed-modifier NBS glasses and the currently accepted single-modifier borosilicate model at these compositions. With reference to the Na-borosilicate model of Dell [1], it is possible to speculate as to the types of structural units in existence.

Samples NBS 10, 14 and 9 (K = 1.23, 1.51 and 1.4) lie within the $0.5 < R < R_{max}$ composition region where, according to the model, the formation of reedmergnerite ($NaBSi_4O_{10}$) borosilicate units has just started. The similarity of the compositions of these samples and the fact that N_4 is directly proportional to the modifier content up to the diborate composition ($R = 0.5$) accounts for the change in the observed values of N_4.

In addition, samples NBS 8, MW and NBS6 (K = 2.51, 3.26 and 4.90) lie within the ($R_{max} < R < R_{d1}$) composition region in which the added modifier does not produce an increase in tetrahedral borate units but is assumed to be associated with NBOs on silicate tetrahedra. The observed increase in N_4 can be explained by the fact that as the K of the glass increases, so does the threshold of R at which the added modifier stops creating [BO_4] units and instigates the production of reedmergnerite units. The expected change in N_4, according to the model, is shown in Fig. 5.02 and agrees very well with the observed experimental results.

Sample NBS 7 (K = 7.94) lies within the ($R_{d1} < R < R_{d2}$) composition range, wherein added modifier continues to associate with NBOs on silicate tetrahedra until such point as the network is saturated. The addition of further modifier leads to the formation of asymmetric trigonal borate units with one, two or three NBOs. The experimental value of N_4 for this sample shows the greatest deviation from the model. As will be shown in Chapter 7, over a greater range of K and R values, the experimental data for the mixed-modifier borosilicate system deviates from the Dell

model after R_{dl} for all K series. This suggests differences between the two systems in the structural rearrangements taking place.

5.1.3 Physical properties

5.1.3.1 Glass transition temperature (T_g) and thermal expansion coefficient (α)

Fig. 5.03 illustrates the details of the DTA spectra for all NBS samples. The glass transition temperature of each glass is visible at approximately 773 K, the known T_g of the MW composition.

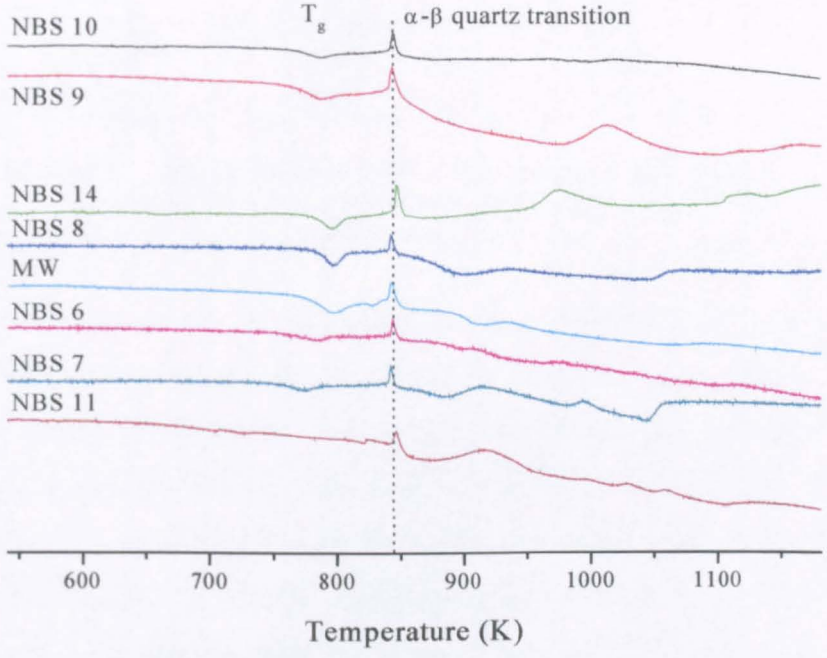

Fig. 5.03 DTA spectra for the NBS series of glasses

It can be seen from Table 5.02 that the change in composition from NBS 7 to NBS 8 leads to an increase in T_g of ~30 K, well outside the bounds of experimental error. At first thought, this behaviour seems somewhat anomalous since we have shown that the connectivity of the glass network is anticipated to decrease with the reduction of N_4, leading to a subsequent decrease in T_g. It is also interesting that samples NBS 14 and NBS 9 exhibit T_gs that differ by ~17 K, despite having compositions that differ by only 1 mol% in each component and N_4 values of 0.48 and 0.53, respectively. Much research by several workers [5,6] has concentrated on investigating the effect of adding modifier to sodium borosilicate glasses. Eventually, the added modifier introduces non-bridging oxygens on the silica

tetrahedra, leading to depolymerisation of the glass network. It is highly likely that the competing processes of increasing N_4 and conversion of silica Q^4 units to Q^3 and Q^2 units account for the unusual variation in T_g, with the change being dominated by the silica unit speciation.

Sample	T_g (K) (± 4K)	$\alpha_{100\text{-}300}$ (MK^{-1}) (± 0.4)
NBS 10	767 (756)*	8.21
NBS 9	762	7.15
NBS 14	779	7.02
NBS 8	783 (785)*	7.67
MW	772	8.44
NBS 6	755 (767)*	8.47
NBS 7	754	9.33
NBS 11	701*	11.4

*Table 5.02 Thermal properties of the NBS compositions deduced from DTA spectra and dilatometer measurements. * - T_g obtained from dilatometry.*

If it is assumed that all the added modifier which is not associated with tetrahedral boron units is used to create non-bridging oxygens (NBOs) on silica tetrahedra, it is possible to use the ^{11}B NMR N_4 data obtained to calculate the total non-bridging oxygen content. Since, for sample NBS MW, N_4 = 0.69, then 12.8mol% modifier oxide is presumed to be associated with tetrahedral boron sites, leaving the remaining 8.04mol% modifier oxide to be associated with other structural units. For the majority of samples, this can be assumed since their compositions place them in regions within which no NBOs on borate units are expected to form. Hence, data for sample NBS 7 has not been included in Fig. 5.04 showing how T_g and the thermal expansion coefficient change for each sample as the number of oxygens that are NBOs on each silicon tetrahedron varies.

It is unsurprising that sample NBS 11 shows the lowest glass transition temperature and largest corresponding number of NBOs per silicon atom. This composition contains no B_2O_3 so the modifier available must be associated with NBOs on silicate tetrahedra, depolymerising the glass network and, consequently, reducing T_g.

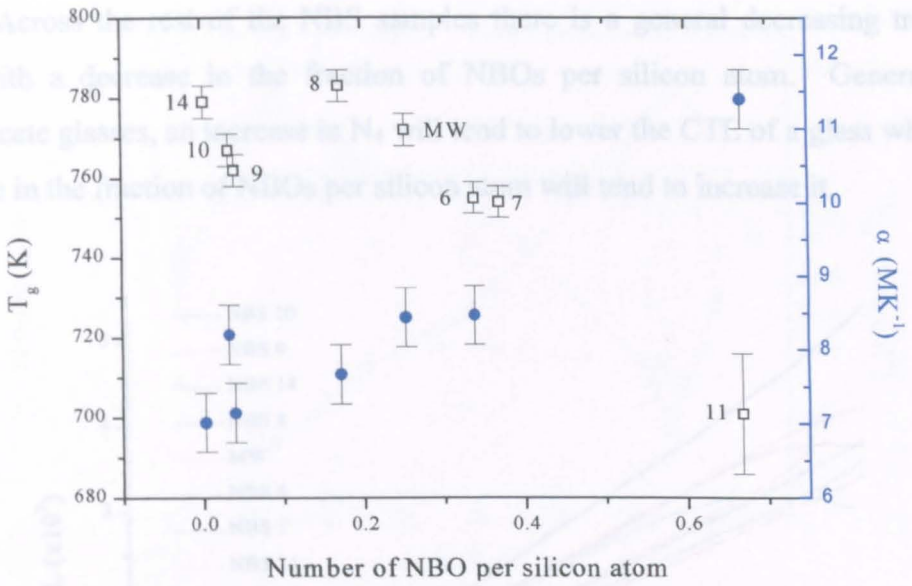

Fig. 5.04 Comparison across the NBS series of the change in T_g (□) and CTE (•)with the average number of NBOs associated with silicate tetrahedra.

Sample NBS 7 can again be considered independently of the other NBS compositions since its analysed composition places it in the ($R_{d1} < R < R_{d2}$) region of the Dell model. Since it is unknown whether the modifier remaining after conversion of $[BO_3]$ units to $[BO_4]^-$ units is associated with the silicate network, calculation of the number of NBOs/Si cannot be made for sample NBS 7.

Samples NBS 8, MW and NBS 6 are found in the ($R_{max} < R < R_{d1}$) model region and although the value of N_4 increases NBS 8 > MW > NBS 6, the transition temperature decreases in the same order. It is known that N_4 is a strong indicator of the trend in T_g but in the case of these compositions the dominating process must be the decrease in NBOs per silicon atom concentration.

Finally, samples NBS 9, NBS 14 and NBS 10 lie within the ($R < R_{max}$) model region. NBS 14 exhibits the largest value of T_g of the three samples since although the concentration of tetrahedral boron units is approximately equal in each glass, the difference in modifier content results in an increasing number of NBOs associated with silicate units, in the order NBS 14 < NBS 10 < NBS 9.

Similarly, the trend in coefficient of thermal expansion can be explained most easily if both N_4 and NBOs/Si are considered together. Sample NBS 11 exhibits by far the largest CTE since it contains no B_2O_3 and hence the largest fraction of NBOs per silicon atom, leading to a greater degree of freedom within the network.

Across the rest of the NBS samples there is a general decreasing trend in CTE with a decrease in the fraction of NBOs per silicon atom. Generally in borosilicate glasses, an increase in N_4 will tend to lower the CTE of a glass whilst an increase in the fraction of NBOs per silicon atom will tend to increase it.

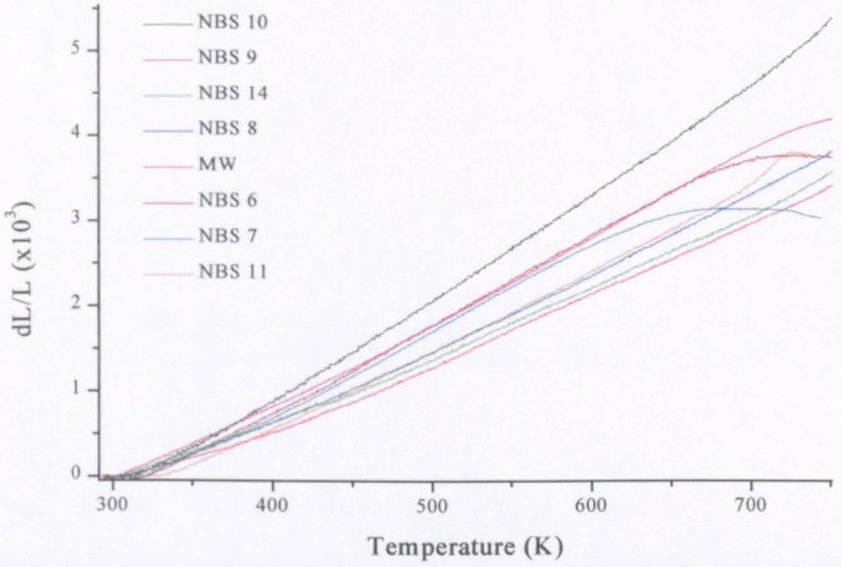

Fig. 5.05 Comparison of the thermal expansion behaviour of the NBS glass compositions.

5.1.3.2 Density and molar volume

Fig. 5.06 shows how the density of the NBS glasses changes with boron content. According to the model of Feil & Feller [7] using the NMR fractions of Dell, Bray & Xiao [1], density changes may be described by accounting for the changes in abundance, volume and mass of the individual borate and silicate units hypothesised to exist at various compositions. It is possible to compare the densities predicted by Feil & Feller with the current data, making a few assumptions regarding the distribution of the modifier species in the glass. This has also been included as the red data points in Fig. 5.06. It can be seen from Fig. 5.02 that the N_4 value for these glasses corresponds closely to the accepted ^{11}B NMR model. This leads to the suggestion that the observed differences between the model and experimental data arise as a result of incorrect assumptions regarding the concentration of NBOs on the silica tetrahedra and perhaps the way in which the modifier atoms apportion themselves between the individual silicate and borate species. At the same time, it is reasonable to state that the only sample that shows a large deviation from the model is NBS 6.

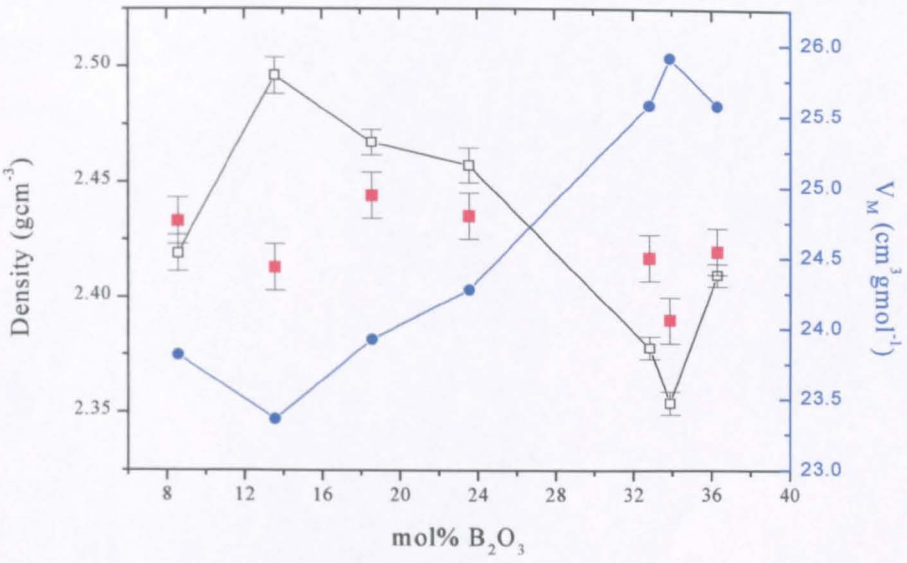

Fig. 5.06 The variation in density of the NBS glass samples with boron content. Theoretical densities from [7] and the corresponding change in molar volume, V_M, are also shown.

5.1.4 Chemical durability

5.1.4.1 Leach testing - introduction

The chemical durability of the chosen wasteform is of prime importance in the isolation of nuclear waste as it is the major barrier to the release of toxic elements and radionuclides into the surrounding area. The process of corrosion of the isolating material can be simulated using a soxhlet apparatus, as described in Chapter 4.

a) Chemical analysis and pH

Fig. 5.07 shows the results of chemical analysis of the leachates produced by soxhlet tests of several NBS glasses. Under the conditions of the leaching process the amount of modifier leached from the samples increases with boron content. Sample NBS 9 is the exception to this, with less modifier being leached than sample NBS 8. Both samples NBS 7 and 6 have only trace amounts of Li and Na in their leachate after 14 days leaching at 75°C, indicating that they are at least as resilient as commerical pyrex. This is reflected in the condition of the samples as described in Table 5.03. The pH of the leachates was measured after the samples had cooled and in all cases was more alkaline than that of the blank run alongside each sample. Sample NBS 11, containing no B_2O_3, showed the greatest change in pH, as did its corresponding blank, though the physical effects were not as pronounced as other samples exhibiting large changes in pH. Sample NBS 10 was attacked most readily,

with large amounts of Li and Na being leached from the glass and very little sample remaining at the end of each of the tests.

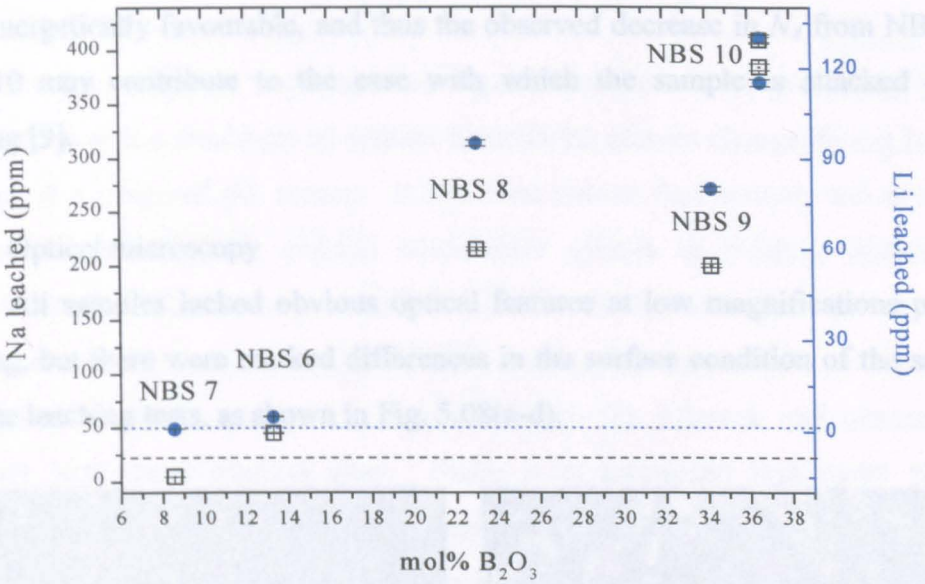

Fig. 5.07 Variation in the quantity of leached material detected by chemical analysis of leachates from glasses NBS 6, 7, 8, 9 and 10. Dashed lines indicate quantity of material leached from glassware of apparatus: --- - Na; --- - Li.

Though no chemical analysis methods were employed to detect the amount of boron leached from each of the samples, a substantial amount, if not all, was obviously removed from samples NBS 14, 10, and 9.

Sample ID code	*pH (± 0.2)*	*Condition of sample after leaching*
NBS 7B	8.10	no noticeable change, transparent
NBS 6A	8.80	scarred surface, opaque
NBS 10V	9.06	75% disintegrated
Blank for 7B, 6A, 10V	8.03	-
NBS8G	9.27	extensive wear, transparent
NBS 9D	8.97	completely disintegrated
NBS 10Y	9.12	completely disintegrated
Blank for 8G, 9D, 10Y	8.75	-
NBS 11H	10.06	cracked in two, abrasions, opaque
Blank for 11H	7.42	-
NBS 6C	-	slight wear, opaque
NBS 14F	-	severe attack, 50% disintegrated
Blank for 6C, 14F	-	-

Table 5.03 Details of changes to the pH and physical appearance of glass samples leached for 14 days at 348K.

In work on the leaching of sodium borosilicate glasses by Zhdanov, it is suggested that an increase in the concentration of boron-oxygen links (i.e. increasing N_4)

reduces the stability of the glass owing to the formation of a less compact silica skeleton [8]. However, the $[BO_3]$ and $[BO_4]^-$ structural units are hydrated by different mechanisms, the acceptor-donor hydration pathway of the $[BO_3]$ unit being more energetically favourable, and thus the observed decrease in N_4 from NBS 7 to NBS 10 may contribute to the ease with which the sample is attacked during leaching [9].

b) Optical microscopy

All samples lacked obvious optical features at low magnifications prior to leaching, but there were marked differences in the surface condition of the samples after the leaching tests, as shown in Fig. 5.08(a-d).

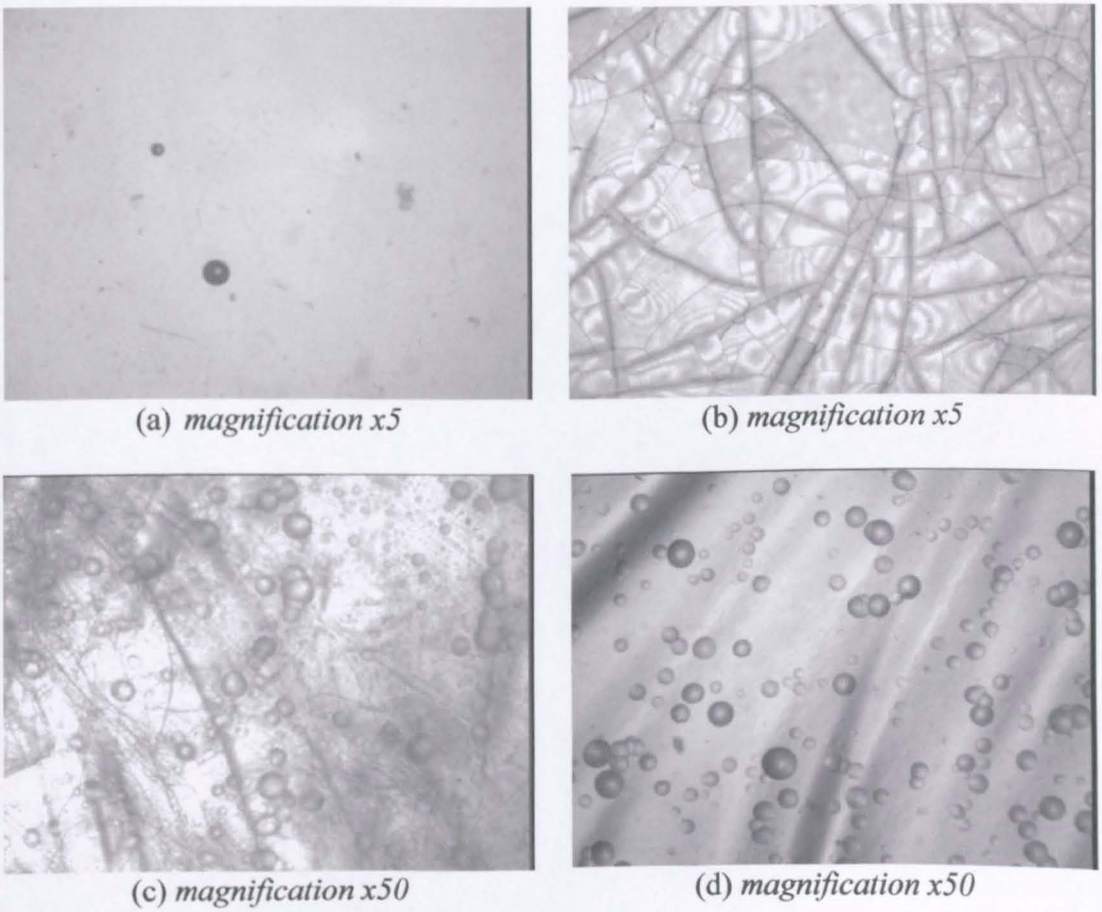

(a) *magnification x5*

(b) *magnification x5*

(c) *magnification x50*

(d) *magnification x50*

Fig. 5.08 Optical micrographs of (a) sample NBS 7B, (b) sample NBS 6A, (c) sample NBS 10V and (d) sample NBS 8G, after leaching for 14 days at 348 K

The sample of NBS 7B (Fig. 5.08(a)) used in the tests withstood the damage processes responsible for the near complete disintegration of sample NBS 10V (Fig.

5.08(b)), which showed extensive crazing features. The presence of bubbles was most marked in samples NBS 6A and NBS 8G.

c) ^{11}B NMR spectroscopy

Nuclear magnetic resonance techniques have been used previously [10] to investigate how the structures of sodium borosilicate glasses change during leaching in water at a range of pH values. It has been shown that sodium and boron are selectively removed from sodium borosilicate glasses to produce hydrosilicate leached layers [11]. Cross polarisation (CP) MAS methods have indicated that glasses leached in a solution of 0.1M HCl undergo an increase in the fraction of $[BO_3]$ sites as –O-H- groups are introduced into the network and preferentially associate with these trigonal sites. Since it is postulated that many physical properties of the final HLW isolation matrix are directly dependent on the short-range structural characteristics of the material, changes to the structure brought about by leaching processes should be anticipated and accounted for. Figs. 5.09(a-c) show, qualitatively and quantitatively, how the leaching process affects the ^{11}B NMR spectra.

It can be seen that there is little noticeable difference between the shapes of the leached and unleached samples and the relative fractions of the tetrahedral and trigonal boron sites, though the intensities of the peaks vary. Any effects induced by interaction of the leaching agent with the surface of the sample are probably masked by the dominance of the bulk sample material.

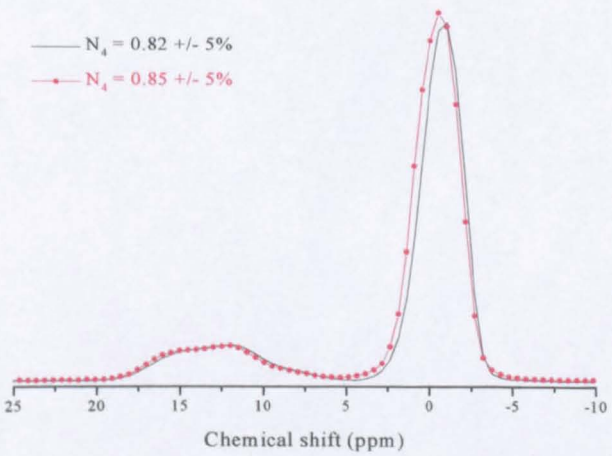

(a) NBS 7

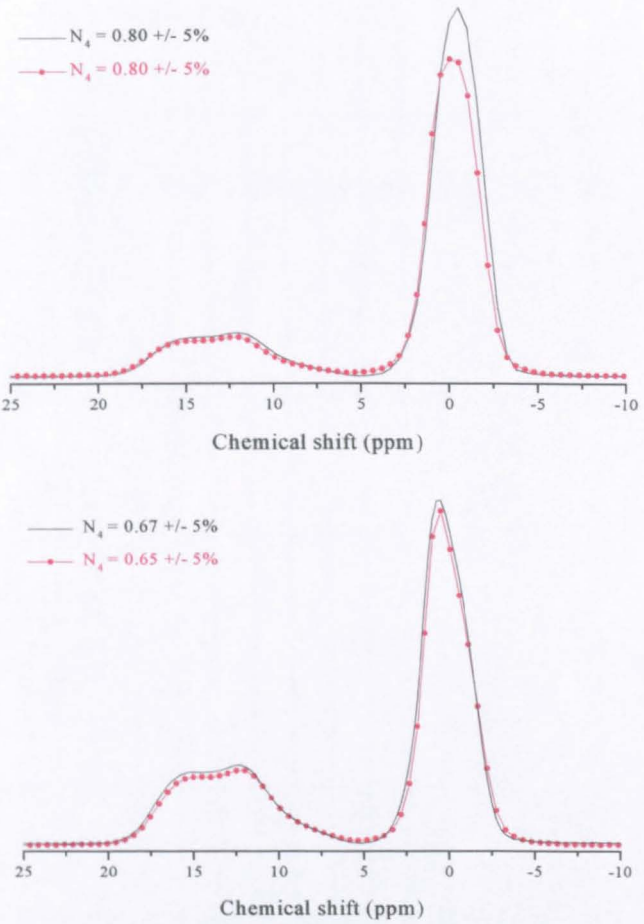

Fig 5.09 Comparison of the ^{11}B NMR spectra of samples NBS 7, 6 and 8 before and after leaching in deionised water at 70°C for 14 days.

5.2 LBS series

5.2.1 Composition details

Samples used to simulate the effect on structure of a typical HLW component were prepared by adding 2.42, 4.84, 9.68 and 12mol% La_2O_3, respectively, to the base composition, MW. Full compositional details are shown in Table 5.04.

Glass ID	Mol% composition					
	SiO_2	B_2O_3	Na_2O	Li_2O	La_2O_3	N_4
LBS 1	59.1	18.12	10.29	10.04	2.42	0.69
LBS 2	57.67	17.67	10.03	9.80	4.84	0.62
LBS 3	54.74	16.77	9.53	9.30	9.68	0.54
LBS 4	53.34	16.34	9.28	9.06	12.00	0.51

Table 5.04 Mol% compositions of La-doped LBS samples.

5.2.2 Structural characterisation

5.2.2.1 NMR spectroscopy

a) ^{11}B NMR – spectra

The ^{11}B MAS NMR spectra obtained from the four LBS samples are shown in Fig. 5.10.

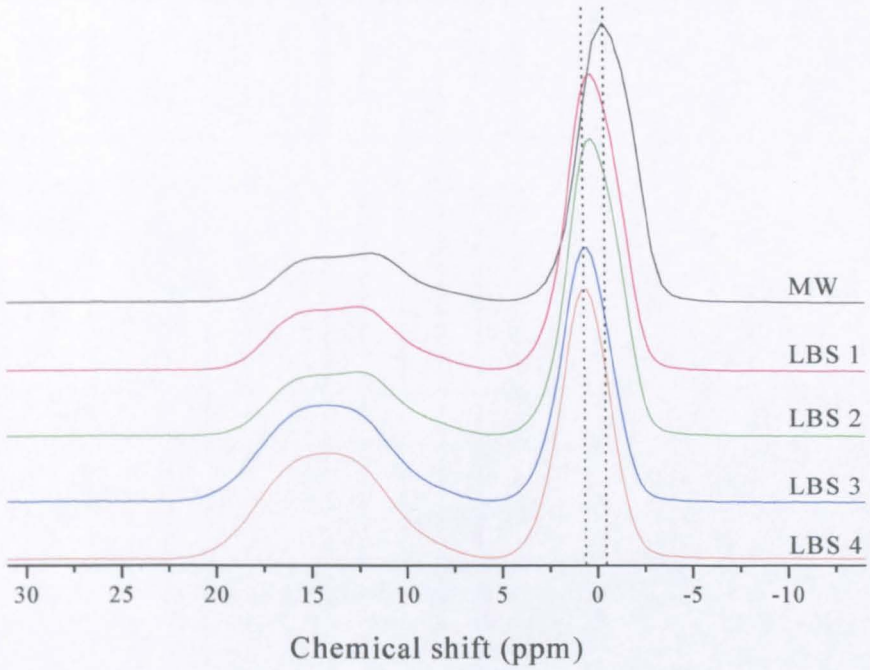

Fig. 5.10 ^{11}B MAS NMR spectra of the La_2O_3-doped MW glass.

The ^{11}B NMR spectra of the LBS glasses exhibit features similar to those seen in the NBS series. However, samples LBS 3 & 4 display a markedly different spectrum, with one broad, featureless peak from B_3 units. All sample spectra were obtained in the same experimental session so this effect is real and not a consequence of experimental inaccuracy. The difficulties encountered in the deconvolution of individual contributions to the B_3 signal for the NBS series are also present in the LBS series, even more so for samples LBS 3 & 4. The suggestion, discussed in further detail in Chapter 7, that there also exists a contribution to the trigonal B_3 site from linkages other than the expected B-O-B linkages is also supported by the ^{11}B NMR spectra of the LBS glasses. Possible explanations for the change in shape of the $[BO_3]$ signal at high La_2O_3 concentrations will be discussed later.

b) ^{11}B NMR – B_3/B_4 co-ordination

The change in boron coordination of the MW composition, upon the addition of La_2O_3, is illustrated in Fig. 5.11. As the proportion of La_2O_3 in the glass increases, the fraction of tetrahedrally co-ordinated borons, N_4, decreases.

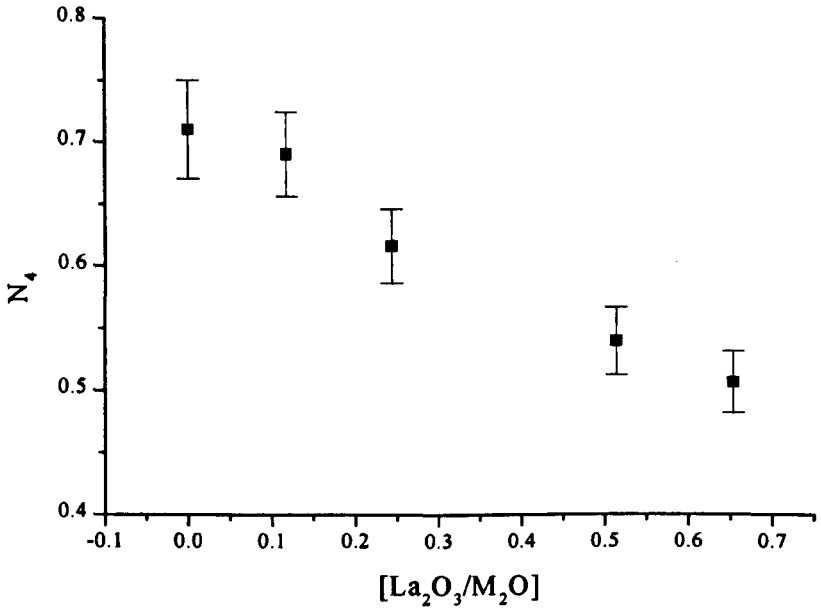

Fig. 5.11 The variation in the fraction of tetrahedrally co-ordinated boron atoms in the MW composition. with increasing amounts of La_2O_3.

Related work by El-Damrawi *et al* [12] on Na_2O-Al_2O_3-B_2O_3-SiO_2 glasses has shown that the addition of Al_2O_3 to borosilicate glasses slows the conversion to BO_4 units to an extent dependent on the molar ratio of $[Al_2O_3]/[M_2O]$. They therefore conclude that the oxygen ions provided by the modifier are consumed first for the formation of the $[AlO_4]^-$ unit. Alongside this observation, the addition of Al_2O_3 to silicate glasses has been shown to reduce the concentration of NBOs and lead to the formation of -Al-O-Si- linkages [13]. It would be useful know the amount of added modifier that is associated with the silicate network and hence work out the amount of R_2O available to create the equivalent $[LaO_4]^-$. If we assume that the La_2O_3 behaves in an analogous fashion to Al_2O_3 then network units of the form $[LaO_4]^-R^+$ could be formed, leading to the consumption of R^+ which would otherwise be involved in $[BO_4]^-R^+$ or $Si\text{-}O^-R^+$ units. Using the observed values of N_4 and making the assumption that all La_2O_3 does in fact form $[LaO_4]^-R^+$ units, it is possible to calculate the change to the proportion of Si in Q^3 units and hence see how the presence of La_2O_3 affects the predictions of the Dell model. The decrease in N_4

already indicates that R^+ are being removed from the borate network. If all the La_2O_3 is converted to $[LaO_4]^-R^+$ units, then an amount of modifier $R^a_2O = R_2O\text{-}La_2O_3$ is available to associate with the borate and silicate networks. It is known that the amount of modifier associated with the borate network is equal to $R^b_2O = N_4 * b$, where b is the amount of B_2O_3 in the glass, so the amount available to the silicate network, after the conversion of $[BO_3]$ to $[BO_4]^-$ units, is given by $R^{Si}_2O = R^a_2O\text{-}R^b_2O$, from which the number of NBO/Si atom can be calculated. Table 5.05 shows how the modifier would be distributed between the structural units as the La_2O_3 concentration increases, assuming all the La_2O_3 is converted to $[LaO_4]^-R^+$ units.

Mol% La_2O_3	N_4	R^a_2O	R^b_2O	R^{Si}_2O	NBO/Si
0	0.71	20.85	13.18	7.67	0.25
2.42	0.69	17.92	12.5	5.42	0.18
4.84	0.62	14.99	10.95	4.04	0.14
9.68	0.54	9.15	9.06	0.09	0.003
12.0	0.51	6.34	8.33	0	0

Table 5.05 Proposed sharing of alkali between the $[BO_4]$, $[LaO_4]$ and $[SiO_4]$ units.

Hence, if all the La_2O_3 is associated with modifier, there is a gradual decrease in the fraction of NBO/Si atom as the La_2O_3 concentration of the glass increases. This would result in a predominance of Q^4 units above ~9.7mol% La_2O_3. Glass stability is curtailed at 12 mol% La_2O_3 which may be a consequence of the lack of sufficient R_2O to charge compensate $[LaO_4]^-$.

c) ^{29}Si NMR

In order to be able to make more substantial comments regarding the structural role of La_2O_3 in these mixed-modifier glasses, ^{29}Si NMR was carried out on several LBS glasses doped with 0.1 mol% Fe_2O_3, the spectra of which are shown in Fig. 5.12. The results of the ^{29}Si NMR indicate that, as the amount of La_2O_3 in the glass increases, there is a small shift of the peak centre 'downfield', from –99 ppm to –89ppm. It is assumed that the MW composition has 0.26 NBOs per Si atom, corresponding to a Q^3:Q^4 ratio of approximately 1:3. This is due to the fact that its composition lies outside the Dell model region in which modifier is associated with NBOs on trigonal borate units and so any residual modifier oxide is assumed by Dell to be associated solely with silicon tetrahedra.

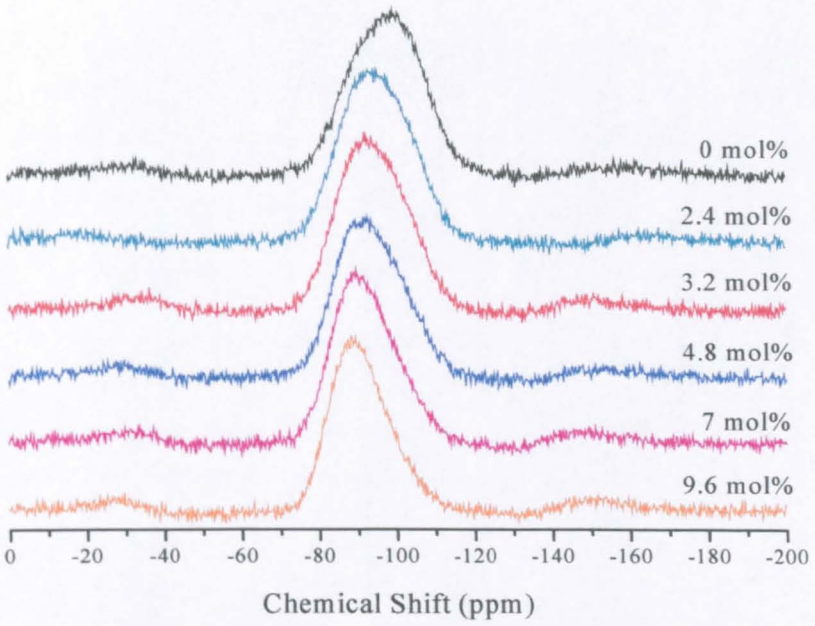

Fig. 5.12 ^{29}Si NMR spectra obtained from several glasses based on the MW composition and doped with La_2O_3.

Table 5.06 gives details of the peaks used to fit each of the LBS ^{29}Si spectra. The spectra were fitted satisfactorily with two gaussian peaks using only the widths of the peaks as linear constraints and it can be seen that the introduction of La_2O_3 into the composition leads to little change in the positions of the fitted peaks. In addition, the spectra were successfully simulated using three peaks representing contributions from Si-O-B, Si-O-La and Q^3 sites. These contributions were constrained by the stoichiometry arising from the conversion of the La_2O_3 to $[LaO_4]^-$, with any modifier remaining after the conversion of BO_3 to $[BO_4]^-$ producing NBOs on silicon tetrahedra. It is assumed that 1 La atom forms links with 4 silicon tetrahedra. Several structural scenarios involving the role of La_2O_3 can be envisaged that are restricted in their likelihood by the ^{11}B and ^{29}Si NMR results. It is known that the MW base glass lies within the $R_{max} < R < R_{D1}$ region of the Dell structural model, where the modifier goes to forming B_4 and introducing NBOs on the silicate tetrahedra only. If the La_2O_3 assumes a role similar to Al_2O_3 in forming $[LaO_4]^-$, then it might be expected that, alongside decreasing the rate of conversion of $[BO_3]$ to $[BO_4]^-$ units, the concentration of NBOs on Si would decrease with the formation of La-O-Si links.

La_2O_3 conc^n (mol%)	Unconstrained		Constrained	
	C of G of fitted peaks (± 1ppm)	Ratio of fitted peaks (± 10%)	C of G of fitted peaks (± 1ppm)	Ratio of fitted peaks (± 10%)
0	–102	66	–101	74
	–91	34	–89	26
2.4	–98	62	–99	66
	–90	38	–91	16
			–86	18
3.6	–100	45	(1)	(1)
	–89	55		
4.8	–99	35	–98	53
	–90	65	–89	33
			–88	14
7	–99	30	(1)	(1)
	–89	70		
9.6	–100	26	–98	30
	–89	74	–88	70

(1) ^{11}B NMR data unavailable to complete calculation

Table 5.06 Information extracted from the fitted ^{29}Si NMR spectra of the La-doped MW glass.

El Damrawi *et al.* have postulated, from the ^{29}Si NMR spectra of Al_2O_3-Na-borosilicates, that the presence of Si-O-Al linkages leads to an observed chemical shift of –90 ppm [12]. This suggests that the fitted peak at ~–99 ppm represents Q^4 units with an Si-O-B link (as will be substantiated in Chapter 7) and the peak at ~–91 ppm arises from Q^4 units with some kind of Si-O-La link, whilst another peak of low abundance would represent the presence of NBOs associated with silicate tetrahedra. The assignment of contributions from Q^4(B),Q^4(La) and Q^3 links to the ^{29}Si spectra is made difficult by the fact that the chemical shifts of these species are not well defined and thus uncertainty arises over whether the role of La_2O_3 is primarily as a modifier or an intermediate oxide. It was possible to fit the some of the spectra using three peaks representing the three sites mentioned previously. The spectrum obtained from the MW glass was fitted satisfactorily with 2 peaks both with and without constraint on the ratios of the peaks deduced from the number of NBOs expected from ^{11}B NMR results.

If all the La_2O_3 is converted to $[LaO_4]^-$ and each of these units is associated with 4 silicons, then the number of Si-O-La linkages of this kind has been calculated to be 16%, 33% and 70% of total Si, for concentrations of 2.4, 4.8 and 9.6 mol% La_2O_3, respectively. The consequence of this is that gradually there is less and less

modifier available to convert Q^4 units to Q^3 units and this can be demonstrated, in Fig. 5.13, by the decrease to zero of the fitted Q^3 contribution.

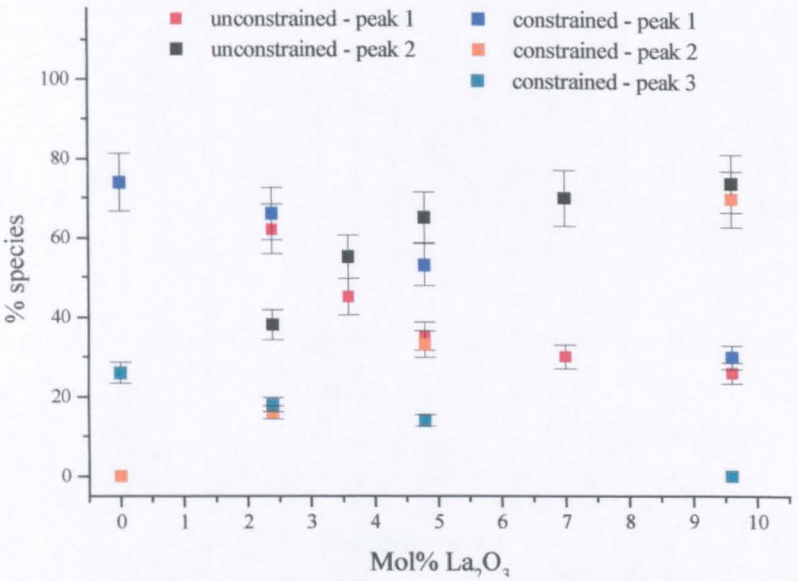

Fig. 5.13 Change in concentration of both the constrained and unconstrained peaks used to fit the ^{29}Si NMR spectra of the La-doped samples.

It can also be seen from Fig. 5.13 that the peak attributed to Si-O-La links has refined to zero in the MW spectrum, whilst still satisfying the NBO concentration requirements. Reference to the ^{11}B NMR spectra for the LBS glasses shows a distinct change in the nature of the trigonal site above 9.68mol% La_2O_3. This could mean that the B-O-La links, which form as the La_2O_3 concentration increases, could be B_3-O-La links as opposed to B_4-O-La.

5.2.3 Physical properties

5.2.3.1 Glass transition temperature (T_g)

Fig. 5.14 shows the DTA traces obtained from the four La-doped samples alongside the MW base glass. It can be clearly seen that, as La_2O_3 is added to the base glass, the glass transition temperature rises. It can also be seen that the crystallisation event at approximately 990 K becomes much more pronounced as the La-content reaches 12 mol%. Visual inspection of this sample revealed the presence of opaque swirls inside the bulk glass, a possible indication of phase separation and that the solubility limit of La_2O_3 in this composition range has been reached. This

could help to explain the change in shape of the LBS 4 ^{11}B NMR spectrum shown in Fig. 5.10.

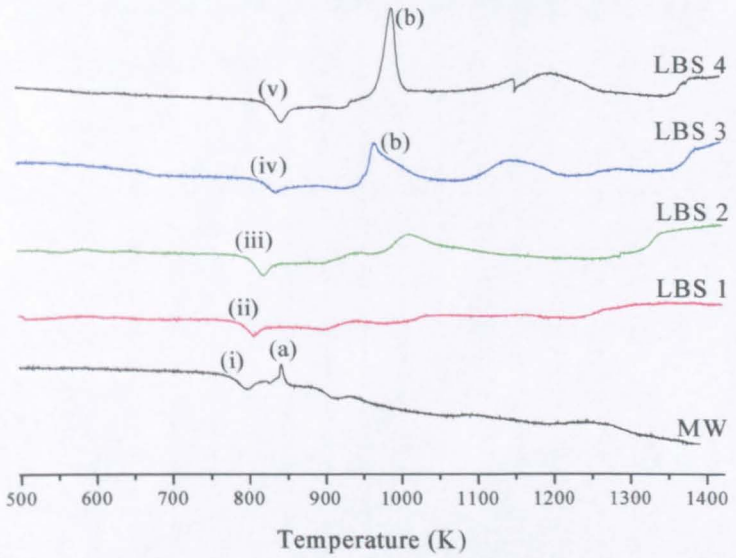

Fig. 5.14 DTA traces obtained from each of the four La-doped glasses and the undoped MW glass. (a) - α-β quartz phase transition, (b) crystallisation event, (i-v) T_g event

Studies of the role of La_2O_3 in sodium silicate glasses [14] have also reported an increase in T_g with the replacement of silica and/or modifier oxide, the greatest variation occurring when the silica content remains unchanged and the modifier oxide is gradually replaced by La_2O_3. Since, the relatively low T_gs of sodium silicate glasses are caused by the introduction of NBOs on silica tetrahedra, the removal of modifier oxide should cause an increase in T_g. For the case of adding La_2O_3 to the mixed-modifier borosilicate MW composition, the ratios of modifier-oxide, B_2O_3 and SiO_2 remain constant so any changes to the physical properties must be caused solely by the introduction of the La_2O_3. Our ^{11}B NMR data shows clearly that N_4 decreases as the composition changes from MW to LBS 4 and a decrease in N_4 should be accompanied by a corresponding decrease in T_g. In fact, the opposite is seen here, with both the density and T_g of the LBS samples increasing with decreasing N_4. As has been shown in section 5.3.1.2 in Table 5.04, the fraction of NBO/Si atom decreases to zero as the La_2O_3 content of the glass increases.

5.2.3.2 Thermal expansion coefficient (α)

Fig. 5.15 shows the thermal expansion behaviour of the MW and La-doped compositions between 300 K and the approximate onset of T_g. It can be seen from

Table 5.07 that the addition of La_2O_3 leads to an increase in the calculated thermal expansion coefficient of the glass. It is known in single-modifier borosilicate glasses [15] that an increase in the coherency of the network, brought about by the conversion of borate units from the trigonal to tetrahedral units, leads to a decrease in the thermal expansion coefficient.

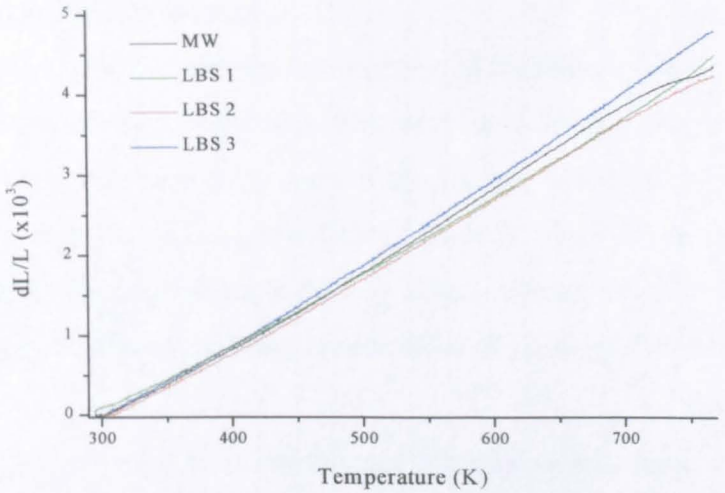

Fig. 5.15 Comparison of the thermal expansion behaviour of the LBS glass compositions.

It may be concluded that the observed decrease in N_4 and NBO/Si concentration and growing concentration of $[LaO_4]^-$ units leads to the observed increase in α. Investigation of the effect of Al_2O_3 on the linear thermal expansion of a series of sodium borosilicate glasses [15] has shown that if sufficient NBOs are attached to $[SiO_4]$ units, the role of the Al_2O_3 is to convert the NBOs into BOs and thus lower the expansion coefficient. Study of the Pr-Na-silicate system [16] has shown that whilst there is a corresponding increase in T_g, there is a decrease in α, characteristic of the role of an intermediate oxide.

Sample	T_g (K) ($\pm$ 4K)	α (MK^{-1}) ($\pm$ 0.4)
MW	772 (778)	8.44
LBS 1	786	8.24
LBS 2	800	8.62
LBS 3	813 (815)	9.24
LBS 4	826	-

Table 5.07 Variation in the thermal properties of the MW and La_2O_3-doped glasses with composition. T_g values in brackets are obtained from dilatometry.

Conversely, the co-ordination number of Pr in this system has been observed to be 6 or 7, typical of a modifying oxide. This apparent dichotomy is present in the LBS system, where the available ^{29}Si and ^{11}B NMR data are unable to explain the change in physical properties satisfactorily if the La_2O_3 is assumed to behave as either a modifier *or* an intermediate.

5.2.3.3 Density and molar volume

Fig. 5.16 shows the change in density of the LBS glasses as the amount of La_2O_3 in the composition is increased. The increase is density can be most easily be explained by considering the large mass of the La ion, which far exceeds that of the other glass components. As suggested by Coon & Shelby [14], the physical effects of any structural rearrangements involving boron, silicon and the modifier oxides will be dominated by the increasing concentration of La_2O_3 in the glass.

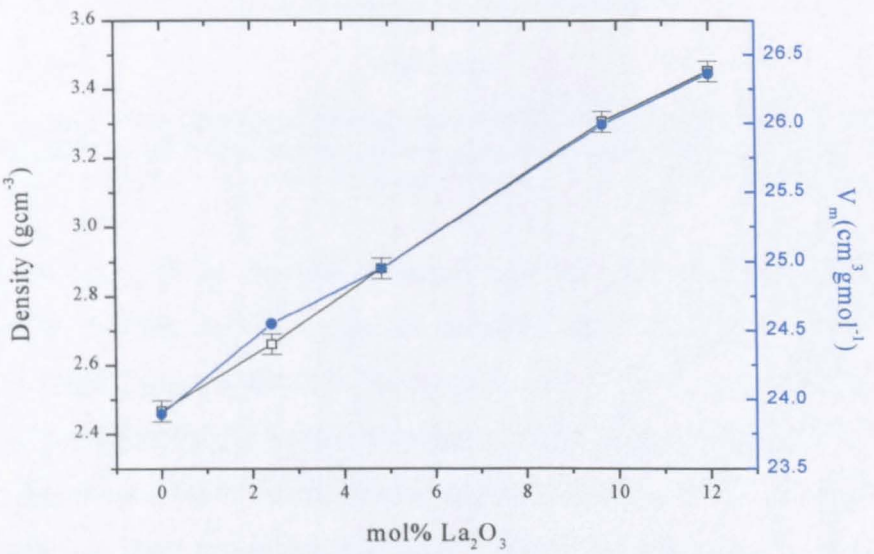

Fig. 5.16 Change in density and corresponding molar volume, V_m, of the LBS glasses with La_2O_3 content.

It can be seen from Fig. 5.16 that there is a steady increase in the molar volume of the each glass as the lanthanum content of the glass is increased. If it is assumed that the effect of the La^{3+} ion is to displace a tetrahedral boron atom and introduce $[LaO_4]^-$ species, it is obvious that both unit masses and volumes will increase. Hence an explanation for the simultaneous increase in ρ and V_m.

5.2.4 Chemical durability

5.2.4.1 Leach testing

a) Chemical analysis and pH

Fig. 5.17 shows a summary of the leaching data obtained from each La-doped composition.

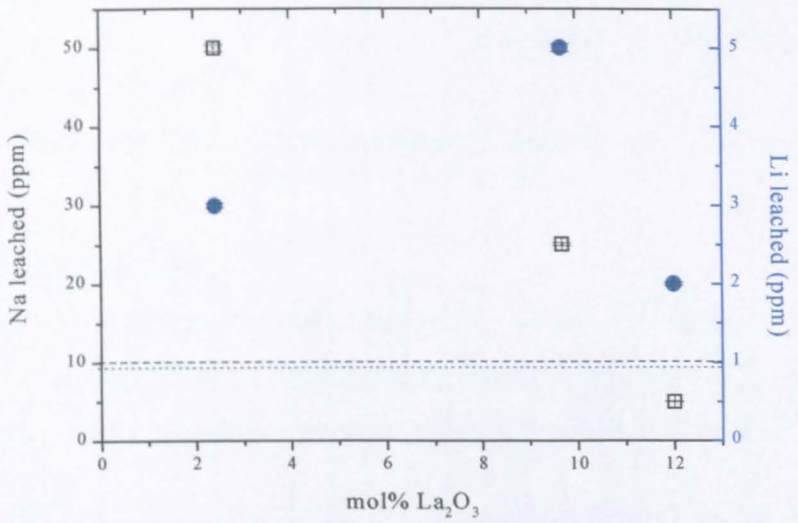

Fig. 5.17 Variation in the quantity of leached material detected by chemical analysis of glasses LBS 1, LBS 3 and LBS 4. Dashed lines indicate quantity of material leached from glassware of apparatus : --- - Na; --- - Li.

Comparison of the leachate chemical analysis of the NBS and LBS glasses shows that the resistance of the glass to chemical attack is greatly increased if as little as 2.4mol% La_2O_3 is added to the composition. There is a gradual decrease in the sodium loss between the 3 glasses so that the level of sodium leached from LBS 4 is indistinguishable from the contribution from the experimental apparatus. The loss of lithium is more pronounced in LBS 3 than the other glasses. If we assume that the effect of the La_2O_3 is to introduce $[LaO_4]^-$ units, then there will be a corresponding decrease in the concentration of $[BO_4]^-$ units available to associate with modifier ions, as observed. The mechanism by which modifier ions are leached out is influenced by the structural unit with which the modifier ions are associated [8]. This implies that one of the effects of incorporation of La_2O_3 into the composition could play would be to increase the chemical durability of the glass.

As mentioned earlier, evidence of immiscibility could be seen in samples LBS 3 and 4, which could lead to more rapid degradation of the glass should the separated phase be less chemically stable than the host glass. The final pH of the

leachates, shown in Table 5.08, was close to that found from the control experiment and little damage to the physical structure of the glasses could be discerned by visual inspection.

Sample	pH	Condition of sample after leaching
LBS 1D	8.73	Minimal damage, sample opaque
LBS 3C	8.75	""
LBS 4A	8.27	Crystalline surface material present
Blank for LBS 1D, 3C and 4A.	8.51	-

Table 5.08 Details of changes to the pH and physical appearance of the La-doped glass samples leached for 14 days at 348K.

b) Optical microscopy

Figs. 5.18 (a-f) are optical micrographs of the LBS glasses showing the condition of a large section of each prior to leaching, whilst (d-f) are examples of surface features of the same samples after leaching for 14 days at 348 K.

(a) *magnification x5*

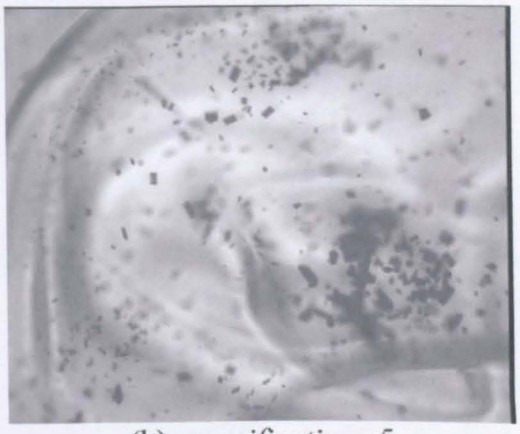

(b) *magnification x5*

(c) magnification x5

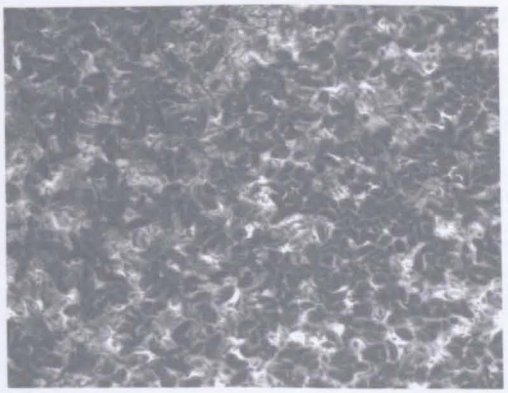

(d) magnification x50

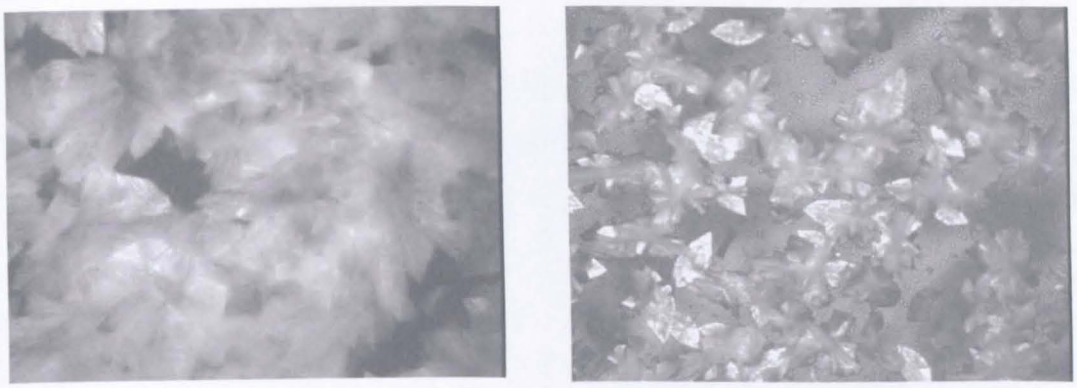

(e) magnification x50 *(f) magnification x20*

Fig. 5.18 Optical micrographs of samples LBS 1, 3 and 4 (a, b, c) prior to and (d,e,f) after leaching in deionised water for 14 days at 348 K.

The most interesting features appear to be the crystal-like growths seen at higher magnification on the surface of samples 3C and 4A. It was particularly obvious on the surface of sample 4A as a light dust was detected upon touching. Sample 4A was subsequently analysed using a high-resolution X-ray diffractometer and the spectrum obtained is shown in Fig. 5.19 below.

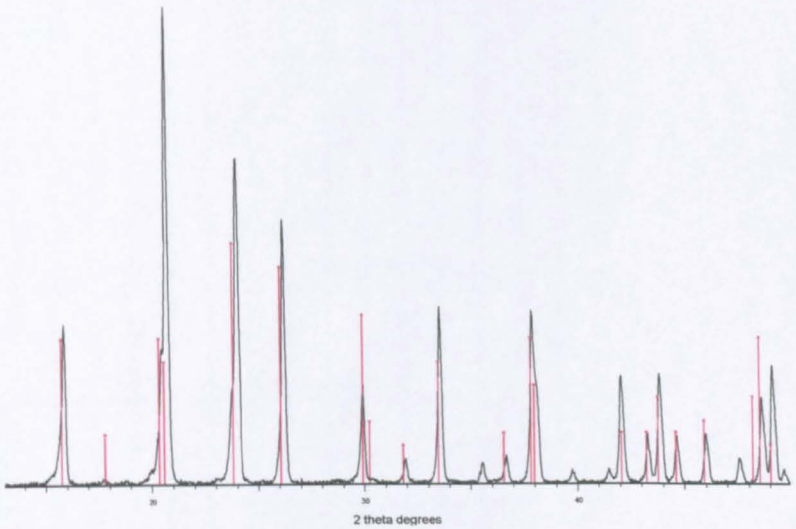

Fig. 5.19 High resolution XRD trace of sample LBS4 after leaching in deionised water for 14 days at 348 K.

Some X-ray diffraction peaks were also observed from the leached LBS3 sample but with a much reduced intensity. The best fit to the peaks comes from the X-ray diffraction spectrum of lanthanum oxide carbonate hydrate ($La_2O(CO_3)_2.xH_2O$) [17].

c) ^{11}B NMR spectroscopy

As with the NBS samples, ^{11}B MAS NMR of the leached LBS samples was carried out to detect the presence of O-H groups bonded to borate units, illustrated in Fig. 5.20(a-c).

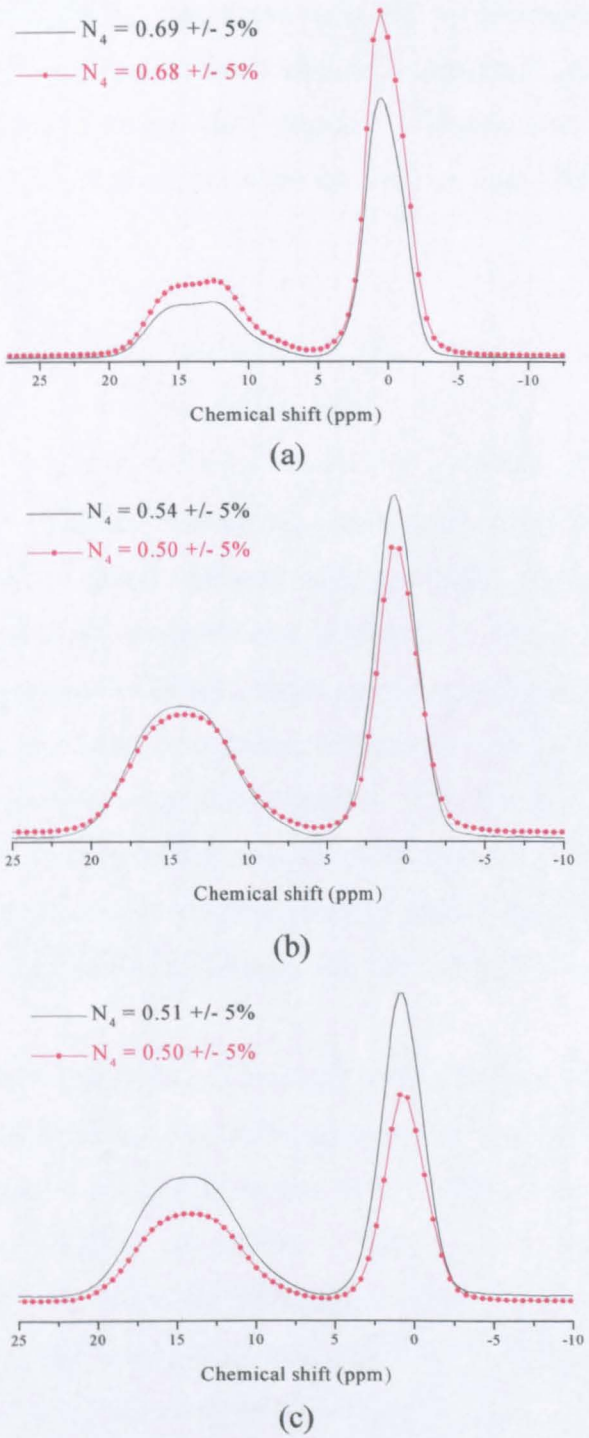

Fig 5.20 Comparison of the ^{11}B NMR spectra of samples a) LBS 1, b) LBS 3 and c) LBS 4 before and after leaching in deionised water at 70°C for 14 days.

The sample of pyrex used as a reference for all the ^{11}B NMR work was also used as a crude estimate of the boron content of some of the samples, particularly those La-containing glasses used in the leach testing, but this proved to be too inaccurate a method to provide useful information. Little difference in the fraction of tetrahedral boron units was detected after leaching and no alteration to the shape of the trigonal and tetrahedral contributions could be detected. As with the NBS glasses, this is probably due to the surfeit of un-leached glass dominating any structural changes induced by the leach process. It should also be noted that the B-OH groups reported by Bunker [11] were carried out under very acidic conditions (pH of leachant ~ 1).

5.3 Summary

Physical and structural techniques have been used to characterise glass compositions related to those currently used by BNFL in its waste vitrification program. The effect of removal and addition of B_2O_3, one of the critical components, on the properties of the glasses has been studied in detail. Explanations have been given for the observed decrease in N_4 and corresponding increase in T_g as the B_2O_3 content increased from 0 to 36mol%. The effect of composition on the chemical durability has been studied using high-temperature dynamic leach tests and it has been shown that the most resilient glasses (containing between 8 and 14 mol% B_2O_3), exhibiting little physical damage, are as resistant to attack as commercial pyrex.

The effect of incorporation of La_2O_3, a waste simulant, has also been studied using similar analytical techniques. It has been shown that the fraction of tetrahedral boron units decreases as the La_2O_3 content is increased, whilst T_g, density and the thermal expansion coefficient all increase. This has led to the development of a structural theory similar to that hypothesised for Al_2O_3 in Al-Na-borosilicate glasses. It is suggested that all the La_2O_3 is converted to $[LaO_4]^-$ units by the required amount of modifier, after which trigonal borate units are converted to $[BO_4]^-$ units and any remaining modifier creates NBOs on the silicon tetrahedra. This theory can be seen to satisfy the observed ^{11}B and ^{29}Si NMR spectra but ambiguity still exists over the

assignment of peaks corresponding to contributions from the proposed Q^4(B), Q^4(La) and Q^3 links. A further possibility can be envisaged in which the growing contribution to the observed Si^{29} spectra results from an increase in NBO concentration generated by the suggested $(LaO_n)^-$ units. It is acknowledged that the coordination of La (6 or 8) is larger than that of B (3 or 4) and hence a more complex mixture of 4 stronger BO and 4 weaker NBO links may be present. The actual La coordination could be increased by contributions from bridging oxygens in neighbouring polyhedra.

Chemical durability tests have shown that the inclusion of La_2O_3 leads to an order of magnitude decrease in the amount of modifier detected in the leachate after conclusion of the leach tests. X-ray diffraction also detected the presence of a crystalline material on the surface of the samples containing 9.68 and 12 mol% La_2O_3, identified as lanthanum oxide carbonate hydrate ($La_2O(CO_3)_2.xH_2O$), probably arising from interaction between the $La(OH)_3$ corrosion layer and CO_2 in the atmosphere.

5.4 References

[1] W. J. Dell, P. J. Bray & S. Z. Xiao, J. Non-Cryst. Solids **58** (1983) p.1

[2] J. E. Shelby, Introduction to glass science and technology, Royal Society of Chemistry, Cambridge (1997) p.90

[3] L. van Wüllen & W. Müller Warmuth, Solid State Nuclear Magnetic Resonance **2** (1993) p.284

[4] R. J. Bunker, D. R. Tallant, R. J. Kirkpatrick & G. L. Turner, Phys. Chem. Glasses **31** (1) (1990) p.30

[5] G. Bhasin, A. Bhatnagar, S. Bhowmik, C. Stehle, M. Affatigato, S. Feller, J, MacKenzie & S. Martin, Phys. Chem. Glasses **39** (5) (1998) p.269

[6] J. W. MacKenzie, A. Bhatnagar, D. Bain, S. Bhowmik, C. Parameswar, K. Budhwani, S. A Feller, M. L. Royle & S. W. Martin, J. Non-Cryst. Solids **177** (1994) p.269

[7] D. Feil & S. Feller, J. Non-Cryst. Solids **119** (1990) p.103

[8] S. P. Zhdanov, R. L. Yastrebova, E. V. Koromaldi & L. V. Aleksandrova, Proc 5th All Union Conf. on the Vitreous State, [ed.] Nauka, Leningrad, (1971) p.302

[9] T. V. Antropova, Optica Applicata, **XXIV** (3) (1994) p.135

[10] B. C. Bunker, D. R. Tallant, T. J. Headley, G. L. Turner & R. J. Kirkpatrick, Phys. Chem. Glasses **29** (3) (1988) p.106

[11] B. C.Bunker, G. W. Arnold, D. E. Day & P. J. Bray, J. Non-Cryst. Solids **87** (1986) p.226

[12] G. El-Damrawi, W. Müller-Warmuth, H. Doweidar and I. A. Gohar, Phys. Chem. Glasses **34** (2) (1993) p.52

[13] R. Dupree, D. Holland & M. G. Mortuza, Phys. Chem. Glasses **29** (1) (1988) p. 18

[14] J. Coon & J. E. Shelby, Phys. Chem. Glasses **35** (2) (1994) p. 47

[15] W. L. Konijnendijk, Philips Res. Repts. Suppl. (1) (1975) p.199

[16] A. Mekki, K. A. Ziq, D. Holland & C. F. McConville, Phys. Chem. Glasses (in press)

[17] K. Nagashima, H. Wakita & A. Mochizuki, Bull. Chem. Soc. Jpn. **46** (1973) p.152

Chapter 6 - Radiation damage of NBS & LBS glasses.

6.1 Introduction

The aim of the irradiation analysis has been to carry out a preliminary study of glasses containing boron and lanthanum under irradiation. The objectives have been: firstly, to determine how neutron generation depends on the amount of boron present in the glass and secondly, to investigate the effect of inclusion of a waste simulant, La_2O_3, on the response of the glass to two different types of applied radiation.

6.2 Glass compositions

Glass compositions used in the irradiation studies can be found in Tables 5.01 and 5.02 in Chapter 5, the NBS and LBS series glasses. Table 6.01 shows details of the samples and corresponding α-doses delivered during the irradiation tests.

6.3 Radiation damage analysis

6.3.1 Cyclotron α-irradiation

6.3.1.1 γ-ray spectroscopy

Fig. 6.01 illustrates the decay of the radioactive species present in the NBS glasses after irradiation by the various doses of α-particles given in Table 6.01.

Sample	*Identification code*	*Total α-particle dose ($x10^{15}$)*	*α-particle dose $gram^{-1}$ ($x10^{16}$)*	*α-particle dose cm^{-3} ($x10^{17}$)*
NBS 7	A	22.7	42.8	8.04
NBS 6	B	7.93	14.4	2.81
	D	22.6	41.1	8.02
MW	2a	2.0	3.70	0.71
	2b	2.0	3.70	0.71
	2c	2.0	3.70	0.71
	2d	3.0	5.56	1.06
	B	4.79	8.87	1.70
	III	8.71	16.1	3.09
	(II)D	11.0	20.4	3.90
	D	12.2	22.6	4.33
	A	15.9	29.4	5.64
	II	16.2	30.0	5.75
	IV	30.1	55.7	10.65
	E	43.4	80.4	15.4
NBS 8	A	3.27	60.6	1.16
	H	8.51	15.8	3.02
	B	25.4	47.0	8.98
NBS 14	A	3.66	7.04	1.29
	C	7.82	15.0	2.77
	E	9.37	18.0	3.33
	D	13.2	25.4	4.68
NBS 9	B	4.10	7.9	1.45
	C	8.28	15.9	2.94
	A	21.0	40.4	7.44
NBS 10	B	3.8	7.17	1.35
	C	5.13	9.68	1.82
	D	9.11	17.2	3.23
	E	15.8	29.8	5.61
LBS 1	A	14.9	25.3	5.28
LBS 2	A	16.6	26.3	5.89
LBS 3	A	14.1	19.3	5.00
LBS 4	C	15.7	20.7	5.57

Table 6.01 Details of the irradiated samples and identifying codes, value of total received radiation dose and radiation dose per unit mass and per cm^{-3}.

The origin of the decay sequence responsible for the γ-ray signal can be found from its characteristic half-life, $\tau_{1/2}$, given by:

$$\tau_{1/2} = \frac{\ln 2}{\lambda} \tag{6.01}$$

where λ is the gradient of the data plot. The half-lives measured for samples NBS 10E, NBS 8B & H and MW(II)D are 10.4 ± 0.3, 13.3 ±0.9, 15.2 ±0.3 and 9.79 ±0.1 minutes, respectively, and the radiation exposure details of these samples along with four other irradiated base glass samples are shown in Table 6.02.

	α-particle dose gram^{-1}	*Activity at end of irradiation (MBq)*	*Irradiation current (μA)*	*Half-life of decay species (mins)*
MW(II)D	17.9	253.5	2	9.8
MW(2a)	3.28	0.28	1	10.5
MW(2b)	3.28	1.35	0.3	6.96
MW(2c)	3.28	0.21	0.3	10.4
MW(2d)	4.92	1.75	0.5	9.62
NBS 8B	41.6	80.1	1.5	13.3
NBS 10E	26.4	380.4	1.5	10.4
NBS 8H	13.9	144.1	1.5	15.2

Table 6.02 Details of the irradiation parameters and half-lives of observed decay species obtained from theγ-ray spectra of several NBS glasses.

The relatively wide spread of values obtained from the decay data could indicate the presence of a contribution from another decay process, leading to an incorrect estimate of the half-life.

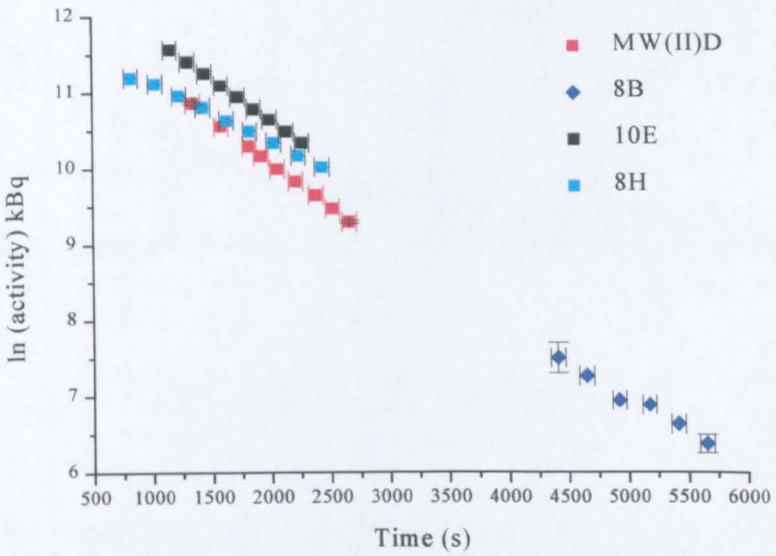

Fig. 6.01 Characteristic γ-ray decay spectrum of some NBS samples after irradiation with varying α-particle dose. Some of the error bars are smaller than the symbols.

The results from samples 10E and MW(II)D and examination of the table of isotopes, a section of which is included in Fig. 6.03, shows that the most promising candidate for the source of the observed γ-decay is given by Eq. 6.02

$$^{10}B + {}^{4}_{2}\alpha \xrightarrow{(a,n)} {}^{13*}N + {}^{1}n \xrightarrow{\gamma\text{-}decay} {}^{13}N \qquad (6.02)$$

$$\tau_{1/2} = 9.965 \text{ minutes [1]}$$

Examination of the possible decay routes and half-lives of the radioactive nuclei produced leads to the conclusion that Eq. 6.02 is the only reasonable candidate for the source of the reaction. The excited ^{13*}N isotope decays via positron annihilation with a characteristic energy of 511 keV. This peak was observed in the γ-ray spectra taken from the irradiated samples, an example of which is shown in Fig. 6.02 below.

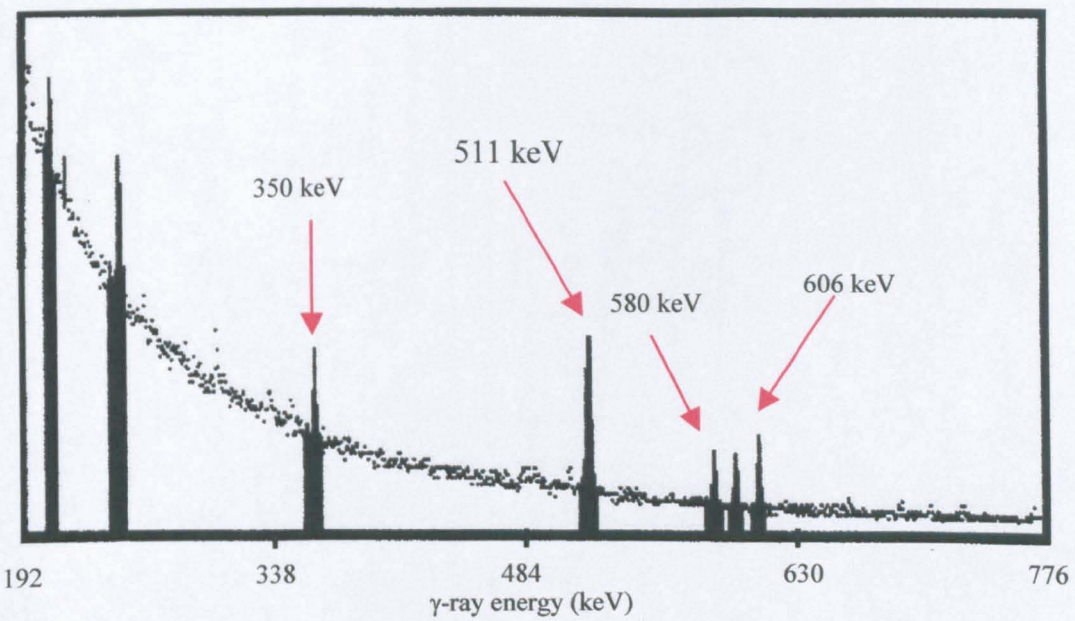

Fig. 6.02 A γ-ray spectrum taken from sample MW (2a) after exposure to $2x10^{15}$ α-particles. In addition to the peak at 511 keV (detected only with the irradiated sample in place) are shown peaks due to background radiation in the laboratory.

The total dose given to each sample was converted to a dose per unit volume and mass by estimation of the area of the sample exposed to radiation. The particle beam irradiated an area approximately 1cm in diameter to a maximum penetration depth of 0.028 cm, which leads to the total irradiated volume. In reality, the α-particles incident on the target will have a distribution of penetration depths

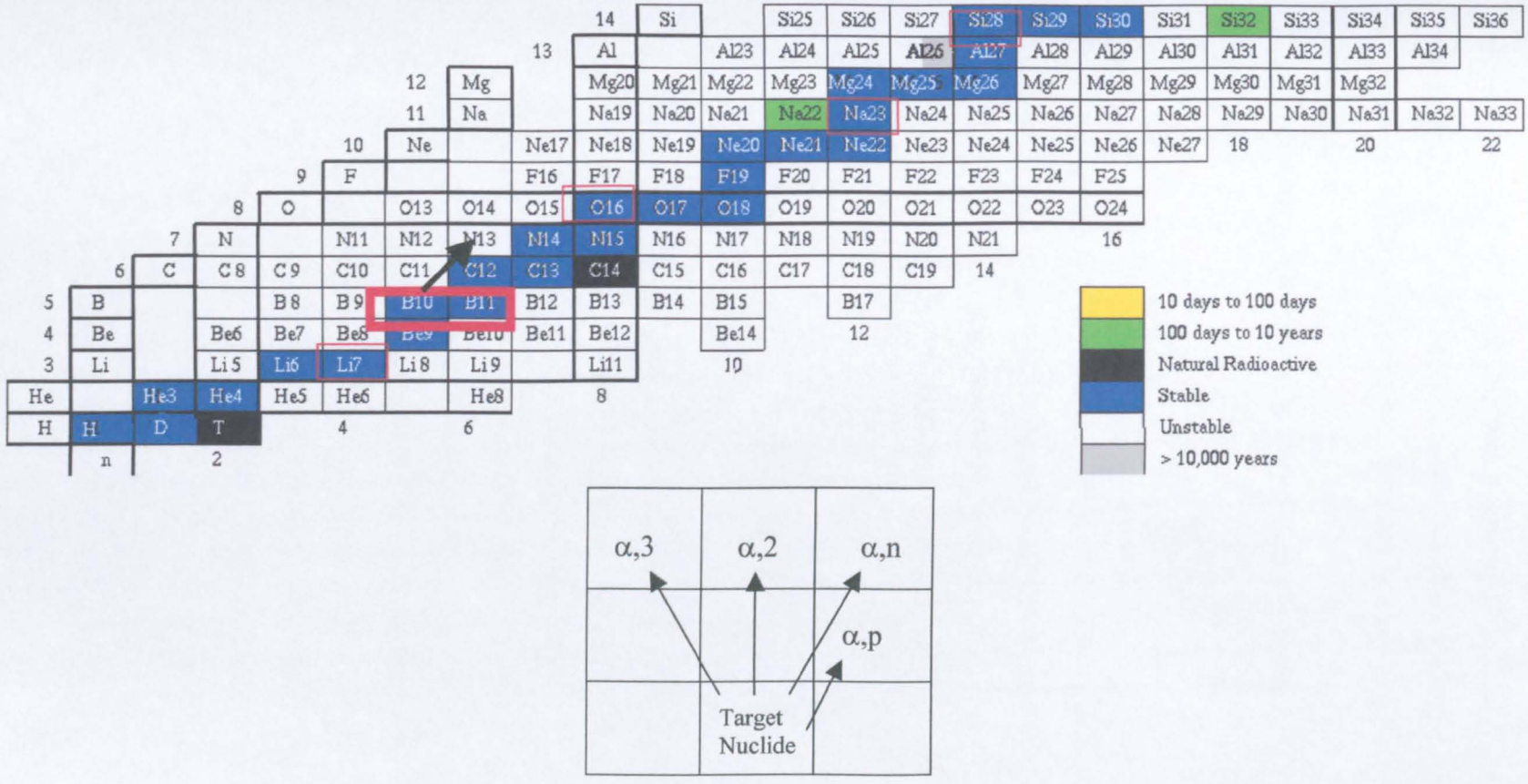

Fig. 6.03 Table of the isotopes of the NBS glass components and the nuclear reaction paths available. Details of the most likely source of the observed γ-decay are also shown (taken from [1]).

depending on the reactions and collisions they undergo, but for the purposes of this analysis the maximum volume has been considered.

It is possible, using the decay information obtained from Fig. 6.01, to estimate the number of boron nuclei that react with the incoming α-particles. From this value, the reaction cross-section for the ^{10}B nuclei can be calculated, as shown below.

From theory, the activation cross section for the reaction, σ, is expressed by:

$$\sigma = \frac{dNAQe}{IN} \tag{6.03}$$

where dN = number of nuclei which react with a beam of α-particles incident on a target containing N nuclei in an irradiation area A, Q is the charge state of incident ion and I is the integrated current in μC.

In a sample of glass of thickness t, the total number of ^{10}B atoms is given by the relationship:

$$N = AtmBRSN_a \tag{6.04}$$

where m is the molar volume of the glass, B is the concentration of B_2O_3 in mol%, R is the ratio of ^{10}B nuclei to the total B nuclei, S is the number of boron atoms per B_2O_3 molecule and N_a is Avogadro's constant.

The molar volume can be calculated from the density and molar mass of each glass, whilst B is known from the composition, S is equal to twice B (since there are 2B in every B_2O_3 unit) and the ratio of $^{10}B/^{11}B$ in natural isotopic boron is 0.2.

From experimental γ-decay data, the number of nuclei (dN) which have reacted with the incident beam of particles, (the derivation of this expression is included in Appendix D) can be calculated from Eq. 6.05:

$$dN = \frac{d_{am}}{[\lambda \exp(-\lambda t_m)(1-\exp(-\lambda t_a))]} \tag{6.05}$$

where d_{am} = measured activity after a total time $t_a + t_m$, λ = decay constant, t_a = activation time and t_m = some time after activation is completed. The results

obtained from the γ-decay spectra enable the decay constant to be determined and hence *dN*. The activation cross-section, σ, can then be calculated.

The ^{10}B (α,n) ^{13}N activation cross section has been studied in detail by Van der Zwan and Geiger [2] whilst studies of neutron production from the general B(α,n)N reaction have been carried out by Marsh *et al.* [3] and Bair and del Campo [4]. Reported values for the neutron yield from the B(α,n)N reaction depend on the energy of the incident α-particle and range from ~6 to ~24 high-energy neutrons (~3 MeV) per 10^6 α-particles, for the ^{10}B and ^{11}B reactions, respectively. The presence of these fast-neutrons could initiate further nuclear reactions between susceptible components of the wasteform and its immediate surrounding environment. The extent to which the production of neutrons can be reduced to an acceptable level is of importance to the current vitrification process since boron plays several important roles in ensuring that desirable chemical and physical properties are maintained.

The number of ^{10}B atoms cm^{-3} and ^{10}B(α,n) activation cross section have been calculated for the other NBS samples and are shown in Table 6.03, alongside the calculated α-particle dose per unit volume of glass.

Sample	*^{10}B atoms volume^{-1} ($x10^{19}$)*	*Reacting nuclei, dN ($x10^{11}$)*	*α-particle dose cm^{-3} ($x10^{17}$)*	*Years of storage** (a)	(b)	*σ(^{10}B(α,n)) (mbarns)*
MW(II)D	4.13	2.34	3.90	18	$2x10^4$	4.05
NBS 8B	5.01	3.39	8.98	70	$2x10^5$	2.09
NBS 10E	7.50	3.67	5.61	45	$5x10^4$	2.44
NBS 8H	5.01	2.95	3.02	12	$3x10^3$	5.43

*Table 6.03 Comparison of useful irradiation parameters calculated for each of the irradiated NBS glasses. *The corresponding years of storage are based on the cumulative decay events g^{-1} from (a) commerical high-level waste and (b) defence waste (taken from [5]).*

It can be seen from Table 6.02 that sample NBS 10E shows the greatest initial activity, determined from interpolation of the gradient of the best fit to the data, despite having received a much smaller α-particle dose $gram^{-1}$ than that of sample NBS 8B, which displayed the lowest initial activity. Since the controlling factors are the number of ^{10}B nuclei available to take part in the (α,n) reaction and the number of incident particles, it is expected that the sample containing the greatest number of ^{10}B nuclei, and receiving the largest α-dose, per unit volume would have the greatest number of reacting nuclei at the end of the irradiation. The number of

nuclei (dN) which react with the incoming beam of particles, as determined from Eq. 6.04, is also shown in Table 6.03. It can be seen that sample NBS 10E contains the greatest number of ^{10}B atoms per unit irradiation volume, and largest number of reacting nuclei, over the course of the irradiation. It would appear that reducing the number of potential reacting nuclei in the glass, rather than limiting the number of incident particles, has a greater effect on the number of interactions that take place. It can be seen from Eq. 6.04, however, that there is a linear relationship between the number of reacting nuclei, the concentration of B atoms and the number of incident particles. It is also assumed that the activation cross-section for the $^{10}B(\alpha,n)$ reaction depends only on the nature of the nucleus and the energy of the incident particle and should remain the same for all the glasses studied here. It is most likely that errors in the extrapolation of the γ-ray data obtained for these samples, as discussed previously, bring about the spread of cross-section values reported here. Unfortunately, no data are available for the NBS 6 or NBS 7 glasses to determine how reducing the B_2O_3 content below the MW composition affects the efficiency of the $^{10}B(\alpha,n)$ reaction. There are factors of 6 and 60 between the equivalent years of storage produced by the irradiation in samples 8H and 8B, respectively, and though the dose given to sample 8B was three times that given to sample 8H, there was only a 14% increase in the number of reacting nuclei.

One of the most interesting points that can be inferred from the results obtained from the irradiation tests and γ-ray decay spectra is that the strong evidence for the $^{10}B(\alpha,n)$ reaction implies, with even more certainty, the presence of the $^{11}B(\alpha,n)$ reaction and this generates more neutrons per reaction [4]. Often investigated in the simulation of radiation damage effects, and of importance to the structural integrity of the glass, is the generation of ^4He, either by the capture of electrons by an incident α-particle or elemental transmutation. Unlike ^{13}N, the product of the $^{11}B(\alpha,n)$ reaction, ^{14}N, is the naturally occurring isotope. The possibility arises, therefore, that in the same way bubbles of ^4He have been observed in actinide-doped glasses [6], the physical properties of the glass could be compromised by the presence of bubbles of nitrogen. Furthermore, the conversion of boron to the isotopes of nitrogen leads to a gradual depletion of one of the glass network formers, with consequences for the stability of the structural framework itself.

6.3.1.2 ESR spectroscopy

Fig. 6.04 shows the X-band ESR spectra obtained from an unirradiated sample of composition $K = 3$, $R = 1.6$ and examples of spectra from several NBS glasses irradiated with varying doses of 5.5MeV α-particles.

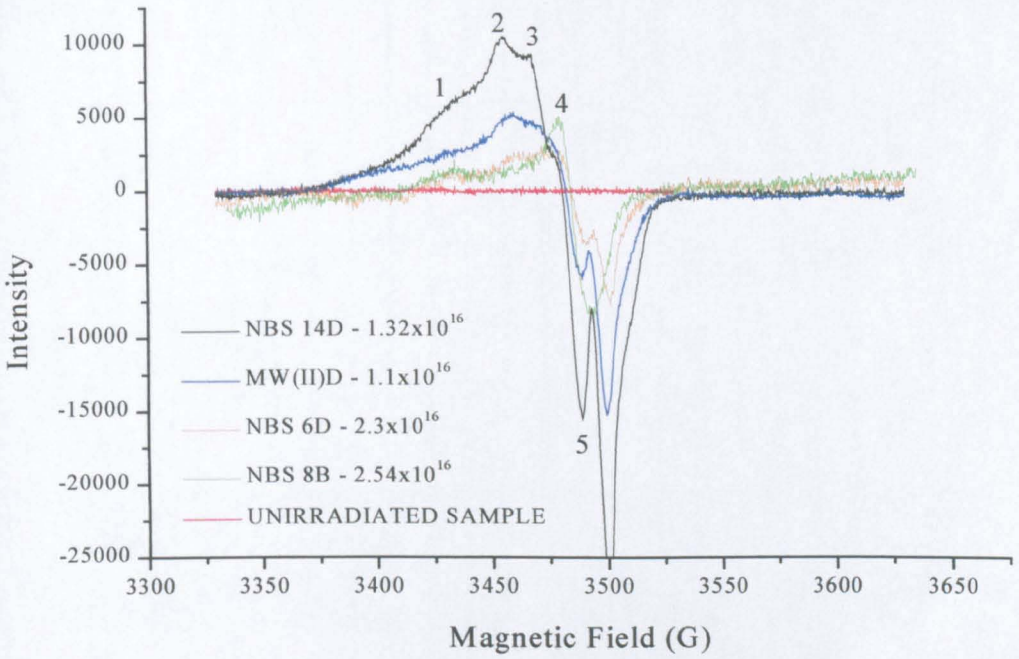

Fig. 6.04 X-Band ESR spectra obtained from five mixed-modifier glasses. The insert gives details of the identity and total dose given to the sample.

The numbered features probably arise from the well-documented 5-line hyperfine interaction on the ^{11}B nucleus and the comparison with the unirradiated sample is obvious. No information regarding the population of paramagnetic sites was obtainable and though Fig. 6.05 gives the indication of an increase in the intensity of the ESR signal with α-particle dose, no quantitative conclusions could be gathered. Past glass irradiation studies [7,8] carried out in-situ ESR measurements of damaged samples and were thus able to detect the presence of short-lived defects as well as the more stable $B\text{-}O^-/h^+$ and $Si\text{-}O^-/h^+$ hole centres. Though it is possible to make quantitative estimates of the number of sites contributing to the observed ESR signal, no such information could be gained from the samples studied because of the low concentrations of defect sites diluted further by unirradiated material.

Fig. 6.06 shows the ESR spectrum obtained from irradiated samples of NBS 10 and NBS 8. Despite containing the greatest concentration of B_2O_3 and, hence, sites that may be probed by ESR techniques, the signal resulting from a total dose of

$5.13x10^{15}$ α-particles is relatively featureless and of reduced quality. It was noticed from several other irradiated samples that, even after receiving a total α-dose above that which resulted in the spectra shown in Fig. 6.03, poor quality ESR spectra were obtained yielding little information about the behaviour of the glass under irradiation.

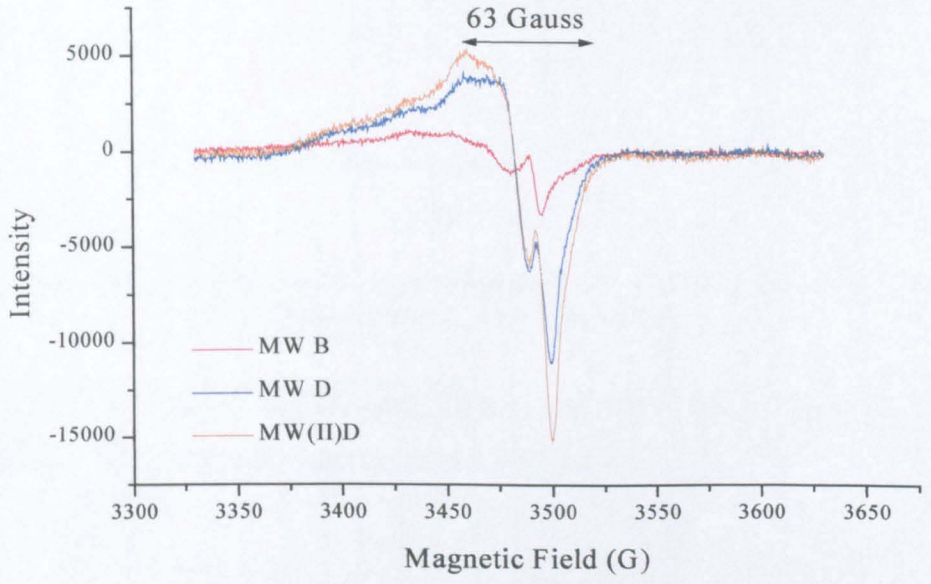

Fig. 6.05 Comparison of the X-band ESR spectra obtained from several MW glasses. The insert gives details of the identity of each sample, whilst the total dose corresponds to: MW- B = $0.48x10^{16}$ α-particles, MW – D = $1.22x10^{16}$ α-particles and MW(II)D = $1.101x10^{16}$ α-particles.

The possibility arises that extreme heating of the samples, which caused the majority to melt or fracture, obscured any details about the effect of the incident radiation on that particular sample by a process of annealing. An example of the change in ESR spectrum of a borate glass given in Chapter 3 (p.53) [9], initially exposed to γ-radiation and subsequently heat treated at 250°C, shows that the distinct 5-line structure is destroyed by the thermal bleaching that takes place upon heating. Though it is obvious that not all the features of the ESR spectra are obscured, the severely altered condition of some of the samples after removal from the irradiation apparatus must suggest that a similar thermal bleaching has taken place during, and immediately after, the irradiation.

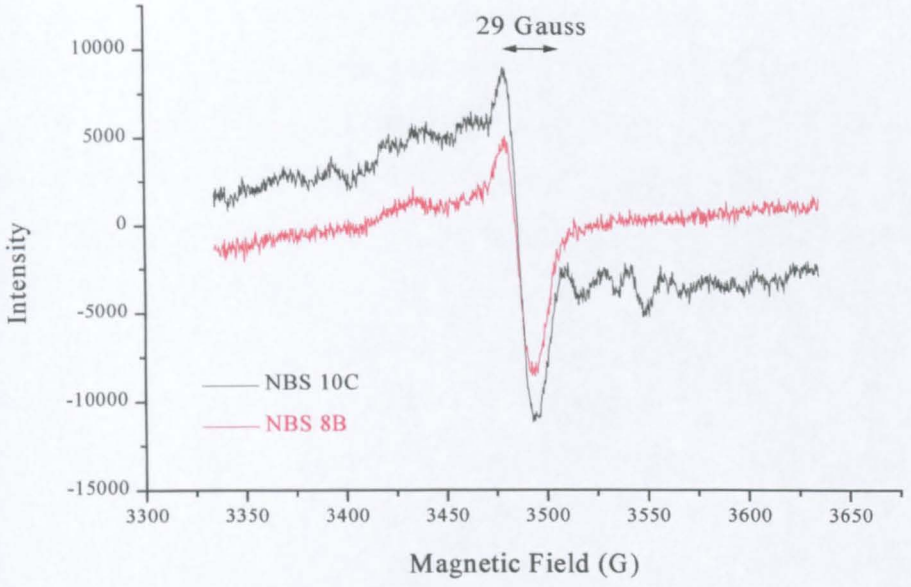

Fig. 6.06 ESR spectrum of sample 10C, irradiated with $5.13x10^{15}$ α-particles and sample 8B irradiated with $2.54x10^{16}$ α-particles.

Fig. 6.07 shows the X-band ESR signal from one of the LBS glasses, containing 2.42 mol% La_2O_3 and its parent MW glass

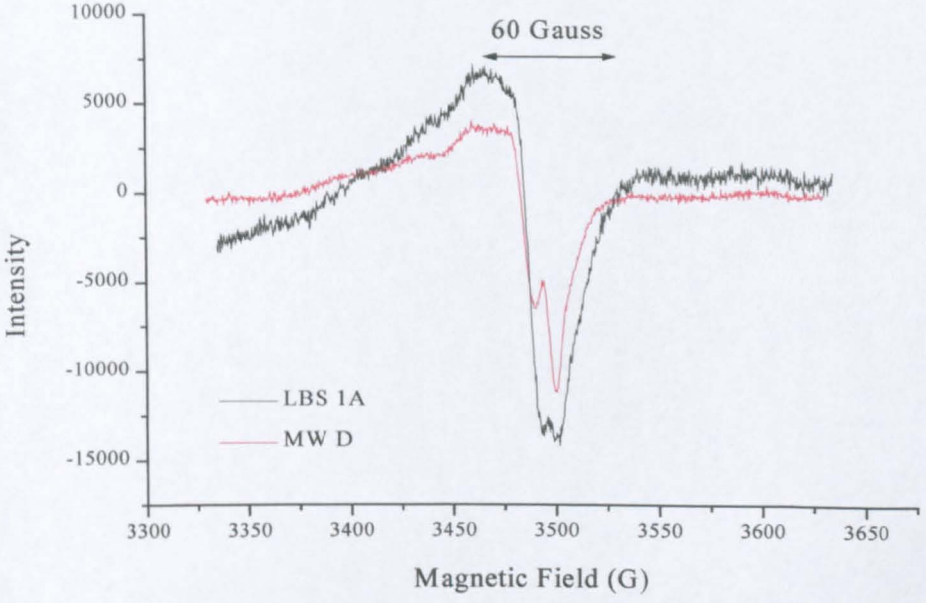

Fig. 6.07 Comparison of the X-band ESR spectrum of sample LBS 1A and a sample of MW glass, irradiated with a similar α-particle dose.

Several points of interest stand out in Fig. 6.07. Firstly, the intensity of signal from the LBS glass is substantially greater than that of the MW glass, suggesting a greater number of sites responsible for the observed features being present in the irradiated LBS glass. However, results shown in Fig. 6.05 do not

show a clear correlation between the total α-particle dose and spectrum intensity. It has been proposed that the addition of La_2O_3 to the MW composition leads to the formation of $[LaO_4]^-$ units, at the expense of $[BO_4]^-$ units. In conjunction with the suggestion of Lee and Bray [9], that the contribution to the 5-part ESR lineshape is caused by ^{11}B nuclei at the centre of $[BO_4]$ tetrahedra, it may be postulated that the observed decrease in the number of such sites would lead to a decrease in intensity of the resulting ESR signal. Insufficient experimental data is available to be able to comment with certainty on the effect of incorporating La_2O_3 but other possible effects might be expected. For instance, also of interest in the LBS 1 spectrum is the change in nature of the large feature attributed to the $Si\text{-}O^-/h^+$ trap. In all the NBS glasses showing well-defined ESR spectra, though the intensity varies, the shape of the line is relatively stable. One of the only tentative conclusions that could possibly be drawn from this is that the added La_2O_3 in some way interferes or competes with the effectiveness of the $Si\text{-}O^-/h^+$ sites, perhaps by formation of $La\text{-}O^-/h^+$ traps.

6.3.2 Cyclotron and UV-irradiation

6.3.2.1 ESR spectroscopy

One of the NBS samples exposed to α-radiation from the cyclotron was subsequently exposed to 248nm U-V radiation in an attempt to detect changes in the ESR signal with the optical bleaching effect of the U-V light, shown in Fig. 6.08.

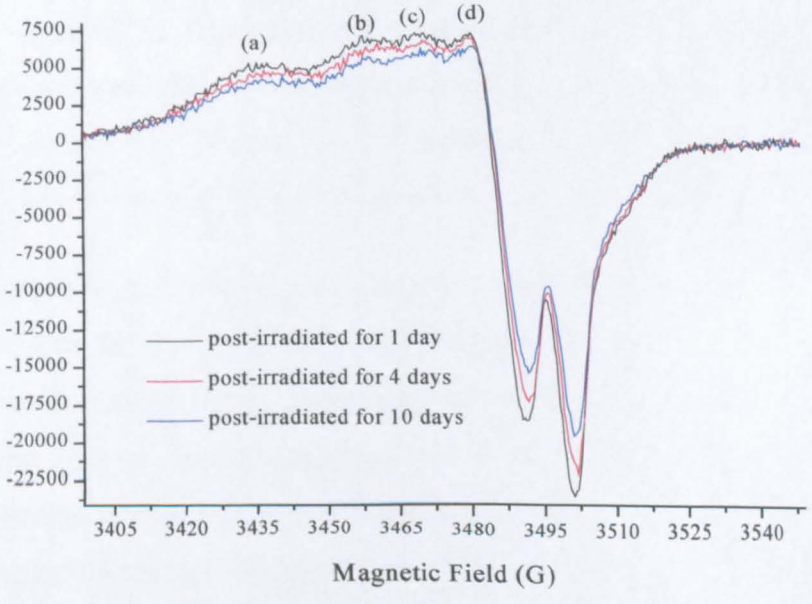

Fig. 6.08 Comparison of the ESR spectra obtained from sample NBS9A after exposure to 5.5MeV α-particles and 248nm UV radiation.

It can be seen that there is a small gradual decrease in the overall intensity of the spectra as the U-V radiation exposure progresses but no great change in the relative intensity or shape of the observed features. The intensity of both the suggested spectral contributions from the ^{11}B hyperfine structure and silicon NBO hole traps ($Si\text{-}O^{-}/h^{+}$) can be seen to decrease in intensity relatively slowly over a period of days, as shown in Fig. 6.09.

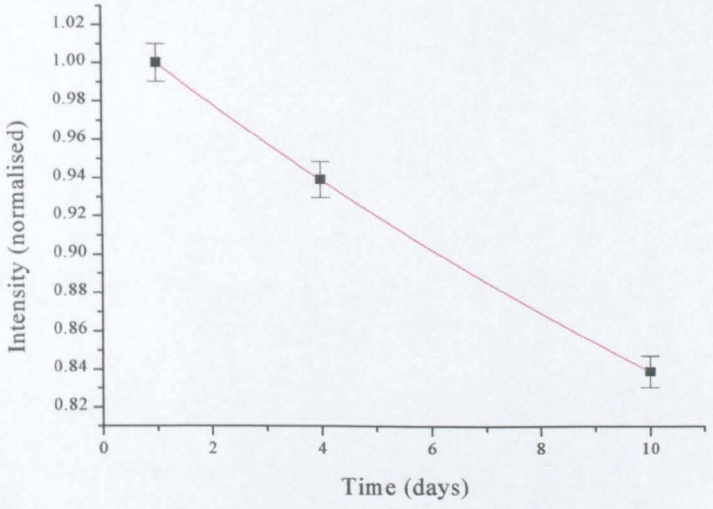

Fig. 6.09 Variation in intensity of the proposed $Si\text{-}O^{-}/h^{+}$ site with U-V radiation dose in sample NBS 9A (previously irradiated with $2.1x10^{16}$ α-particles).

Work by Nofz *et al.* [8] has indicated that the defects ($Si\text{-}O^{-}/h^{+}$ traps and electron centres) present in alkali silicate glasses are annealed at the same rate, their intensities dropping to ~20% after 20 minutes irradiation by an 800W Hg(Xe) optical lamp. The longevity of the signals observed to decay in the current UV-bleached samples results from the low energy of the UV-source used. It can also be acknowledged that the origins of the signals are very stable under normal atmospheric conditions of light and temperature.

6.3.2.2 UV-Visible absorption spectra – irradiated glasses

Several of the cyclotron irradiated NBS glass samples were retrieved intact and a distinct darkening of the area exposed to the α-particle beam was observed. One of the samples was then exposed to a 100W U-V lamp, operating at 252nm, for increasing periods of time and the UV-visible spectrum acquired after each exposure. Fig. 6.10 shows the change in optical properties of the sample with exposure to the U-V radiation.

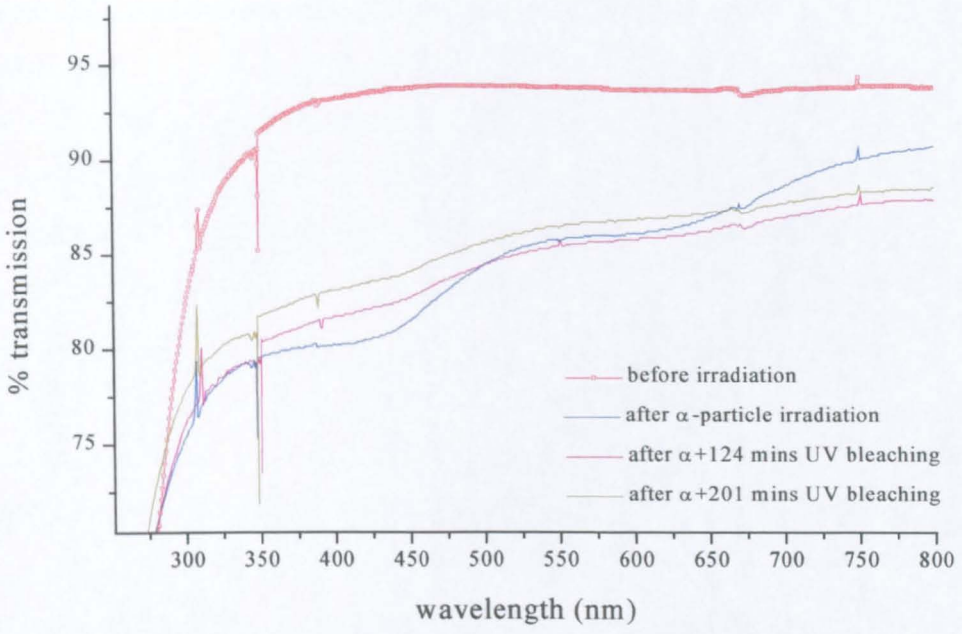

Fig. 6.10 Change in the UV-Visible transmission characteristics of glass NBS 11D after α-particle irradiation and UV-bleaching.

Sample NBS 11D contains no B_2O_3 but shows a marked difference in its post α-irradiation visible absorption spectrum and that obtained prior to irradiation. It is therefore reasonable to conclude that the processes responsible for the darkening observed after bombardment with α-particles are not related to the features, due to defects associated with ^{11}B nuclei, observed in the ESR spectra of the other NBS compositions. Subsequent bleaching with UV radiation led to a decrease in the intensity of the darkened region with increasing time, as seen by the increase in transmission of visible light in Fig. 6.10.

6.3.2.2 UV- Visible absorption spectra – unirradiated glasses

The UV-visible absorption spectra of several LBS compositions were also obtained and are shown in Fig. 6.11. It can be seen that there is a variation in the UV absorption edge of the LBS glasses from LBS 1 = 341nm < LBS 3 = 345nm < LBS 4 = 355nm, though the overall difference between the 2.42mol% (LBS 1) and 12mol% (LBS 4) glasses is not considerable. All the glasses exhibit a faint yellow colour that grows in intensity as the composition becomes more saturated with La_2O_3 and this can be seen to have an effect on the transmission of light between infrared and UV wavelengths. In alkali-doped silica, the gradual increase in UV cut-off wavelength

has been attributed by Stevels [10] to the generation on NBOs on the $[SiO_4]$ tetrahedral units.

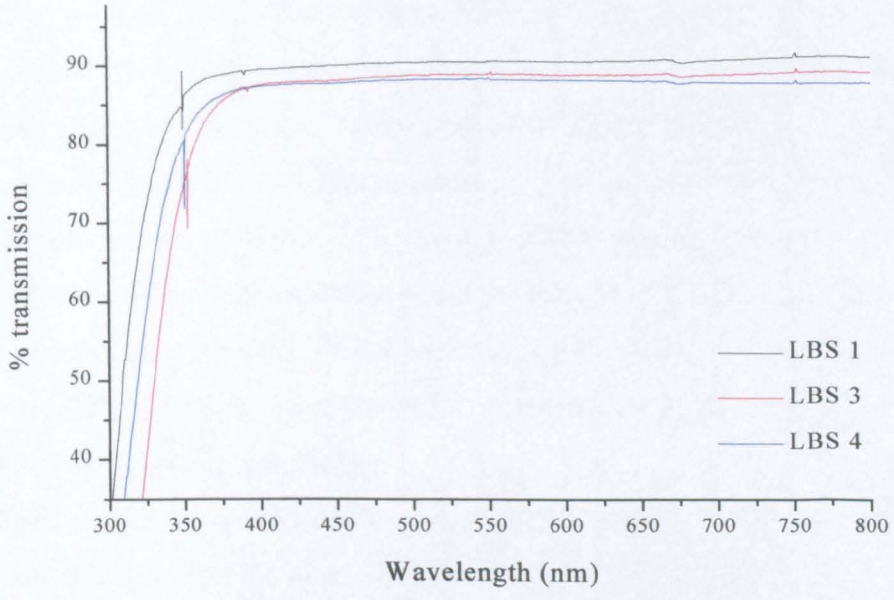

Fig. 6.11 Variation in the UV-visible absorption characteristics of the MW glass with increasing concentration of La_2O_3. The UV cut-off is measured from the onset point.

In the structural studies of the LBS glasses detailed in Chapter 5, an increased interaction between the $[LaO_4]^-$ units and silicon tetrahedra has been suggested, leading to the removal of NBOs as the La_2O_3 content increases. This situation would not correlate with the ideas of Stevels in explaining the observed increase in UV cut-off wavelength for these LBS glasses but the presence of more and more Si-O-La links could have a similar effect.

6.4 Summary

Preliminary investigation of the interaction of the NBS and LBS glasses with two different types of radiation has been carried out. Approximately 30 samples of varying NBS compositions and 4 samples of the LBS glasses were irradiated with 5.5 MeV α-particles and analysed for the presence of decay products and defect centres using γ-ray and ESR spectroscopy. Initial results have given evidence for the $^{10}B(\alpha,n)$ reaction and an interaction between the incident α-particles and the ^{10}B nucleus. This provides evidence that is of importance to the use of this glass system

as a HLW disposal solution. Previous research has shown that a substantial number of fast-neutrons are generated by reactions involving the ^{10}B and ^{11}B nuclei. The dose given to each sample could not be correlated simply to the observed intensity or nature of the defect signals observed from ESR analysis, though the total number of nuclei available to take part in the (α,n) reaction could be of more importance than the number of incident particles. Interpretation of the ESR spectra for the irradiated samples shows evidence of defect centres located on both B and Si atoms, in agreement with other workers. It is thought that annealing processes which can occur during and after the irradiation obscure some of the defect centres produced and fine detail is not observed. What has been shown from UV-irradiation of some of the α-irradiated samples is that the defect sites are stable and long-lived in normal temperatures and lighting-conditions.

The incorporation of La_2O_3 has been seen to interfere with the contribution to the ESR signal from $Si\text{-}O^-/h^+$ sites, possibly through the formation of $La\text{-}O^-/h^+$ sites. Investigation of the UV-Visible transmission characteristics of the La-doped glasses has shown that there is a small but definite increase in the UV cut-off wavelength as the La_2O_3 concentration is increased. This could be as a result of the supposed interaction between the $[LaO_4]^-$ units and silicate network discussed in Chapter 5.

6.5 References

[1] J. Chang, Table of the Nuclides, Korea Atomic Energy Research Institute, http://atom.kaeri.re.kr/ton/nuc8.html

[2] L. Van der Zwan and K. W. Geiger, Nuclear Physics A **246** (1975) pp.93-103

[3] J. W. Marsh, D. J. Thomas & M. Burke, Nuclear Instruments and Methods in Physics A **366** (1995) p.340

[4] J. K. Bair & J. Gomez del Campo, Nuclear Science and Engineering **71** (1979) p.18

[5] W. J. Weber, R. C. Ewing, C. A. Angell, G. W. Arnold, A. N. Cormack, J. M. Delaye, D. L. Griscom, L. W. Hobbs, A. Navrotsky, D. L. Price, A. M. Stoneham & M. C. Weinberg, J Mater. Res. **12** (8) (1997) p.1950

[6] W. J. Weber & F. P. Roberts, Nuclear Technology **60** (1983) p.178

[7] D. L. Griscom, C. I. Merzbacher, R. A. Weeks & R. A. Zuhr, J. Non-Cryst. Solids **258** (1999) p.34

[8] M. Nofz, C. Reich, R. Stösser, J. Bartoll & E. Janata, Glastech. Ber. **72** (1999) (3) p.76

[9] S. K. Lee & P. J. Bray, J. Chem. Phys. **39** (11) (1963) p.2863

[10] J. M. Stevels, Proc. 11th Int. Congress on Pure and Appl. Chemistry **5** (1953) p.315

Chapter 7 – General system characterisation and modelling

7.1 ABS series

7.1.1 Composition details

Samples used in the general system characterisation studies were prepared by varying the amount of silica and modifier present according to the general formula, $\boldsymbol{K}SiO_2 \cdot B_2O_3 \cdot \boldsymbol{R}M_2O$, where K describes the ratio of silica to boron oxide, and R the ratio of modifier oxide to boron oxide. Table 7.01 presents details of those compositions used in the present work.

	Mol% composition			
R	SiO_2	B_2O_3	Na_2O	Li_2O
		K=1		
0.2	45.45 45.39	45.45 45.35	4.59 4.68	4.50 4.56
0.32	43.1	43.1	6.97	6.83
0.352	42.5	42.5	7.575	7.425
0.4	41.66	41.66	8.42	8.25
0.5	40	40	10.1	9.9
0.666	37.5 37.65	37.5 37.47	12.62 12.36	12.37 12.50
0.753	36.5	36.5	13.64	13.37
0.857	35	35	15.15	14.85
1	33.33	33.33	16.83	16.83
1.5	28.57 28.88	28.57 28.73	21.64 21.14	21.22 21.23
		K=2		
0.15*	63.49	31.74	2.40	2.36
0.25*	61.54	30.77	3.88	3.81
0.33	60 59.27	30 30.39	5.05 4.99	4.95 5.33
0.5	57.14	28.57	7.21	7.07
0.6*	55.54	27.77	8.43	8.26
0.636*	55.00	27.50	8.84	8.66
0.64*	54.94	27.47	8.88	8.71
0.7*	54.05	27.03	9.55	9.36
1	50	25	12.625	12.375
1.22*	47.4	23.7	14.59	14.31
1.44	45.05	22.52	16.38	16.05
1.7*	42.56	21.28	18.26	17.9
2	40	20	20.2	19.8
2.26	38.02	19.01	21.70	21.27

2.5	36.36 36.75	18.18 18.40	22.95 22.84	22.50 22.00
2.6	35.71	17.86	23.45	22.98
		K=2.4		
0.15	67.72	28.1	2.11	2.07
0.25	65.84	27.32	3.46	3.38
0.379	63.54	26.38	5.05	4.95
0.6	60.11	24.94	7.55	7.40
0.723	58.29	24.19	8.83	8.64
0.781	57.50	23.86	9.41	9.21
0.852	56.48	23.46	10.1	9.9
1.136	52.95	21.99	12.63	12.37
1.29	51.18	21.26	13.89	13.61
1.46	49.42	20.52	15.15	14.85
1.75	46.71	19.38	17.13	16.79
2.26	42.43	17.60	20.2	19.9
		K=3		
0.15	72.29	24.10	1.82	1.79
0.25	70.59	23.52	2.97	2.91
0.375	68.58	22.86	4.32	4.24
0.5	66.66	22.22	5.61	5.5
0.545	66.00	22.00	6.06	5.94
0.753	63.16	21.05	7.97	7.81
1	60	20	10.1	9.9
1.26	57.00	19.00	12.12	11.88
1.6	53.57	17.86	14.42	14.14
1.7	52.63	17.54	15.1	14.72
2.26	47.91	15.97	18.22	17.86
		K=4		
0.15	77.68	19.42	1.465	1.435
0.25	76.2	19.05	2.40	2.35
0.33	75.00 74.69	18.75 18.49	3.16 3.10	3.10 3.70
0.5	72.72	18.18	4.60	4.50
0.714	70.00	17.5	6.31	6.187
0.753	69.57	17.39	6.58	6.46
1	66.66	16.66	8.42	8.24
1.153	65.00	16.25	9.46	9.28
1.66	60.00 60.33	15.00 15.30	12.63 12.22	12.38 12.14
2.26	55.00	13.75	15.78	15.46
2.56	52.91 53.2	13.22 13.6	17.09 16.55	16.77 16.64
3	50	12.5	18.94	18.56
3.88	45 45.38	11.25 11.41	22.09 21.60	21.66 21.60

*Table 7.01 Mol% compositions of ABS series samples. Note: chemical analyses are highlighted in red. * - 0.1mol% Fe_2O_3 added to facilitate Si^{29} NMR measurements.*

7.1.2 Structural Characterisation

7.1.2.1 NMR spectroscopy – introduction

The structural details that have been elucidated from the NMR spectra of these glass samples are central to further understanding of other physical properties such as density and the coefficient of thermal expansion, so it is right that these results should be presented and discussed before all others. The glasses studied in the general system characterisation will be discussed first.

a) ^{11}B NMR - spectra

Firstly, the ^{11}B spectra of the samples in each *K* series are shown in Fig. 7.01(a-e). All the peaks corresponding to tetrahedrally coordinated boron atoms, labelled B_4 in each spectrum, have been referenced to the frequency of the B_4 peak from Pyrex®, arbitrarily assigned a chemical shift value of zero, which enables comparison of results taken at different times. Other studies have referenced their ^{11}B NMR data to $Et_2O{:}BF_3$ and assigned the contribution from the tetrahedral boron site in pyrex a chemical shift of +1.8 ppm. Hence, to compare the current work with any other, a factor of 1.8 ppm must be added to the observed chemical shifts. In addition, all the spectra have been normalised to the intensity of the B_4 peak of the sample with the lowest R value.

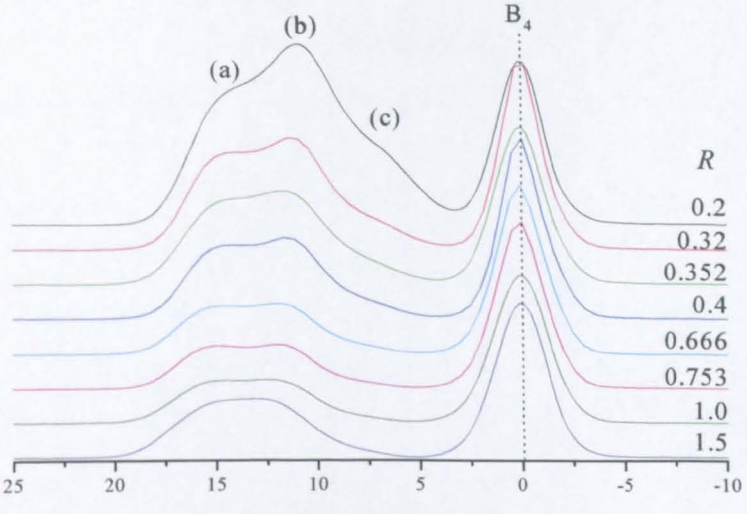

(a) K = 1

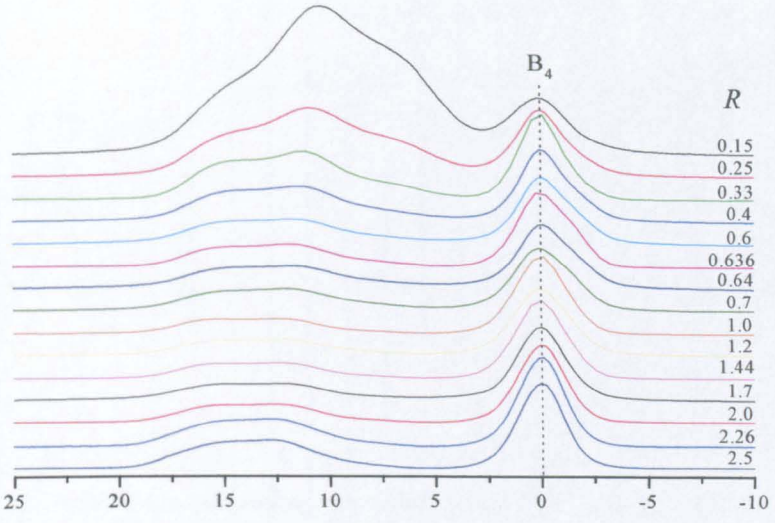
B4
R
0.15
0.25
0.33
0.4
0.6
0.636
0.64
0.7
1.0
1.2
1.44
1.7
2.0
2.26
2.5
25
20
15
10
5
0
-5
-10
Chemical Shift (ppm)

(b) K = 2

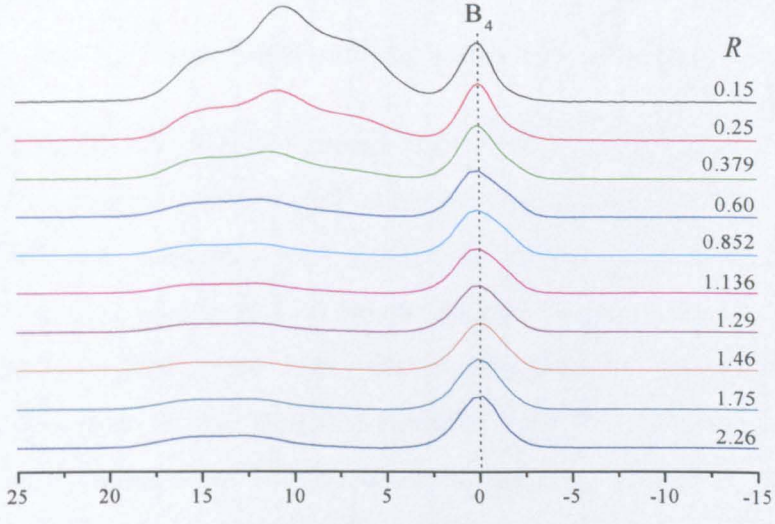
B4
R
0.15
0.25
0.379
0.60
0.852
1.136
1.29
1.46
1.75
2.26
25
20
15
10
5
0
-5
-10
-15
Chemical Shift (ppm)

(c) K = 2.4

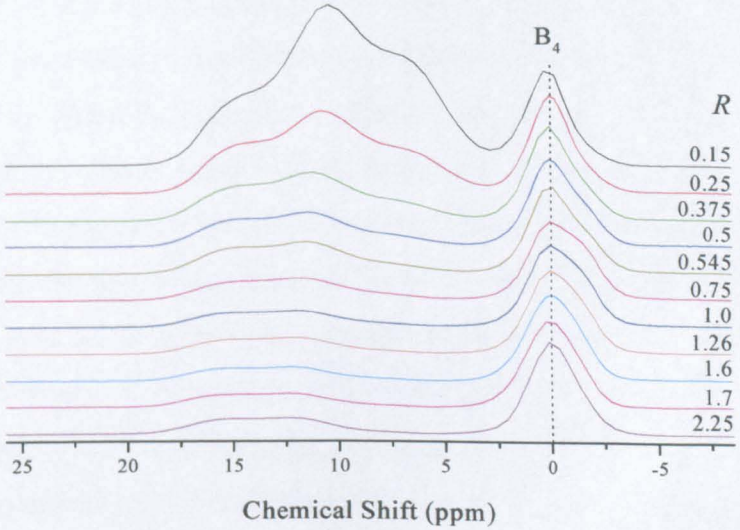
B4
R
0.15
0.25
0.375
0.5
0.545
0.75
1.0
1.26
1.6
1.7
2.25
25
20
15
10
5
0
-5
Chemical Shift (ppm)

(d) K = 3

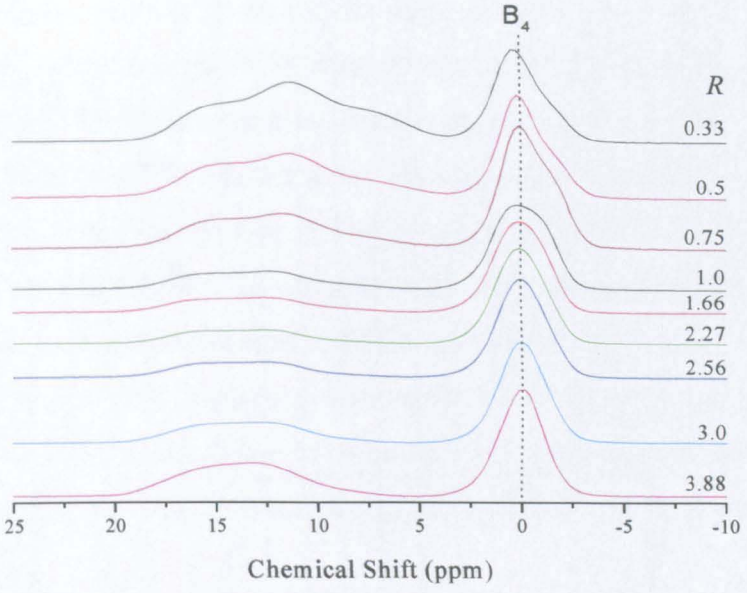

(e) K = 4

Fig. 7.01 ^{11}B MAS NMR spectra of samples with varying K and R

Inspection of each series of spectra shows that, superficially, the shape of the B_4 peak remains relatively unchanged across varying K and R, whilst the nature of the B_3 peak changes noticeably as R increases. At very low R, according to the model [1], there must be only two borate species present, based on the known concentrations of modifier, boron and silicon atoms present. The measured value of N_4 confirms this since all the available modifier goes towards producing B_4 units, none is available to introduce NBOs on silicate units or to produce trigonal boron units with one NBO, the f_3 unit described earlier. Similar B^{11} NMR work [2] has shown that the trigonal signal in Na-borosilicate glasses can be simulated with two peaks that they assign to symmetric (f_1) and asymmetric (f_3) boron sites.

Closer inspection of the NMR spectra shows that the majority of the B_3 peak shapes cannot be simulated using fewer than 2 peaks, but the Dell model, which will be taken as the most successful to date, indicates that the asymmetric contribution cannot be from an f_3 unit at these compositions. Another source of the asymmetry of the boron unit may be the presence of B-O-Si links, rather than the presence of NBOs. This may be thought of as asymmetry in the second co-ordination sphere rather than the first. A visual inspection of each sample was made to detect phase separation since it is believed [1] that the borate and silicate matrices do not interact at low R. Interestingly no obvious evidence (large-scale phase separation) was found, again lending support to the idea that there is an interaction between the

borate and silicate matrices at an earlier stage than has been previously thought. Whether this arises from the B-O-Si links present at the interfaces of phase separated regions or from a more extensive interaction is hard to say, but further comment will be made in light of the ^{29}Si NMR spectra discussed in section 7.1.2.1(c). It can be seen that the B_4 signal in the $K = 4$, low R spectra is in fact quite asymmetric in nature, though it is possible to fit the peak with one quadrupolar lineshape, so there are changes in B_4 local environment as a function of K and R.

As with the NBS glasses, a deconvolution of the contributions to several spectra in the all the K series has been carried out, assuming the presence of one tetrahedral site and two trigonal sites, all exhibiting a quadrupolar interaction.

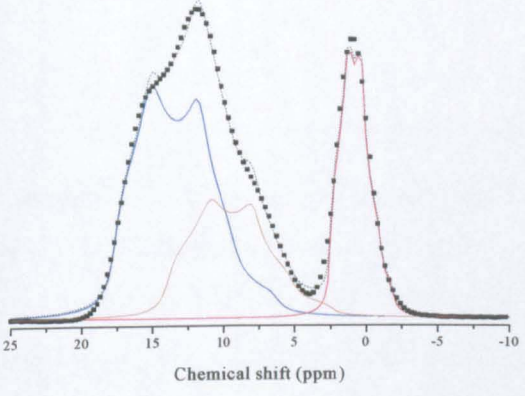

(a) K = 1; R = 0.2

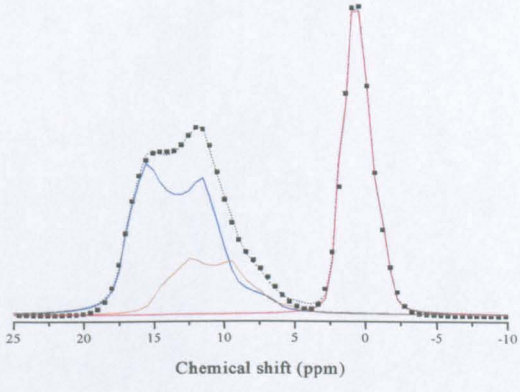

(b) K = 1; R = 0.32

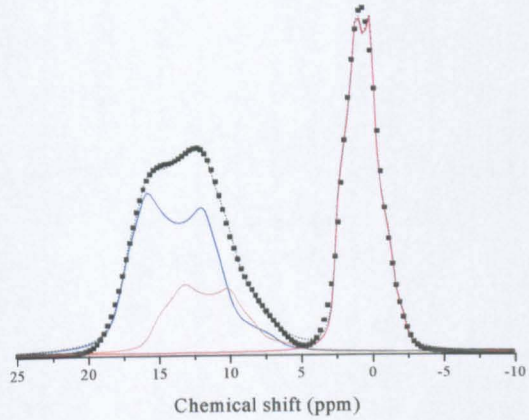

(c) K = 1; R = 0.352

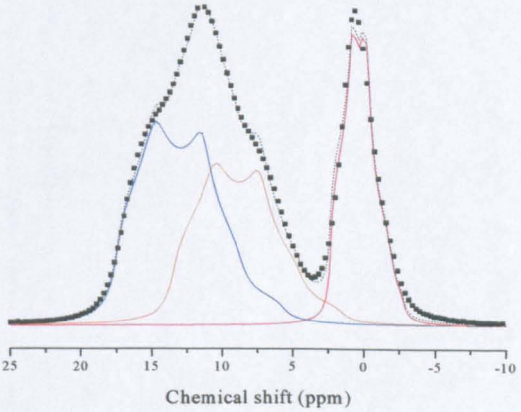

(d) K = 2; R = 0.25

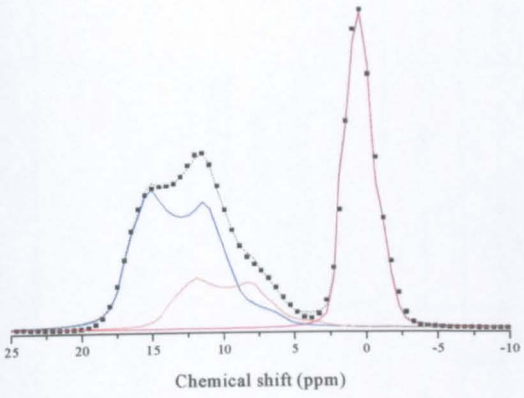

(e) K = 2; R = 0.33

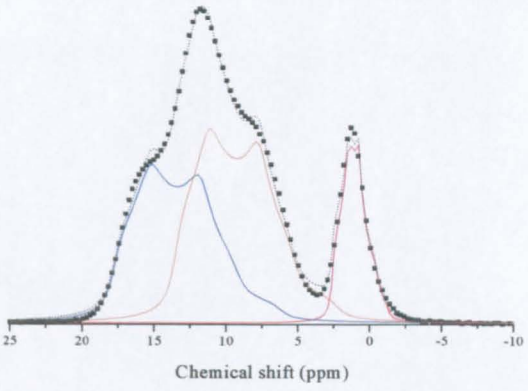

(f) K = 2.41; R = 0.15

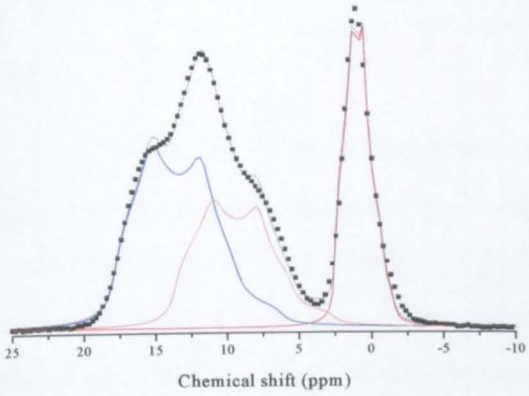

(g) K = 2.41; R = 0.25

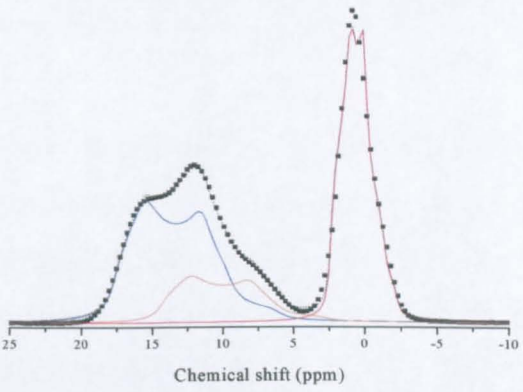

(h) K = 2.41; R = 0.379

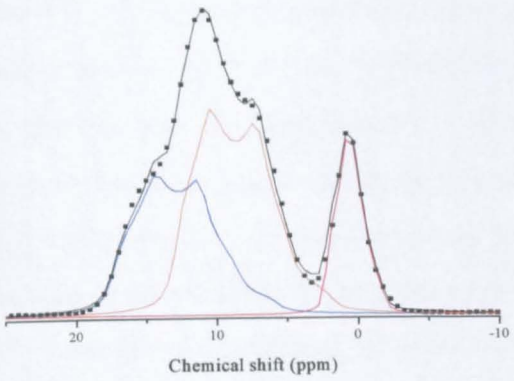

(i) K = 3; R = 0.15

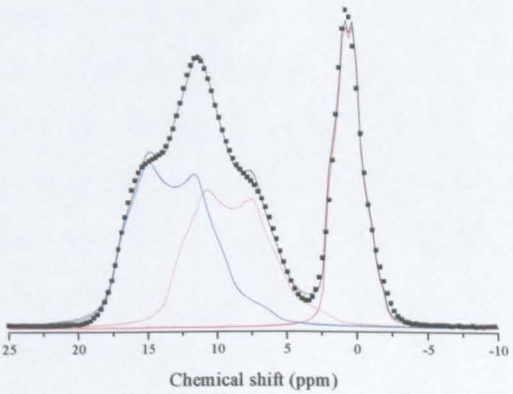

(j) K = 3; R = 0.25

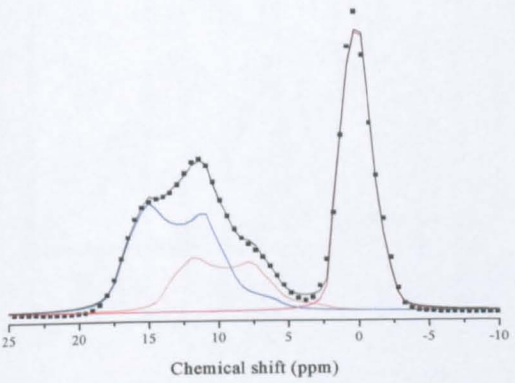

(k) K = 3; R = 0.375

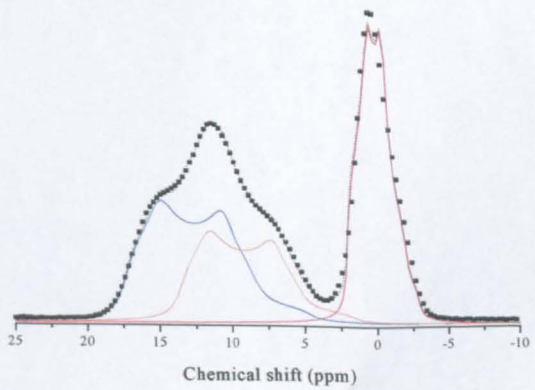

(l) K = 4; R = 0.33

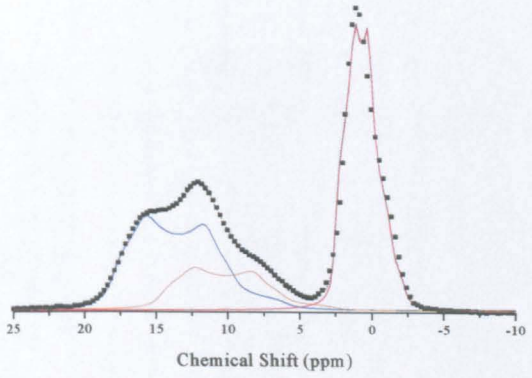

(m) K = 4; R = 0.5

Fig 7.02 Comparison of the experimental ^{11}B NMR spectra and simulations of several ABS glasses for different values of K and R given beneath the corresponding spectrum.
—— = BO_4, —— = BO_{3S}, —— = BO_{3A}, ····· = experimental data, - - - = fit.

The values of the isotropic chemical shift, δ_I, quadrupolar coupling constant, Q_{CC}, and asymmetry parameter, η, of each contribution were recorded. A complete table of parameters for all the $K = 3$ compositions is included in the appendix along with their respective spectra, whilst the parameters for the spectra shown in Fig. 7.02 are given in Table 7.02. Good agreement exists between the values of N_4 generated by the peak fitting and determined by simple integration of the B_3 and B_4 peaks from the ^{11}B NMR experiments carried out, though this gives no indication of the uniqueness of the fit to the trigonal [BO_3] contribution since there is good separation of the B_3 and B_4 contributions. Values for Q_{cc}, δ_i and η obtained from the deconvolution of experimental spectra of Na-borosilicate glasses have been reported by other workers [1,3] and agree well with the value of Q_{cc} obtained for the B_3 site and the chemical shifts observed for the two B_3 sites. Fig. 7.03 shows the ^{11}B MAS NMR spectra obtained from a boron-containing mineral and a borosilicate glass [4].

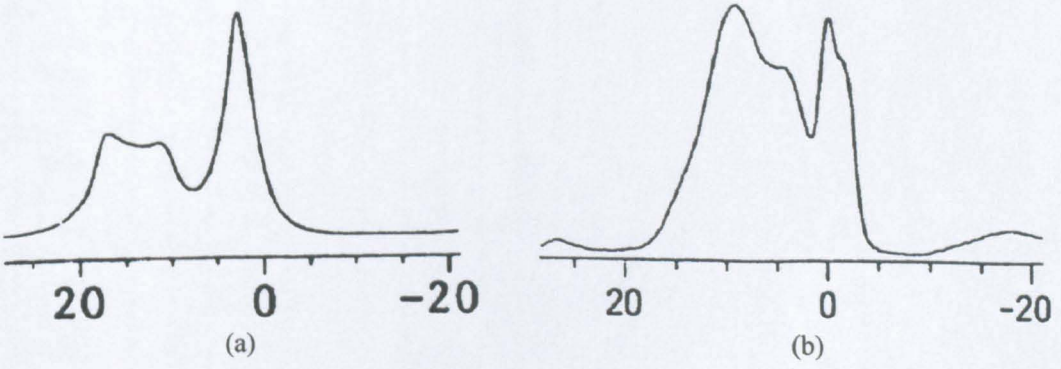

Fig. 7.03 Examples of ^{11}B MAS NMR lineshapes obtained from (a) kernite ($Na_2B_4O_6(OH)_2{\cdot}3H_2O$) and (b) pyrex glass (taken from [4]).

Sample *(K,R)*	*δ_i (ppm)* *(±0.5)*	*Qcc (MHz)* *(±0.05)*	*η* *(±0.05)*	*Species %* *(±5%)*
Site				
(1,0.2)				
BO_4	2.6	1.59	0.57	22/25.0
BO_{3S}	18.2	2.63	0.39	52
BO_{3A}	14.4	2.61	0.46	26
(1,0.32)				
BO_4	2.3	1.55	0.64	36/36.2
BO_{3S}	18.1	2.63	0.27	47
BO_{3A}	15.5	2.53	0.42	17
(1,0.352)				
BO_4	2.8	1.69	0.58	39/40.0
BO_{3S}	18.6	2.63	0.28	43.
BO_{3A}	16.1	2.51	0.37	18
(2,0.25)				
BO_4	2.40	1.70	0.61	25/27.0
BO_{3S}	18.1	2.68	0.41	42
BO_{3A}	14.0	2.66	0.45	33
(2,0.33)				
BO_4	2.2	1.56	0.68	38/35.2
BO_{3S}	18.1	2.68	0.30	45
BO_{3A}	14.9	2.67	0.31	17
(2.41,0.15)				
BO_4	2.60	1.44	0.58	14/16.8
BO_{3S}	18.4	2.65	0.41	40
BO_{3A}	14.0	2.60	0.38	46
(2.41,0.25)				
BO_4	2.5	1.51	0.61	25/26.4
BO_{3S}	18.4	2.65	0.38	45
BO_{3A}	14.2	2.58	0.40	30
(2.41,0.379)				
BO_4	2.50	1.62	0.57	40.2/37.7
BO_{3S}	18.4	2.68	0.31	43
BO_{3A}	15.2	2.71	0.29	17
(3,0.15)				
BO_4	2.21	1.55	0.61	15/17.5
BO_{3S}	17.8	2.65	0.45	36
BO_{3A}	13.4	2.60	0.38	49
(3,0.25)				
BO_4	2.30	1.55	0.61	26/27.7
BO_{3S}	18.10	2.64	0.36	40
BO_{3A}	13.9	2.63	0.38	34
(3,0.375)				
BO_4	1.9	1.62	0.55	40/41.6
BO_{3S}	17.9	2.70	0.30	40
BO_{3A}	14.6	2.72	0.29	20
(4,0.33)				
BO_4	2.1	1.66	0.58	35/37.4
BO_{3S}	18.2	2.81	0.32	38
BO_{3A}	14.5	2.74	0.27	27
(4,0.5)				
BO_4	2.6	1.66	0.57	45/47.2
BO_{3S}	18.8	2.74	0.31	38
BO_{3A}	15.5	2.73	0.32	17

Table. 7.02 ^{11}B NMR simulation parameters for the glasses shown in Fig. 7.02. Values highlighted in red are the % values of N_4 determined by standard integration of the B_3 and B_4 peaks.

Turner *et al.* [4] have reported the simulation of the pyrex spectrum using a 4-component peak fit with the following parameters: Q_{cc} = 2.5 MHz, δ_i = 12.6 ppm; Q_{cc} = 2.3 MHz, δ_i = 16.0 ppm; Q_{cc} = 0.5 MHz, δ_i = 1.8 ppm; Q_{cc} = 0.5 MHz, δ_i = 0.2 ppm. They suggest the presence of BO_3/BO_4 bonded to similar units (BO_3, δ_i = 16.0 ppm; BO_4, δ_i = 1.8 ppm) as in alkali borate glasses together with BO_3/BO_4 units whose spectra are modified as a result of interaction with the silicate network (BO_3, δ_i = 12.6 ppm; BO_4, δ_i = 0.2 ppm).

The spectra exhibiting the most well-defined structural features (*$R \approx 0.15 - 0.4$*) were fitted with a line broadening of 9-9.5 Hz and this produced the most satisfactory fit to the data. For higher *R* spectra, the lack of structure meant that though the amount of broadening applied to the lineshapes could be varied widely whilst still providing a satisfactory fit, the nature of each lineshape was altered drastically, leading to a large spread in possible values of δ_I, Q_{cc} and η. Somewhat tentatively, Fig. 7.04 shows the variation in abundance of the three contributions used to fit each of the experimentally obtained spectra. It can be seen that, as R increases, N_4 decreases, N_{3S} remains constant and N_{3A} decreases.

What can be considered in isolation, and with confidence, is that the trigonal boron sites in the *R = 0.15, 0.25* and *0.375* samples exhibit a complex shape which implies that there is a significant contribution from another [BO_3] site that has not been reported in previous work on similar systems. It may be concluded that the candidates for such a site are: a) a [BO_3] unit linked to an [SiO_4] unit, b) a [BO_3] unit linked to a $[BO_4]^-$ unit and c) a [BO_3] unit with one NBO. Situation c) can be ruled out because the experimentally determined fractions of tetrahedral boron units, discussed in the following section, show that all the available modifier is associated with $[BO_4]^-$ units. It may instead be the case that the signal arises from the asymmetry of a [BO_3] unit with a [BO_4] unit as a next nearest neighbour but it is doubtful whether this situation would cause a chemical shift of the magnitude observed in the spectra, particularly at the lowest values of *R*. In addition, no modification to the B_4 signal is observed, which might reasonably be expected if situation b) were occurring. However, it can be seen from Fig. 7.04(b) that the amount of silica present in the glass (i.e. *K*) has little effect on the rate at which N_4 increases, whereas there is a noticeable general increase in the fraction of asymmetric [BO_3] units with *K*. This behaviour could be a result of the inaccuracy

of the fitting procedure but at the same time it lends support to the only remaining candidate for the structure observed at low R for all the samples, that of a $[BO_3]$ unit with an $[SiO_4]$ unit as a next nearest neighbour. It can be seen that the B_{3A} contribution diminishes following an increase in the modifier content of the glass. If B_3-O-Si linkages are responsible for the unusual signal, then a decrease in their concentration is expected as more of the trigonal borate units are converted to tetrahedral units with, perhaps, the formation of B_4-O-Si.

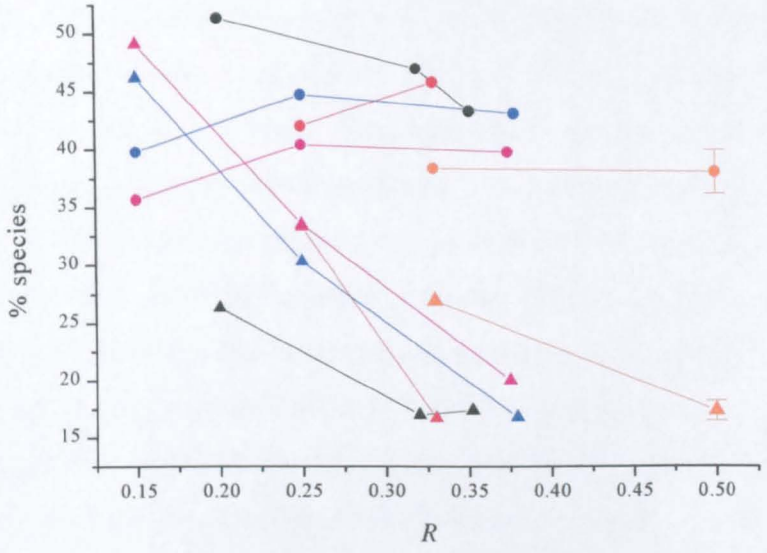

(a) N_{3S} & N_{3A} variation

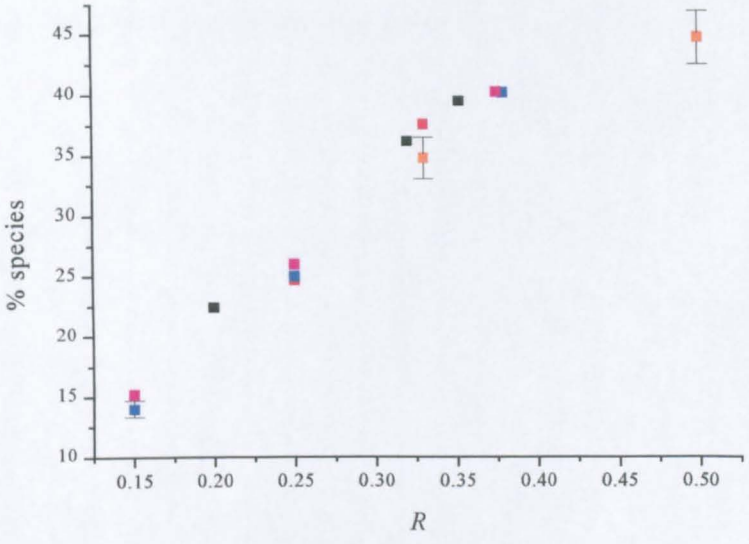

(b) N_4 variation

Fig. 7.04 Summary of the abundance of ^{11}B NMR spectral contributions as deduced from fitting of experimental data of several ABS glasses with varying K and R. Key: square – N_4, circle – N_{3S}, triangle – N_{3A}; —— : K = 1; —— : K = 2; —— : K 2.41; —— : K = 3; —— : K = 4.

b) ^{11}B NMR – B_3/B_4 co-ordination

Figs. 7.05(a-e) illustrate the trends in the variation of N_4 as K and R increase. It can be seen that the data follow the Dell model closely up to a point, after which the model then overestimates the value of N_4 before underestimating it at higher values of R. Recent data published by Martens and Muller-Warmuth [5] include several data points from the $K = 2$ series glasses and these have also been plotted in Fig. 7.05(b). These few points do not follow the Dell model and are much closer to the results of the present work. The extra modifier required to maintain this concentration of tetrahedral boron units would result in less than the expected amount of modifier being available to produce NBOs associated with silicon tetrahedra and trigonal boron units. The explanation for this change in behaviour between the single- and mixed-modifier systems and the Dell model is unclear. The extent of the deviation does not appear to be affected by the amount of silica in the glass. Because of this observed deviation from the Dell model, it is very difficult to predict the rate of formation of f_3, f_4 and f_5 units as R increases. It is also impossible to apportion alkali not associated with f_2 units between these borate units and the silicate network. The development of a comprehensive structural model based on NMR data has not been the objective of the current work but the inability to account for the possible modifier associations means that the discussion of trends based on NBO concentrations can be continued only up to $R = R_{D1}$ at most.

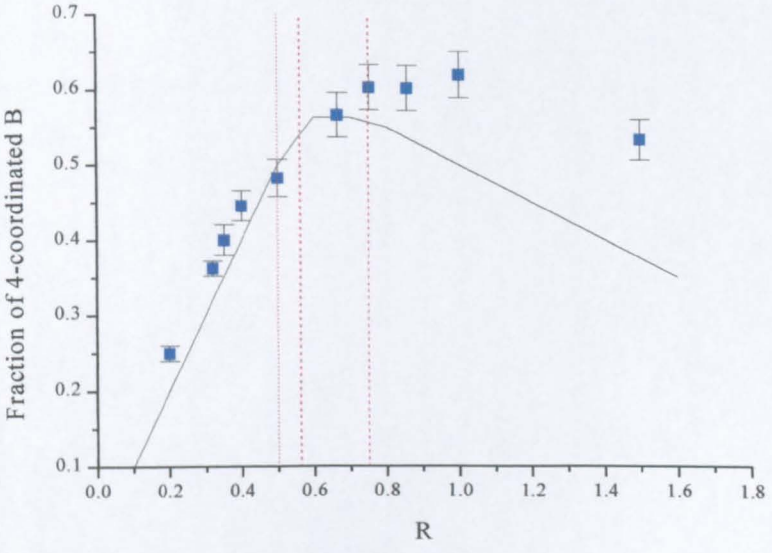

(a) K = 1

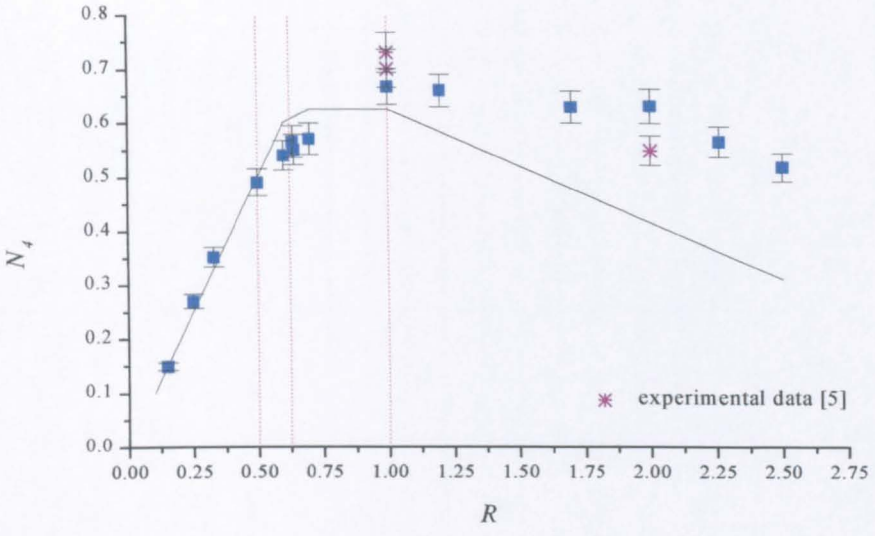
0.8
0.7
0.6
0.5
0.4
0.3
0.2
0.1
0.0
N_4
experimental data [5]
0.00 0.25 0.50 0.75 1.00 1.25 1.50 1.75 2.00 2.25 2.50 2.75
R

(b) K = 2

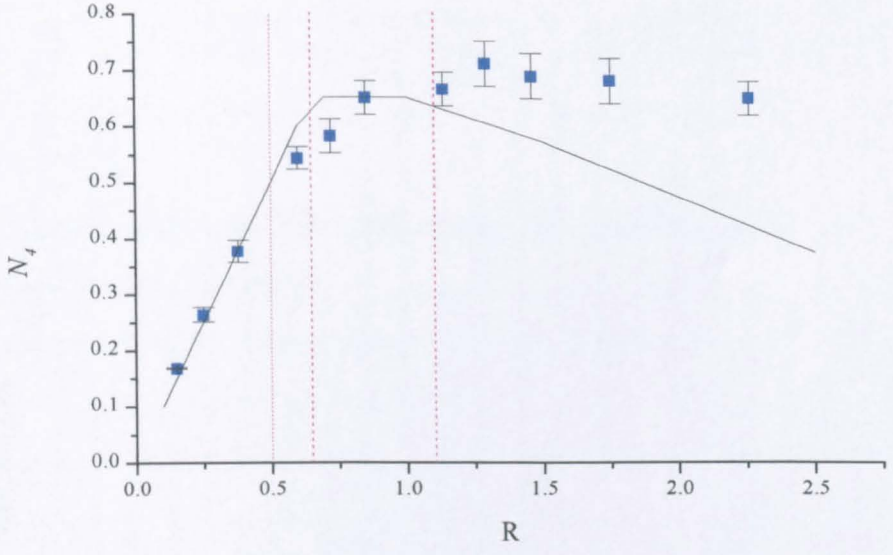
0.8
0.7
0.6
0.5
0.4
0.3
0.2
0.1
0.0
N_4
0.0 0.5 1.0 1.5 2.0 2.5
R

(c) K = 2.4

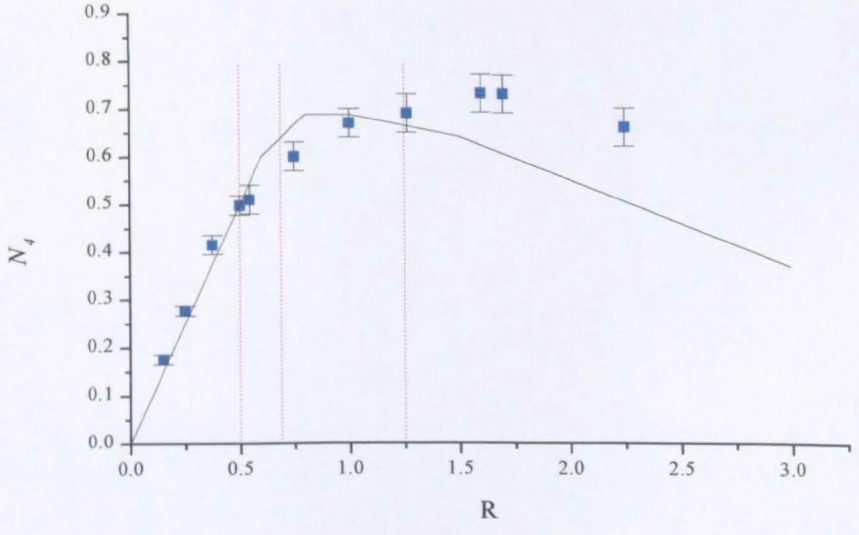
0.9
0.8
0.7
0.6
0.5
0.4
0.3
0.2
0.1
0.0
N_4
0.0 0.5 1.0 1.5 2.0 2.5 3.0
R

(d) K = 3

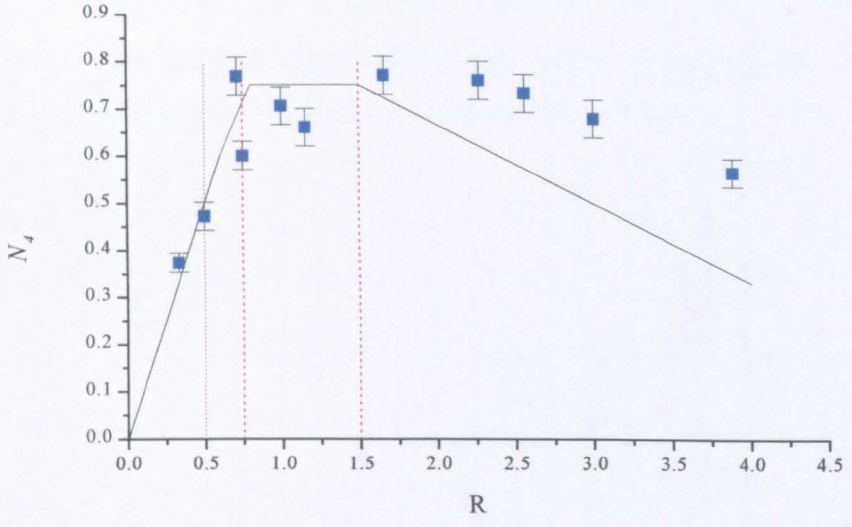

(e) K = 4

Fig. 7.05 The variation in fraction of 4-co-ordinated boron, N_4, of the ABS samples with varying K and R. Key: ■ : current data; —— : Dell model [1]. The dotted lines indicate the break points of the Dell model.

c) ^{29}Si NMR

Fig. 7.06 shows the ^{29}Si NMR spectra obtained from the K=2 glasses that were doped with 0.1mol% Fe_2O_3.

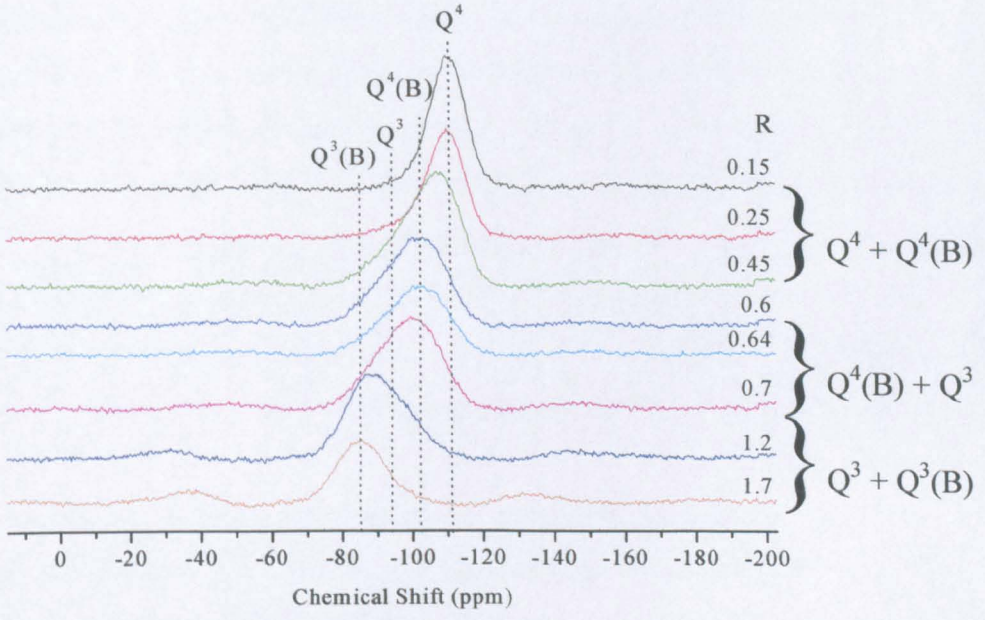

Fig. 7.06 ^{29}Si MAS NMR spectra obtained from K=2 samples doped with 0.1mol% Fe_2O_3. Also indicated are the structural units hypothesised to exist at various compositions.

Fig. 7.07(a,b) shows the result of fitting the ^{29}Si spectra obtained from the first two K = 2 glasses, whilst Table 7.03 gives details of the peaks and their

associated intensities for all K = 2 glasses. It should be noted that the spectra were fitted with two Gaussian lineshapes without any constraints and so the values given in the asterisked columns are subject to question as *R* increases.

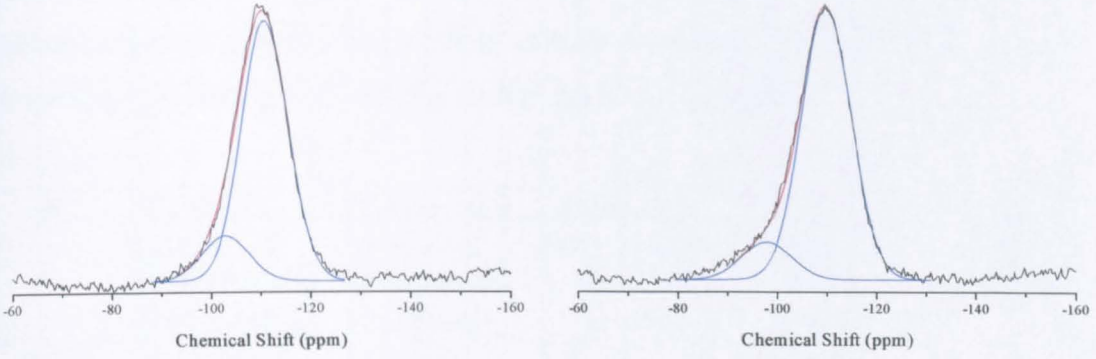

Fig. 7.07 Examples of the peaks used to fit the ^{29}Si spectra obtained from glasses with K = 2 and R = a) 0.15 and b) 0.25. Individual peaks are shown in blue and the fit is highlighted in red.

It can be seen that at low modifier concentrations, *R = 0.15, 0.25 and 0.45*, the vast majority of the silicon atoms possess a chemical shift of approximately –110 ppm, characteristic of Q^4 units bonded to other Q^4 units, as in vitreous silica. There is however, an increasing contribution from another species with a chemical shift of between –96 and -103 ppm that grows as the modifier concentration is increased. At this low modifier concentration, it is unlikely that Q^3 species have started to be formed since the model of Dell [2] assumes only Q^4 units exist until the critical modifier content is reached, corresponding to *R = 0.625* for *K = 2*. In addition, observed values of N_4 confirm that all modifier is associated with borate units. The spectra representing samples with *R = 0.15, 0.25* and *0.45* cannot be simulated with a single Gaussian peak, even though the model predicts only one silicate unit present.

At higher modifier concentrations, the resonance moves 'downfield' and samples with R = 0.6 to 0.7 exhibit a resonance around –100 ppm, again made up of two peaks with shifts of approximately –103 ppm and -92 ppm, respectively. Most of the intensity is now found in the –103 ppm peak and there is little change in the relative intensity of each peak between R = 0.6 and 0.7. Fig. 7.07 has shown that not all of the modifier expected to convert B_3 units to B_4 units actually does so and there is a consistent overestimation of the value of N_4 in this region. The ^{11}B NMR data

indicates that between 6 and 13% of the oxygen atoms associated with silicon tetrahedra would be non-bridging, equivalent to a dominance of Q^4 units over Q^3 units. It is impossible, with the available data, to calculate the number of NBOs per silicon atom above $R \sim 1$ since the Dell model predicts that some of the added modifier will produce NBOs on some of the $[BO_3]$ units. Since no quantitative information on the evolution of these units is available, the amount of modifier remaining to be associated with the silicate network is unknown.

R	Centre of gravity of ^{29}Si peak (± 1ppm)	Centre of gravity of fitted peaks* (± 1ppm)	Ratio fitted Peak 1: fitted Peak 2* (± 10%)	N_4 (from ^{11}B data)	NBOs/Si (from ^{11}B data)
0.15	−108	−110	85	0.15	0
		−102	14		
0.25	−108	−110	88	0.27	0
		−98	12		
0.45	−105	−109	69	0.45	0
		−98	31		
0.6	−100	−104	65	0.54	0.06
		−93	35		
0.64	−101	−104	68	0.55	0.09
		−93	32		
0.7	−99	−102	68	0.57	0.13
		−91	32		
1.2	−90	−96	40	0.66	-
		−86	60		

Table 7.03 Information extracted from the fitted ^{29}Si NMR spectra of several K=2 glasses.

Using the ^{11}B N_4 values for these compositions, the amount of modifier available to associate with the silicate network can be calculated as follows:

In a glass with general composition rR_2O bB_2O_3 $sSiO_2$, the number of tetrahedrally coordinated borons present at a given composition is given by

$$B^4 = N_4 * 2 * b \tag{7.01}$$

which also corresponds to the number of R^+ associated with B^4. Hence, the total amount of R_2O associated with B^4 is given by:

$$[R_2O] = N_4 * b \tag{7.02}$$

therefore, the amount of 'spare' modifier available to associate with the silicate network is:

$$r' = r - (N_4 * b) \tag{7.03}$$

Since there are 2 R^+ for each O^{2-} in R_2O, the number of NBO produced will be equal to:

$$2 * r' = 2 * [r - (N_4 * b)] \tag{7.04}$$

Hence, the number of NBOs introduced per silicate unit equals:

$$NBO_{Si} = 2 * [r - (N_4 * b)] / s \tag{7.05}$$

It can be deduced from this that if $R\ (=r/b) < 1$, virtually none of the oxygen atoms attached to the silicon atoms should be non-bridging. Therefore, it must be concluded that the second contribution to the ^{29}Si spectra arises either from Si-O-B linkages at the boundaries of the respective borate and silicate phases, or as a result of more intimate network interaction.

In addition, if Peak 1, obtained by fitting the spectra of compositions $R = 0.6 - 0.7$ and shown in Fig. 7.10, represented the fraction of Q^3 units present, the calculated values of N_4 are lower than those observed for ^{11}B NMR data. Bhasin *et al.* [6] have investigated the short range order in Na-borosilicate glasses using ^{29}Si NMR and report values of $Q^4 = 89\%$, $Q^3 = 11\%$ *and* $Q^4 = 0\%$, $Q^3 = 93\%$, $Q^2 = 7\%$ for compositions $K = 2$ and $R = 0.5$ and 1.0, respectively. This implies N_4 fractions for these compositions of 0.39 and 0, respectively, and obviously differs radically from the values expected (and generally observed) from the Na-borosilicate model [2] of 0.5 and 0.625. Misinterpretation of the results of the deconvolution process may have caused this error to occur.

As explained in Chapter 2, several workers [7-9] have developed alternative theories based on ^{11}B NMR results and have suggested that the proportional sharing of the modifier between the borate and silicate networks begins at a much lower

modifier composition. This would agree with the explanation that the second deconvolved peak is generated by the presence of Si-O-B linkages, despite previous studies suggesting that the effect of these bonds on the ^{29}Si chemical shift is a few ppm at most [10,11]. The value of N_4 that would be expected from looking at the ^{29}Si NMR data alone can be calculated using Eqs 7.01-7.05 in reverse order. In order to do this, assumptions regarding the fractions of silicate units with NBOs must be made from the ^{29}Si NMR data. Since the fractional contribution of the 2nd peak to the whole is known (from the fitted peaks), and if it is assumed that this arises because of Si-O-B linkages, knowing the composition of the glass allows the number of boron atoms, required to satisfy the experimental data, to be calculated. In other words, for compositions $R = 0.15, 0.25$ *and* 0.45, 14%, 12% and 31% of silicon atoms have one boron atom associated with them. Since, from the known concentrations of SiO_2 and B_2O_3, the ratio of total boron atoms: total silicon atoms = 1, it is known that 14%, 12% and 31% of boron atoms are associated in this way in each composition, respectively. Although no evidence (e.g. TEM) for the scale and extent of any phase separation is available, it is interesting to be able to comment on what consequences this information may have for the structure of the glasses. At the extreme, having 30% of the silicon tetrahedra associated with a boron atom implies an extensive number of Si-O-B links with "phase separated" regions of no more than several nm.

Using the information given in the last column of Table 7.04, the spectra were now *simulated* using Gaussian peaks where the ratio of two peaks were constrained by the fraction of NBOs predicted by ^{11}B NMR to be present at each composition (2-peak fitting). A further simulation was made using these constraints and including the intensity from the spinning side-bands (4-peak fitting), but this simulation produced a result that was little different from the 2-peak analysis.

Figs. 7.08(a-f) below compare the simulated spectra with and without the constraints dictated by the ^{11}B NMR data. (—— = data, —— = simulated peaks and —— = fit). The results of these simulations serve to show that a wide combination of peaks can be sufficient to simulate the experimental data, but the simulations are consistent with the data. This highlights the fact that, only in combination with other NMR data can a detailed picture be produced, as illustrated by [6] whose ^{29}Si NMR data does not make sense in the light of other NMR information.

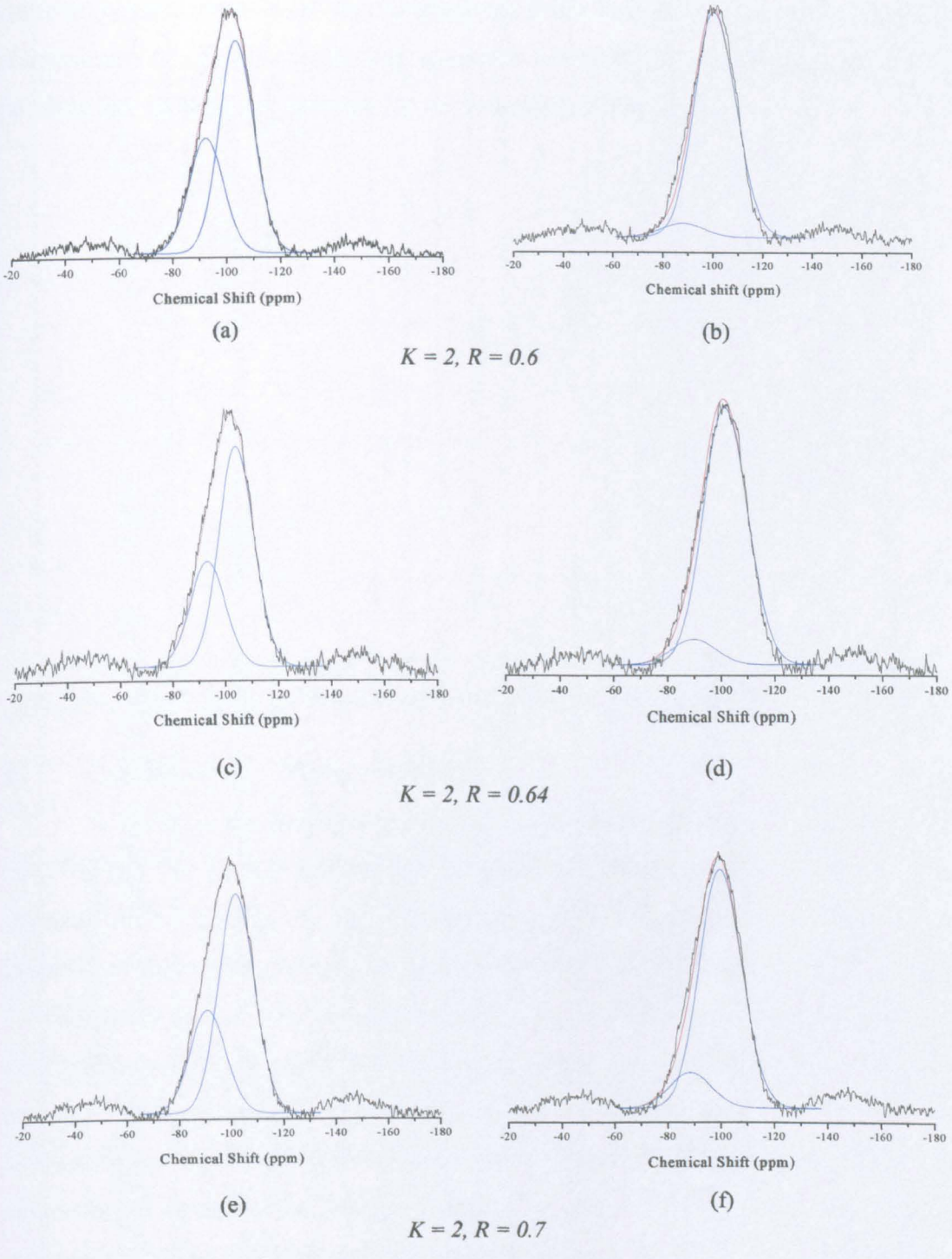

Fig. 7.08 Comparison of ^{29}Si peak fitting methods where a),c) and e) were unconstrained whilst b),d) and f) were constrained according to ^{11}B NMR information.

Fig. 7.09 compares the shift in centre of gravity of the ^{29}Si peaks from the present work with results obtained by MacKenzie *et al.* [7] for the Li- and Na-borosilicate systems and by Martens and Müller-Warmuth [5] for the Na-borosilicate system, showing there is generally good agreement between the mixed-modifier and single modifier data. No comment on the nature of the ^{29}Si lineshapes has been

made in previous work involving the single-modifier borosilicate systems. Since this phenomenon poses some interesting questions about the structure of the glass, it is possible that the effect is reserved for the mixed-modifier system.

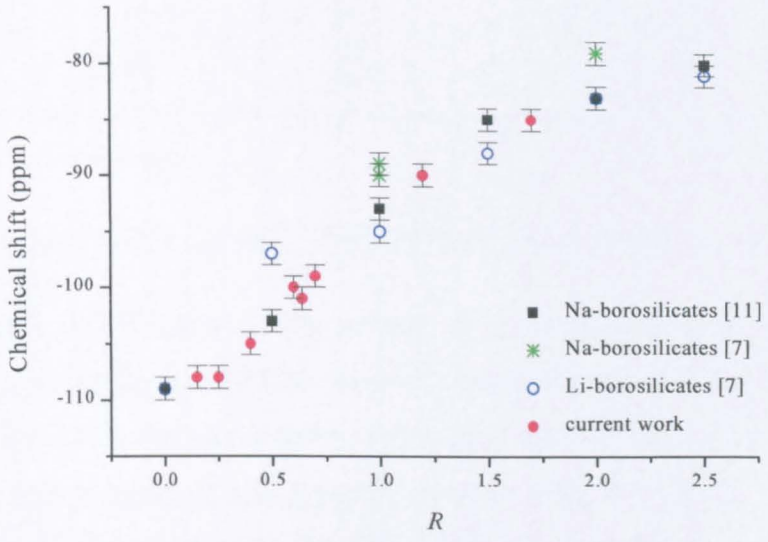

Fig. 7.09 Variation in ^{29}Si chemical shifts with modifier oxide content in K=2 borosilicate glasses.

d) Combination of ^{11}B and ^{29}Si NMR

A model of the structure determined from NMR must explain the features of both ^{11}B and ^{29}Si spectra and the way in which they change with composition. The intensity of the B_{3A} peak in Fig. 7.04 decreases rapidly as *R* increases, whereas the intensity of the second contribution needed to fit the ^{29}Si NMR spectra shown in Fig. 7.06 increases with *R*. The suggestion that the B_{3A} is a $[BO_3]$ unit with a Si atom as a next nearest neighbour could not be consistent with the trends unless B_4 effectively replaces B_{3A} from the B-O-Si link. As mentioned previously, this has been assumed in the fitting of the ^{11}B MAS NMR spectrum of pyrex [4]. Fig. 7.10 shows how it is necessary to combine the results of both ^{11}B and ^{29}Si NMR into one coherent explanation of the structural arrangement of the glass. At low R, ^{11}B NMR tells us that there is a significant contribution from asymmetric trigonal boron sites but the asymmetric contribution to the ^{29}Si NMR of the same sample is relatively small. Hence, it may be suggested that the asymmetry observed in the ^{11}B spectra, at low R, arises from B_3-O-B_4 linkages, whilst the signal seen in the ^{29}Si spectra arises from small numbers of Si-O-B_3 links. This would then explain the asymmetry of the B_4 peak observed in many of the samples. The use of ^{17}O NMR would allow accurate assignment of the sources of the contributions to the ^{11}B and ^{29}Si spectra.

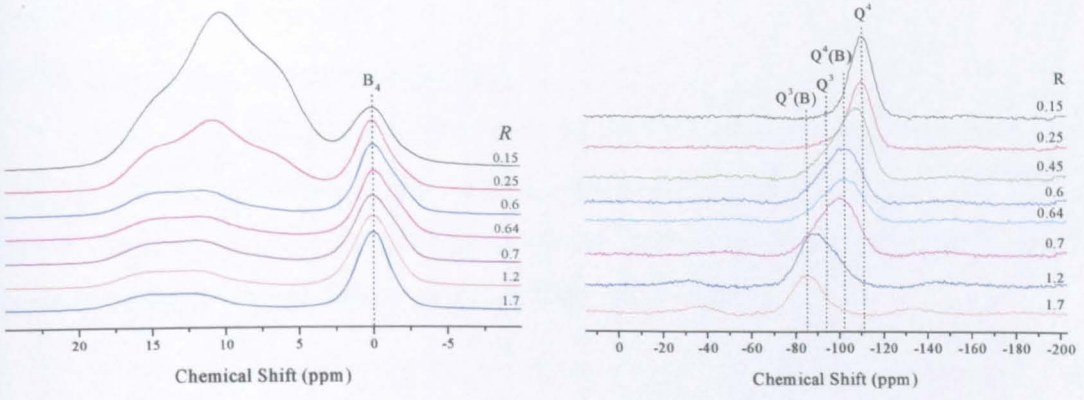

Fig. 7.10 Comparison of the ^{11}B and ^{29}Si NMR spectra obtained from the K = 2 series samples.

The lack of sphericity of the nuclear charge distribution, described by the nuclear quadrupole moment, inhibits the resolution that can be obtained under MAS conditions. The first order quadrupole contribution can be removed by magic angle spinning but second order effects can still be quite large. Removal of the second order quadrupole contribution to the line width can be achieved using multiple quantum magic angle spinning (MQMAS) by mixing single quantum and multiple quantum nuclear magnetisation together. In recent work, Wang and Stebbins [12] have made use of MQMAS ^{17}O NMR studies of borate and borosilicate glasses to test the assumptions of the Dell model and have made some interesting observations. They report evidence supporting the idea that there is intimate interaction between trigonal boron units and the silicate network. They also estimate that glasses of low *R*, showing relatively high concentrations of Si-O-B links, would require immiscibility domains on the scale of 2-3nm.

It is difficult to make a general statement covering all possible compositions given that ^{29}Si NMR data only exist for the $K = 2$ compositions. However, the agreement of the experimental variation in N_4 with the Dell model (i.e. $N_4 = R$, $N_3 = 1-R$) at low *R* enables the elimination of NBOs on silicon tetrahedra as the explanation for the asymmetry observed in the ^{29}Si NMR lineshapes and it may be assumed that this is the case for all values of *K*, given that the same trend in N_4 has been observed. At higher *R*, the emergence of what has been assigned a Q^3 peak is observed at approximately –90 ppm and this can be simulated fairly satisfactorily using constraints imposed by results of the ^{11}B NMR analysis. It is acknowledged that this shift is somewhat larger than that observed for Q^3 units in alkali silicate glasses and could result from the influence of B as a next nearest neighbour.

7.1.3 Physical properties

7.1.3.1 Glass transition temperature (T_g)

Figs. 7.11(a)-(d) show the variation in glass transition temperature with *R* for varying *K* for a range of single- and mixed-modifier borosilicate glasses. Also shown, for K = 1, is the variation in *Z*, the number of bridging oxygens per boron atom according to the structural model of Dell, Bray and Xiao.

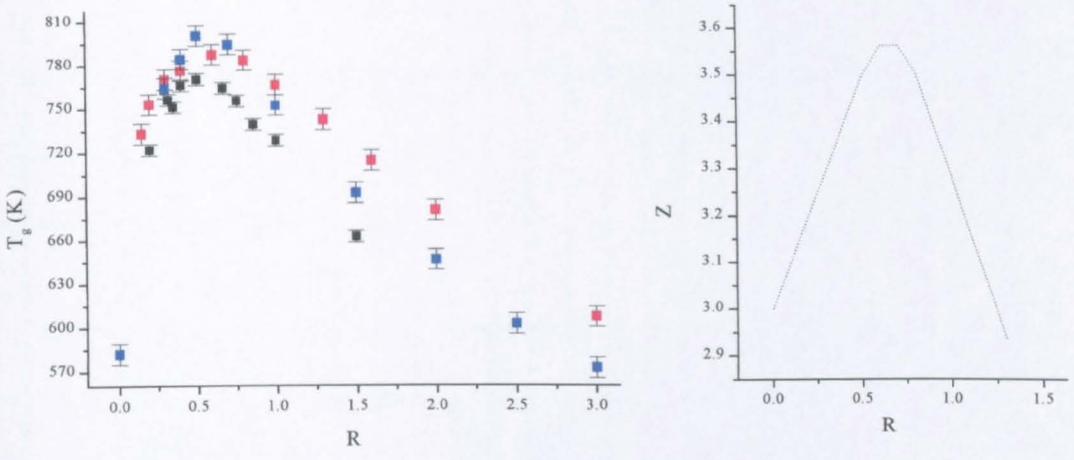

(a) K = 1

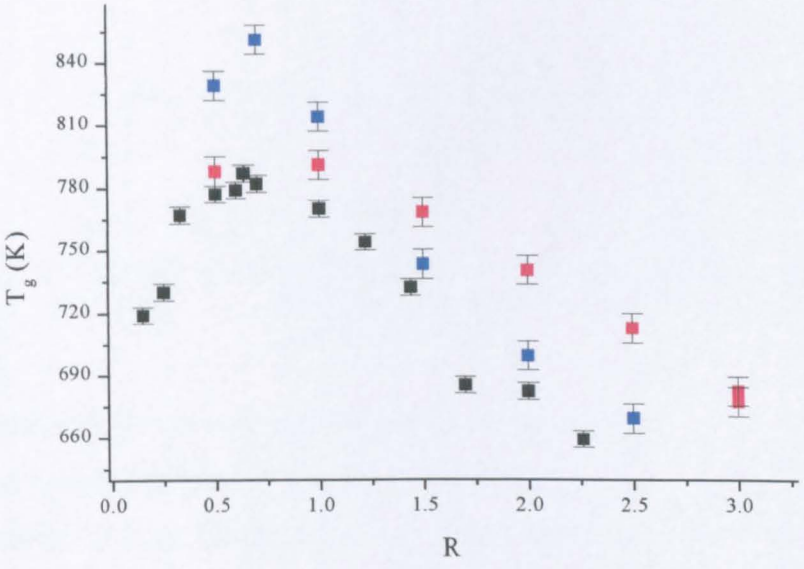

(b) *K = 2*

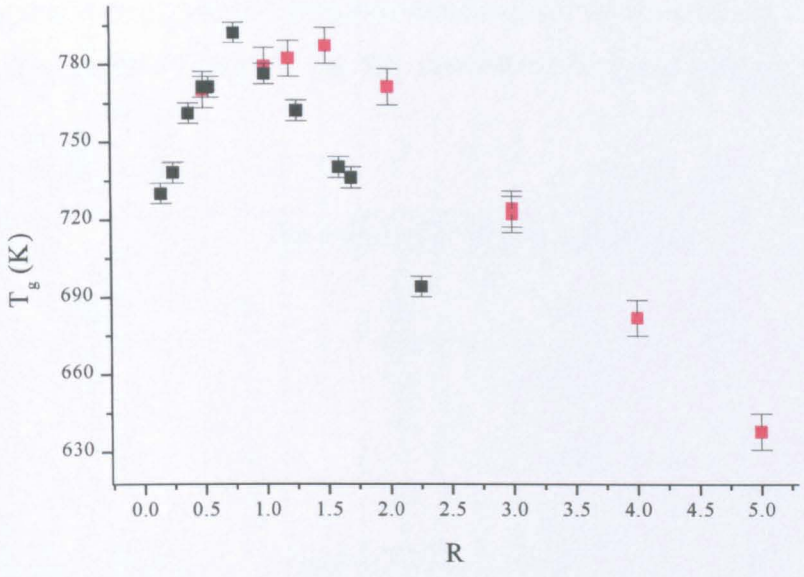

(c) $K = 3$

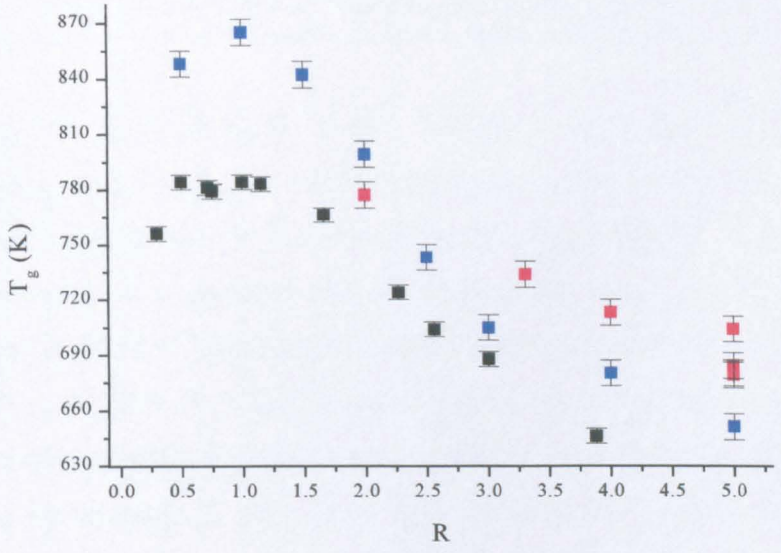

(d) $K = 4$

Fig. 7.11 The variation in T_g of a range of single- and mixed-modifier borosilicate glasses with K and R. Key: ■ *= data;* ■ *= Li-borosilicate system (from [16]);* ■ *= Na-borosilicate system (from [16])*

Kamitsos [13] first investigated the idea that a change in the number of BOs per boron atom is a significant factor in T_g behaviour in the caesium borate system. As mentioned previously, an increase in bridging oxygen content can be thought of as an increase in the connectivity of the network, whereby structural rearrangements require more energy to take place. The predicted values of Z are based on the ^{11}B NMR model of Dell *et al.* [1] and although the ^{11}B NMR data for this mixed-modifier system only shows close agreement up to $R = R_{D1}$, the model has still been used at higher R, in order to continue the comparison of T_g and Z with the Li- and

Na-borosilicate systems. Table 7.04 gives details of the values of R and Z that have been seen to maximise T_g and N_4 in the current work and in the Li-borosilicate system.

K	The value of R which maximises:					
	T_g		N_4		Z	
	(a)	(b)	(a)	(b)	(a)	(b)
0	0.5	-	0.8	-	0.4	(1)
1	0.6	0.52	1.0	0.883	0.5	"
2	0.6	0.69	1.1	1	0.6	"
2.4	-	0.8	-	1.25	-	"
3	1.5	0.8	1.8	1.65	0.9	"
4	-	0.85	-	1.75	-	"

(1) Insufficient data to determine maximum Z in the current system

Table 7.04 Comparison of the values of R which maximise glass properties including T_g and N_4. Included are data for the (a) Li-borosilicate system (taken from [15]) and (b) current work.

From Figs. 7.11(a,b) it can be seen that there is some agreement between the way in which T_g and Z vary with composition, though the variation in Z, calculated from the Dell NMR model, is not able to predict the variation in T_g for all three systems illustrated. It is probable that the assumptions made for the binary borate system do not translate to the borosilicate system due to the added effect of the silica network. The best fit of T_g with Z comes from the Na-borosilicate system since the ^{11}B NMR model on which Z is based was originally formulated from NMR study of that system. Comparison of the current T_gs with those from the single Li- and Na-borosilicate systems shows that there is a noticeable mixed-modifier effect present, with the peak T_g being much closer in value to that of the Li- than the Na-borosilicate. As R increases beyond the maximum in T_g for each system, the T_g of the Na-borosilicates has been shown to decrease at a much faster rate than the Li-borosilicates [16], which results in the Na-Li-borosilicate system following the Na-system at low R and the Li-system at higher R.

In addition to the analysis of the way in which T_g, N_4 and Z are maximised with *R*, Boekenhauer *et al.* [15] have studied the way in which the post T_g-maximum slope varies with the value of K, based on a proportional sharing of the modifier between the borate and silicate networks. They show very good agreement between the measured slope S(K) of the Li-borosilicate system glasses and the slope of the binary borate system modified for the silica content of the corresponding Li-

borosilicate. The same procedure was carried out for the current work and details are given in Table 7.05.

K	*S(K) (K/unit R)*		*(1/1+K) x S(0) (K/unit R)*	
	(a)	(b)	(a)	(b)
0	-196 ± 9	-173 ± 4	-196	-173
1	-122 ± 4	-80 ± 4	-98	-87
2	-85 ± 8	-57 ± 2	-65	-58
2.4	-80 ± 7	-	-58	-
3	-65 ± 2	-43 ± 1	-49	-43
4	-53 ± 4	-31 ± 2	-39	-35

Table 7.05 Post maxima slopes, S(K), of T_g curves as a function of K for a) the current work and b) the Li-borosilicate system (taken from [15]). Also shown is the slope of the corresponding ternary borate system, modified by proportional sharing of modifier between the borate [17] and silicate networks.

The post T_g-maximum slope of the ternary sodium-lithium borate system was calculated from the data reported by Affatigato *et al.* [17]. It can be seen that there is a significant difference between the measured slope of the current T_g data and that determined from modification of the ternary borate system. The decrease in magnitude of the slope of the measured T_gs proceeds at a slower rate than that of the single-modifier Li-borosilicate system reported by Boekenhauer *et al.* [15]. The implication of this is that the structural rearrangements induced by incorporation of increased amounts of silica into the mixed-modifier system proceed less rapidly than in the single-modifier system. Table 7.05 shows that the T_g maxima also do not vary with *K* as rapidly as in the single-modifier system and though the N_4 maxima would appear to coincide with those of the single-modifier system reported by Boekenhauer, Figs. 7.07(a-e) show that there is significant difference between the current system and the currently accepted Dell model.

Figs. 7.12(a-c) compares the value of T_g obtained for a range of lithium- and sodium-borosilicate glasses by Feller *et al.* [16] with the current work.

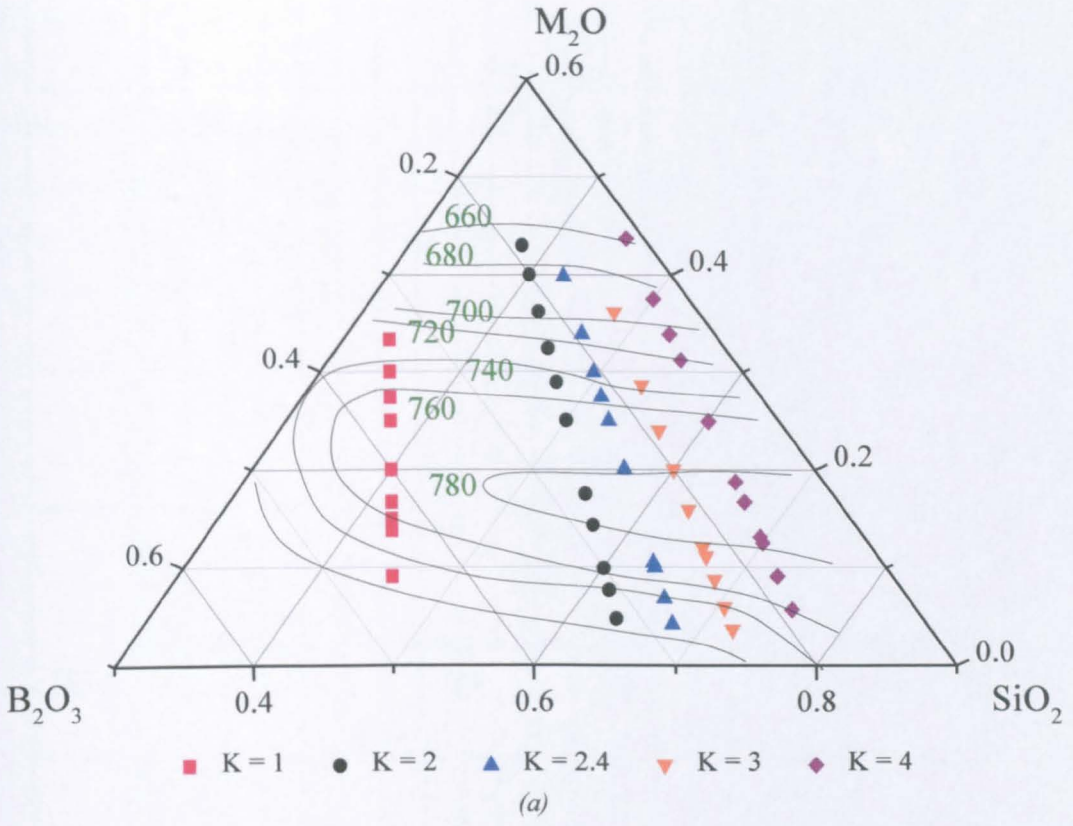
M2O
0.6
0.2
660
680
0.4
700
720
0.4
740
760
0.2
780
0.6
0.0
B2O3
0.4
0.6
0.8
SiO2
K = 1
K = 2
K = 2.4
K = 3
K = 4

(a)

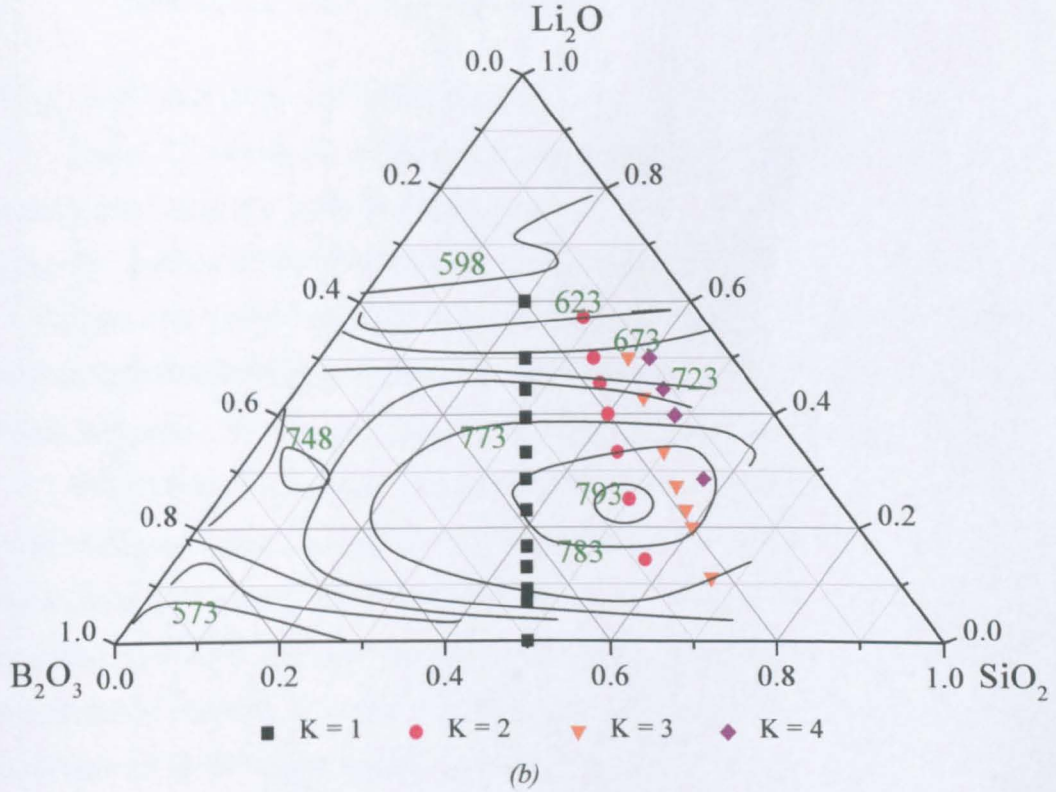
Li2O
0.0
1.0
0.2
0.8
598
0.4
623
0.6
673
723
0.6
0.4
748
773
0.8
793
0.2
783
573
1.0
0.0
B2O3
0.0
0.2
0.4
0.6
0.8
1.0
SiO2
K = 1
K = 2
K = 3
K = 4

(b)

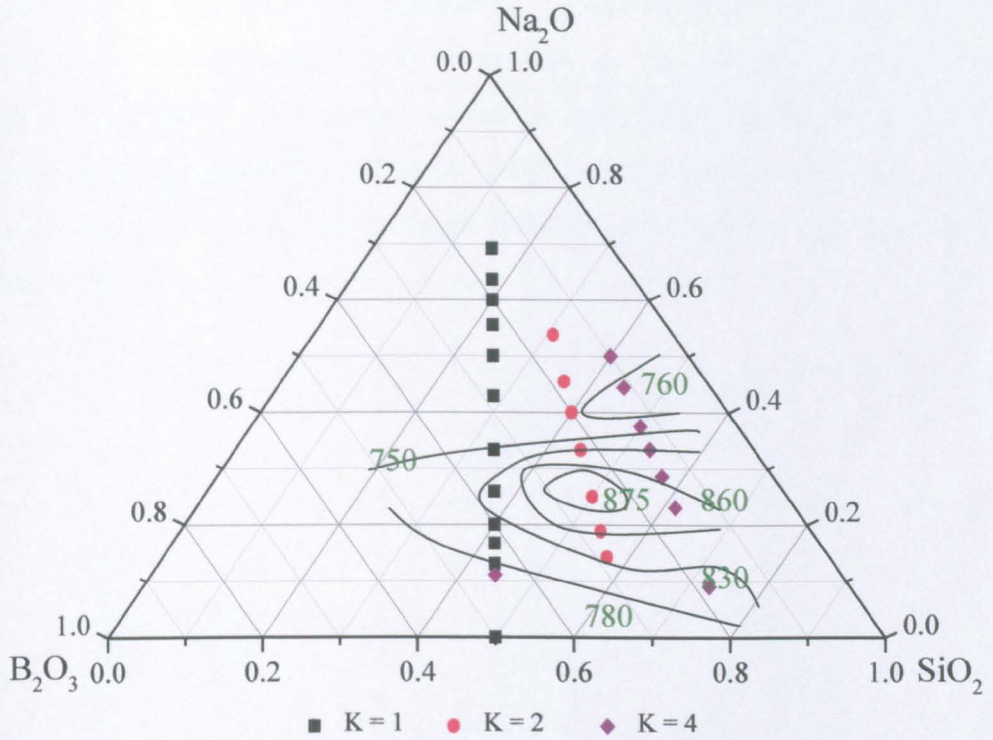

(c)

Fig. 7.12 Ternary plots illustrating the transition temperature isotherms of a) the current work, b) the Li-borosilicate system and c) the Na-borosilicate system (taken from [16]).

7.1.3.2 Coefficient of thermal expansion (α)

Fig. 7.13 shows the change in thermal expansion coefficient of the ABS glasses with *K* and the number of NBOs per Si atom. It is only really possible to display the fraction of NBOs associated with silicate tetrahedra up to the model limit $R < R_{DI}$ since at this point, NBOs are suggested to form on trigonal borate groups. Since insufficient information exists to enabling modelling of the current system beyond this point with any confidence, some data points have been excluded.

With a few exceptions, it can be seen that after an initial steep increase, there is a gradual near-linear increase in α as the modifier content of the glass increases, with a slight gradient change at higher modifier concentrations. It is known that the expansion coefficient of modifier-silicate glasses increases as the modifier ions fill the interstices between the structural units and prevent the transverse vibrations by which pure silica is thought to achieve a negative expansion coefficient. By contrast, modifier borate glasses exhibit the *borate anomaly* wherein the expansion coefficient first decreases with the addition of modifier as trigonal borate units are converted to a tetrahedral configuration but the introduction of NBOs then leads to a subsequent

increase at higher modifier concentrations. Studies of sodium- and potassium-borosilicates by Konijnendijk [18] show that as the modifier concentration is increased (keeping the silica content constant), there is a slight decrease followed by an increase in the expansion coefficient. As the silica content is increased, the initial decrease becomes less pronounced until there is an almost linear progression with modifier content.

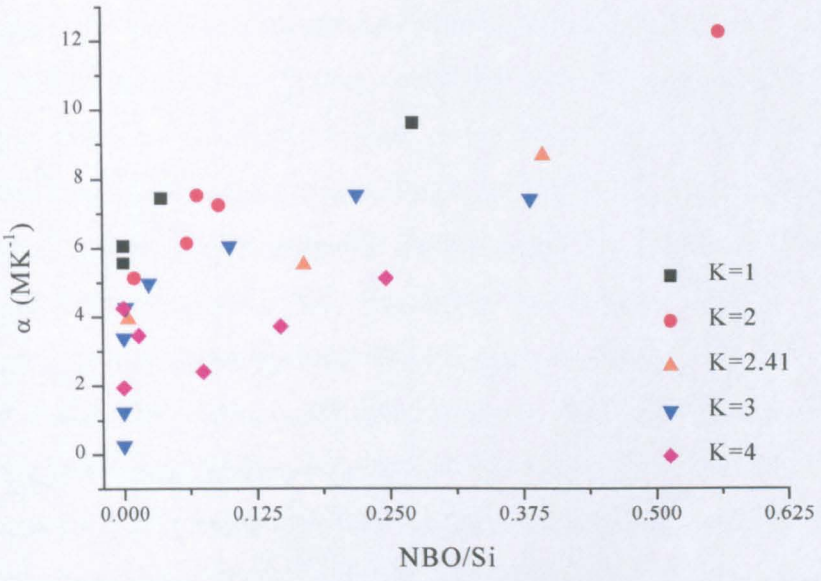

Fig. 7.13 Comparison of the variation in thermal expansion coefficient, between 373 and 573 K, of the ABS glasses with NBO/silicon concentration deduced from ^{11}B NMR results

There is no discernible initial decrease in the thermal expansion coefficient of the ABS glasses and it must be deduced that the dominant factors are the filling of interstices and subsequent NBO production on the silicate and borate units. In addition, the increase in order of the network as the concentration of tetrahedral borate units increases is outweighed by the increasing numbers of SiO_4 tetrahedra as K increases. It is noticeable that initially there is an appreciable increase in the expansion coefficient without a corresponding change in the number of NBOs per silicon unit. Therefore the effect that the conversion of tetragonal boron units to tetrahedral units has on α is outweighed by the effect of incorporation of the modifier into interstitial network space.

7.1.3.3 Density and molar volume

a) Comparison with single-modifier systems

Figs. 7.14(a-e) show the changes in density that take place as the modifier content of the glass increases. Where available, data from the Na- and Li-borosilicate systems have been included for comparison, alongside the density for the Na-borosilicate system predicted using the models of Feil and Feller [19] and Budhwani and Feller [20].

For the $K = 1$ and 3 mixed-modifier glasses, the densities lie midway between those of the individual modifier glasses. As R increases the mixed-modifier density tends towards the Na-borosilicate system rather than the Li-borosilicate system. Other workers have commented that this could suggest the heavier sodium ion has a dominant effect on the physical properties of the glass [17]. At low K and low R, the densities of all three systems are very similar and only begin to diverge as first more modifier and then more silica is added. The delineated regions of the ^{11}B NMR Na-borosilicate model have been superimposed on the graphs to illustrate where the major structural rearrangements are thought to take place. It can be seen that the rate at which the density reaches a relatively constant value decreases with K. This has also been observed in previous ^{29}Si NMR studies [6] and can be explained by the fact that as K increases, more modifier is required to introduce NBOs on the silicate units.

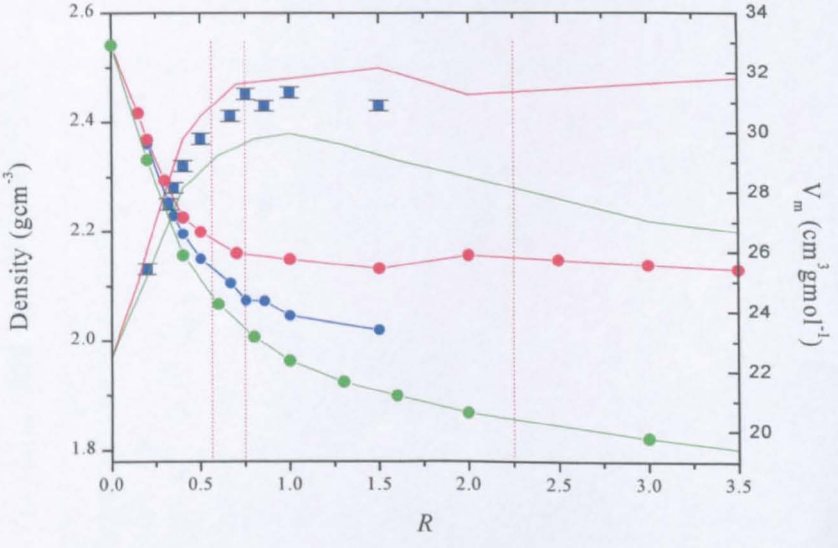

(a) K = 1

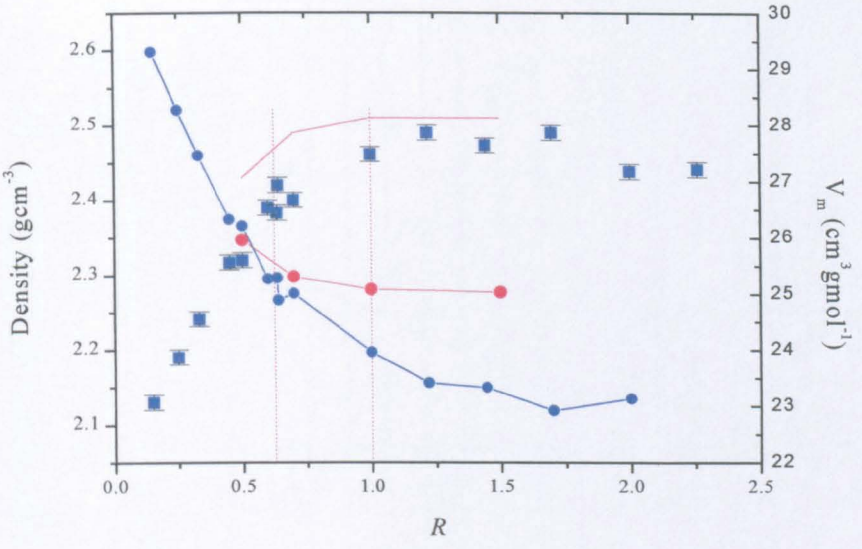
Density (gcm^{-3})
V_m (cm^{3}gmol^{-1})
R

(b) K = 2

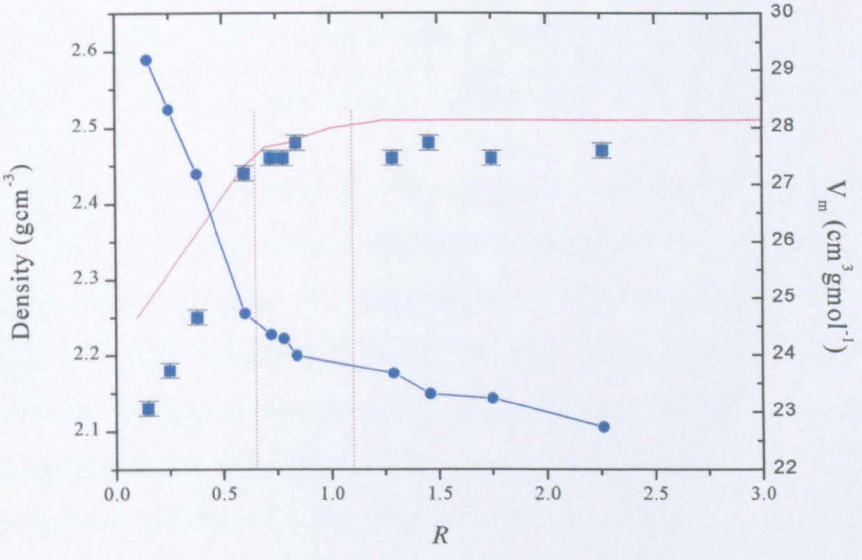
Density (gcm^{-3})
V_m (cm^{3}gmol^{-1})
R

(c) K = 2.4

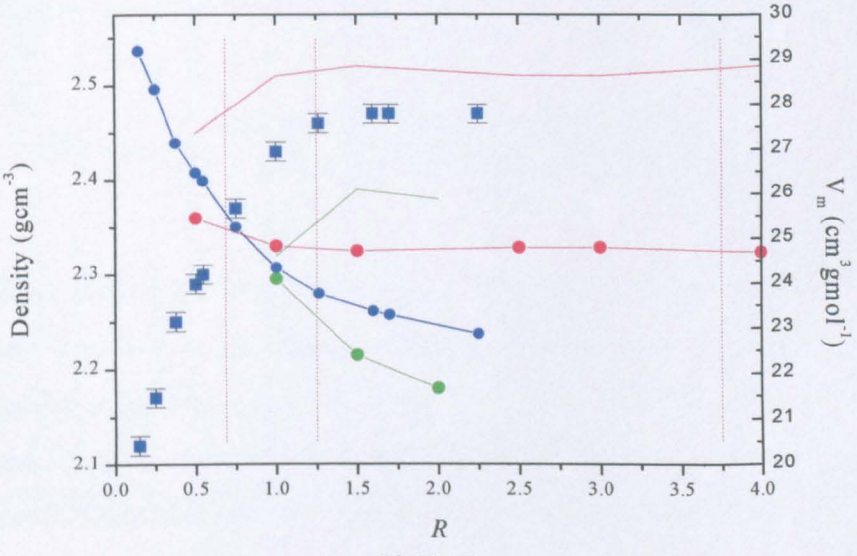
Density (gcm^{-3})
V_m (cm^{3}gmol^{-1})
R

(d) K = 3

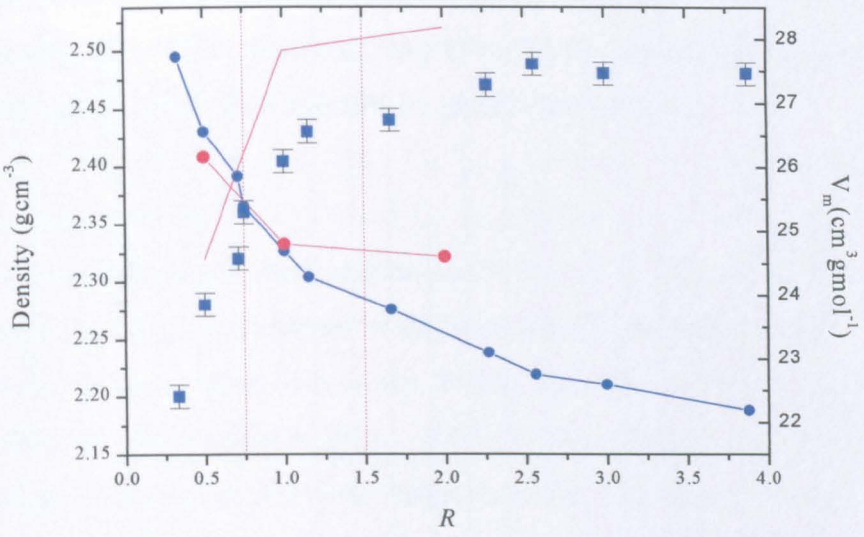

(e) K = 4

Fig. 7.14 The variation in density and molar volume, V_m, of the ABS samples with increasing modifier content. Key: □ – density data; ○ –V_m data; — : current system; — : Na-borosilicate system [16]; — : Li-borosilicate system [16].

A more detailed explanation of the method by which the ^{11}B NMR model is incorporated into this density model is given in Chapter 2. As a reminder, the semi-empirical density model used in this study takes into account the volumes (V_n,) masses (M_n) and mole fractions (f_n, deduced from NMR studies) of the structural units assumed to be present in borate and silicate glasses. All masses and volumes are referenced to that of the $[BO_3]$ unit (B_3, n=1), i.e. the mass of the $[BO_4]^-M^+$ unit (B_4, n=2) is given as {Mass{(B+2O+M)/(B+1.5O)}} and so on. Initially, the value of M_{Si} is assumed to be that of the silicate Q^4 unit. Therefore, an equation can be written that defines ρ, as follows

$$\rho(R) = \rho_o \frac{f_1M_1 + f_2M_2 + f_3M_3 + f_4M_4(K/2)^* M_{Si}}{f_1V_1 + f_2V_2 + f_3V_3 + f_4V_4(K/2)^*(V_6 + N^* dV_6)} \qquad (7.06)$$

where $\rho(R)$ is the density for a given value of R and K and N is the number of ($M^+ + \frac{1}{2}O^{-1}$) added to the silica system per silica unit. The structural units represented by successive values of n are n=1 $[BO_3]$, n=2 $[BO_4]M$. Initially, since only silicate Q^4 units are assumed to be present, N=0 and a least squares analysis of the data enables determination of a value for V_6, the associated volume of the silicate Q^4 unit.

The primary difference between the single- and mixed-modifier systems is that in the mixed-modifier system the way in which the two modifier ions apportion themselves between the borate and silicate units is not known.

b) Density modelling

Examination of Eq. 7.06 shows that below $R = R_{max}$, only the mass and volume of f_1, f_2 and Q_4 units are taken into account. The current ^{11}B and ^{29}Si NMR data support this assumption and so the density data and model can be compared with confidence. Inspection of Figs. 7.14(a-e) shows that at all values of K the model overestimates the density of the mixed-modifier system. The reason for this is not clear but one possible explanation is given by the work of Chong *et al.* [21] who demonstrate that the inclusion of more than one modifier into a borate glass leads to variation in the volumes of the five borate units, from those of the single-modifier borate system. In modelling the data, several combinations of values for the volumes and masses of the borate units were considered and used to determine values for the V_6 and dV_6, the only completely unknown quantities in Eq. 7.06. The combinations used were:

1. Average Na-Li borate and silicate unit masses; Na-Li borate unit volumes.
2. Na-borate unit masses and volumes; Li-silicate unit masses.
3. Li-borate unit masses and volumes; Na-silicate unit masses.

corresponding to the scenarios described in Table 7.06. The masses and volumes of each borate unit for each scenario in all regions are outlined in Table 7.06.

	Scenario 1	*Scenario 2*	*Scenario 3*
V_1	0.98	0.96	0.98
V_2	1.03	1.19	0.91
V_3	1.49	1.65	1.32
V_4	1.87	2.15	1.69
M_1	1	1	1
M_2	1.66	1.89	1.43
M_3	1.66	1.89	1.43
M_4	2.32	2.78	1.86

Table 7.06 Summary of the masses and volumes of the borate units considered in each of the fitting scenarios.

The volumes have been determined by least-squares fitting of density data from the corresponding system by Chong *et al.* [21] and the masses were calculated from the atomic mass of each constituent atom ($f_1 = B+1.5O$, $f_2 = B+2O+R$, $f_3 = B+2O+R$, $f_4 = B+2½O+2R$; where B = boron atom, O = oxygen atom, R = modifier atom and all masses and volumes used in the simulation are referenced to that of the f_1 unit). The mass of the silicate unit remains constant up to $R < R_{max}$ and is equal to 1.73. For each scenario, a least-squares fit was applied to the density data for each K series using Eq. 7.06 in the region $R < R_{max}$, from which a value for V_6 was determined. The values found were V_6 = 1.39(3) for scenario 1, 1.42(2) for scenario 2 and 1.38(4) for scenario 3. The model was then applied to the region $R_{max} < R < R_{D1}$ whereby values for V_6 and dV_6 were obtained. The values found were V_6 = 1.39(1) and dV_6 = 0.31(5) for scenario 1, 1.41(2) and 0.29(6) for scenario 2 and 1.36(2) and 0.31(5) for scenario 3. Figs. 7.15 (a)-(d) demonstrate how well the averages of these values fit the data of each K series.

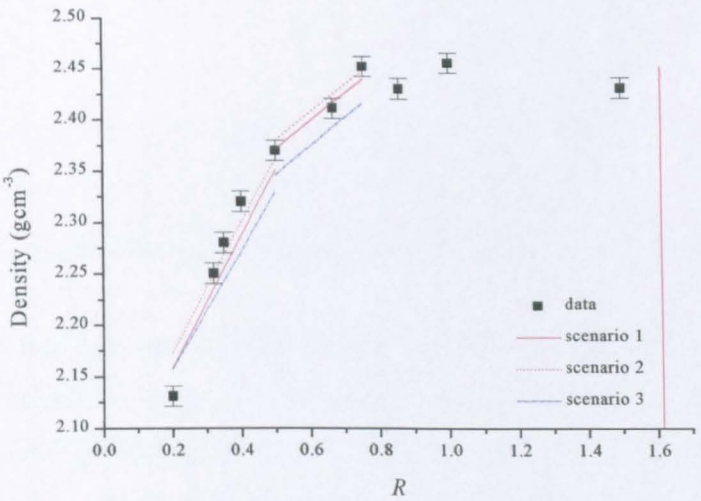

(a) K = 1

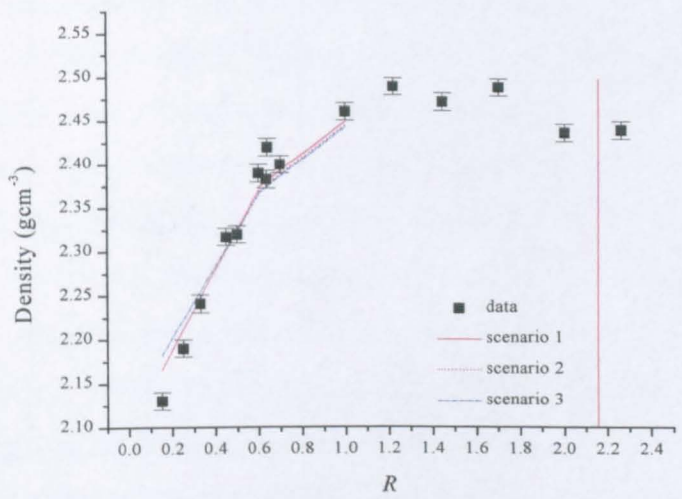

(b) K = 2

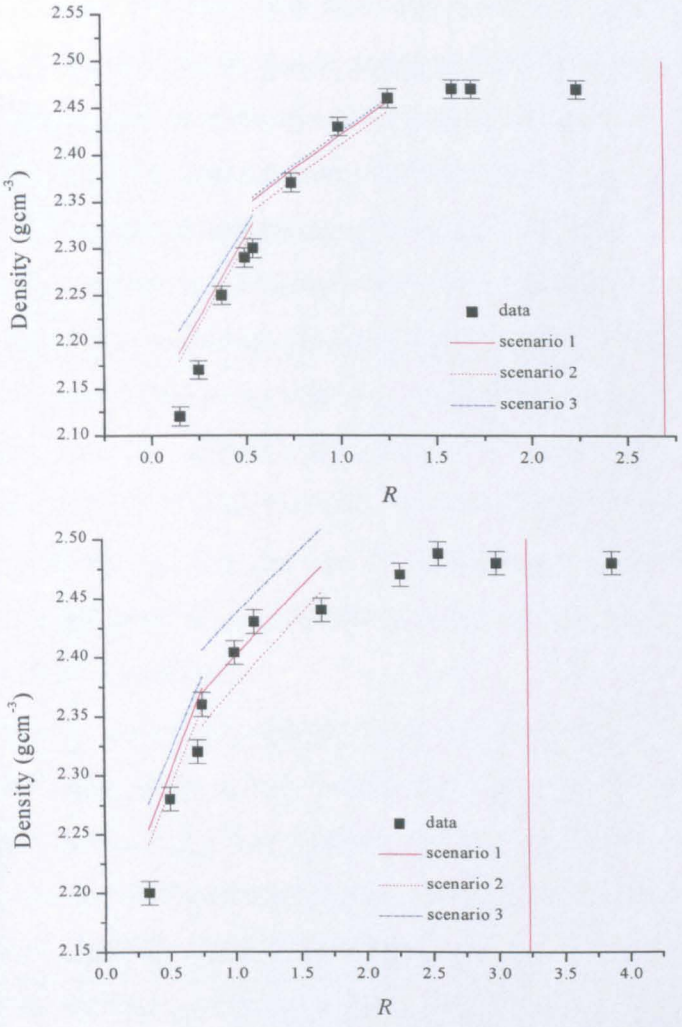

Fig. 7.15 Results of the density modelling using different structural scenarios with increasing K.

It can be seen that each of the modifier distribution scenarios considered lead to comparable values for V_6 and dV_6 across the composition range used in the fitting process. The most consistent fit to the data comes from scenario 1, where the volumes and masses of the borate units are calculated using the average mass of the two modifiers. Actually, little difference is seen between the fits produced using the values of V_6 and dV_6 from the other scenarios considered, apart from the K= 4 result, where there is a noticeable difference between the fit from each scenario. Comparison of the values of V_6 and dV_6 found for each scenario and those determined for the Li- and Na-borosilicate systems by Budhwani and Feller [20] is interesting. As expected, since V_6 represents the volume of the [SiO_4] tetrahedron and no modifier is associated with it, they report the same value of V_6 (=1.43) for each of the single modifier systems. There is a relatively small difference between the values of V_6 obtained, via the different scenarios, for the current system and the

average of all V_6 values (=1.39). The fact that there is a difference between V_6 (Budhwani) and V_6 (current work) could indicate that the presence of the mixed modifiers could have an effect on the nature of the [SiO_4] tetrahedron, though earlier work by Feil and Feller [19] reported vastly different values for V_6 (=1.32) and dV_6 (=0.55) for the Na-borosilicate system using a virtually identical empirical formula. Inaccuracies on this scale are more likely to have been introduced by the scarcity of data points than by density variations initiated at a structural level. Of more interest is the change in volume of the [SiO_4] unit, dV_6, which, though relatively static across the different scenarios, is significantly different to the value determined by Budhwani for the Li- (= 0.24) and Na- (=0.47) borosilicate systems. The value of dV_6 determined from the current data can be considered a rough average of these values, suggesting that there is no preferential association with the silicate network of one particular alkali over another

No explanation can be determined, from the results of the modelling, for the way in which the density of the mixed-modifier system varies so widely from that of the single-modifier system. The only interaction anticipated in the empirical formula is the change in volume of the trigonal borate unit as it is converted to a tetrahedral unit by the added modifier. Insufficient data is reported for the single-modifier systems to be able to make a more complete comparison with the current work. In this calculation the ^{11}B NMR model serves as an acceptable starting point up to $R = R_{max}$. Above this point, it has been shown that the fraction of tetrahedral boron deviates from the model, for all values of K. Attempts to use this model above $R = R_{DI}$ were not made because the ^{11}B NMR based model does not support the variation in N_4 seen for this system.

It is worth considering the implications for the density modelling of this series of glasses of the unexpected ^{11}B NMR data discussed previously, since the composition range of interest in both cases is in the low R region. It has been proposed that there is a significant concentration of B-O-Si links at a much lower modifier content than previously suggested by structural models based on ^{11}B NMR analysis. However, it is clear from the way in which N_4 varies up to the first critical model point, R_c, that only tetrahedral borate and silicate units exist in this region, so the assumptions made by the model in that regard are accurate. It has been observed, from the data, that even in this relatively simple region with few different types of units and limited structural arrangements, there is still a large deviation in density

between the single- and mixed-modifier systems. The effect grows noticeably with silica content and could give an indication as to what structural linkages are actually present at low modifier concentrations.

It has been mentioned several times that it is often the case that one set of NMR data is insufficient to generate an all-inclusive structural model, and that conflicts arise when comparisons are made between results from several sources. In this case, more concrete statements could be made if comparison of ^{29}Si NMR could also be made.

7.1.3.4 Ionic conductivity

a) Arrhenius plots

The conductivities of several compositions of the general formula $0.25M_2O.B_2O_3.KSiO_2$ were measured and the results are shown in Fig. 7.16.

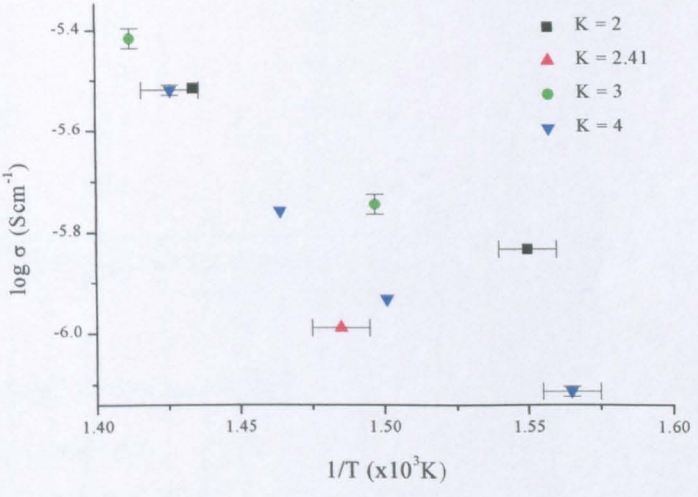

Fig. 7.16 The variation in conductivity of several ABS glasses of composition $0.25M_2O.B_2O_3.KSiO_2$.

There is insufficient data available to be able to calculate a value of E_A for each K series due to the high temperatures required to observe a measurable conductivity. However, fitting of the K = 4 data to a straight line gives an E_A value of 80.3 kJ mol^{-1}. This is comparable with the activation energy calculated for the mixed-modifier glass with K = 2, R = 1 and a Na:Li ratio of 0.5.

7.2 Mixed-modifier series

7.2.1 Compositions details

Samples used to investigate the mixed-modifier effect in this glass system were prepared by taking the composition K=2, R=1 and varying the Li_2O content from 0% to 100%, whilst keeping the overall modifier content constant. Table 7.07 presents details of the compositions of the prepared samples.

	Mol% composition							
Glass	SiO_2		B_2O_3		Na_2O		Li_2O	
MA 1	50	50.35	25	25.19	25	24.44	0	0
MA 2	50	50.43	25	25.24	22.5	22.00	2.5	2.31
MA 3	50		25		20		5	
MA 4	50	50.06	25	25.48	17.5	17.01	7.5	7.44
MA 5	50		25		15		10	
MA 6	50		25		12.5		12.5	
MA 7	50		25		10		15	
MA 8	50		25		7.5		17.5	
MA 9	50		25		5		20	
MA 10	50		25		2.5		22.5	
MA 11	50		25		0		25	

Table 7.07 Mol% compositions of the MA series samples. Note: results from chemical analysis are highlighted in red.

7.2.2 Structural Characterisation

7.2.2.1 NMR spectroscopy

a) ^{11}B NMR – spectra

Fig. 7.17 shows the ^{11}B NMR spectra obtained from each of the mixed-alkali glasses. As the ratio of Li_2O to total alkali content changes from 0 to 1 the shape of the spectrum remains largely unchanged. There are two contributions to the B_3 signal, as seen in the majority of the ABS glasses, and a small downfield drift in the chemical shift of the B_4 peak, from 0.21 to 0.73 ppm as the Li content increases. However, this is within the ± 1ppm experimental error expected and so the positions of the spectra have been normalised to 0 ppm.

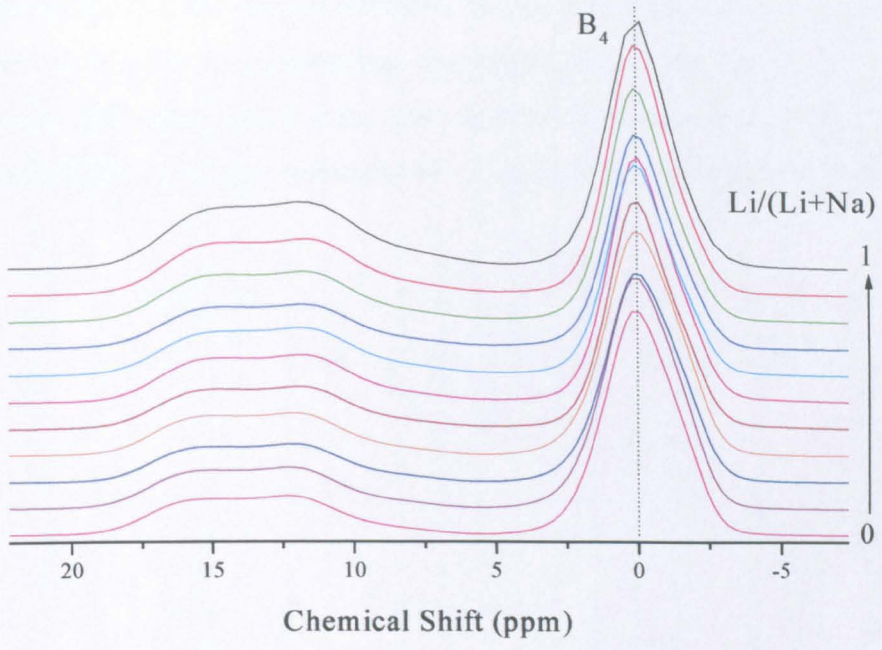

Fig. 7.17 ^{11}B MAS NMR spectra of mixed-alkali glass samples (normalised and referenced to pyrex).

It can be seen from Fig. 7.17 that there is a slight but real decrease in N_4 as the amount of lithium in the glass increases. At first glance this interesting result provides evidence for the possibility of preferential association of each alkali with either boron or silicon and not simply an averaged random distribution between both. Previous work [22,23] has shown that different alkali species do lead to a variation in N_4 of between approximately 5 and 20% as the alkali content is increased. However, the mixed-alkali glasses maintain the composition $K = 2$, $R = 1$ and so the overall alkali content is constant. The small deviations from stoichiometry indicated by the chemical analyses in Table 7.07 show that any differences in the properties of the samples are not as a result of compositional variations.

b) ^{11}B NMR – B_3/B_4 co-ordination

Comparison of N_4 with data obtained for the Na-borosilicate system [5] and the Dell N_4 model, which does not take into account any effect of the presence of different alkali atoms, shows that, as the ratio Li/(Li+Na), A, approaches 0.5, N_4 settles around the expected model value. The data for A=1 may be misleading as the glass was obviously phase separated. As mentioned in Chapter 2, variation in the type of modifier included in modifier-borate glasses leads to a change in the maximum fraction of tetrahedral borate units, in the order Li > Na > K > Rb > Cs. The opposite case is observed in this system and it can be seen that there is great

disagreement between the way in which N_4 is seen to change in the MA glasses and that reported for the corresponding single-modifier borosilicate compositions. Larger errors have been included for these systems because the data were obtained from wideline spectra as opposed to the MAS technique used in the current study.

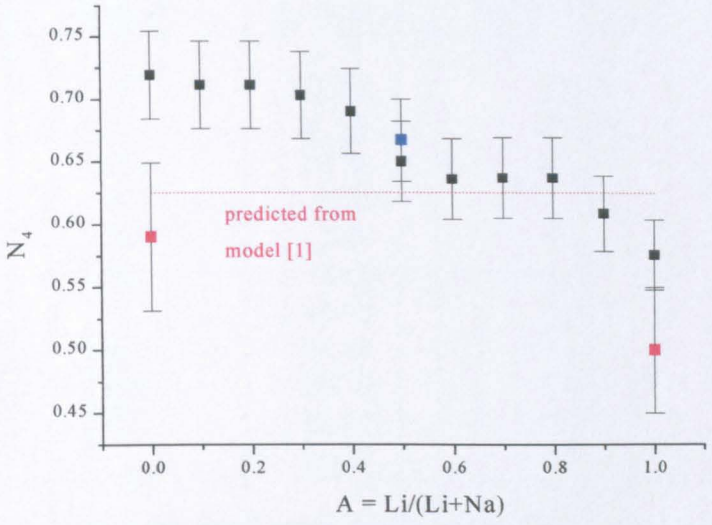

Fig. 7.18 The variation in fraction of tetrahedral boron units, N_4,, with the gradual change in composition from a sodium- to a lithium-borosilicate glass. Also shown are the N_4 values obtained for the Na- [1] and Li-borosilicate [8] systems.

It has already been shown that above R = R_{D1}, the current system displays a marked difference to the established Na-borosilicate NMR model and this has been reiterated in the MA glasses by comparison of data from the K = 2, R = 0.5 sample prepared for the general system characterisation (shown in blue).

The ^{11}B NMR data for the MA series shows that the tetrahedral boron concentration is at a minimum for the MA11 composition and in-line with the general decreasing trend across the series. The fraction of tetrahedral boron units may be expected to increase or decrease if all the alkali oxide usually associated with the silicate network interacts only with the borate network as the glass phase-separates. If the Dell model prediction of borate unit fractions can be applied here, it is possible to say tentatively how much of the modifier oxide is producing NBOs on silicate units. The general MA composition lies on the boundary where all the alkali oxide is expected to associate with the borate network and where added oxygen leads to NBOs being formed on silicate units. Close to this composition (allowing *R* to vary by +10-20%), the concentration of f_3 and f_4 units will be between 2 and 5% of the total boron speciation and therefore within the range of experimental error of the

technique. The fraction of tetrahedral boron units and composition of each sample predict that more modifier should be available to produce NBOs on the silicate tetrahedra, as shown in Table 7.08, assuming that NBOs are not yet associated with any trigonal borate units.

Li/(Na+Li)	N_4 (± 5%)	NBOs/Si atom
0	0.719	0.281
0.1	0.711	0.289
0.2	0.711	0.289
0.3	0.703	0.297
0.4	0.69	0.31
0.5	0.65	0.35
0.6	0.636	0.364
0.7	0.637	0.363
0.8	0.637	0.363
0.9	0.609	0.391
1	0.576	0.424

Table 7.08 Change in the concentration of NBOs/Si across the MA series.

Therefore, a small but definite increase in the number of Q^3 and Q^2 units might be expected as the sodium is replaced by the lithium, which could be detected using ^{29}Si NMR.

Sharing of the alkali oxide between the borate and silicate networks has been an integral part of previous structural models developed from NMR data but preferential alkali association has either not been considered or not been observed and several questions arise from this idea. Although one of the samples was obviously phase separated, the possibility that all the samples are phase separated to some degree should be considered. Separation of the glass into a pure silica region and a borosilicate glass region, containing all the alkali oxide, could be envisaged. Though R would remain unchanged for all compositions, the effective value of K would change with the amount of silica removed from the glass into its own region. Fig. 7.19 shows a ternary plot of the variation in N_4 in the Na-borosilicate system, allowing us to see how it would vary if K were reduced for a fixed R. The arrow highlighted in red in Fig. 7.19 shows the path that the actual composition of our phase separated glass could follow if a pure silica phase is extracted from the borosilicate network. The extent of the immiscibility has not been determined and so

the fraction by which *K* has been reduced cannot be known. It is possible, however, to estimate what the composition of the borosilicate phase might be by using the

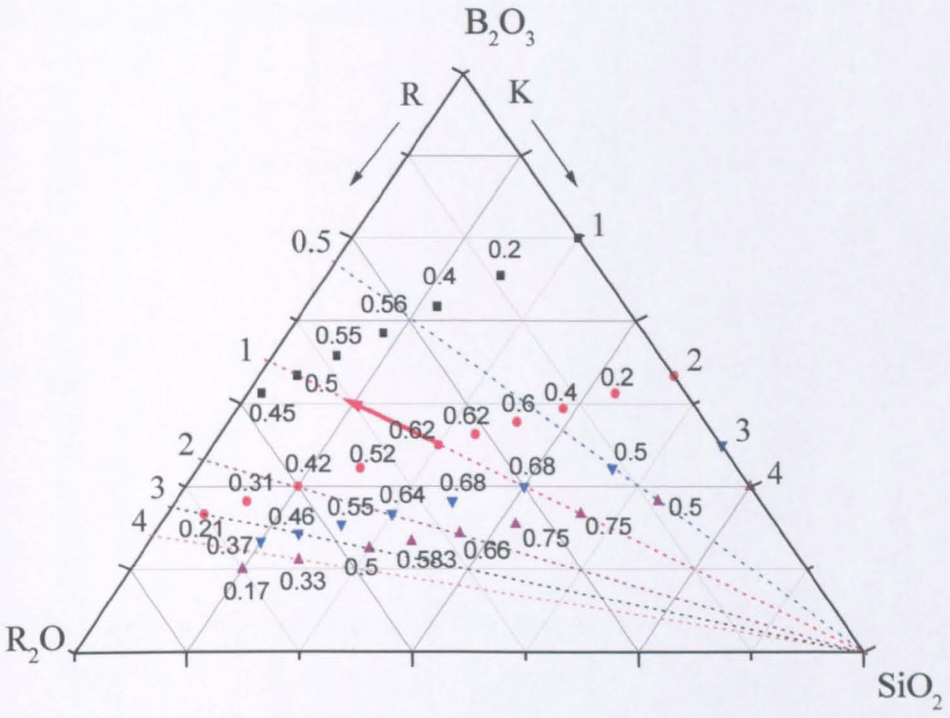

Fig. 7.19 A ternary plot illustrating how the concentration of tetrahedral boron units varies for a wide range of K and R.

known value of N_4 = 0.576 and the composition dependence shown in the ternary plot. A possible *K* for the borosilicate phase could be estimated to be 1.71 rather than 2. This could be investigated using ^{29}Si NMR, which would show the presence of a greater concentration of Q^4 units than would otherwise be expected as this composition.

7.2.3 Physical properties

7.2.3.1 Glass transition temperature (T_g)

Fig. 7.20 shows the change in transition temperature of the mixed-alkali glasses as *A*, the fraction of Li in the glass, increases from 0 to 1. For comparison, the T_gs of the *K = 2, R = 1* Li- and Na-borosilicate glasses are 791 and 814 K [16], respectively, shown in red in Fig. 7.19. Some evidence of a mixed-alkali effect can be seen, as suggested by Affatigato [17], though it is noticeable that the minimum in T_g occurs between 60 and 80% Li content and not at the 50%Li composition.

Chemical analysis of the MA samples has shown that there is excellent agreement between the batched and actual compositions which rules out errors introduced by unexpected losses on melting. There is no correlation between the changes in T_g and Z, as shown in the general characterisation study.

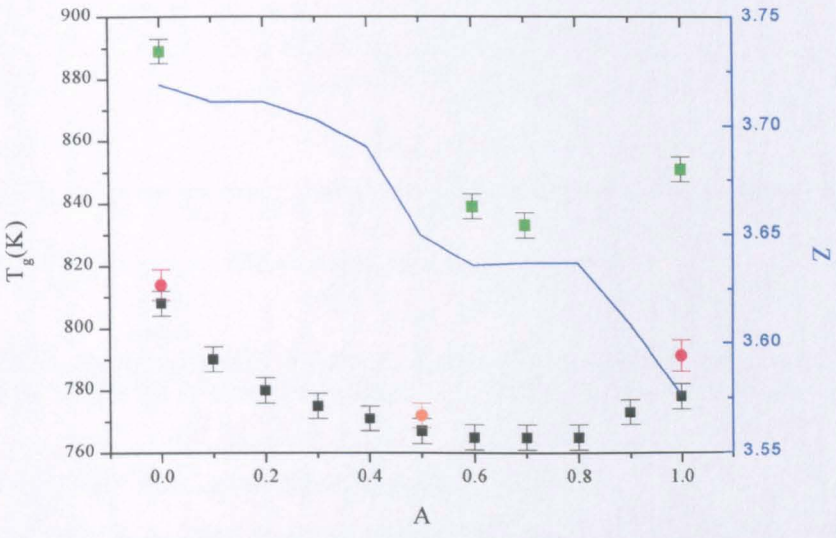

Fig. 7.20 The variation in glass transition temperature, T_g, of the mixed-alkali samples with the gradual change in composition from a sodium- to a lithium-borosilicate glass.

The transition temperature of sample MA1 and its equivalent Na-borosilicate glass agree within experimental error, unlike the difference between MA11 and its corresponding Li-borosilicate glass. The phase separation observed in sample MA11 and the calculated increase in silicon NBO concentration across all compositions could explain this phenomenon. As expected, the increase in NBOs/Si leads to a decrease in the T_g of the glasses until large-scale phase-separation occurs and the effective K of the borosilicate phase is reduced as explained in the previous section.

Convincing evidence for phase separation across all samples can be seen from the two T_g events seen by DTA (Fig. 7.21). The glass transition temperatures of the suggested second T_g event are also plotted in green in Fig. 7.17, indicating that the variation across the samples is similar to that of the first T_g event. The phase separation only became visible to the naked eye at the Li-borosilicate extremum, suggesting that the composition K = 2, R = 1 lies within a region of metastable immiscibility and would not be suitable for use as a composition for HLW vitrification.

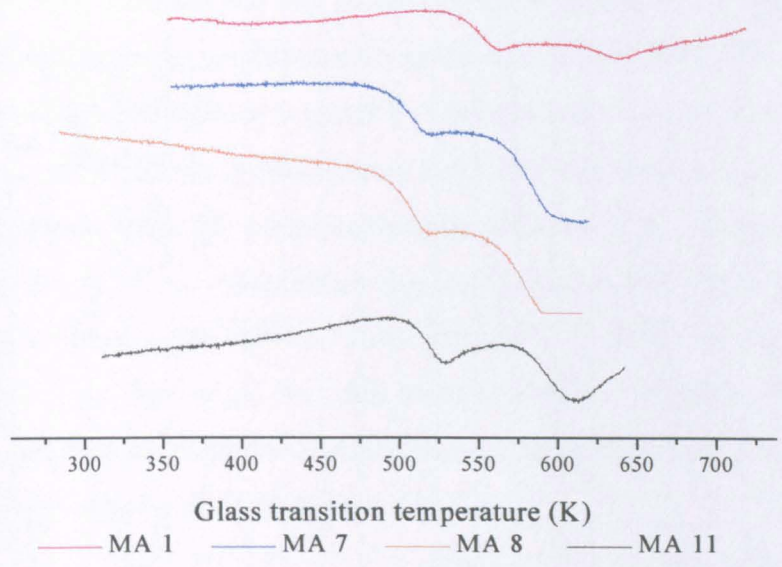

Fig. 7.21 Illustration of the DTA lineshapes obtained from several of the MA samples, possibly indicating the double T_g events arising from phase separation throughout the compositions.

7.2.3.2 Coefficient of thermal expansion (α)

Fig. 7.22 shows the change in thermal expansion coefficient of the mixed-alkali glasses with ratio of Li to the total alkali content, illustrating an approximately linear interpolation between extrema.

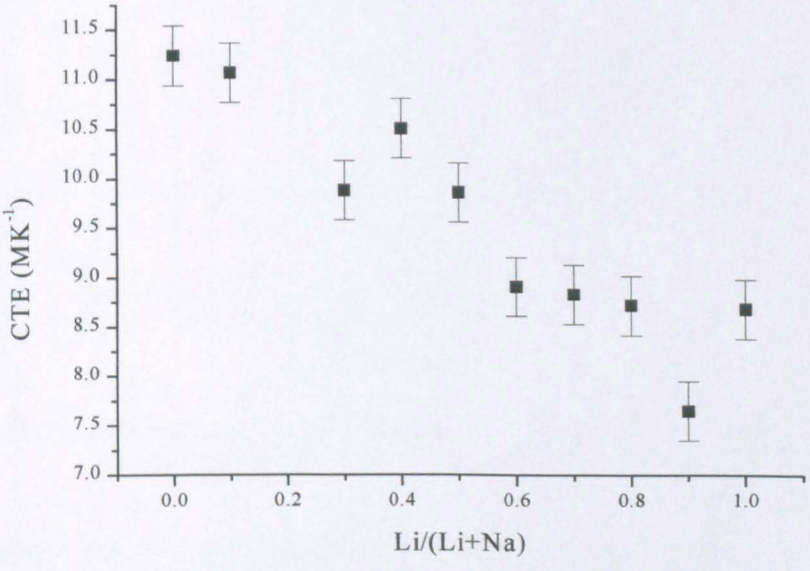

Fig. 7.22 Variation in thermal expansion coefficient of the mixed-alkali glasses with the change in composition from a sodium- to a lithium-borosilicate glass.

We observe no mixed-alkali effect in the Li-Na borosilicate system despite the presence of a small mixed-alkali effect in the thermal expansion coefficient of

silicate glasses and a general decrease according to Cs > Rb > K > Na > Li in borate glasses [24]. It is thought that the coefficient decreases with an increase in the coherence of the network, i.e. the concentration of tetrahedral boron units, but our NMR results show that there is a small but definite *decrease* in N_4 alongside the decrease in α. It is difficult to detect, from the ^{11}B NMR results, any change in the nature of the borate units, for instance, the generation of NBOs on $[BO_3]$ units. In addition, this $K = 2$, $R = 1$ composition is on the boundary only after which NBOs are expected to form. Alternatively, considering the relative sizes of the modifier cations ($Na^+ > Li^+$), the larger Na^+ will be less strongly bonded to the network, resulting in anharmonic vibrations and a higher thermal expansion coefficient, as observed in the results for the MA glasses.

7.2.3.3 Density and molar volume

Fig. 7.23 shows the change in density and molar volume of the mixed-alkali glasses with the ratio of Li to the total alkali content.

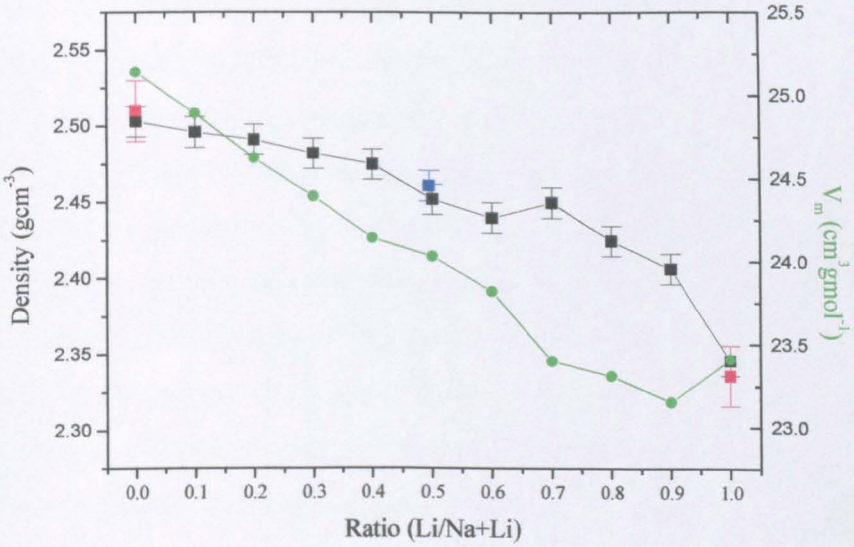

Fig. 7.23 The variation in density of the mixed-alkali samples with the gradual change in composition from a sodium- to a lithium-borosilicate glass.

In alkali silicate glasses, for a given composition the density of a Na-silicate glass is greater than that of a Li-silicate glass, whereas in the borate and germanate systems, the reverse is true.

It has already been shown that the density of an alkali-borosilicate glass can be adequately modelled by taking into account the changes in abundance and nature

of the structural units present in the glass. Since the mixed-alkali glasses MA1-MA11 possess the same $K = 2$, $R = 1$ composition, it is a much simpler task to say how the density changes as we change from one alkali to another. For the mass of the boron units, a $[BO_4]^-$ unit associated with a Na^+ ion will have a larger mass than the same unit associated with a Li^+ ion, as will a silicate Q_3 unit. In opposition to this, the smaller Li^+ ion will possess a greater charge density than the Na^+ ion, helping it to distort the interstitial free space in which it is located to a greater extent than the Na^+ ion, reducing the volume of the network unit with which it is associated. The change in molar volume in Fig. 7.23 has been highlighted in green and shows a gradual decrease as the sodium is replaced by lithium. The 100% lithia glass was observed to phase separate readily despite rapid cooling and there is a slight increase in the molar volume of the glass at this composition. From knowledge of the ionic radii of each constituent atom, it is possible to calculate a value for the ionic volume of each of the borate and silicate units [19]. It is known that the single alkali borosilicate glasses exhibit regions of immiscibility, leading to isolated alkali-borate and silicate networks, but there is no corresponding increase in the fraction of tetrahedrally coordinated boron units or decrease in the glass transition temperature, that might be expected as a result of this phase separation.

It can be seen from the data in Fig. 7.21 that the density gradually decreases as the soda is replaced by lithia, suggesting that the process is dominated by the change in mass of the borate and silicate units. The data highlighted in red was obtained using the density model of Feil & Feller as a comparison and the data shown in blue gives the density of the $R = 1$ glass from the $K = 2$ series. The ^{11}B NMR data for the mixed alkali have shown that, unexpectedly, the fraction of tetrahedral boron units is, initially, greater than the expected *Dell* model value but subsequently decreases below the model value as the sodium is replaced by lithium. In addition, DTA analysis has shown that the transition temperatures of the 100% Na- and Li-borosilicate samples are lower than those reported by other studies [16], whilst the densities are very close to those reported by other workers and the density model of Feil & Feller.

7.2.3.4 Ionic conductivity

Fig. 7.24(a) shows the variation in conductivity with frequency across the whole range of MA samples, whilst Fig. 7.24(b) provides evidence for a small

mixed-modifier effect at fixed temperature of 507 K. It can be seen from both Figs. that the most highly conducting glasses are those at the extremes of modifier content, i.e. the nearly 100% single modifier glasses, and that the 100% Li-borosilicate glass shows an anomalously high conductivity.

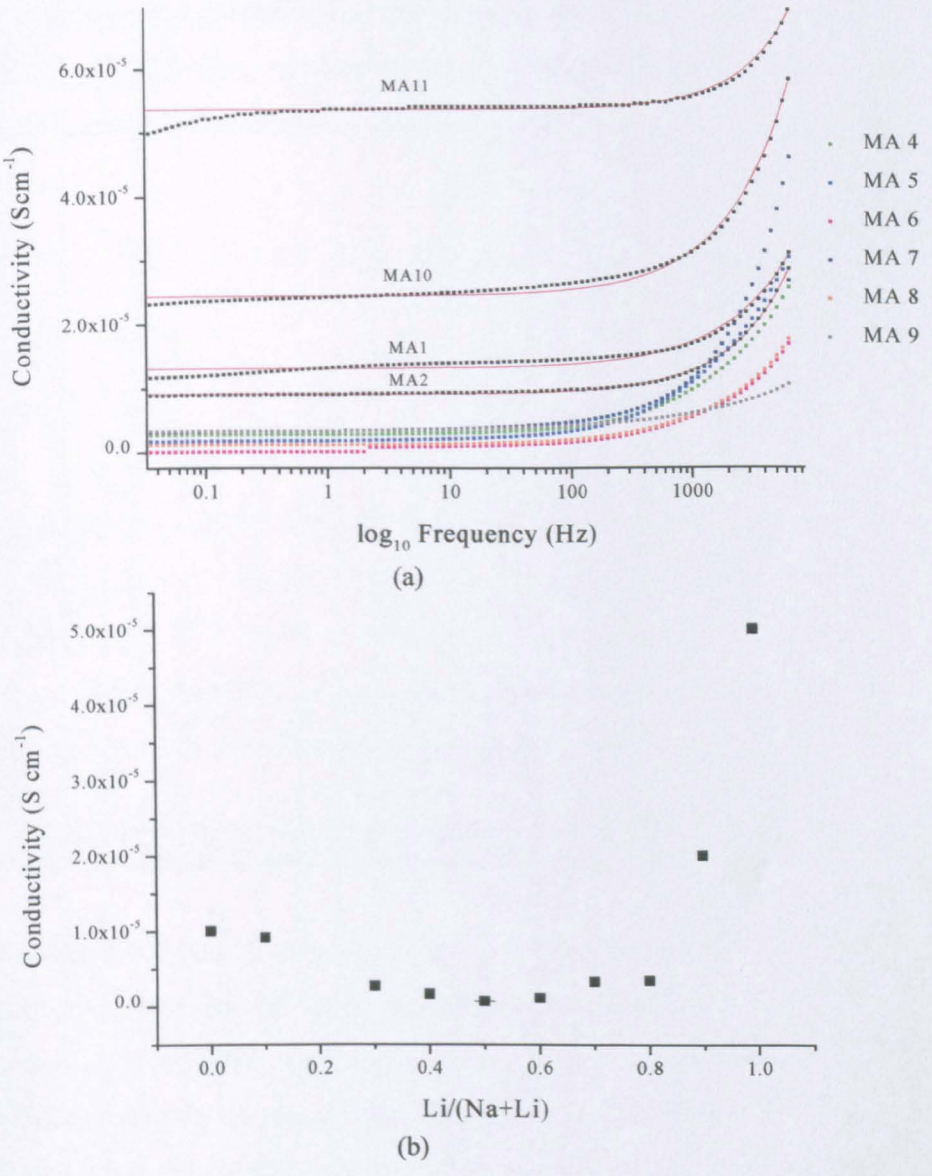

Fig. 7.24 Illustration of (a) the frequency dependence of the conductivity of the MA glasses and (b) demonstration of the mixed-alkali effect observed in the conductivity of the MA samples at 507 K (± 7K). Error bars are smaller than the symbols.

What is more interesting is that samples MA 1, MA 10 and MA 11 show evidence of two contributions to the d.c. conductivity plateau, indicative of multiple conduction mechanisms possibly due to extensive phase-separation.

The anomalous conductivity of the pure Li-borosilicate glass may give some indication as to the nature of the phase-separation that has taken place, since the morphology of the glass can have a large effect on the conductivity. The high conductivity could be explained if the glass were separated into areas of low conductivity interspersed in a high-conductivity phase containing the alkali cations. It is known that there is a gradual reduction in the concentration of tetrahedral borate units and it is possible that separation into a pure silica phase and an alkali-borosilicate phase could be responsible for this.

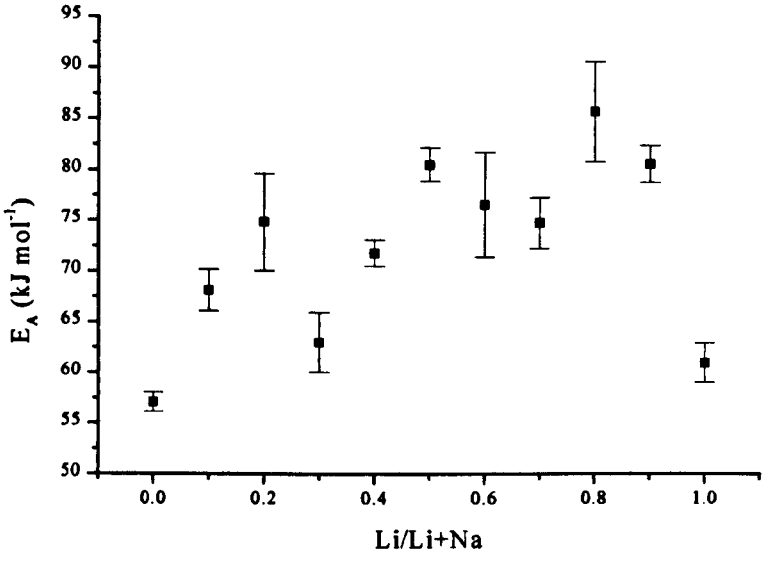

Fig. 7.25 The variation in activation energy of conduction of the mixed-alkali samples with the gradual change in composition from a sodium- to a lithium-borosilicate glass.

How would this then impact properties such as ionic conductivity? Consider how their association with different network units affects the mobility of the conducting species. An alkali cation will probably be less strongly bound to a $[BO_4]^-$ unit than a NBO because of the greater charge delocalisation and reduced charge density of the symmetric tetrahedral unit. The decrease in concentration of these units over the MA series would reduce the mobility of the cations at these sites, resulting in an increase in E_A, the activation energy of conduction. This increase, over the whole series, has been observed but the change from sample to sample is somewhat erratic, as shown in Fig. 7.25.

The 100% Li- and Na-borosilicate glasses possess much smaller activation energies than the 50/50 Na-Li samples, in agreement with data observed in Li-K-borate glasses [25], though it is reported here that the maximum in E_A is less

pronounced than for other combinations of alkali and is displaced to Li/(Li+Na) ≅0.65.

7.3 Summary

General characterisation of the Na-Li-B-Si system has made use of such structure-sensitive properties as T_g, density, and NMR analysis. The properties of this system, of particular interest because of its application in the field of HLW vitrification and disposal, have been compared with those of the already well-documented single-modifier borosilicate system. ^{11}B NMR results have shown that at low modifier concentrations the system is seen to behave similarly to the single-modifier system, whereby added modifier is used to convert trigonal $[BO_3]$ units to tetrahedral $[BO_4]^-$ units. At increasing modifier concentrations, the conversion of trigonal sites to tetrahedral sites proceeds beyond the point at which it has been shown to cease in the single-modifier systems, and then subsequently decreases at a similar rate. Recent work by Martens & Müller-Warmuth [5] has shown agreement between the variation in N_4 in the Na-borosilicate system and the current work, whereby B_4 production continues to a higher modifier concentration than expected. No comment has been made on the structural rearrangements behind this deviation from the accepted model since the creation and abundance of NBOs on trigonal borate units, hypothesised to lead to the observed decrease in N_4, is beyond the scope of the current work.

In agreement with suggestions put forward by workers [8-10] that interaction between the, supposed, isolated borate and silicate networks occurs as soon as modifier is introduced into the system, both the ^{11}B and ^{29}Si NMR data shows evidence of linkages other than the expected Si-O-Si and B-O-B. The ^{29}Si NMR results indicate the presence of a site other than the Q^4 expected, and observed, at compositions with $R < 0.5$. This is also reflected strongly in the ^{11}B NMR spectra, where two contributions to the trigonal signal are observed. The possibility that these additional signals are caused by NBOs on any borate or silicate units can be eliminated since all the modifier capable of producing NBOs is associated with $[BO_4]^-$ units. It is proposed that, at low R there exist B_3-O-B_3 (B_{3S}); B_3-O-B_4 (B_{3S})

and B_3-O-Si (Q^4(B)) links. On increasing R these are replaced by B_{3S} and B_4-O-Si (Q^3(B)) links.

The glass transition temperatures of the glasses within this system appear to follow a trend also similar to that observed in the single-modifier systems. The addition of modifier leads to a sharp rise in T_g until a limit is reached, after which it decreases at a rate dependent on the amount of silica in the glass. An interesting mixed-modifier effect is observed in which the maximum T_g attained for a particular silica content is lowest for the current system than for either of the Na- or Li-borosilicate systems. At increased modifier concentrations, the T_g of the current system follows that of the Na-borosilicate system more closely, which has been seen to fall below that of the Li-borosilicate at higher R. This could be indicative of the dominant effect of the Na^+ ion, as suggested by Affatigato [17] in the mixed-modifier borate system. Information regarding the thermal expansion of single-modifier borosilicates with the same range of K and R values as those in the current study is relatively scarce. The initial decrease and subsequent increase in α has not been observed in the current work, possibly due to the effect of the increase in tetrahedral borate unit concentration being outweighed by the numbers of SiO_4 tetrahedra as K increases.

The density variations in the current system have been shown to be most similar to those in the Na-borosilicate system, again suggesting that the Na^+ ion plays a more dominant role in determining the physical properties of the glasses. The density of each K series increases with R before levelling out at higher R. Comparison of the volume of the silicate unit (V_6) and change in volume upon the addition of NBOs (dV_6) between the single-modifier and mixed-modifier systems shows that the best fit to the data of the empirical density formula comes from assuming that the effect of the mixed-modifier is to produce borate and silicate unit masses and volumes that are an average of the individual alkali. The best fit value of V_6 was calculated to be 1.39(1) (the value reported by Budhwani and Feller is 1.43), whilst the best fit value of dV_6 was calculated to be 0.31(5) (the value reported by Budhwani and Feller is 0.24 for the Li-borosilicate system and 0.47 for the Na-borosilicate system.

Physical and structural characterisation of the mixed-modifier glasses has also been carried out as a function of the type of alkali present, by varying the ratio

Li/(Li+Na) between 0 and 1. The change in N_4 as the sodium is replaced by lithium may suggest preferential association of the lithium with the silicate network, but this has been deemed unlikely from the density modelling results of the system as a whole. More likely is that phase separation occurs across the majority of the compositions, ending with the 100% Li_2O glass separating very easily after melting. Removal of SiO_2 from the borosilicate phase could be used to explain the observed decrease in N_4 and thermal expansion. At the composition extrema, there is good agreement with T_g data reported by others for the single-modifier systems. The observed decrease in T_g across the compositions is probably related to the increased concentration of NBOs on silicon tetrahedra. The ionic-conductivity of the samples has displayed a small mixed-alkali effect with conductivities only in the region of 1-$2x10^{-5}$ S cm^{-1}. The 100% Li_2O sample showed an anomalously high value of ~$5.5x10^{-5}$ S cm^{-1}, almost certainly due to extensive phase-separation, also observed in several other MA samples.

7.4 References

[1] W. J. Dell, P. J. Bray & S Z Xiao, J. Non-Cryst. Solids **58** 1(1983) p.1

[2] R. J. Bunker, D. R. Tallant, R. J. Kirkpatrick & G. L. Turner, Phys. Chem. Glasses **31** (1) (1990) p.30

[3] L. van Wullen & W. Müller-Warmuth, Solid State Nuclear Magnetic Resonance **2** (1993) p.281

[4] G. L. Turner, K. A. Smith, R. J. Kirkpatrick & E. Oldfield, J Mag Res **67** (1986) p.547

[5] R. Martens, W. Müller-Warmuth, J. Non-Cryst. Solids **265** (2000) p. 167

[6] G. Bhasin, A. Bhatnagar, S. Bhowmik, C. Stehle, M. Affatigato, S. Feller, J, MacKenzie & S. Martin, Phys. Chem. Glasses **39** (5) (1998) p.269

[7] J. W. MacKenzie, A. Bhatnagar, D. Bain, S. Bhowmik, C. Parameswar, K. Budhwani, S. A. Feller, M. L. Royle & S. W. Martin, J. Non-Cryst. Solids **177** (1994) p.269

[8] J. Zhong, X. Wu, M. L. Liu & P. J. Bray, J. Non-Cryst. Solids **107** 1988 p.81

[9] X. W. Wu, F. Tian, X. Q. Zhang, L. Z. Pan & S. L. Wu, Collected Papers XIV Intl. Congress on Glass **1** (1986) p.32

[10] S. W. Martin, A. Bhatnagar, C. Parameswar, S Feller, J. Am. Ceram. Soc. **78** (4) (1995) p.952

[11] S. W. Martin, J. W. MacKenzie, A. Bhatnagar, S. Bhowmik, S. Feller & M. L. Royle, Phys. Chem. Glasses **36** (2) (1995) p.82

[12] S. Wang & J. F. Stebbins, J. Am. Ceram. Soc. **82** (6) (1999) p. 1519

[13] E. I. Kamitsos, G. D. Chryssikos & M. A. Karakassides, Phys. Chem. Glasses **29** (3) (1988) p. 121

[14] J. E. Shelby, Introduction to Glass Science & Technology, Royal Society of Chemistry, Cambridge, (1997) p.74

[15] R. Boekenhauer, H. Zhang, S. Feller, D. Bain, S. Kambeyanda, K. Budhwani, P. Pandikuthira, F. Alamgir, A. Michael Peters, S. Messer and K. L. Loh, J. Non-Cryst. Solids **175** (1994) p.142

[16] S. Feller, J. Kottke, J. Welter, S. Nijhawan, R. Boekenhauer, H. Zhang, D. Feil, C. Parameswar, K. Budhwani, M. Affatigato, A. Bhatnagar, G. Bhasin, A. Bhowmik, J. MacKenzie, M. Royle, S. Kambeyanda, P. Pandikuthira and M. Sharma, Proc. *2nd Int. Conf. on Borate Glasses, Crystals and Melts*, (1997) p.246

[17] M. Affatigato, S. Feller, E. J. Khaw, D. Feil, B. Teoh & O. Matthews, Phys. Chem. Glasses **31** (1) (1990) p.21

[18] W. L. Konijnendijk, Philips Res. Repts Suppl. (1) (1975) p.196

[19] D. Feil & S. Feller, J. Non-Cryst. Solids **119** (1990) p.103

[20] K. Budhwani & S. Feller, Phys. Chem. Glasses **36** (4) 1995 p.183

[21] B. C. L. Chong, S. H. Choo, S. Feller, B. Teoh, O. Mathews, E. J. Khaw, D. Feil, K. H. Chong, M. Affatigato, D. Bain, K. Hazen & K. Farooqui, J. Non-Cryst. Solids **109** (1989) p.105

[22] M. Shibata, C. Sanchez, H. Patel, S. Feller, J. Stark, G. Sumcad & J. Kasper, J. Non-Cryst. Solids **85** (1986) p.29

[23] A. Karki, S. Feller, H. P. Lim, J. Stark, C. Sanchez & M. Shibata, J. Non-Cryst. Solids **92** (1) (1987) p.11

[24] J. E. Shelby, Introduction to Glass Science & Technology, Royal Society of Chemistry, Cambridge, (1997) p.150

[25] A. A. El-Mongy, Phys. Stat. Sol.(a) **136** (1993) p.K11

Chapter 8 – Conclusions and Future Work

8.1 Characterisation of the Na_2O-Li_2O-B_2O_3-SiO_2 system

8.1.1 Introduction

The mixed-modifier borosilicate system studied here is currently used by British Nuclear Fuels as part of their high-level waste vitrification process. The system as a whole has attracted little reported study but is part of a family of technologically important glass-forming systems. Hence, elucidation of the structural arrangements underlying the physicochemical properties of these glasses can be used to augment the knowledge base and improve the application of glasses in their various roles.

8.1.2 General characterisation using NMR

Of the numerous analytical techniques available to investigate the short-range order in glasses, NMR has been used to the greatest effect. The current system has been shown to exhibit features similar to the well-investigated single-modifier borosilicates, confirming assumptions made concerning the types and abundance of various borate and silicate structural units. Over a range of SiO_2/B_2O_3 ratios (K), added modifier is seen to be associated solely with the borate network, converting trigonal $[BO_3]$ units to tetrahedral $[BO_4]$ units up to R (M_2O/B_2O_3) ~ 0.5, in agreement with the ^{11}B NMR model developed by Dell *et al.* However, ^{29}Si NMR results from a wide range of K = 2 glasses indicate that there is a growing contribution from a site other than the Q^4 unit bonded to other Q^4 units predicted to exist below $R<Rd_1$. Since the ^{11}B NMR results show that all the available modifier is associated with $[BO_4]$ units the unknown contribution to the ^{29}Si spectrum must result from the presence of Si-O-B links, despite the model assumption that there is no intimate mixing of the individual networks below R_{max}. There are three B species indicated by the ^{11}B spectra; a tetrahedral B_4, a symmetric trigonal B_{3S} and an asymmetric trigonal B_{3A}. As the amount of modifier is increased, the B_{3A} concentration decreases fairly rapidly whereas the Si-O-B concentration increases. Hence, it appears that initially Si-O-B_{3A} are replaced by Si-O-B_4, although it is

surprising that the chemical shift resulting from Si-O-B_4 should be as large as ~15 ppm.

At higher modifier concentrations, the Dell model is seen to slightly overestimate and then greatly underestimate the population of tetrahedral boron units determined from the current work and recent studies of single-modifier borosilicates.

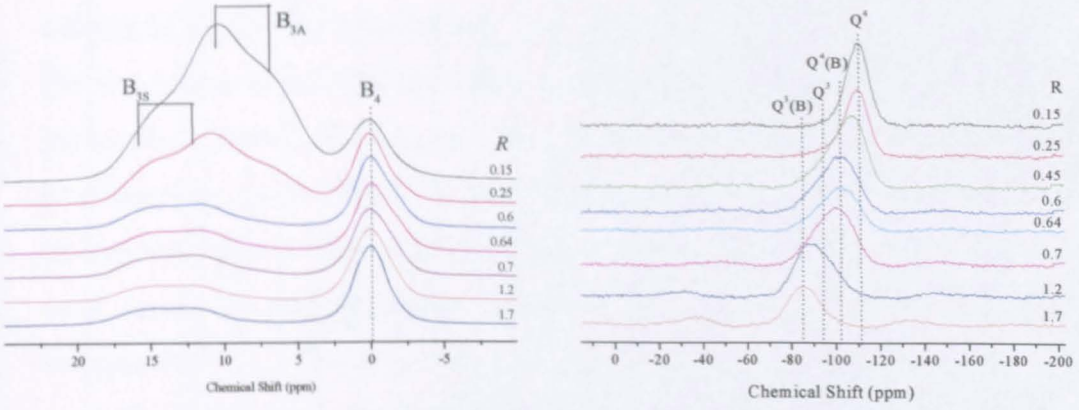

Fig. 8.01 Comparison of the ^{11}B and ^{29}Si NMR spectra obtained from the K = 2 series samples.

The observations of the NMR studies can be summarised in the following points:

- There is a small, but increasing, additional contribution to the ^{29}Si NMR signal at very low modifier content, possibly from Si-O-B_3 links. At higher modifier concentrations, the presence of Si-O-B_4 links is proposed.
- There is a significant second trigonal contribution to the ^{11}B NMR signal at very low modifier content, which can be satisfied from the concentrations of Si-O-B_3 and B_4-O-B_3 links calculated using known compositions, N_4 values and simulated ^{29}Si site concentrations.
- The current system agrees closely with the Dell model up to R ~ R_{d1} but deviates significantly at higher R.

8.1.3 General characterisation using physical properties

It has been suggested in previous work that the glass transition temperature of borate glasses is influenced by the arrangements of structural units within the glass, specifically the f_2 tetrahedral borate unit, and also by the connectivity of the borate network represented by Z, the number of bridging oxygens per boron unit. Results have shown that there is some agreement between Z and T_g for all three

systems, suggesting that the simple assumptions made about the borate system can be translated to the borosilicate system but some way of incorporating the effect of the silicate network should be introduced.

- The current system has shown a similar trend in T_g to that seen in the single-modifier borosilicate system, wherein there is an increase in T_g as modifier is added, up to a certain point, whereupon it decreases at a rate dependent on the amount of SiO_2 in the composition.
- Evidence for a mixed-modifier effect in the variation in T_g has been observed in the current system indicating that, for a particular value of R, a higher T_g could be attained by use of *either* Na_2O or Li_2O but not both. However, the Li_2O plays an important part in the solubility of heavy metals from the high-level waste and so it would be undesirable to remove it from the waste-glass composition completely.
- It can be seen that the mixed-modifier system follows the Li-borosilicate system more closely at lower R before switching to the Na-borosilicate system at higher R.
- There is a general near-linear increase in the CTE of the Na-Li borosilicate system over a range of K values as R increases. The rate of increase is greatest for the K =1 glasses and decreases as K increases. There also appears to be a strong correlation with the concentration of non-bridging oxygens on silicate tetrahedra. Even though trigonal borate units are converted to tetrahedral borate units at low R, shown in alkali borate glasses to decrease the expansion coefficient, there is no corresponding decrease in α in the current borosilicate system. The depolymerisation of the silicate network and filling of interstitial space with modifier ions is thought to play a dominant role in determining α.
- Density variation over the Na-Li borosilicate system shows similarity to the single-modifier systems, increasing with added modifier before leveling off to a constant value at higher R. At lower modifier content, there is little difference between the mixed- and single modifier systems, but as R increases, the density eventually settles on values between the corresponding single-modifier system but tends towards that of the Na-system rather than the Li-system. The rate at which the constant value is approached decreases with K across all three systems.

- Empirical modelling up to $R = R_{D1}$ using the Feil and Feller model, augmented by Budhwani and Feller, has produced best fit values for V_6 and dV_6 and shown no evidence for preferential association of added modifier with the silicate or borate networks. The best fit to the data were a Q^4 unit volume (V_6) = 1.39(1) and a change to V_6 upon addition of $[M^+ + \frac{1}{2}O^-]$ (dV_6) = 0.31(5). This compares with values reported by Budhwani and Feller of V_6 = 1.43, dV_6 = 0.24 and V_6 = 1.43, dV_6 = 0.47 for the Li- and Na- borosilicate systems, respectively. No evidence for a mixed-alkali effect has been observed.

8.2 Structural & physical study of the NBS glasses

^{11}B NMR study has shown that the NBS compositions produced by variation of the B_2O_3 content of the MW base glass agree closely with the structural model developed by Dell. Sample NBS 7 (K = 7.9, R = 2.7) deviates from the model prediction but this composition lies in the region $R_{d1} < R < R_{d2}$, within which the general characterisation studies have shown that the current system differs from the NMR model considerably. The changes in N_4 that have been observed between the samples can be satisfactorily explained with reference to the structural NMR model of Dell.

- There is a gradual decrease in N_4 of the NBS glasses as the B_2O_3 content is increased, accompanied by an increase in T_g to a maximum value of 783 K for sample NBS 8. The overall variation in T_g is approximately 82 K and an improvement of only 10 K over the MW composition is seen.
- Consideration of the number of NBOs per Si atom shows that the samples with the highest T_gs contain the lowest percentage of NBOs and vice versa. This is also reflected in the variation in thermal expansion coefficient, where the majority of the samples exhibit a lower value of α if the number of NBOs per Si atom is low. This is to be expected since it is known that the more coherent the network, i.e. greater N_4 and fewer NBOs per Si atom, the lower the thermal expansion coefficient.

8.3 Structural & physical study of the LBS glasses.

The incorporation of La_2O_3, a simulant of the rare-earth elements in the wastestream, into the base glass composition has enabled detailed investigation of the structural and physical changes that take place.

- The density, thermal expansion and glass transition temperature all increase steadily with increasing amounts of La_2O_3, whilst at the same time the fraction of tetrahedral boron units is observed to decrease.
- The addition of 12mol% La_2O_3 increases the T_g of the base glass from 773 K to 826 K and leads to a modest increase in the CTE from 8.44 MK^{-1} to 9.94 MK^{-1} for the 9.68mol% La_2O_3 glass.
- A satisfactory explanation of these trends can be made if it assumed, in analogy with the role of Al_2O_3 in the Na_2O-Al_2O_3-B_2O_3-SiO_2 system, that the introduction of La_2O_3 could lead to the formation of $[LaO_4]^-$ units at the expense of $[BO_4]^-$ production. Firstly, the modifier is used to convert all the added La_2O_3 to $[LaO_4]^-$, then conversion of $[BO_3]$ units to $[BO_4]^-$ units takes place before any remaining modifier introduces NBOs on the silicate tetrahedra. Gradually less modifier oxide is available to associate with the silicate network and the number of NBOs per silicon atom drops to zero with the inclusion of 12mol% La_2O_3.
- However, ^{29}Si NMR of the LBS glasses has shown that it is difficult to confirm the formation of $[LaO_4]^-$, and there is the possibility that the coordination could be greater, giving rise to more Si-O-La bonds but of greater covalency than typical modifier links.

8.4 Chemical durability studies of the NBS and LBS glasses

Dynamic leach testing has enabled comparison of the chemical durability of the NBS and LBS compositions under conditions currently employed by BNFL.

- Samples NBS 10 (K = 1.23, R = 0.53), 9 (K = 1.4, R = 0.8) and 14 (K = 1.51, R = 0.53) were most severely attacked and often completely disintegrated during the course of the tests. Samples NBS 11, containing 0mol% B_2O_3, and NBS 7 (K

= 7.94, R = 2.72) showed the greatest resistance to attack and little physical damage was observed at the end of the tests.

- Chemical analysis of the leachates of the samples showed that samples NBS 6 (K = 4.9, R = 1.65) and 7 were at least as resilient as the experimental apparatus used in the tests (Pyrex® borosilicate glass), whereas approximately 8 times as much sodium and nearly 50 times as much lithium was leached from samples of the NBS 10 composition. Extensive physical damage was observed from optical micrographs, including cracking, crazing and bubble formation.
- Similar study of the LBS samples showed a marked decrease in the amount of material leached from the samples as the La_2O_3 concentration was increased. The amount of sodium leached from the glass was reduced to a level equivalent to that removed from the glassware of the apparatus used and all the samples showed little physical damage.
- A crystalline material was detected on the surface of the sample containing 12mol% La_2O_3 and this was identified as lanthanum oxide carbonate hydrate ($La_2O(CO_3)_2.xH_2O$) from X-ray diffraction methods. This results from the fact that there is a well-known tendency for lanthanum oxides and hydroxide to react with CO_2 in the atmosphere. No evidence for migration of -OH- into the glass matrix was observed in either the NBS or LBS samples.

8.5 Radiation interaction studies of the NBS and LBS glasses.

A preliminary study into the effect of α-radiation on the NBS and LBS glasses has shown that damage sites created within the glass network are detectable by ESR spectroscopy and this provides evidence of an interaction between the incident radiation and boron atoms in the glass. A total of 33 samples were irradiated with α-particle doses equivalent to several tens to several thousands of years of storage, depending on the exact waste composition.

- The correlation between the dose delivered to the glass and the amount of detectable damage is unclear, possibly because of annealing processes that take place during and after the irradiation that mask the damage caused.

- The observed defect signals were shown by ESR to be relatively stable and long-lived.
- The introduction of La_2O_3 was seen to interfere with the shape of the signal, possibly through competition between LaO^-/h^+ and SiO^-/h^+ sites.
- Gamma-ray spectroscopy of several NBS samples, after completion of the irradiation, has indicated the presence of a radioactive species with a half-life of approximately 10 minutes. Based on the composition of the glass and known radioactive decay pathways, the most likely source of the observed decay is shown to be the $^{10}B(\alpha,n)$ reaction, resulting in an excited ^{13}N nucleus that decays via positron annihilation with a characteristic γ-ray energy of 0.511 MeV.
- During α-irradiation, darkening of the glass samples occurred which was subsequently removed by exposure to high-intensity UV light.
- UV-Visible spectrophotometry of the LBS glasses has shown that there is a slight increase in the UV cut-off wavelength with increasing La_2O_3 content. Usually attributed to an increase in the non-bridging oxygen concentration of the glass, this does not strictly agree with the assumption that the number of NBOs decreases as the La_2O_3 concentration increases.

8.6 Vitrification matrix refinements

In the light of the results obtained from the structural and physical characterisation of the Na_2O-Li_2O-B_2O_3-SiO_2 system, it is possible to highlight improvements to the current vitrification composition that could be made. It has been shown from the NBS glasses that a modest increase of 10 K is obtained from modification of the B_2O_3 content (+5mol%) and in the general characterisation study, the maximum T_g obtained is 792 K (K = 3, R = 0.75). It has been proposed that a mixed-modifier effect takes place which suppresses the T_{gs} in this system to below those of the single-modifier systems, so the high T_gs seen in Li-borosilicate glasses would be unobtainable in the current system.

The current base glass, MW (K = 3.26, R = 1.12), exhibits a low thermal expansion coefficient (8.4 MK^{-1}) but it has been found that the NBS 8 (K = 2.51, R = 0.82) composition exhibits a thermal expansion coefficient of 7.7 ($\pm$ 0.4) MK^{-1}. In

the general study of the system, low values of α, a desired property of the isolating matrix, occur at low modifier concentrations and values < 5 MK^{-1} are achievable with compositions (K = 4, R = 1.15) similar to that of MW (K = 3.3, R = 1.12).

It has been seen that there is a significant improvement in the corrosion resistance of the NBS glasses as the B_2O_3 content is decreased, but this also leads to a decrease in the glass transition temperature. Sample NBS 7 (K = 7.9, R = 2.7) exhibited the greatest durability, but it was found that the addition of La_2O_3 also greatly improved the leach resistance.

8.7 Future Work

Extensive study of numerous borosilicate systems has shown even two sets of NMR data can be insufficient to fully describe the structural arrangements within the glass. Further investigation using ^{17}O NMR would allow more detailed identification of the types of Si-O-B links prevalent at different compositions. Multiple-quantum MAS NMR would allow more accurate quantification of the second trigonal site observed from the ^{11}B NMR spectra and enable closer comparison with the acquired ^{29}Si NMR data. Further series with increasing *K* and *R* should be produced to give as wide a picture a possible of the physical and structural properties of the current system.

A more detailed study of the interaction of radiation with the NBS samples could be performed by improvement of the method of irradiation and subsequent analysis. Direct evidence for the proposed $^{10}B(\alpha,n)$ reaction could be obtained using fast-neutron spectroscopy. Further study of the influence on the radiation interaction of the glass of simulants such as La_2O_3 should be carried out. Under suitable experimental conditions, the effect of radiation on the leaching behaviour of the NBS and LBS compositions could also be studied.

In order to make more substantiated observations regarding the role of La_2O_3 in this system, knowledge of the co-ordination state of the La^{3+}, determined by EXAFS, would enable accurate assignment of its role as predominantly a modifier or intermediate oxide.

Finally, it would be of interest to see how a move away from the 50:50 modifier composition would affect the chemical durability of the glass, since the single-modifier borosilicate systems exhibit greatly improved T_gs.

J M Roderick, D Holland & C R Scales, Proc. 3rd Int. Conf. on Borate Glasses, Crystals and Melts, Phys. Chem. Glasses, **41** (6) (2000) p.392-395

CHARACTERISATION AND RADIATION RESISTANCE OF A MIXED-ALKALI BOROSILICATE GLASS FOR HIGH-LEVEL WASTE VITRIFICATION

J.M. RODERICK *, D. HOLLAND *, C.R. SCALES **

*Physics Department, Warwick University, Coventry, CV4 7AL, UK, phrxi@csv.warwick.ac.uk

**British Nuclear Fuels Ltd, Sellafield, Seascale, Cumbria, UK

Glasses related to those used for the vitrification of high-level waste (HLW) have been produced from the sodium-lithium borosilicate system. Their thermal and structural characteristics have been measured for a wide range of boron oxide contents and for a range of alkali oxide to boron oxide ratios, R, for several fixed silica to boron oxide ratios, K. The NBS series of glasses was seen to exhibit a maximum in the glass transition temperature, T_g, and a minimum in the fraction of 4-coordinated borons, N_4, at 22 mol% and 29 mol% boron oxide, respectively. With variation of K and R, initial results indicate an increase in T_g to a maximum before a gradual decrease. Density measurements show a general increase before remaining within experimental error at larger R. Initial α-particle irradiation tests have been carried out on several base glass samples and show evidence of B(α,n) reactions, the occurrence of which could have important consequences for the future viability of the wasteform.

J M Roderick, D Holland, A P Howes & C R Scales, Proc. 8th Int. Conf. On Non-Crystalline Materials, J. Non-Cryst. Solids, in press.

Density-structure relations in mixed-alkali borosilicate glasses by ^{29}Si and ^{11}B MAS-NMR

J.M. Roderick [a], D. Holland [a], A.P. Howes [a] & C.R. Scales [b]

[a] *Department of Physics, Warwick University, Coventry, CV4 7AL, UK.*

[b] *British Nuclear Fuels Ltd, Sellafield, Seascale, Cumbria, CA20 8PG, UK.*

Densities and boron and silicate speciation of the mixed-alkali borosilicate glass system $R(½Na_2O+½Li_2O)•B_2O_3•KSiO_2$, have been measured over a wide range of R and K values. Previous models for the density of single alkali borates and borosilicates and mixed-alkali borates have been used in an attempt to identify the roles of the two alkalies in this mixed-alkali borosilicate. Results are discussed in terms of the type and abundance of structural units present and the manner in which the alkali species apportion themselves between the borate and silicate units. Structural data obtained from ^{11}B and ^{29}Si Magic Angle Spinning Nuclear Magnetic Resonance (MAS-NMR) illustrate the similarities and differences between the mixed and single alkali systems. Below a critical value of R (R_{max}), the current system exhibits a variation in N_4, the fraction of tetrahedrally coordinated borons, similar to the Na-borosilicate system. Beyond this point, model N_4 predictions initially overestimate, then underestimate the experimental results seen in the current work. A semi-empirical formula, developed previously, has been employed to investigate the trends in density variation. Comparison, with previous reports, of the associated volumes of the silica Q^4 units shows a larger initial volume, V_6, but a smaller value of dV_6, the incremental change in volume of the $[SiO_4]$ unit on introducing non-bridging oxygens. Some preliminary evidence is also presented for the existence of borosilicate units, below R_{max}, not accounted for in most borosilicate density models.

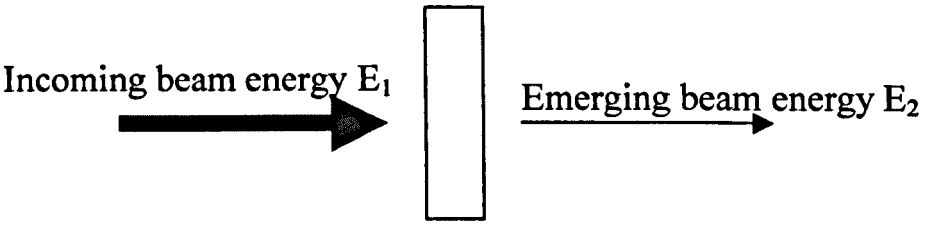

$Range_z(E_2) = Range_z(E_1) - Z$ where $Range_z(E)$ is the range in mg cm^{-2} at energy E. Expressing the range in mg cm^{-2} is more accurate since it takes into account the different density of materials.

Hence, the incoming beam of α-particles has energy of 24MeV and we require the emerging α-particles to have an energy of 5.5MeV. From tables, we know the ranges of α-particles of varying energies in materials of different compositions, hence the degrader thickness can be calculated using the equation given above.

Therefore, $Range_z(E_2)$ = 7.22 mg cm^{-2}, $Range_z(E_1)$ = 76.09 mg cm^{-2}* and therefore the thickness of Al-foil required to degrade the 25MeV α-particles to 5.5MeV = 68.87 mg cm^{-2} of Al.

*** Code DEDX, Daresbury Laboratory (unpublished), derived from the code SPRAT, report ORNL 4869 (1973) (unpublished)**

Comparison of the experimental ^{11}B NMR spectra and simulations of the NBS glasses.

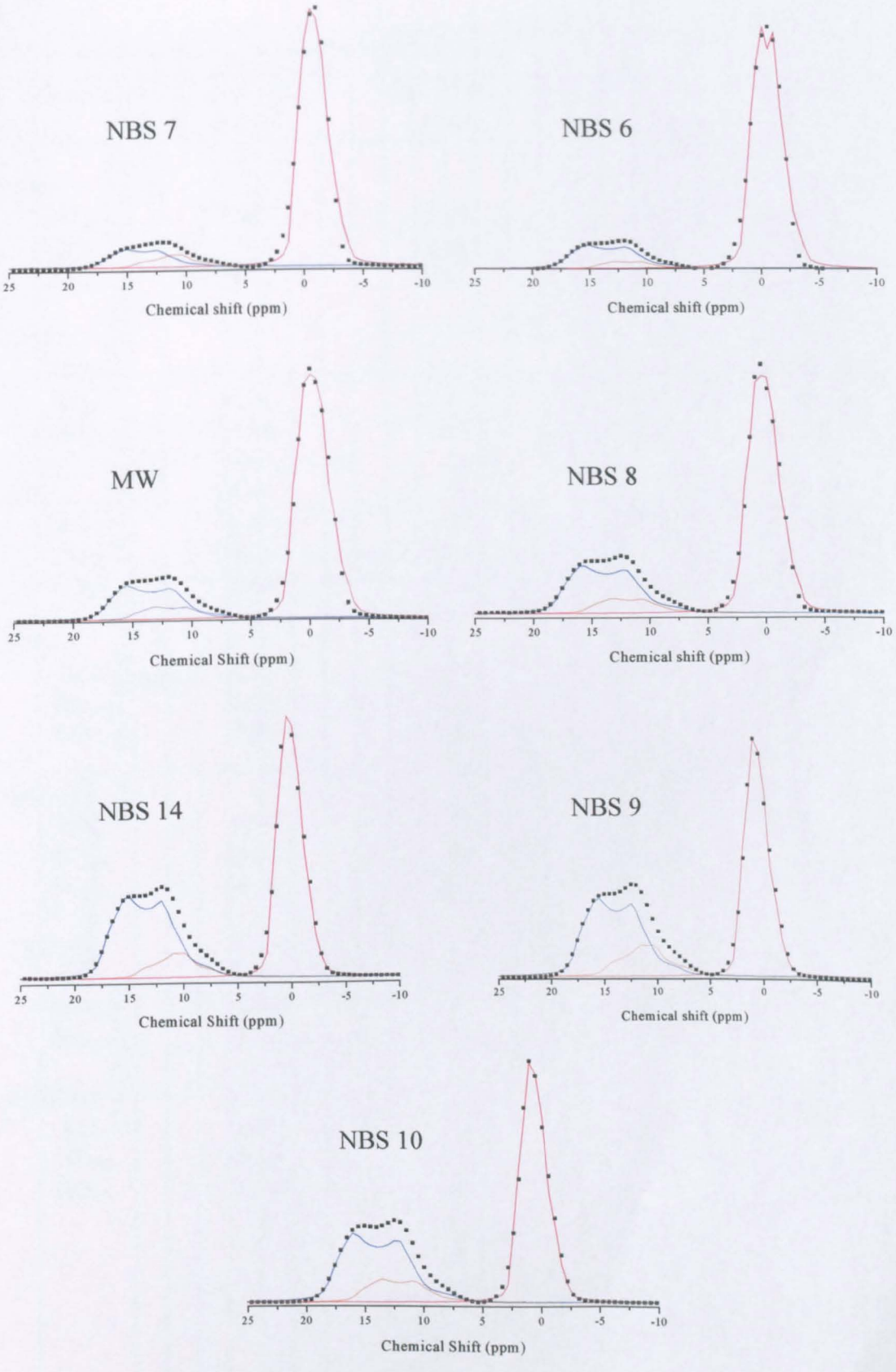

^{11}B NMR simulation parameters corresponding to NBS glass spectra shown in Appendix C-1

N_4 fractions deduced from ^{11}B NMR are highlighted in red

Sample	*δ_I (ppm) (±0.5)*	*Qcc (MHz) (±0.05)*	*η (±0.05)*	*Species %*
NBS 7				
BO_4	0.98	1.64	0.52	81.74 / 85.2
BO_{3S}	17.71	2.38	0.38	11.85
BO_{3A}	14.51	2.13	0.71	6.41
NBS 6				
BO_4	1.49	1.74	0.47	80.38 / 82.2
BO_{3S}	18.00	2.55	0.31	15.97
BO_{3A}	15.06	2.20	0.40	3.65
MW				
BO_4	1.83	1.75	0.54	73.13 / 71.0
BO_{3S}	18.19	2.59	0.28	20.23
BO_{3A}	15.65	2.34	0.39	6.64
NBS 8				
BO_4	2.31	1.73	0.54	65.17 / 60.9
BO_{3S}	18.59	2.61	0.30	27.40
BO_{3A}	15.91	2.38	0.40	7.43
NBS 14				
BO_4	1.99	1.63	0.56	52.88 / 53.3
BO_{3S}	18.03	2.54	0.35	38.35
BO_{3A}	14.38	2.22	0.70	8.77
NBS 9				
BO_4	2.41	1.61	0.59	48.92 / 45.2
BO_{3S}	18.39	2.52	0.34	38.29
BO_{3A}	15.18	2.29	0.69	12.79
NBS 10				
BO_4	2.44	1.62	0.59	52.39 / 50.6
BO_{3S}	18.64	2.61	0.28	36.75
BO_{3A}	16.17	2.40	0.38	10.86

Determination of the number of nuclei that react in a beam of incident particles

During an activation experiment which creates a non-stable nucleus, the number of nuclei d_{na} created is affected by the decay of those nuclei created, and rises as

$$d_{na} = d_n[1 - \exp(-\lambda t_a)] \quad (1)$$

where λ = decay constant = $\ln 2/t_{1/2}$ and t_a = activation time. Hence, any measurements must be corrected for the time of activation, t_a, to obtain the correct number of nuclei that would be created if the activation was continued until the saturation value, d_n, was reached.

The value of d_{na} is calculated by measuring the activity d_{am} of the sample at some time t_m after the activation is finished, and obtaining the value for d_{aa} at the end of the activation time by correcting for the measurements delay t_m via

$$d_{am} = d_{aa} \exp(-\lambda t_m) \quad (2)$$

and

$$d_{na} = d_{aa} / \lambda \quad (3)$$

hence $$d_n = d_{am} / [\lambda \exp(-\lambda t_m)(1 - \exp(-\lambda t_a))] \quad (4)$$

where d_{am} is the measured activity of the sample after a total time $t_a + t_m$, and d_n is the saturated value of the number of atoms which would be created in the sample if activation was continued for more than about 4 half lives.

Comparison of the experimental and simulated ^{11}B NMR spectra for K = 3 glasses.

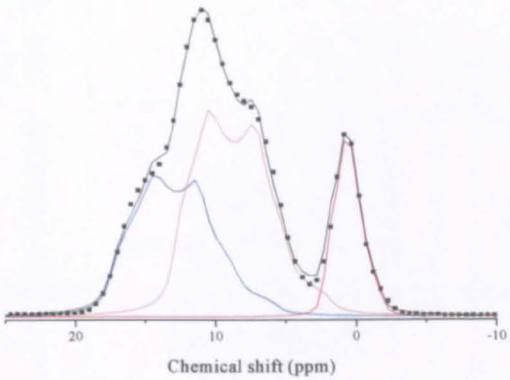

(a) R = 0.15

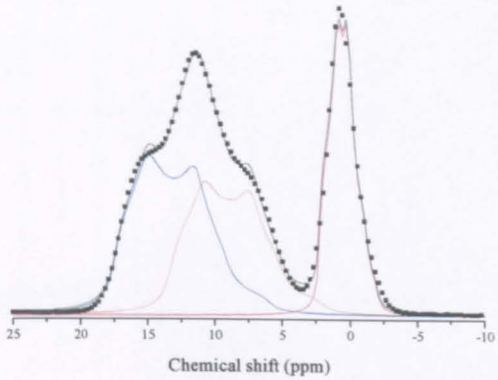

(b) R = 0.25

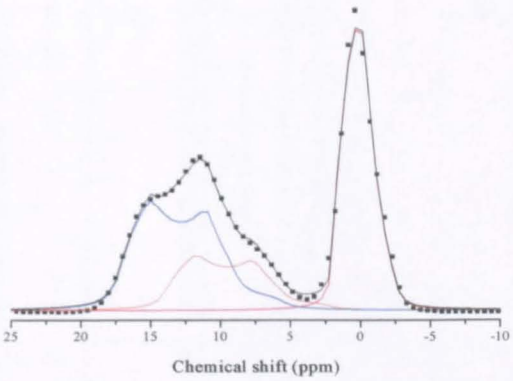

(c)R = 0.375

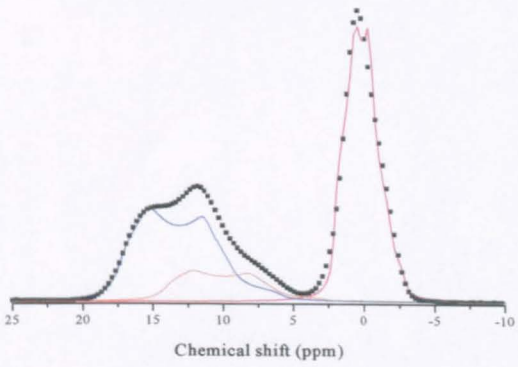

(d) R = 0.5

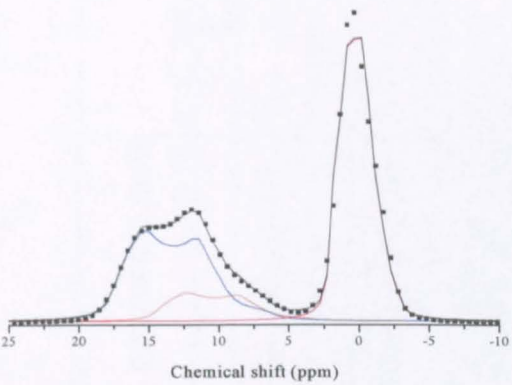

(e) R = 0.545

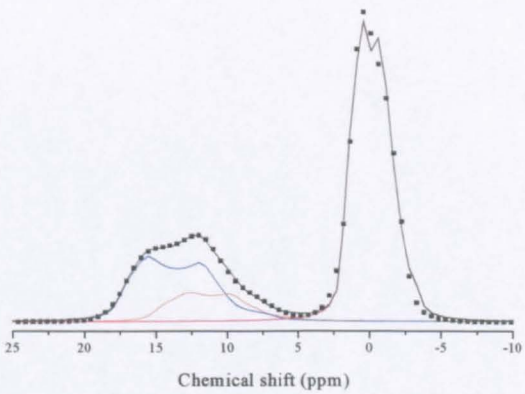

(f) R = 0.75

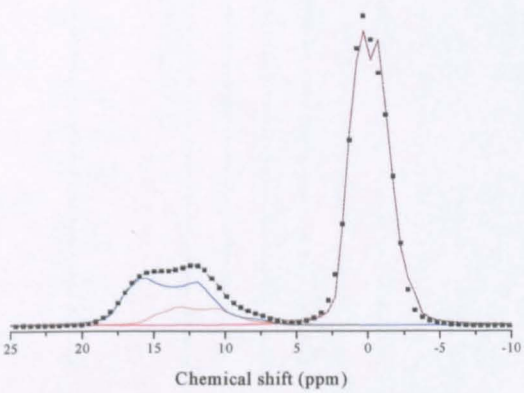

(g) R = 1.0

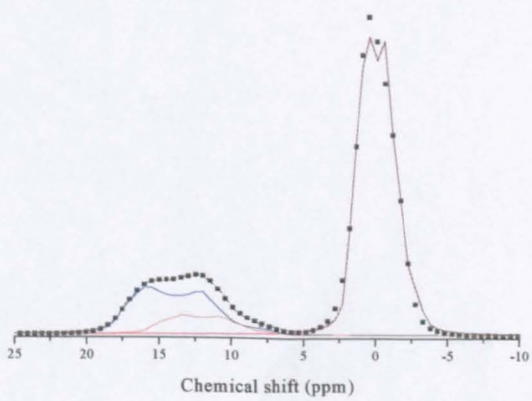

(h) R = 1.26

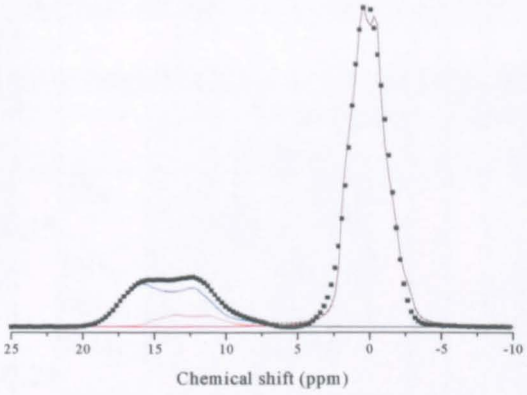

(i) R = 1.6

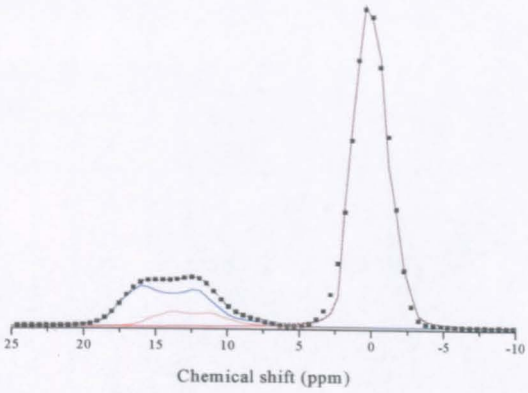

(j) R = 1.7

= BO_4, = BO_{3S}, = BO_{3A}, ····· = *experimental data,* - - - = *fit.*

^{11}B NMR simulation parameters for K=3 glasses shown in Appendices E1-2

Values highlighted in red are the values of N_4 determined from ^{11}B NMR.

R	*δ_i (ppm) (±0.5)*	*Qcc (MHz) (±0.05)*	*η (±0.05)*	*Species %*
Site				
0.15				
BO_4	2.21	1.55	0.61	15.21 / 17.5
BO_{3S}	17.77	2.65	0.45	35.64
BO_{3A}	13.36	2.60	0.38	49.15
0.25				
BO_4	2.28	1.55	0.61	25.99 / 27.7
BO_{3S}	18.07	2.64	0.36	40.40
BO_{3A}	13.88	2.63	0.38	33.51
0.375				
BO_4	1.87	1.62	0.55	40.27 / 41.6
BO_{3S}	17.92	2.70	0.30	39.70
BO_{3A}	14.64	2.72	0.29	20.02
0.5				
BO_4	2.18	1.68	0.56	48.51 / 49.8
BO_{3S}	18.22	2.67	0.31	38.53
BO_{3A}	15.10	2.68	0.29	12.96
0.545				
BO_4	2.19	1.68	0.53	51.54 / 51.0
BO_{3S}	18.26	2.65	0.31	37.14
BO_{3A}	15.21	2.63	0.31	11.32
0.75				
BO_4	2.00	1.78	0.44	61.78 / 60.0
BO_{3S}	18.30	2.61	0.28	26.7
BO_{3A}	15.62	2.49	0.40	11.5
1.0				
BO_4	2.02	1.78	0.43	69.7 / 67.0
BO_{3S}	18.43	2.60	0.28	22.6
BO_{3A}	15.90	2.38	0.39	7.70
1.26				
BO_4	2.03	1.74	0.46	69.49 / 69.0
BO_{3S}	18.59	2.61	0.30	22.53
BO_{3A}	16.04	2.37	0.40	7.98
1.6				
BO_4	2.13	1.69	0.55	73.65 / 73.0
BO_{3S}	18.57	2.58	0.30	21.6
BO_{3A}	15.89	2.23	0.38	4.75
1.7				
BO_4	1.91	1.66	0.56	72.57 / 73.0
BO_{3S}	18.60	2.62	0.30	21.19
BO_{3A}	16.20	2.34	0.38	6.25

Tables of T_g, N_4, density and thermal expansion data for NBS & LBS glasses studied.

	T_g (± 4K)	N_4 (± 5%)	ρ (± 0.01)	α (MK^{-1}) (± 0.4)
NBS 11	701	-	-	11.4
NBS 7	754	0.85	2.42	9.33
NBS 6	755	0.82	2.50	8.47
MW	772	0.71	2.47	8.44
NBS 8	783	0.61	2.46	7.57
NBS 14	779	0.53	2.38	7.02
NBS 9	762	0.45	2.35	7.15
NBS 10	767	0.51	2.41	8.21
LBS 1	786	0.69	2.66	8.24
LBS 2	800	0.62	2.88	8.62
LBS 3	813	0.54	3.30	9.24
LBS 4	826	0.51	3.45	-

Tables of N_4 and density data for ABS glasses studied

K (±0.05)	*R* (±0.01)	ρ (gcm^{-3}) (±0.02)	N_4 (±5%)	*K* (±0.05)	*R* (±0.01)	ρ (gcm^{-3}) (±0.02)	N_4 (±5%)
1	0.2	2.13	0.25	2.4	0.72	2.46	0.582
1	0.32	2.25	0.34	2.4	0.78	2.46	-
1	0.35	2.28	0.4	2.4	0.85	2.48	0.59
1	0.4	2.32	0.42	2.4	1.14	-	0.65
1	0.5	2.37	0.482	2.4	1.29	2.46	0.69
1	0.66	2.41	0.563	2.4	1.46	2.48	0.7
1	0.75	2.45	0.564	2.4	1.75	2.46	0.68
1	0.86	2.43	0.581	2.4	2.26	2.47	0.61
1	1	2.46	0.62				
1	1.5	2.43	0.532	3	0.15	2.12	0.178
				3	0.25	2.17	0.277
2	0.15	2.13	0.149	3	0.38	2.25	0.37
2	0.25	2.19	0.27	3	0.5	2.29	0.5
2	0.33	2.24	0.352	3	0.55	2.3	0.51
2	0.45	2.32	-	3	0.75	2.37	0.61
2	0.5	2.32	0.49	3	1	2.43	0.67
2	0.6	2.39	0.54	3	1.26	2.46	0.69
2	0.636	2.38	0.565	3	1.6	2.47	0.73
2	0.64	2.42	0.55	3	1.7	2.47	0.71
2	0.7	2.40	0.57	3	2.25	2.47	0.66
2	1	2.46	0.667				
2	1.22	2.49	0.66	4	0.33	2.2	0.37
2	1.7	2.49	0.63	4	0.5	2.28	-
2	2	2.44	0.632	4	0.71	2.32	0.68
2	2.26	2.44	0.567	4	0.75	2.36	-
2	2.5		0.52	4	1	2.404	0.71
				4	1.15	2.43	0.66
2.4	0.15	2.13	0.168	4	1.67	2.44	0.77
2.4	0.25	2.18	0.264	4	2.27	2.47	0.76
2.4	0.32	2.25	-	4	2.56	2.488	0.73
2.4	0.38	-	0.377	4	3	2.48	0.68
2.4	0.59	2.44	0.543	4	3.88	2.48	0.57

Table of T_g data for the ABS glasses studied

K *(±0.05)*	*R* *(±0.01)*	T_g *(K) (± 4)*	*K* *(±0.05)*	*R* *(±0.01)*	T_g *(K) (± 4)*
1	**0.2**	722	**2.4**	**0.781**	774
1	**0.32**	756	**2.4**	**0.852**	-
1	**0.352**	751	**2.4**	**1.136**	772
1	**0.4**	766	**2.4**	**1.29**	752
1	**0.5**	770	**2.4**	**1.46**	735
1	**0.66**	764	**2.4**	**1.75**	710
1	**0.75**	755	**2.4**	**2.26**	680
1	**0.86**	739			
1	**1**	728	**3**	**0.15**	730
1	**1.5**	662	**3**	**0.25**	738
			3	**0.379**	761
2	**0.15**	719	**3**	**0.5**	771
2	**0.25**	730	**3**	**0.545**	771
2	**0.33**	767	**3**	**0.75**	792
2	**0.45**	777	**3**	**1**	776
2	**0.5**	779	**3**	**1.263**	762
2	**0.6**	787	**3**	**1.6**	740
2	**0.636**	787	**3**	**1.7**	736
2	**0.64**	782	**3**	**2.25**	694
2	**0.7**	770			
2	**1**	754	**4**	**0.333**	756
2	**1.22**	732	**4**	**0.5**	784
2	**1.7**	685	**4**	**0.714**	781
2	**2**	682	**4**	**0.75**	779
2	**2.26**	659	**4**	**1**	784
			4	**1.153**	783
2.4	**0.15**	705	**4**	**1.666**	766
2.4	**0.25**	740	**4**	**2.27**	724
2.4	**0.32**	766	**4**	**2.56**	704
2.4	**0.379**	768	**4**	**3**	688
2.4	**0.4**	-	**4**	**3.88**	646
2.4	**0.723**	-			